Transcriptional Regulation and Epigenetic Landscape of the Glomerulus

INAUGURAL-DISSERTATION

zur

Erlangung des Doktorgrades

der Mathematisch-Naturwissenschaftlichen Fakultät
der Universität zu Köln

vorgelegt von

He Chen
aus Zheng Zhou

Dissertation accepted by the Faculty of Mathematics and Natural Sciences of the University of Cologne

Köln 2024

Berichterstatter: Prof. Dr. Thomas Benzing
(Gutachter) Prof. Dr. Niels Gehring

Contents

List of Figures

List of Tables

List of Abbreviations

µL	microlitre
µM	micromolar
mL	millilitre
mM	millimolar
nM	nanomolar
bp	base pairs
DNA	Deoxyribonucleic acid
RNA	Ribonucleic acid
DNase	Deoxyribonuclease
RNase	Ribonuclease
FSGS	Focal segmental glomerulosclerosis
DN	Diabetic nephropathy
MCD	Minimal change disease
ADR	Adriamycin-induced nephropathy
SD	slit diaphragm
FP	foot processes
GBM	Glomerular basement membrane
GEC	Glomerular endothelial cell
TF	Transcription factor
Tn5	Transposase 5
SE	super-enhancer
PAS	Periodic acidic schiff
STED	Stimulated emission depletion
ELISA	Enzyme-linked immunosorbent assay
Cre	Cre recombinase
Rosa26	(Gt(ROSA)26Sor)
GFP	Green fluorescent protein
tdTomato	Tandem dimer Tomato
PCR	Polymerase chain reaction
snRNA-seq	Single nuclei RNA-sequencing
ATAC-seq	Assay of Transposase Accessible Chromatin sequencing
CUT&RUN	Cleavage under targets and release using nuclease
CUT&Tag	Cleavage under targets and tagmentation
ddH2O	Double distilled water
HBSS	Hanks' Balanced Salt Solution
PBS	Phosphate-buffered saline
TAE	Tris-acetate-EDTA
PFA	Paraformaldehyde
TEMED	N,N,N',N'-tetramethylethylenediamine
APS	ammonimum persulfate
DAPI	4',6-diamidino-2-phenylindole

EDTA	Ethylenediaminetetraacetic acid
BSA	Bovine serum albumin
Tam	Tamoxifen
TMB	3,3',5,5'-Tetramethylbenzidine
LMX1B	LIM homeobox transcription factor 1-beta
WT1	Wilms' tumor protein
TCF21	Transcription Factor 21
PHB2	Prohibitin-2
MAFb	V-maf musculoaponeurotic fibrosarcoma oncogene homolog B
CD2AP	CD2-associated protein
MAGI-2	Membrane-associated guanylate kinase, WW and PDZ domain-containing protein 2
ZO-1	Tight junction protein ZO-1
YAP	Transcriptional coactivator YAP1
TEAD1	Transcriptional enhancer factor TEF-1
FOXC1	Forkhead box protein C1
ACR	Albumin-to-creatinine ratio
H3K4me1	Histone 3 lysine 4 mono-methylation
H3K4me3	Histone 3 lysine 4 tri-methylation
H3K27ac	Histone 3 lysine 27 acetylation
H3K27me3	Histone 3 lysine 27 tri-methylation
CTCF	CCCTC-binding factor
IGV	Integrative Genomics Viewer
PDS	Podocyte damage score
PONDR	Predictor of Natural Disordered Regions
IDR	Intrinsic disordered domains
LLPS	liquid liquid phase separation
FRAP	Fluorescence recovery after photobleaching

1 Abstract

Disease heterogeneity presents challenges in the understanding of disease progression of individual cells or cell types within complex tissues, particularly when the cells that are undergoing damage progress at different rates. In progressive renal diseases that lead to focal segmental glomerulosclerosis (FSGS), the loss of podocyte number and function is a major contributing factor for renal pathogenesis and our understanding of the underlying damage mechanisms in damaged podocytes has been limited. The present work addresses this gap in understanding by investigating the dysregulation of transcription networks, alterations in the epigenetic landscape, modulation of cellular pathways, and regulation by transcription factor (TF) in podocytes during FSGS development. By employing mouse models, single-cell technologies, and molecular assays, we developed a podocyte damage score (PDS) to decipher TF and pathway rewiring, explored changes in the epigenetic landscape, and investigated the molecular actions of LMX1B, which is a key TF essential for podocyte maintenance. Our findings highlighted the robustness and specificity of the PDS in scoring damage at single-cell resolution across murine and human chronic kidney diseases and demonstrated the versatility of the PDS in identifying unique cellular mechanisms across diverse disease models. We performed comprehensive mappings of the epigenetic landscape for various glomerular cell types in health and disease and revealed differential regulation of glomerular cell-specific enhancers through chromatin accessibility and by acetylation of histone 3 lysine 27 which correlated with target gene expression and key signaling pathways. Additionally, functional podocyte-specific knockout studies of *Lmx1b* using single-cell multiomic approaches revealed its potential role as a novel regulator of the non-canonical Wnt signaling pathway in injured podocytes and *in vitro* studies implicated the C-terminal end of LMX1B in liquid-liquid phase separation (LLPS), and offered additional mechanistic insight into the function of LMX1B. In summary, our integrated approach utilizing single-cell technology allowed for a comprehensive investigation of the intricate gene regulatory mechanisms and epigenetic rewiring of podocytes undergoing FSGS and shed light on differential regulation related to key TFs and signaling pathways critical for podocyte function.

2 Introduction

2.1 Podocyte biology

The glomerulus is the filtration unit of the kidney and is responsible for maintaining body homeostasis as well as fluid and electrolyte balance by filtering blood into urine [1]. The filtration process begins when blood plasma passes through the glomerular filtration barrier, which only permits free passage to small molecules like water, ions, glucose, amino acids and waste products, yet remains impermeable to macromolecules [1]. The resulting glomerular filtrate collects in the Bowman's capsule, travels through the proximal tubules and along various segments of the renal tubules where essential substances such as glucose, amino acids, and the majority of the filtered water undergo reabsorption back into the bloodstream before nitrogenous wastes, salts and excess water are excreted as urine [2]. The integrity of the glomerular filtration barrier ensures appropriate size and charge selection against macromolecules to prevent protein wastage in the urine (proteinuria). Proteinuria is a hallmark of kidney disease [3]. The glomerular filtration barrier preventing proteinuria consists of three components: the fenestrated endothelium, the basement membrane, and the podocytes [1]. The endothelium layer of the glomerular capillaries is layered by endothelial cells while podocytes are terminally differentially epithelial cells that wrap around the capillaries to create filtration slits with thin diaphragms in between [1]. The glomerular basement membrane (GBM) is an extracellular matrix that forms between the glomerular endothelial cells (GECs) and the podocytes. The function of the filtration barrier is dependent on the integrity and interplay between the three constituents but the specific molecular mechanisms remain largely unknown [4, 5].

Podocytes are highly specialized epithelial cells located on the outer surface of the glomerular capillaries [2] (Figure 1). They have unique finger-like extensions called foot processes, which interdigitate with neighboring podocyte foot processes forming cell-cell junctions but leaving narrow gaps or slits between them forming the slit diaphragm (SD) [6, 7]. These specialized adherens junctions contain unique podocyte-specific integral membrane proteins including nephrin, podocin and Neph1. These proteins serve as a signaling platform to maintain the filtration function and to regulate the shape of foot processes through interaction with the actin cytoskeleton [8]. Mutations in nephrin, podocin, podocalyxin and Neph1 are associated with foot processment effacement and proteinuria. Scaffolding proteins including ZO-1, CD2AP, MAGI-2 and various actin-binding proteins including actinin-4 are associated with the junction and also localized to the slit diaphragm [9]. Podocytes are terminally differentiated cells without the capacity to renew and podocyte damage is suggested to be one of the critical factors in determining renal prognosis [3, 10]. Mechanical injury to podocytes, genetic susceptibility, drug treatment, and aging may all contribute to podocyte damage and deteriorating filtration ability of the slit [11, 9, 12]. The disruption of the podocyte slit diaphragm can occur in various kidney diseases, such as Focal Segmental Glomerulosclerosis (FSGS), Diabetic Nephropathy (DN) and Minimal Change Disease (MCD), where the selective filtration properties of the slit diaphragm are compromised, resulting in abnormal filtration rate and proteinuria [3, 9, 6]. The filtration process across the glomerular capillary exerts physical forces on the capillary wall but the gel-like structure of the GBM counteracts this hydrostatic pressure by dynamic organization of the highly regulated actin cytoskeleton network in podocytes [13]. Thus the coordinated transcriptional regulation from the nucleus to signaling effectors at the SD is essential for correct mechanosensing and preservation of the structural integrity required to maintain podocyte function. The failure to provide mechanical resistance against blood pressure by the podocytes to compress the GBM leads to poor permselectivity of the filtration barrier and loss of albumin and other macromolecules into the urine [14]. Therefore, a deeper understanding of how transcription regulatory

mechanisms contribute to the maintenance of podocyte function in health and undergo alterations during disease progression can provide valuable insights for the development of therapeutic strategies.

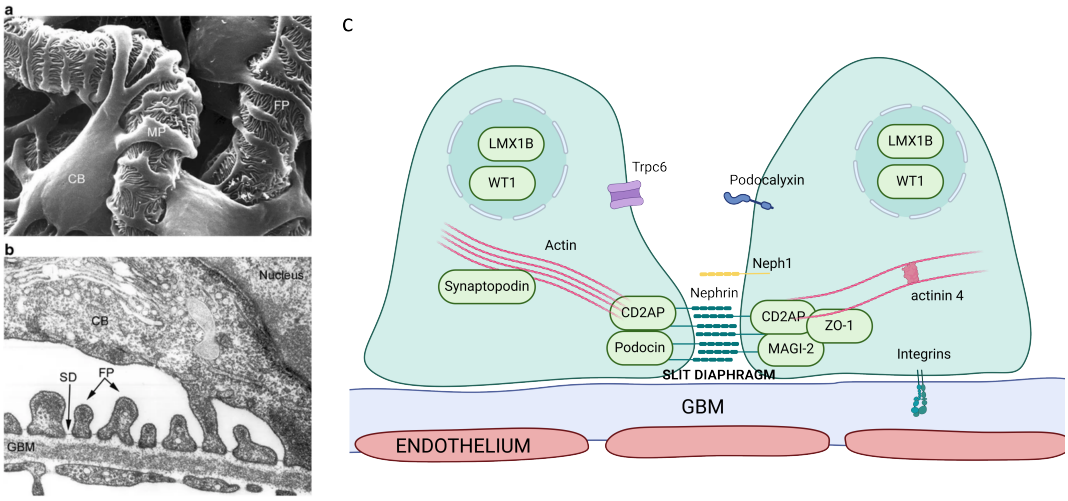

Figure 1: The structure of podocytes. A. Scanning electron microscopy view from Bowman's space. Major or primary processes (MP) link the cell body (CB) to foot processes (FP), which interdigitate with that of the neighboring podocytes to form the filtration slits. B. Transmission electron microscopy image of the cross-section of the filtration barrier showing the fenestrated endothelium, GBM, and podocyte FP with the slit diaphragm (SD). C. Schematic representation of the slit diaphragm and key proteins that play a role in the the maintenace of podocyte function. Figures A and B are adapted from Mundel et al. [15]. Figure C is adapted from Benzing et al. using Biorender [13].

2.1.1 Focal segmental glomerulosclerosis

Focal segmental glomerulosclerosis (FSGS) is a histological pattern of the glomeruli characterized by scarring and lesions in segments of a subset of glomeruli [16]. Clinical manifestations of FSGS encompass proteinuria or hypoalbuminemia, edema, decreased kidney function, and can result in chronic kidney disease (CKD) [17]. The loss of and injury to podocytes are associated with the development of FSGS [18]. The medical intervention aims to mitigate the severity of symptoms, preserve renal function, and slow disease progression [3, 17]. In severe cases, FSGS may progress to end-stage renal disease (ESRD), which necessitates dialysis or kidney transplantation as a final treatment option [18]. FSGS is a heterogeneous glomerular damage pattern with diverse presentations and underlying causes. It encompasses various subtypes, including primary, secondary, and genetic FSGS [18, 19]. Primary FSGS, also known as "idiopathic" FSGS, arises spontaneously without an identifiable cause, and its exact mechanisms are not well understood. On the other hand, secondary FSGS emerges as a consequence of stress imposed on the glomeruli by secondary associated risk factors from outside of the kidney. The contributing conditions may include obesity, hypertension, diabetes, infections, or medications [19]. Additionally, genetic mutations can play a significant role in FSGS pathogenesis where mutations in genes encoding proteins important for podocyte function and glomerular filtration can result in hereditary forms of FSGS [17, 3].

The identification of key proteins that are essential for podocyte function led to the discovery of numerous mutations responsible for the onset of FSGS. For example, mutations in the nephrin (NPHS1) [20], and podocin (NPHS2) [20, 14], genes cause childhood- and adult-onset FSGS. α-Actinin-4 is an actin-filament crosslinking protein and missense mutations in the ACTN4 gene leading to nonsynonymous substitution at

L228E, T232I or S235P have been identified as direct causes of FSGS [21]. CD2-associated protein (CD2AP) is an adaptor protein that can directly interact with nephrin and F-actin to regulate the actin cytoskeleton [22]. Patients with mutations in the CD2AP genes resulting in truncated proteins were affected by idiopathic FSGS [23] and early onset nephrotic syndrome [24], and heterozygous mutations at K301M [25] and T374A [26], as well as point mutations within introns [27] were established FSGS-causing variants. Transcription factors (TFs) are also crucial regulators of podocyte function. Wilm's tumor gene (WT1) is a zinc finger TF important for the development of kidneys and the differentiation of podocytes, and WT1 variants are pathogenic for the Denys–Drash syndrome which is presented with renal failure [28], and mutations in the zinc finger domain show dominant negative activity via loss of binding to DNA of target genes [29, 28]. Another example is the Lim homeobox transcription factor 1B (LMX1B) which belongs to the LIM-homeodomain TF family and amino acid substitution at arginine 246 has been shown to cause FSGS [30, 3, 31, 32]. In contrast to WT1, whose target genes have been identified via glomerular ChIP-seq [33, 34, 35], knowledge of transcriptional mechanisms of LMX1B and the function of its target genes remains to be explored due to the lack of high-quality antibodies for ChIP-seq.

2.2 Transcriptional regulation

Mutations in podocyte-specific TFs, including WT1 and LMX1B, are well-established contributors to FSGS. Consequently, our work investigates the molecular functions of these regulatory factors in order to understand the regulatory role of TFs underlying podocyte damage. Gene expression can be regulated at two key stages, transcription and translation, wherein the former regulates the conversion of DNA to RNA and the latter controls the expression of proteins synthesized from its mRNA. Transcriptional regulation is the core feature of cell development including acquisition of cell fate, differentiation of cell type, maintenance of cell metabolism, and response to external stimuli. Transcriptional regulation is a complex and highly orchestrated process that intricately controls gene expression and precise gene expression, occurring at the appropriate spatial, temporal, and quantitative levels, is vital for the development and maintenance of the correct cell identity [36].

2.2.1 Transcription factor regulation in podocytes

The role of several TFs that are essential in the development and maintenance of podocyte function have been elucidated [37, 38]. The WT1 gene encodes a four Krüppel-type Cys2-His2 zinc finger and a tumor suppressor protein that is indispensable for the initial stages of kidney development, but also the maintenance of the integrity of the final differentiated podocyte [39]. WT1 defines podocyte identity by activation of other podocyte-specific TFs, including Mafb, Lmx1b, FoxC2, and Tcf21 [40, 33, 34]. Mutations in WT1 are associated with a spectrum of diseases including Wilms's tumor, the Denys-Drash syndrome, the Frasier syndrome, and the isolated steroid-resistant nephrotic syndrome, then eventually progress to end-stage renal failure [37]. The alternative splicing of WT1 leads to the protein expression of two major isoforms: +KTS and -KTS both have distinct biological functions in development [41]. The predominant +KTS isoform has a higher affinity for RNA binding and is implicated in gene regulation, and direct regulation of Scribble gene, which regulates cell apical-basal polarity, in cultured podocyte models [42]. Downstream targets of Wt1 are also implicated in podocytophathy in FSGS, including Tead1 [43, 44], Tcf21 [45, 46, 47] and Mafb [48, 49, 50, 51]. Foxc1/2 has been to interact with WT1 in zebrafish to regulate podocyte formation [52]. RE1-silencing transcription factor (REST), which is a repressor of neuronal genes during embryonic develop-

ment has also been whon to play a role in the adaptation to injury and aging in podocytes [53]. In summary, the transcriptional regulation enabled by TFs can further lead to signaling cascades of downstream TFs to form interconnected auto-regulatory loops within a gene regulatory network, and the intricate interaction orchestrated by a network of TFs underscores the complexity of transcriptional control in podocytes. Understanding how the cell type-specific regulatory network is dynamically modulated upon podocyte damage remains challenging to decipher.

2.2.2 Gene regulatory networks in the kidney

The elucidation of the gene regulatory network of podocytes is highly relevant for understanding molecular functions and pathogenesis of FSGS. Meta-analysis of gene expression in hyperglycemic zebrafish showed altered gene expression of key TF genes which led to morphological abnormalities in glomeruli, pronephric tubules, proximal and distal ducts [54]. Integrated network analysis identified key changes in gene expression and regulatory mechanism in FSGS [55], and research has shown that TAGLN-mediated regulatory network may be involved in the progression of proteinuria [56]. Novel calcium-regulated gene networks have been identified in podocytes [57]. Genes associated with the Wnt signaling cascade were dysregulated, while classical podocyte-specific genes appeared widely unaltered [58]. In the diphtheria toxin (DT)-mediated podocyte depletion mouse model, differential gene expression analysis in isolated GECs showed significant changes in pathways related to cell adhesion, actin cytoskeleton, cell proliferation, angiogenesis, as well as apoptosis [59]. Podocyte-specific gene regulatory networks revealed alternative splicing of key genes that regulated cellular processes important for the function of the cytoskeleton, endosomes, and peroxisome [60]. However, current investigations of cell type-specific gene regulatory networks rely mostly on bulk transcriptomic and proteomics and are technically limited in capturing subtle cellular changes in damaged podocytes. In this thesis, we harness the power of single-cell technologies to comprehensively characterize temporal-dependent transcriptional changes in podocytes undergoing progressing FSGS at single-cell resolution.

2.3 Epigenetic regulation of gene expression

Another layer of regulation beyond transcription control includes epigenetic mechanisms. The term epigenetics was first coined by Waddington in 1942 to study "mechanisms by which the genes of the genotype bring about phenotypic effects" [61] but its definition has since drifted beyond the vague yet ambitious term aimed to explain the intriguing fact that multiple cell types can arise from one single fertilized egg. Epigenetics first echoed Herring's definition used later in the year 1993 to refer to "the entire series of interactions among cells and cell products which leads to morphogenesis and differentiation" [62]. Both references redeliberated the Latin root word, epigenesis, which is an idea propelled by Aristotle who contrasted epigenesis with preformation to draw his philosophical interpretation of nature and nurture based on observations made from the embryonic development of chick eggs [63]. Indeed, before the 1990s, the primary focus of epigenetics research pertained to developmental biology. However, the modern most widely accepted definition of epigenetics came instead from Riggs' review in 1996 summarized as "the study of mitotically and/or meiotically heritable changes in gene function that cannot be explained by changes in DNA sequence" [64]. Therefore, in this thesis, epigenetic mechanisms describe changes in the way genes are accessed or utilized in response to input cues in flexible and reversible manners.

Examples of epigenetic mechanisms include DNA methylation, histone modifications and variant exchange, modification by chromatin remodelers and RNA-based regulation, including long non-coding RNAs

[65]. Methylation is a direct modification wherein a methyl group is covalently transferred to the C-5 position of the cytosine ring in DNA molecules, and this reaction is catalyzed by methyltransferases and predominantly occurs in the promoter regions of target genes that are enriched with CpG dinucleotides, called CpG islands [66, 67]. Histones interact with and compact nuclear DNA into nucleosomes while regulating the access to regulatory elements. Nucleosomes consist of 146bp of DNA wrapped around a histone octamer, comprising two copies each of four core histone proteins (H2A, H2B, H3, and H4) and are connected via linker histone H1 [68]. The precise arrangement of nucleosomes along the DNA sequence is subject to dynamic modifications and regulation by chromatin remodelers, via direct acetylation, methylation, or phosphorylation on histones, which in turn influence chromatin structure and gene expression patterns [69]. The acetylation of histone 3 lysine 27 (H3K27ac), and monomethylation of histone 3 lysine 4 (H3K4me1) are often associated with open chromatin and active gene expression [70], while histone deacetylation or tri-methylation of histone 3 lysine 27 (H3K27me3) is linked to gene repression [71]. Chromatin remodeling complexes control gene expression by modifying nucleosome shuffling or positioning to allow access to condensed DNA regions to regulate transcription machinery protein [72]. Non-coding RNAs, such as microRNAs (miRNAs) and long non-coding RNAs (lncRNAs), are RNA molecules that do not code for proteins but regulate gene expression at the post-transcriptional level [73]. Active transcription of enhancers generates lcRNAs known as enhancer RNAs (eRNAs) and eRNAs are also implicated in transcriptional regulation of target genes via phase separation and the formation of nuclear transcriptional condensates [74, 75, 76]. The complexity of the multifaceted epigenetic regulation of gene expression reflects the dynamic interplay between various epigenetic mechanisms that can collectively modulate chromatin structure and accessibility in response to changes in stimuli, cellular signals or damages. Potential combinatorial regulatory effects of epigenetic modifications and their interaction with TFs and regulatory elements add additional layers of complexity and research is still needed to understand how epigenetic mechanisms modulate kidney function and podocyte biology.

2.3.1 Epigenetic mechanisms in kidney and podocytes

Regulation of DNA regulatory elements and chromatin structure in the kidney DNA regulatory elements such as promoters, enhancers, insulators and repressors are key regions in the genome that determine the efficacy of transcriptional regulation and the connectivity of the gene regulatory networks (Figure 2). These regulatory elements and networks are highly cell type-specific and context-dependent and remain technically challenging to determine for podocytes, thus necessitating careful annotation and then understanding of rewiring of the interconnecting epigenetic landscape of podocytes undergoing damage. Promoters are generally 1-2 kilobases upstream of the transcription start site (TSS) and are essential for the recruitment of RNA polymerase II transcription machinery. In podocytes, the analysis of the murine Nphs1 promoter led to the identification of a 1.25-kb fragment promoter-enhancer element that can drive transgene expression in podocytes without expression in extrarenal tissues and this promoter was further exploited to generate a podocyte-specific Cre recombinase activatable mouse line that is now widely used in *in vivo* investigation of podocyte biology [77, 78, 79]. In contrast, enhancers are *cis*-regulatory sequences that work in concert with the promoter of a gene to control the spatiotemporal expression of its gene targets and can serve as a scaffolding platform for recruitment and binding of transcription factors and DNA modifying complexes. The regulation of enhancers is irrespective of their orientation, distance or position to their TSS target. Clusters of enhancers, called super-enhancers (SEs), may act synergistically or redundantly to regulate transcription [80]. The analysis of primary cultures of human cortices and tubules

discovered that genetic variants associated with kidney diseases (GWAS) and kidney expression quantitative trait loci were mostly enriched in DNA regulatory regions [81]. In the glomerulus, FOXC1/2 are suggested to play meaningful roles in core regulatory circuits as they associate with SEs [82]. On the other hand, CTCF is a protein that can bind to insulator elements and partition chromatin into higher-ordered topologically associating domains (TADs) which act as single functional units for co-regulation in the genome. The podocyte-specific inducible ablation of CTCF has been shown to develop rapid podocyte loss, severe progressive albuminuria, hyperlipidemia, hypoalbuminemia, and impairment of renal function [83, 84]. Due to technical limitations, mapping the 3D chromatin organization of podocytes presents a considerable challenge. However, the promoter-enhancer contacts have been profiled in human cultured podocytes, where the glucocorticoid receptor binding sites were shown to be enriched at SEs [85]. The 3D chromatin conformation map has also been investigated human cultured glomeruli by Hi-C to identify the target genes of risk variants associated with kidney diseases but Hi-C generally lacks sufficient resolution to fully delineate the chromatin interaction associated with transcription [81], thus the generation of an epigenetic map that fully annotates and characterizes the glomerular cell type-specific landscape in health and disease will be a prerequisite to understanding epigenetic remodeling in FSGS.

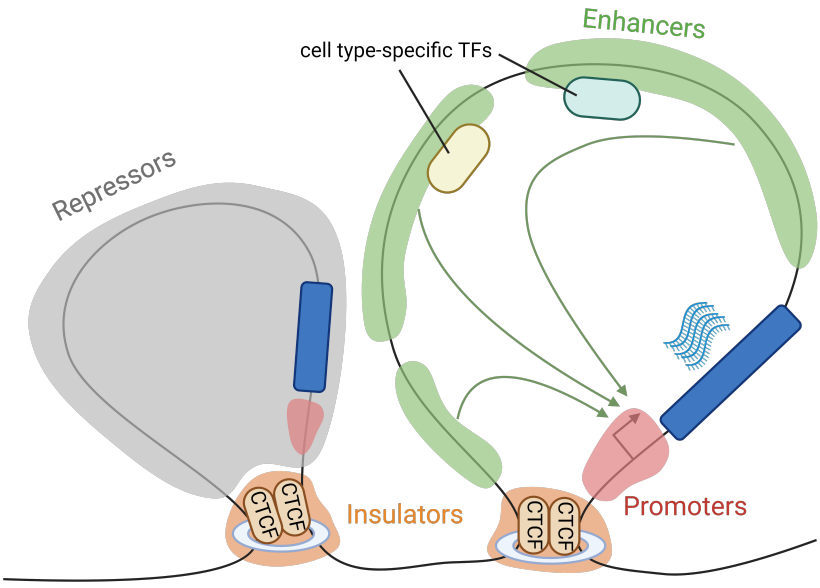

Figure 2: Schematic of DNA regulatory elements where cell-type-specific TFs can associate with enhancers or SEs to activate gene expression via enhancer-promoter contacts within CTCF-defined TADs but repressors inhibit transcription.

Regulation by histone modifications Numerous research have explored the role of histone modifications and histone-modifying enzymes in kidney diseases. In patients with FSGS or diabetic nephropathy, podocytes showed reduced H3K27me3 levels, and the loss of H3K27me3 in cultured podocytes in vitro encouraged podocyte dedifferentiation [86]. Additionally, the deletion of enhancer of zeste homolog 2 (EZH2), an enzyme responsible for catalyzing H3K27me3 methylation, decreased H3K27me3 levels in the promoter

region of the Notch ligand Jag1 and increased susceptibility to glomerular disease in mice [86]. In diabetic kidney diseases, advanced glycation end products (AGEs) were found to reduce the level of H3K27me3 through modulation of the expression of nuclear inhibitor of protein phosphatase 1 (NIPP1) and concurrently decreased the expression of its interactor EZH2 [87]. Furthermore, the induction of chronic kidney injury in mice through lipopolysaccharide injection led to increased serum creatinine and urine albumin levels [88], accompanied by heightened H3K4me3 levels in podocytes [89]. Podocyte-specific deletion of the Pax Transactivation Domain-Interacting Protein (PTIP), an essential component of a H3K4 methyltransferase complex, resulted in proteinuria and podocyte effacement in 12-month-old mice [90]. In addition, in murine podocytopathy models, the activities of histone deacetylases 1 and 2 (Hdac1, Hdac2) in podocytes were increased [91]. VPA is a Hdac1/2 inhibitor and treatment with VPA ameliorated podocyte effacement, decreased levels of albuminuria and inhibited podocyte loss [92, 93]. Interestingly, the genetic ablation of podocyte-associated Hdac1 and Hdac2 provided renal protection, improved proteinuria, and mitigated the progression of glomerular injury in podocyte-specific Tln1-KO mice [91]. However, the germline podocyte-specific deletion of Hdac1 and Hdac2 in mice displayed severe proteinuria and showed characteristics of DNA damage, cell cycle arrest, and senescence [94]. The conflicting evidences of the regulation of gene expression by histone modifiers in mice highlight the complexity of the epigenetic regulation in podocytes thus necessitating mapping the exact genome-wide epigenetic landscape of podocytes by various DNA regulatory elements and their changes as well as changes in upstream effectors in podocyte damage.

2.3.2 Interplay between transcription factors and chromatin regulation

The interplay between TFs function and epigenetic regulation presents a complicated yet pivotal aspect in unraveling the intricate mechanisms underlying podocyte biology in FSGS. TFs can modulate the transcriptional regulatory network by binding to specific DNA motifs and dictating the activation or repression of its target genes through the recruitment and stabilization of the RNA polymerase complex [95]. Additionally, DNA regulatory elements, such as promoters and enhancers, play a crucial role in activating gene transcription and expression, while repressors and silencers work oppositely to hinder these processes. For example, FOXC1/2 has been suggested to regulate podocyte-specific SEs [82], and two distal intronic enhancers of Pbx1 can be bound by BRG1 to regulate nephron progenitor-specific expression in response to Six2 activity [96]. Insulators are DNA elements that form isolated transcriptional hubs and prevent inappropriate interactions between adjacent chromatin domains [97], bound by insulator proteins like CTCF [98], cohesin [99], or YY1 [100], contribute to the organization of chromatin into higher-order, self-associating and loop-like subdomains known as topologically associating domains (TADs) and further facilitate the activation of genes associated within these TADs [101, 102, 85]. Chromatin can also undergo dynamic structural changes and shuffle between closed or open conformations to regulate the recruitment of TFs and general transcriptional machinery to target genes and to elicit downstream transcriptional activity via chromatin remodeling complexes to reorganize TADs and to fine-tune the overall gene expression output [72]. Overall, the intricate interplay of TFs, cis-regulatory elements, chromatin structures, and chromatin remodeling complexes constitutes a sophisticated regulatory network that governs gene expression, ensuring precise, temporal- and context-dependent transcriptional responses [36]. However, the regulatory role and the exact mechanism of action of several TFs important for podocyte function and how they interact with the chromatin to modulate transcriptional activity are still unclear.

2.4 LIM Homeobox Transcription Factor 1 Beta (LMX1B)

In this thesis, we aim to elucidate the functional role of LMX1B in podocytes and its molecular mechanism of action within the nucleus. LMX1B belongs to the LHX transcription factor genes and LIM-homeodomain protein family and contains two protein-interacting cysteine and histidine-rich LIM zinc-binding domains at the N-terminus, one central DNA-binding homeodomain, and a C-terminal glutamine-rich transcriptional activation domain. The homeodomain recognizes AT-rich elements, known as FLAT elements, which contain the 5'-ATTA-3' (reverse 5'-TAAT-3') core sequence in the promoter or intron region of its target genes. Lmx1b expression has been detected in neurons, retinas, and limbs. Lmx1b is required for the formation of dorsal-ventral patterning during development in limbs and organs, including the kidney, brain, and eye. It has been reported that LMX1B can interact with NFkb at target gene transcription. LMX1B is highly expressed in ovarian cancer cells, laryngeal squamous cell carcinoma, and radioresistant esophageal cancer cells. Lmx1b is also implicated in osteogenic differentiation and bone regeneration [103, 104]. The first mutation of LMX1B was described in 1998 [105]. Haploinsufficiency of LMX1B causes Nail-patella syndrome where patients are often presented with defects in limbs, eyes and brain and nephropathy [106, 107]. LMX1B knockout mice are embryonically lethal [105]. In podocytes, Lmx1b is important in glomerular development and is implicated in the dysfunction of the podocytes [108], and a missense mutation (R246Q) in LMX1B causes FSGS without extra-renal manifestations and downregulated the WT1(-KTS) isoforms in podocytes [109]. Podocyte-specific deletion of Lmx1b in mice showed proteinuria yet little foot process effacement in podocytes, as well as dysregulation of actin cytoskeleton organization [110]. In zebrafish, Lmx1b and FoxC combinatorially bind to the nphs2 promoter and regulate podocyte development [111]. Regulatory elements for Lmx1b have been identified in vertebrates using ChIP-seq during development [112], and two associated *cis*-regulatory modules LARM1 and LARM2 have been shown to be bound by Lmx1b in vertebrates during limb development, and both enhancers are associated with active chromatin marks and display enhancer activity within the dorsal mesoderm [112]. Published work on LMX1B from various cell types suggests that LMX1B is essential in the maintenance of cell type differentiation via association with active enhancers to drive gene expression and to modulate downstream cellular pathways but the specific mechanisms of action in podocytes are still unclear. In the context of podocytes, the elucidation of the protein interactors, direct target genes, and associated enhancers of LMX1B will be needed to bridge the gap in the understanding of the regulatory function and mechanisms of LMX1B.

2.5 The role of Wnt signaling in podocytes

Lmx1b has been implicated in the Wnt signaling pathway in the establishment of the dorsal-ventral axis during development [113], but may play a role in regulating podocyte biology which has not been previously investigated. The Wnt signaling pathway consists of the canonical and the non-canonical pathways and transduces different signals via downstream effectors. The canonical Wnt signaling pathway is β-catenin-dependent and signals through the Frizzled receptor to trigger signaling cascades that enable the translocation of β-catenin to the nucleus where it acts as a transcription co-activator for the expression of T cell factor (TCF)-lymphoid enhancer factor (LEF)-dependent genes, wherein non-activated steady state, β-catenin is phosphorylated by a destruction complex formed by GSK3β, APC, CK1 and axin, then targeted for proteosomal degradation [114, 115]. The non-canonical Wnt pathways include the Wnt/Ca^{2+} signaling pathway and the Wnt/planar-cell-polarity (PCP) pathway. The Ca^{2+}-dependent pathway activates PLC and PKC which leads to increased intracellular Ca^{2+} concentration thus triggering the activation of the

CaMKII pathway and downstream transcriptional changes. On the other hand, the Wnt/PCP pathway is mediated through the class of Frizzled, Ror or LRP receptors to recruit Dishevelled (DVL) proteins to trigger the activation of small GTPases, such as RHOA and RAC1, then activates downstream Rho-associated protein kinase (ROCK) or JUN-N-terminal kinase (JNK) proteins to regulate actin cytoskeleton remodeling, adhesion dynamics and polarization that power cell motility. The activation of the non-canonical Wnt pathway can inhibit the canonical pathway [114, 115].

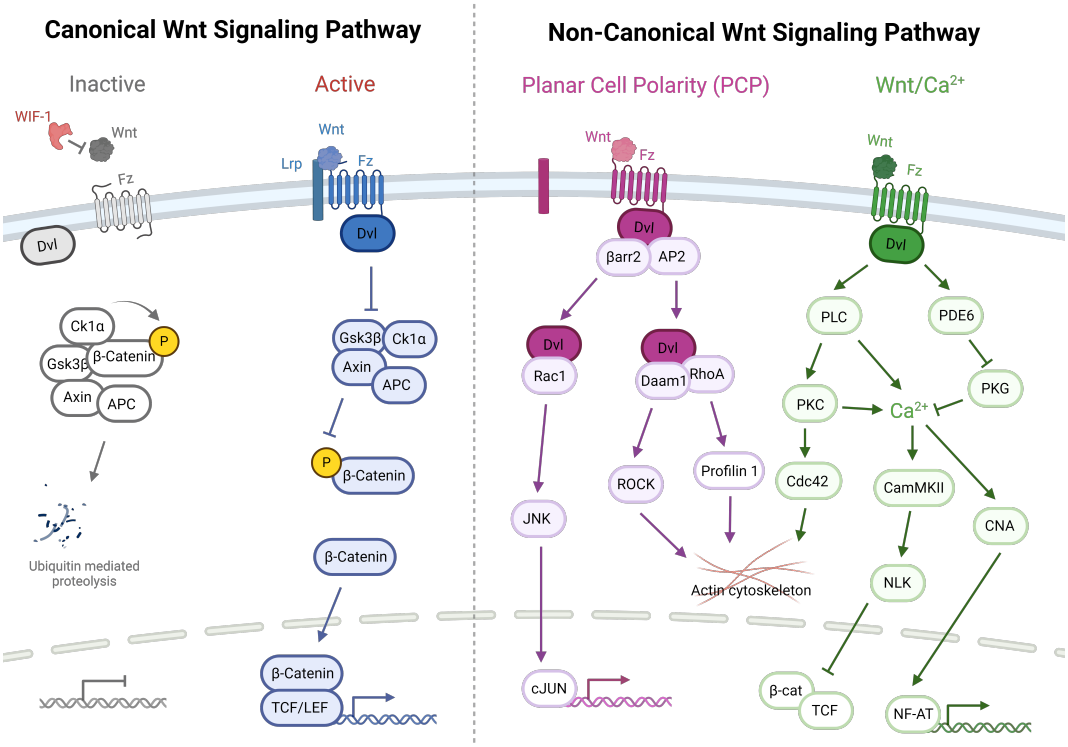

Figure 3: Canonical and non-canonical Wnt signaling pathways. Binding of specific Wnt ligands to the Frizzled class receptors activates the canonical Wnt signaling pathway inhibits the phosphorylation and degradation of β-catenin and instead leads to the translocation of β-cantenin to the nucleus to activate transcriptional responses. The non-canonical Wnt signaling pathway is categorized into the planar-cell-polarity (PCP) pathway or the Ca^{2+} pathway which activates downstream signaling cascades to regulate the actin cytoskeleton or to modulate transcriptional responses.

2.5.1 Canonical Wnt signaling in podocyte damage

The Wnt/β-catenin signaling pathway has been shown to be activated in podocytes in diabetic nephropathy [116, 117, 118], adriamycin-induced (ADR) nephropathy [119] and angiotensin II-induced podocyte injury [120], and the inhibition of the activated Wnt5 signaling pathway generally show renal protective effects. For example, the activation of Wnt/β-catenin by TGF-β1 led to podocyte injury and proteinuria [121], whereas podocyte-specific knockout of β-catenin was protective after adriamycin-induced injury [119] and against oxidative stress [122]. Similarly, the inhibition of the Wnt pathway using peptides and small molecule inhibitors, such as Klotho-derived peptide 6 (KP6) [117], DKK1 [123], ICG-001 [124] or Paricalcitol [125], improved proteinuria and ameliorate glomerulosclerosis and fibrosis. However, it has also been shown that constitutively active podocyte-specific expression of β-catenin led to increased susceptibility to glomerular injury and proteinuria, whereas deletion of podocyte-specific β-catenin or inhibition of the canonical Wnt

pathway also displayed increased susceptibility to diabetic kidney disease [118]. Conflicting evidence presented on the role of β-catenin suggests that the expression of β-catenin needs to be carefully balanced in podocytes for proper glomerular filtration. Mechanistically, WT1 has been implicated in the canonical Wnt signaling pathway. Ectopically overexpressed WT1 has been shown to downregulate active β-catenin expression in cultured podocytes and mouse models, and WT1 demonstrated protective effects on podocytes by inhibiting β-catenin activation [126]. Overall, the specific mechanism of how the canonical Wnt signaling pathway is regulated by TFs in podocytes is still not well understood.

2.5.2 Non-canonical Wnt signaling in podocytes damage

In contrast, the role of the non-canonical Wnt signaling pathway has not been well investigated in podocytes. Podocyte-specific deletion of Wntless, a receptor protein required for Wnt secretion, showed susceptibility to ADR-induced podocyte injury and downregulated NFAT1 and NLK which are downstream mediators of the non-canonical Wnt/calcium pathway [127]. NFAT1 is a TF and a key transcription regulator of calcium and calcineurin signaling, and the activation of NFAT in mice caused progressive proteinuria and FSGS [128]. Mutation in the TRPC6 cation channel which regulates calcium influx into cells caused FSGS and TRPC6 has been implicated in crosstalking with the Wnt signaling pathway to regulate podocyte function [129]. In addition, the Wnt/PCP pathway has been implicated in the organization of the SD proteins and the remodeling of the cytoskeleton mediated by Wnt5a, which induced the mislocalization of Dvl and Daam1, and modified stress fibers morphology and increased cell motility in cultured podocytes [130, 131]. The activation of ROCK, RhoA, and Rac-1 activities, which are downstream signaling transducers of the non-canonical Wnt signaling pathway, have been implicated in podocyte injury [132, 133]. Simiarly, Rap1 activity has been shown to be essential to mediate signaling between nephrin and integrin-β to maintain the integrity of focal adhesion. Overall, the inhibition of the upregulated canonical Wnt signaling pathway in podocyte injury models seems renal protective, although the modulation of the non-canonical Wnt pathway may lead to aberrant podocyte function and the balance between the two pathways may be needed for proper podocyte function. The role of the non-canonical Wnt signaling pathway in podocytes, including the identification and understanding of specific Wnt ligands, interacting receptors, and the mechanisms by which key effector signaling transducers or TF mediate downstream transcriptional rewiring during podocyte damage, remains speculative.

2.5.3 The implication of LMX1B in the Wnt signaling pathway

Lmx1b has been reported to be essential for the dorsalization of distal limb structures though there are conflicting reports for its role in dorsal-ventral patterning during limb development and digit regeneration [113, 134, 135, 112]. Ectopic expression of Wnt7a, a secreted ligand, has been found to induce and maintain the expression Lmx1 from the limb ectoderm to the mesenchyme during development [136]. In chick embryos, β-catenin did not induce ventral expression of Lmx1 suggesting that Wnt7a regulated Lmx1 via the non-canonical Wnt signaling pathway [137, 138, 139]. However, Wnt7a may also act through the canonical Wnt signaling pathway depending on the cell type [140, 141, 139]. Lmx1b has also been shown to maintain Wnt1 expression in brain development [142, 143]. An autoregulatory loop between Wnt1 and Lmx1a/Lmx1b has been described in the midbrain dopaminergic (mDA) neurons to regulate mDA-specific transcription factors to drive differentiation [144]. However, Wnt ligands that may be associated with Lmx1b function has not been previously described in podocytes and remain an interesting aspect of research.

Common Wnt ligands that can act through the canonical Wnt signaling pathway include Wnt1, Wnt2, Wnt3, Wnt3a, Wnt8a, Wnt8b, Wnt10a and Wnt10b, whereas Wnt4, Wnt5a, Wnt5b, Wnt6, Wnt7a, Wnt7b and Wnt11 were implicated in the non-canonical Wnt signaling pathway [145]. The role of Wnt ligands has not been well described in podocyte research. Wnt5b is involved in bone function and limb development [146], though conflicting effects have been attributed to its role in non-canonical signaling. Wnt5b acted via both the calcium-dependent signaling pathways and the Wnt/PCP pathway in chondrocyte differentiation [147], but regulated chondrocyte stacking through Wnt/PCP-independent signaling pathway in zebrafish [148]. Wnt5b has been shown to activate adipocyte differentiation [149], β-cell differentiation [150] and cardiomyocyte differentiation [151]. Wnt ligands are found to be required for nephron formation from nephrogenic mesenchyme and Wnt signaling is important for patterning of the proximal-distal nephron axis [152, 153]. It has been shown that the activation of the Wnt pathway in mesonephric cultures repressed early and late glomerular markers including Wt1 and Pod1 [153] but LMX1B, which is also a key TF that shares similar function to WT1 and directly regulator of podocin has not been implicated in the canonical nor non-canonical Wnt signaling pathway in neither healthy and disease podocytes.

2.6 Next generation sequencing (NGS) technologies

The regulatory relationships between TFs and their target genes within a gene regulatory network and the associated cell-type specific gene expression are very difficult to entangle in a heterogeneous cell population and even more challenging in a heterogeneous disease like FSGS. Genome-wide sequencing is an indispensable tool to investigate gene regulation. The identification of specific binding sites for transcription factors (TFs) of interest and the mapping of the epigenetic landscape yield novel insights into the intricate and spatially dynamic regulation of podocytes in FSGS. Technical advancement in bulk sampling and single-cell technologies provide more robust methods to overcome technical challenges previously encountered in various types of samples, enabling one to uncover novel and key biological pathways underlying the intertwining transcriptional network.

2.6.1 Assay for Transposase-Accessible Chromatin using sequencing (ATAC-seq)

The assay for Transposase-Accessible Chromatin using sequencing (ATAC-seq) is a molecular biology tool pioneered by Buenrostro in 2013 [154], and is now largely favored as an alternative method for MNase-seq [155], DNase-seq [156] and FAIRE-seq [157]. It is widely used to assess genome-wide DNA accessibility from different cells and tissues. ATAC-seq exploits a hyperactive mutant transposase 5 (Tn5) that has a high affinity for open chromatin and is engineered with barcoded sequencing adapters. Upon activation by magnesium, Tn5 inserts loaded adapters into open regions of the genomes and thus fragments DNA that are later amplified by PCR for sequencing in one single step. Omni-ATAC-seq is an improved method of ATAC-seq for low input and frozen tissue [158]. Compared to other sequencing techniques, ATAC-seq benefits from low input, high sensitivity, ease of library preparation and adaptivity for bulk processing. Unsurprisingly in 2015, single cell ATAC-seq was developed where ATAC-seq was integrated with microfluidic devices to capture single nuclei aimed to map the accessible genome of individual cells to investigate the *regulome* within a heterogenous cell population [159].

2.6.2 Cleavage Under Targets & Tagmentation (CUT&Tag)

The conventional and gold standard technique of profiling genome-wide chromatin binding profiles of protein of interest has been Chromatin Immunoprecipitation sequencing (ChIP-seq) which required a large amount of input material (millions of cells) and tedious optimization of cell fixation, sonication and antibody validation. Alternative approaches to study DNA-protein interaction including FARP-ChIP, ChIPmentation and TAF-ChIP aimed to overcome the limitations of ChIP-seq by lowering the prerequisite for input material and by improving signal-to-noise of datasets but may remain challenging to perform. In 2017, the Henikoff lab introduced an improved modification of Laemmli's Chromatin Immunocleaveage (ChIC) method called CUT&RUN which targeted a fusion protein containing Micrococcal Nuclease (MNase) and Protein A (pA-MNase) to antibodies bound to the chromatin in bead-immobilized nuclei or permeabilized cells [160]. This technique is further refined into Cleavage Under Targets & Tagmentation (CUT&Tag) by exploiting the properties of the hyperactive mutant Tn5 transposase to insert barcoded sequencing adapters and to streamline the library preparation process [161]. The most attractive features of CUT&Tag include adaptability to single cell platforms, and faithful reproducibility of data compared to ChIP-seq yet fewer input materials for profiling histone modifications [161]. Though antibody validation remains strictly restricted to ChIP-seq standards, CUT&RUN and CUT&Tag are robust methods for profiling transcription factors and histone markers binding profiles *in situ* and can be a highly attractive method used to study rare cell type populations and to apply on precious tissues [96].

2.6.3 Single cell technologies

Techniques for genome-wide profiling of cell state have been undergoing rapid development toward acquiring high coverage data from bulk samples, but single-cell genomic, epigenomic, and transcriptomic methods have revolutionized the rapidly evolving field of genome analysis by overcoming the need to extract and purify for single populations of cells. Single-cell technology can capture complex heterogeneity of samples at a single-cell resolution and profile the transcriptomic gene expression of thousands of cells at once. The diversity of sample input accommodates a wide range of sample preparation and conditions and can effectively be used to streamline large-scale analysis of novel or rare cell populations [162]. Single-cell RNA-seq (scRNA-seq) profiles RNA from cells and single-nucleus RNA-seq (snRNA-seq) may be more suitable for frozen and hard-to-dissociate tissues due to sample availability though both techniques enable large-scale cell mapping efforts and capture meaningful biological function such as individual cell state and structure [163]. Systematic and comprehensive benchmarking between scRNA-seq and snRNA-seq show little difference in sensitivity and reproducibilities but snRNA-seq vastly increased the datasets of patient-derived samples [164, 165].

In recent years, single-cell-based datasets of the kidney in mice and humans have expanded and vastly advanced the understanding of kidney pathogenesis. scRNA-seq and multiomic analysis of cultured kidney organoids [166, 167, 145, 168] can be directly compared to human fetal kidney [169] are used to investigate kidney development and cell type specification and patterning [170]. Additionally, the analysis using a murine model with cell type-specific gene deletion [84] or injury model [171] lead to in-depth knowledge of gene regulation in various nephropathy [172]. Single-cell ATAC-seq (scATAC-seq) is also widely used to profile open chromatin and the analysis using scATAC-seq in the kidney [173, 174]. Multiome allows for the combination of scATAC-seq with scRNA-seq for the profiling of cell state and RNA expression from the same cell in developing [174], adult [175] or disease kidney [176] and this provided novel insight in the expression of quantitative trait loci (eQTLs) [177]. Bulk and single-cell datasets of patients with kidney diseases can also

be accessed through various biobanks, including the KPMP consortium [178, 179]. Patient-derived primary organoids may lead to promising therapeutics in personalized modeling [180].

Single-cell CUT&Tag (scCUT&Tag) is a novel technique that will further expand the power of genome-wide profiling of cellular epigenome at single-cell resolution [161]. Several more advanced methods of scCUT&Tag utilize the power of nanobody [181, 182] or different barcoding to multiplex several histone markers or TFs of interest to minimize sequencing cost [183]. Presently, there are no kidney or glomerular scCUT&Tag from mice or humans publicly available. Future efforts in the application of scCUT&Tag and the investigation of DNA regulatory genome and TF binding coupled to snRNA-seq in human FSGS will become an exciting field of personalized therapeutic research.

3 Research Aims

Little is known about the regulatory processes governed by gene expression, epigenetic mechanisms and cell type-specific transcription factors in podocytes undergoing damage. This thesis attempts to bridge the gap in knowledge using next-generation bulk and single-cell sequencing, transgenetic mouse models and cellular assay to investigate the multifarious regulation of transcription in podocyte injury in FSGS. Previously, the methods used to quantify podocyte damage often relied on histology without clear knowledge of the underlying molecular pathways involved in glomeruli damage. Transcriptomics can reveal unique gene expression damage-related and temporal-dependent responsive changes but rare cell types within complex tissue, such as podocytes, suffer from poor capture rates and insufficient resolution in order to derive meaningful insights on biological pathways. Furthermore, the understanding of molecular pathway changes based on transcriptomic alone is limited without integration with other layers of transcriptional control such as regulation via epigenetics. The lack of comprehensive cell type-specific experimental data that describe the epigenetic landscape in health and disease hinders further speculation on how various DNA regulatory elements, chromatin modifiers and TFs cooperatively regulate transcriptional changes in podocyte damage. LXM1B is an established TF that is essential for podocyte differentiation and maintenance, but its molecular mechanism of function has not been elucidated in podocytes. The purpose of this thesis is to understand the multifaceted regulation at the transcription level in podocytes in health and disease. The podocyte damage score (PDS) developed in Chapter 1 aimed to unravel the disease-specific changes in cellular signaling pathways and TF activities aligned by temporal dynamics at single-cell resolution. Chapter 2 outlines the epigenetic map of the glomerulus to identify genome-wide DNA cis-regulatory elements that regulate key genes and signaling pathways that are crucial for the maintenance of podocyte function. Finally, the experiments presented in Chapter 3 aim to characterize the regulatory function of LMX1B and to study its molecular mechanism of action via phase separation.

4 Materials

4.1 Chemicals and reagents

Table 2: List of chemicals and reagents used

Item	Company	Catalog number
Tris-HCl	Thermo Fischer Scientific	J22638.AP
Sodium dodecyl sulfate	Carl Roth	CN30.3
EDTA	Thermo Fischer Scientific	AM9260G
Sodium chloride	Carl Roth	3957.1
Potassium choride	Merck	1.04936.0500
Sodium phosphate dibasic heptahydrate	Carl Roth	X987.2
Monopotassium phosphate	Carl Roth	3904.1
Sodium bicarbonate	Carl Roth	6885.1
D-Glucose	Sigma-Aldrich	G7021-1KG
Calcium chloride dihydrate	Carl Roth	HN04.2
Magnesium chloride hexahydrate	Carl Roth	2189.2
Magnesium sulfate heptahydrate	Sigma	230391
Protease inhibitor without EDTA	Sigma	5056489001
Sodium butyrate	Sigma-Aldrich	19-137
Murine RNase inhibitor	NEB	M0314L
UltraPure Water	Thermo Fischer Scientific	10977035
HEPES	Carl Roth	9105.3
Manganese chloride	Carl Roth	T881.3
Spermidine	Sigma-Aldrich	S0266
Digitonin	Fluka	37006
Dimethyl sulfoxide	Sigma	D2650
BSA	Carl Roth	3737.1
Concanavalin A beads	Polysciences	86057-3
40% acrylamide	BioRad	161-0140
VA-044 initiatior	Wako	017-19362
Boric Acid	Sigma	B0252
D-fructose	Sigma	F0127
1-Thiglycerol	Sigma	M1753
Sodium deoxycholate	Applichem	A1531,0100
Polyethylenglykol 8000	Carl Roth	0263.1
Wnt5b	R&D Systems	3006-WN

4.2 Kits and Assays

Kit and assay	Company	Catalog number
REDTaq ReadyMix PCR-Reaction Mix	Sigma-Aldrich	R2523
GoTaq Flexi DNA Polymerase	Promega	M7808
Nuclei EZ Prep	Sigma-Aldrich	NUC101-1KT
DNA Clean&Concentrator-5	Zymo Research	D4013
ChIP DNA Clean & Concentrator	Zymo Research	D5205
Q5 High-Fidelity DNA Polymerase	NEB	M0491L
NucleoSpin Gel and PCR Clean-up	Macherey-Nagel	740609.50
NucleoSpin Plasmid, Mini kit	Macherey-Nagel	740588.50
NucleoBond Xtra Midi kit	Macherey-Nagel	740410.50
Creatinine (urinary) colorimetric assay kit	Cayman Chemical	500701

4.3 Antibodies

Antibody	Company	Catalog number	LOT number
H3K27ac	Active Motif	39133	28518012
H3K4me1	Epicypher	13-0040	20178005-44
H3K27me3	Cell Signaling Technology	9733S	14
H3K4me3	Diagenode	C15410003-50	A5051-001P
Normal rabbit IgG	Cell Signaling Technology	2729	1
Guinea pig anti-rabbit IgG	Antibodies-Online	ABIN101961	NE-200-022001
Lmx1b	Proteintech	18278-1-AP	00009655
Nephrin	Fitzgerald	20R-NP002	P21022412
Podocin	Sigma	P0372	NA
Acetylated Tubulin	Sigma	T6793	0000174802

4.4 Enzymes

Enzymes	Company	Catalog number
Proteinase K	Thermo Fischer	10181030
Protease	Sigma	P5147
Collagenase IV	Worthington	LS004186
DNase	Worthington	9003-98-9
pAG-Tn5	Epicypher	15-1017
SalI-HF	NEB	R3138L
HindIII	NEB	R0104L
MluI-HF	NEB	R3198L
NotI	NEB	R0189L
T5 Exonuclease	NEB	M0663L
Phusion High-Fidelity DNA Polymerase	NEB	M0530L
Taq DNA Ligase	NEB	M0208L

4.5 Oligonucleotides for genotyping

Table 3: Oligonucleotides used for genotyping

Purpose	Strand	Sequence (5' to 3')
Beta-globin	forward	TGC TCA CAC AGG ATA GAG AGG GCA GG
	reverse	GGC TGT CCA AGT GAT TCA GGC CAT CG
Cre	foward	ACC CGA CGG TCT TTA GGG
	reverse	GCA AAC GGA CAG AAG CAT TT
Rosa26	forward	CTC TGC TGC CTC CTG GCT TCT
	reverse	CGA GGC GGA TCA CAA GCA ATA
	reverse	TCA ATG GGC GGG GGT CGT T
Wt1	forward	GTG ACC CCG CAG CTA GCC
	reverse	GGA GCG TTC ATC TCG GAG AC
	reverse	CCA TTT GTC ACG TCC TGC
LMX1B flox	forward	AGG CTC CAT CCA TTC TTC TC
	reverse	CCA CAA TAA GCA AGA GGC AC
Cre:ERT2	forward	TCA ACA TGC TGC ACA GGA GAT
	reverse	ACC ATA GAT CAG GCG GTG GGT
	forward	CCT GAC AGT GAC GGT CCA AAG
	reverse	CAT GAC TCT TCA ACT CAA ACT
Podocin flox	forward	CCA GCA TCC CAT TAG ATA GAT GAG G
	reverse	GCA TCC AAA TGA TCA GAG TTC CCA GG
R231Q	forward	GCC CGG CTC TAT GCT ATA AT
	reverse	ACT GAC TGA CTG ATT CCC CA
	forward	CGC CTC TTG GCA CAT CG
	reverse	CAG GAG AAT TTC AGT CAA GCT TT
A286V	forward	CAC TCC AAT TGC CCT CTT CTG
	reverse	ACA CTA TCA ACA GCG GTG GA
A286V-sequencing	reverse	CAG CCG GAT TCC GTT CAG T

4.6 Oligonucleotides for cloning

Cloning into pEGFP-N1:

Name	Strand	Sequence (5' to 3')
Lmx1b-201	forward	TCA GAT CTC GAG CTC AAG CTG CCA CCA TGG ATA TAG CAA CAG GTC CCG AGT C
	reverse	CGA CTG CAG AAT TCG AAG CTT GGA GGC AAA GTA GGA GCT CT

Cloning into pEGFP-C1:

Name	Strand	Sequence (5' to 3')
Lmx1b-201	forward	GCT TCG AAT TCT GCA GTC GAC ATG GAT ATA GCA ACA GGT CC
	reverse	CGG GCC CGC GGT ACC GTC GAT CAG GAG GCA AAG TAG GAG C
delta180-221	forward	ACT ATG AGA AGG AGA AAC CGA GAA GGC CCA AAC GGC CCC G
	reverse	CGG GGC CGT TTG GGC CTT CTC GGT TTC TCC TTC TCA TAG T
delta288-401	reverse	CGG GCC CGC GGT ACC GTC GAT CAG TGT CTC CGG GCC AGC T

4.7 Equipment

Item	Company	Catalog number
PCR cycler	BioRad	S1000
Nanodrop spectrophotometer	PeqLab	1000
DNA loBind 1.5ml microtubes	Eppendorf	0030 108.051
Qubit 4 Fluorometer and dsDNA kit	Thermo Fisher Scientific	Q32854
Tapestation and D1000 High sensitivity	Agilent	5067- 5584/5067- 5585
CellTrics 30 µm, sterile	Sysmex	04-004-2326
CellTrics 10 µm, sterile	Sysmex	04-004-2324
100 µm cell strainers	Sarstedt	83.3945.100

5 Methods

5.1 Animal work

5.1.1 Animal husbandry and mouse models

Mice were housed and maintained in CECAD *in vivo* Research Facility. All mice were kept under a 12 h light/dark cycle and had *ad libitum* access to food and water. All mouse experiments were performed with approval from The Animal Care Committee of the University of Cologne and LANUV NRW (Landesamt für Natur, Umwelt und Verbraucherschutz Nordrhein-Westfalen, State Agency for Nature, Environment and Consumer Protection North Rhine-Westphalia) for this study. Mice were kept on a C57BL6 background except for Wt1.hetdel mice, which were kept on a FVB/N background. Mice were crossed to cell type-specific Cre lines to generate cell type-specific expression of nuclear GFP reporter.

Mouse line	Purpose	Reference
$Rosa26^{nTnG}$	Visualization of nuclear fluorescent reporter	[184]
$Rosa26^{mTmG}$	Visualization of membrane fluorescent reporter	[185]
$Podocin^{R231Q/A286V}$	Compound heterozygous mutation of NPHS2	[14]
$Phb2^{flox}$	Deletion of PHB2	[186]
$Lmx1b^{flox}$	Deletion of LMX1B	[187]
Wt1.hetdel	Heterozygous deletion of WT1	[188]
Nphs2:cre	Podocyte-specific Cre driver	[189]
Tie2:cre	Endothelial cell-specific Cre driver	[190]
Nphs2:CreERT2	Tamoxifen-inducible podocyte-specific Cre driver	[191]

Table 4: Mouse lines used in the study.

5.1.2 Tamoxifen induction

$Lmx1b^{flox}$ were crossed with $Rosa26^{mTmG}$ and Cre:ERT2 to inducibly express podocyte-specific membrane GFP reporter. For tamoxifen induction, mice are fed ad libitum with a tamoxifen diet for an indicated number of days prior to sacrifice and organ harvest.

5.1.3 Genotyping PCR

DNA from mouse ear tags were extracted by boiling tissues at 95 ℃ for 30 min in base solution (0.025N NaOH, 0.2 mM EDTA), cooled on ice and adding an equal volume of neutralization solution (52 mM Tris-HCl) [192]. Genotyping PCR reactions were performed accordingly (Table 7) and the PCR products were analyzed using a 2% agarose gel. For the $Podocin^{A286V}$ allele, the PCR product was cleaned by enzymatic purification by incubating with 0.25 unit of SAP and 0.5 unit of ExoI for 20 min at 37 ℃ followed by an inactivation step for 15 min at 72 ℃. The resulting product was used for Sanger sequencing.

5.1.4 Glomeruli and nuclei isolation

Glomeruli isolation was performed as described in [193]. Mice were sacrificed by cervical dislocation and kidneys were extracted and perfused *ex vivo* through the renal arteries with magnetic Dynabeads suspension

in HBSS (5.4 mM KCl, 0.3 mM Na_2HPO_4, 0.4 mM KH_2PO_4, 4.2 mM $NaHCO_3$, 137 mM NaCl, 5.6 mM D-glucose, 1.3 mM $CaCl_2$, 0.5 mM $MgCl_2$, 0.6mM $MgSO_4$). Perfused kidneys were minced by scalpel and digested with digestion buffer (1 mg/ mL Pronase E, 1 mg/ mL collagenase type II and 50 unit/ mL DNase I in HBSS) for 15 min at 37 ℃. The kidney suspension was triturated until homogenous and filtered twice through 100 µm cell strainers. The kidney lysates were washed with HBSS and pelleted at 1500 rpm for 5 min at 4 ℃. The pellet was resuspended in HBSS and washed on the magnet until isolated glomeruli were obtained.

Isolated glomeruli were resuspended in 1 mL of lysis buffer (Sigma EZ lysis buffer supplemented with EDTA-free protease inhibitors) and placed on a Thermoshaker at 1400 rpm for 10 min at 4 ℃. After magnetization, the supernatant containing loose nuclei was collected through a 30 µm cell strainer. The leftover beads were resuspended in 1 mL lysis buffer and titurated 10 times. The sample was incubated shaking at 1400 rpm for 5 min and tituration was repeated. After magnetization, the loose nuclei were collected through a 30 µm filter and the leftover beads were resuspended in 1 mL lysis buffer and further lysed through 27G needle 5 times. After the loose nuclei were collected, the beads were resuspended in 1 mL of lysis buffer and further lysed through 30G needle 5 or 10 times to collect the final aliquots of loose glomerular nuclei. The pooled nuclei were centrifuged at 500 g for 5 min at 4 °C. The pellet was resuspended in 300 µL of lysis buffer, transferred to a 1.5 mL Eppi, and placed on the magnet for 3 minutes to remove residual magnetic beads.

5.1.5 Flow assisted cytometry sorting (FACS)

FACS sorting of nuclei was supported by the Max Planck Institute of Aging, FACS & Imaging Facility using the BD FACSAria IIIu or the BD FACSAria Fusion flow cytometers equipped with the 70 µm nozzle with chillers. Isolated glomerular nuclei were stained with DAPI and singlet and DAPI+ nuclei were gated by forward scatter and side scatter and the UV1 laser. DAPI+ nuclei were then sorted by fluorescent signal and GFP+ or tdTomato+ nuclei were collected into lysis buffer.

Nuclei isolated from wildtype mice carrying no $Rosa^{nTnG}$ allele were DAPI+ but GFP- and tdTomato-. Isolated nuclei from $Rosa^{nTnG/wt}$ or $Rosa^{nTnG/nTnG}$ mice are exclusively tdTomato+, while nuclei isolated from Cre transgenic mice (Pod:cre or Tie2:cre) show respective cell-type specific GFP signal.

5.1.6 Coomassie urinary analysis

Urine from mice was collected and 2 µL was combined with 4 µL of water and 6 µL of 2X Lammli buffer supplemented with DTT. The lysate was boiled at 95 ℃ for 5 min and loaded onto 10% polyacrylamide gel. The SDS-PAGE was run at 200V until the dye front had run off. The gel was fixed in fixation buffer (25% v/v Isopropanol, 10% v/v acetic acid) for 30 min and stained with Coomassie buffer (1% w/v Coomassie brilliant blue G-250, 3% w/v ortho-phosphoric acid, 20% v/v methanol, 10% w/v ammonium sulfate) overnight. The gel was destained with water overnight prior to imaging using Odyssey CLx.

5.1.7 Albumin and creatinine ELISA

Urines from mice were first analyzed by coomassie urinary analysis to approximate the dilution for albumin ELISA (usually ranging between 1:100 to 1:100,000). All steps were carried out at room temperature. First, wells were coated for 1 h with 100 µL of anti-mouse albumin coating antibody at 1:10,000 in coating buffer (0.05 M carbonate-bicarbonate, pH 9.6), then washed 5 times with 200 µL of wash solution (50 mM Tris,

0.14 M NaCl, 0.05% Tween-20, pH 8.0) before incubating for 30 min with 200 µL of blocking solution (50 mM Tris, 0.14M NaCl, 1% BSA, pH 8.0). The wells were washed again 5 times with 200 µL of wash solution before incubation for 1 h with 100 µL of standards or samples diluted in diluent buffer (50 mM Tris, 0.14 M NaCl, 0.05% w/v Tween-20, 1% w/v BSA, pH 8.0). Next, the wells were washed 5 times with 200 µL of wash solution before incubation with 100 µL of HRP detection antibody diluted 1:25,000 in the diluent buffer for 1 h. Finally, the wells were washed 5 times with 200 µL of wash solution and developed with 100 µL of substrate solution (100 µg/ mL TMB, 48 mM sodium acetate, 0.01% v/v hydrogen peroxide, pH 5.2) for 15 min in the dark. The reaction was stopped by adding 100 µL of stop solution (0.18 M sulfuric acid) and the absorbance was measured at 450 nm. For the creatinine urinary colorimetric ELISA, urines were diluted 1:20 in water and assayed according to the manufacturer's protocol. All samples were measured in triplicates.

5.1.8 PAS staining

Kidneys were fixed in 4% formalin overnight at 4 ℃ and stored in cold PBS until dehydration and embedding in paraffin. Tissues were cut into 2 µm sections onto a glass slide using the microtome and slides were incubated at 60 ℃ for 2 h. The slides were incubated sequentially twice for 5 min in xylol, thrice for 3 min in 100% ethanol, twice for 2 min in 97% ethanol, once for 1 min in 70% ethanol, and twice for 2 min in water. The slides were stained in 0.9% periodic acid for 10 min and the excess was rinsed off in water for 1 min. The slides were then stained in undiluted Schiff's reagent for 10 min and rinsed in tap water for 2 min. Then, the slides were stained in undilute Mayer's hemotoxylin for 10 min, and rinsed in water water for 8 min. Finally, the slides were incubated sequentially once in 70% ethanol, twice in 97% ethanol, thrice in 100% ethanol, and twice in xylol for 2 min each. The slides were embedded with histomount and scanned with Leica Slidescanner.

5.1.9 STED microscopy

Kidney tissues were fixed in formalin for 4 h at room temperature and stored in cold PBS. The kidney cortex was cut into 1-2 mm pieces and immersed in hydrogel solution (4% acrylamide, 0.25% VA-044 initiator in PBS) at 4 ℃ for 12-16 h. The gel was polymerized by incubation at 50 ℃ for 3 h. The excess polymer was removed and tissues were washed in PBS three times before embedding in 3% agarose prior to cutting into 200 µm sections using a vibratome. Samples were transfered to a clearing solution (200mM boric acid, 4% SDS, pH 8.5) and incubated at 50 ℃ until cleared. Samples were washed briefly in wash buffer (10 mM HEPES, 200 mM NaCl, 3% Triton X-100) before incubation with primary antibodies at 37 ℃ overnight. Samples were washed with wash buffer before incubation with secondary antibodies at 37 ℃ overnight and embedded in saturated fructose solution (80.2% w/w fructose, 0.5% *alpha*-thioglycerol) before mounting in a glass-bottom dish for imaging using the Leica SP8 STED microscope. Quantification of slit diaphragm length was performed using Fiji as described in [14].

5.2 DNA preparation

5.2.1 ATAC-seq and omniATAC-seq

ATAC-seq was performed as described in [154]. Briefly, 50,000 GFP+ or tdTomato+ nuclei were sorted by FACS into lysis buffer and centrifuged at 1000 g for 10 min at 4 ℃. The pellet was resuspended in 50 µL of transposition reaction mix (25 µL of transposition buffer, 2.5 µL of TDE1, and 22.5 µL of nuclease-free

water). The reaction was carried out at 37 ℃ for 30 min. Immediately following transposition, DNA was purified using Zymo DNA clean concentrator-5 per the manufacturer's instructions. The transposed DNA was eluted in 10 µL of elution buffer.

For Podocin$^{RQ/AV}$ and Phb2^{flox} cre transgenic mice where fewer podocytes were recoverable by FACS after glomeruli and nuclei isolation, omniATAC-seq was performed instead of ATAC-seq as described in [158]. Briefly, 10,000 or 5,000 GPF+ or tdTomato+ nuclei were collected by FACS, centrifuged at 1000 g for 10 min at 4 ℃ and the pellet was resuspended in 10 µL or 5 µL of transposition reaction mix respectively (25 µL of transposition buffer, 2.5 µL of TDE1, 16.5 µL PBS, 0.5 µL 1% digitonin, 0.5 µL 10% Tween-20 and 5 µL nuclease-free water). The reaction was carried out at 37 ℃ for 30 min shaking at 1000 rpm on the Thermoshaker. Immediately following incubation, transposed DNA was purified using Zymo DNA clean concentrator-5 per manufacturer's instructions and eluted in 10 µL of elution buffer.

5.2.2 Cut&Tag

Cut&Tag experiments were performed as described in [161]. Briefly, glomerular nuclei were FACS sorted into lysis buffer and conjugated with 5-10 µL of activated Concanavalin A beads per sample. The primary antibody was incubated with the nuclei-bead complex at 1:50 dilution overnight at 4 ℃ in Wash150A buffer (WASH150 buffer, 0.1% BSA, 2 mM EDTA). Incubation of the secondary antibody was performed for 30 min at room temperature using the guinea pig anti-rabbit antibody at 1:100 dilution in Wash150 buffer (20 mM HEPES, pH 7.5, 150 mM NaCl, 0.5 mM spermidine, 0.05% digitonin, 5 mM sodium butyrate, supplemented with protease inhibitors). The pAG-Tn5 adapter complex was used in 1:20 dilution in Wash300 buffer (20 mM HEPES, pH 7.5, 300 mM NaCl, 0.5 mM spermidine, 0.01% digitonin, 5 mM sodium butyrate, supplemented with protease inhibitors) and incubated with the samples for 1 h at room temperature. The transposition reaction proceeded for 1 h at 37 ℃ in tagmentation buffer (20 mM HEPES, pH 7.5, 300 mM NaCl, 10 mM MgCl2, 0.5 mM spermidine, 0.01% digitonin, 5 mM sodium butyrate, supplemented with protease inhibitors), and the reaction was stopped by the addition of SDS, EDTA and Proteinase K and incubated for 1 h at 55 ℃. The transposed DNA was purified using the Zymo ChIP DNA clean and concentrator kit according to the manufacturer's instructions or by phenol-chloroform extraction and eluted in 21 µL of elution buffer.

To determine the cycle number for library preparation, one parallel CUT&Tag reaction was performed and 5 µL eluted DNA was combined with 1 µL of 10 µM Ad1.1 primer, 1 µL of 10 µM Ad2.x primer, 1.25 µL of 10X SYBR Green, 12.5 µL of 2X NEBNEXT HiFi PCR mastermix and 4.25 µL of nuclease-free water. The library was amplified using QuantStudio 5 Real-Time PCR System for 5 min at 72 ℃, 30 s at 98 ℃, cycled 39 times at 10 s at 98 ℃ and 10sec at 63 ℃, before final extension at 1 min at 72 ℃.

5.2.3 Phenol chloroform extraction

One volume of phenol-chloroform isoamyl alcohol was added to the sample, vortex, and loaded onto a pre-packed phase lock gel tube before centrifugation at 16,000 g for 5 min. One volume of chloroform was added to the phase lock gel tube and inverted 10 times before centrifugation at 16,000 g for 5 min. The supernatant was added to an equal volume of 100% ethanol and DNA was precipitated at -80 ℃ for at least 15 min. After centrifugation at 16,000 g for 10 min at 4 ℃, the pellet was rinsed with 1 mL of 100% ethanol before re-centrifugation at 16,000 g for 10 min at 4 ℃. The pellet was air-dried before resuspension in elution buffer.

5.3 Single cell technologies

5.3.1 Single nuclei RNA-seq and multiome

Glomeruli were isolated from mice kidneys and subjected to isolation of nuclei using Sigma EZ lysis buffer supplemented with EDTA-free protease inhibitors and 0.1% murine RNase inhibitor. Isolated nuclei were washed twice in lysis buffer and counted with a hemocytometer. After centrifugation at 1000g for 10 min, nuclei were resuspended in PBS supplemented with 2% BSA to reach an approximate concentration of 1000 nuclei/ µL. Prior to immediate processing, the samples were further filtered through a 10 µm cell strainer. For multiome, nuclei were resuspended to approximately 3000 nuclei/ µL in 1X Nuclei Buffer from Illumina supplemented with protease and RNAse inhibitors.

5.3.2 Library preparation and sequencing

Library preparation and DNA sequencing of ATAC-seq, omniATAC-seq, Cut&Tag, and all single nuclei technologies were performed by the Cologne Centre of Genomics (CCG). 12 cycles of PCR amplification were used for ATAC-seq samples. Cycle numbers of PCR amplification used for Cut&Tag samples were determined by qPCR as described above. For snRNA-seq, libraries and sequencings were prepared per the manufacturer's instructions supported by 10X Genomics.

5.4 Molecular cell biology

5.4.1 Cloning

pEGFP-C1 was linearized by SalI-HF and pEGFP-N1 by HindIII respectively at 37 ℃ for 10 h before gel purification on 1% agarose gel using NucleoSpin Gel and PCR Cleanup kit according to manufacturer's protocol. Inserts were PCR amplified using Q5 polymerase from the mouse cDNA library and cloned into linearized pEGFP-C1 or pEGFP-N1 using Gibson assembly. Ligated DNA products were transformed into DH10 competent cells and grown on appropriate antibiotic plates overnight at 37 ℃. Single colonies were picked into 3 mL of LB supplemented with antibiotics and grown to saturation overnight. Minipreps were prepared using a Nucleospin Plasmid EasyPure kit according to the manufacturer's protocol. The sequence of the inserts was confirmed by Sanger sequencing, then plasmids were prepared and purified by NucleoBond Xtra Midi kit according to the manufacturer's protocol.

5.5 Cell culture work

5.5.1 Cell culture and transfection

HEK293T cells were cultured in monolayers and maintained at 37 ℃ and 5% CO_2 in DMEM media with GlutaMAX supplemented with 10% fetal bovine serum (FBS). Cells were passaged by washing them once with sterile PBS and adding 1 mL trypsin for 5 min at 37µntil detached. Diluted cells were transferred into a fresh culture dish with the pre-warmed medium.

Plasmids were transfected into HEK293T cells using calcium phosphate transfection. 3 µg of DNA was added to 0.25 M calcium chloride and complexed with an equal volume of 2X HEBS buffer by thorough vortexing, then added dropwise to cells for 6-8 h. The next day, cells were used for live cell imaging.

5.5.2 Fluorescence recovery after photobleaching (FRAP)

HEK293T cells were grown on glass bottom 35 mm dishes and transfected with appropriate plasmids prior to live cell imaging using the Leica SP8 STED microscope. 5 frames of images were acquired prior to photobleaching of fluorescent signals at the region of interest (ROI) within the cell and imaged at 1.3 s interval for at least 30 frames for potential signal recovery within the ROI. Images were analyzed using Fiji.

5.6 Bioinformatics

5.6.1 Multiome analysis

For snRNA-seq, the Seurat R package was used to perform filtering, normalization, dimensionality reduction, clustering, and differential expression analysis. The "FindClusters" function was performed to generate different clustering results. Differential gene analysis was performed by the "FindAllMarkers" function and DEGs were identified with Bonferroni-adjusted P values as described in figure legends. For snATAC-seq, the Signac R package was used to perform subsequent analysis. The accessible chromatin peaks for each cell type were identified using MACS2. Differential chromatin accessibility analysis was performed by the "FindAllMarkers" function. Differentially accessible chromatin regions were identified with Bonferroni-adjusted P values as described in the figure legend. The "FindMotifs" function and the JASPAR database were used to identify motif enrichment of transcription factors. The "RunChromVAR" function was used to compute a per-cell motif activity.

5.6.2 GAGE analysis

GAGE was used to assess the gene set enrichment for pathway analysis [194]. The average log2 fold change of differentially expressed gene sets was derived from tamoxifen-induced 6-day, 10-day and 14-day between sick and healthy podocytes and they were each compared to 6-day control to identify significant signaling pathways within the KEGG database.

5.7 Statistics

Statistical calculations were done using the rstatix package within R. Comparison of two groups was done using a t-test and comparison between more than two groups was done using ANOVA.

6 Results

6.1 Gene regulatory network of podocytes and the development of the Podocyte Damage Score (PDS)

6.1.1 Single nucleus map of mouse glomeruli in FSGS

To investigate disease heterogeneity in FSGS, single nuclei were extracted from isolated glomeruli and snRNA-seq was performed using *Nphs2*$^{R231Q/A286V}$ and *Wt1*.hetdel mice at various stages of the disease. Glomeruli were isolated from wildtype or experimental animals from *Nphs2*$^{R231Q/A286V}$ mice at 4w (n=4), 6w (n=3), 8w (n=3) or 12w (n=4) or from *Wt1*.hetdel mice at 12w (n=4) or 25w (n=2). Heatmaps of the top 10 gene markers of each cluster were generated to identify different cell types within the kidney, and snRNA-seq analysis identified the three major cell types in the glomerulus, podocytes, endothelial cells and mesangial cells based on the expression of lineage-specific markers (Figure 4A and D). Globally, a distinct separation between healthy and disease cells in all disease models was observed (Figure 4C and F).

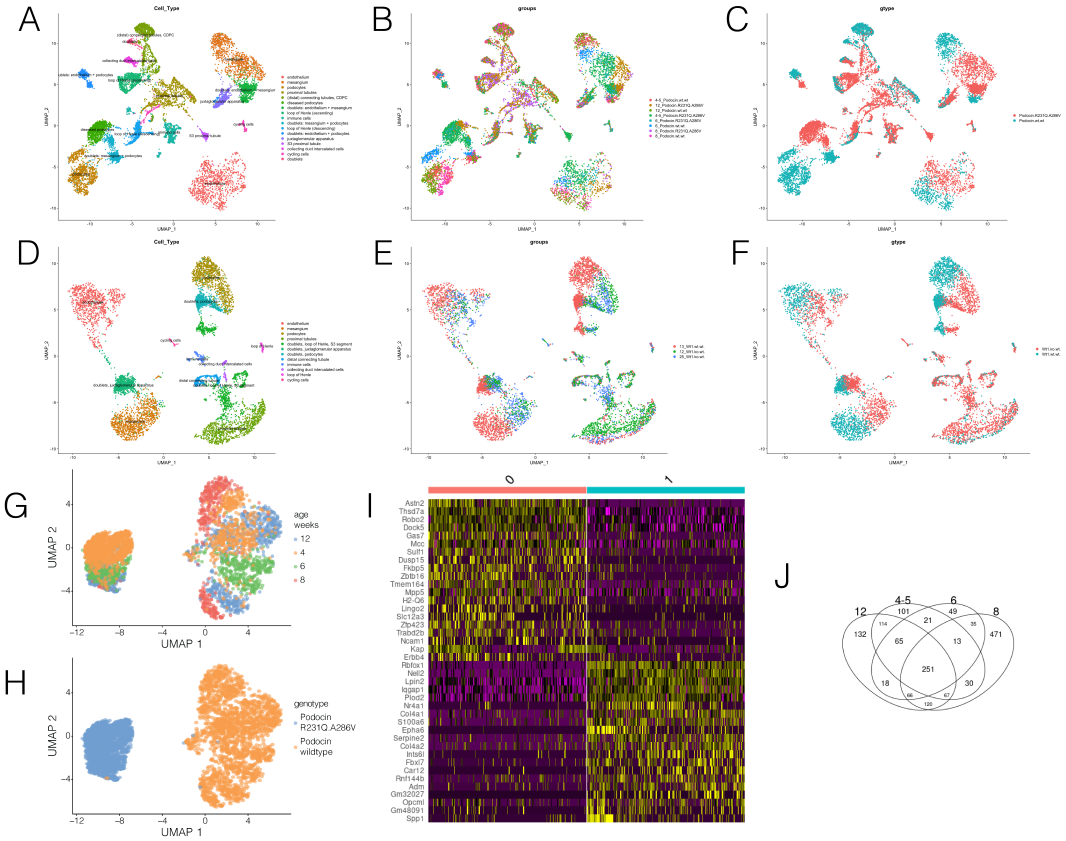

Figure 4: snRNA-seq analysis of FSGS mice revealed a major shift in damage response in all cell types. UMAP showing cells identified in *Nphs2*$^{R231Q/A286V}$ mice by cell type (A), age (B) and genotype (C). UMAP showing cells identified in *Wt1*.hetdel mice by cell type (D), age (E) and genotype (F). There is a clear separation between healthy and damaged cells in all cell types. Subclustering of podocytes in *Nphs2*$^{R231Q/A286V}$ mice show clear distinction by age (G) and by genotype (H) within damaged podocytes. I. Heatmap of top 20 gene clusters of healthy podocytes (cluster 0) and damaged podocytes (cluster 1). J. Differential expression analysis patterns in damaged podocytes show similarily across all four timepoints.

To understand how rare cell types in the kidney, such as podocytes, respond to injury and rewire their gene connectivity and signaling pathways in FSGS. Subclustering of 23,650 podocytes in *Nphs2*$^{R231Q/A286V}$ mice revealed clear separation of podocytes by genotype (Figure 4H) where healthy podocytes showed differential gene expression in known podocyte marker genes including Thsd7a, Sulf1 and Dock5 whereas in damaged podocytes, these genes were downregulated (Figure 4I). There was an age-dependent gene expression change in damaged podocytes from 4w to 12w (Figure 4G) possibly correlating with disease progression yet differential expression analysis between these four timpoints showed large overlap, with 251 commonly significant genes (Figure 4J). To resolve the discrepancy between the lack of gene expression changes in damaged podocytes with podocyte disease progression, we hypothesize that even within damaged podocytes, there were subsets of podocytes where the rewiring and changes in TF and pathway activity correlated with the extent of podocyte damage. Subsequently, we developed a podocyte damage score (PDS) aimed at monitoring the disease trajectory and pathway activity at single-cell resolution and investigating cell type-specific gene regulatory network reconfiguration in FSGS.

6.1.2 Development of the PDS

In order to develop the PDS, approximately 200 publicly available datasets of microarray, bulk and single-cell RNA-seq of different models of podocyte damage, including diabetic nephropathy, FSGS and toxin-induced injury were pooled and considered for the development of the PDS. To maximize the biological representation of podocytes, these studies were filtered by cell types where only FACS-sorted podocytes, whole glomeruli bulk and single-cell RNA-seq from kidneys were retained for further analysis but whole kidney and cultured podocytes studies were removed from consideration due to poor capture of the podocyte population or poor recapitulation of the function of podocytes in cell culture. Approximately 40 datasets were further examined and datasets with confounding phenotypic presentation of podocyte dysfunction were removed. Combined with several in-house generated bulk and single-cell RNA-seq (as shown above), 37 datasets eventually contributed to the development of the PDS (Table 5). The differential expression analysis was performed to identify gene signatures of podocyte damage for each dataset. Genes were more specifically selected if they fulfill the criteria that they are detectable in >75% of the studies and are expressed in the same direction of change between control and disease. Finally, the differential gene expression was ranked by p-value and the top 50 common genes were combined as damage signatures aliased as the PDS (Figure 5). Next, we validated the PDS across different datasets to test its sensitivity in detecting damage in specific cell types, various disease types and along disease progression.

GSE accession	Model group	Type of dataset	Type of cells	Reference
GSE18358	Wt1 KO	MA	glomeruli	[195]
GSE117571	Foxc1/2 KO	MA	glomeruli	[196]
GSE63272	Slit diaphragm	MA	podocytes	[197]
GSE20235	HIV/VHL KO	MA	glomeruli	[198]
GSE106841	diabetes	MA	glomeruli	[199]
GSE108629	toxic damage	MA	podocytes	[200]
GSE112116	diabetes	MA	glomeruli	[91]
GDS3992	diabetes	MA	glomeruli	[201]
GSE17709	PTIP KO	MA	glomeruli	[90]
GSE117987	HIV-mediated damage	bulk	glomeruli	[202]

GSE123179	slit diaphragm	bulk	glomeruli	[203]
GSE126217	glycan metabolism	bulk	glomeruli	[204]
GSE154955	toxic damage	bulk	podocytes	[35]
GSE127235	diabetes	sc	glomeruli	[205]
GSE146912	various	sc	glomeruli	[206]
in-house dataset	slit diaphragm	bulk	glomeruli	
in-house dataset	toxic damage	bulk	glomeruli	
in-house dataset	Wt1 KO	bulk	glomeruli	
in-house dataset	Wt1 KO	sc	podocytes	
GSE119049	light chain deposition	bulk	glomeruli	[207]
GSE131266	diabetes	MA	glomeruli	[208]
GSE138774	actin cytoskeleton	bulk	glomeruli	[209]
GSE134327	diabetes	bulk	glomeruli	[210]
GSE110092	slit diaphragm	bulk	glomeruli	[211]
GSE123853	diabetes	bulk	glomeruli	[212]
GSE104624	focal adhesion	MA	glomeruli	[213]
GSE77717	diabetes	bulk	glomeruli	[214]
GSE84663	diabetes	MA	glomeruli	[215]
GSE79291	diabetes	bulk	glomeruli, podocytes	[216]
GSE85569	diabetes	MA	glomeruli	[217]
GSE56236	immunologic damage	MA	glomeruli	[218]
GSE43061	ageing / DNA damage	MA	glomeruli	[219]
GSE33744	diabetes	MA	glomeruli	[220]
GSE36209	diabetes	MA	podocytes	[221]
GSE136138	ageing	bulk	podocytes	[222]

Table 5: Datasets used for the development of the PDS. MA = microarray, bulk = bulk RNA-seq, sc = scRNA-seq. Published datasets are referenced by GSE accession numbers and datasets without GSE accession numbers (NA) were generated in-house. Datasets are also categorized by cell types that were assayed and classified under different model groups based on disease etiology.

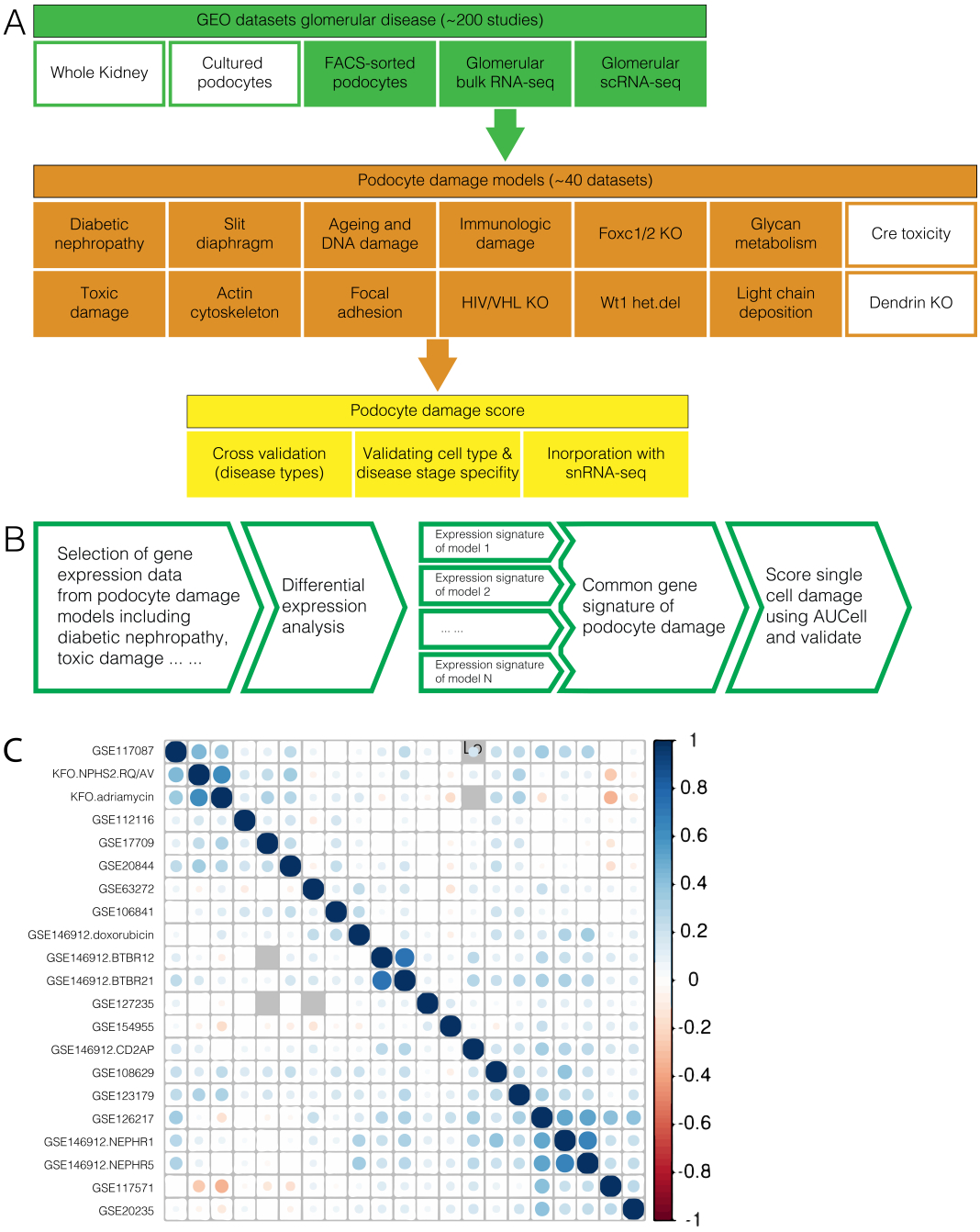

Figure 5: Bioinformatic workflow used in the development of the PDS. A. Selection of publicly available studies and datasets that contribute to the development of the PDS. Approximately 200 studies were filtered by podocyte specificity and only FACS-sorted podocytes, glomerular bulk RNA-seq and glomerular scRNA-seq were collected for further analysis. The models of each dataset were further categorized by the type of podocyte disease and non-representative datasets were excluded. Based on these datasets, the PDS was tested by validating for cell type, disease type, and disease stage specificity using both bulk RNA-seq and snRNA-seq. B. Outline of the selection of genes for AUCell scoring to calculate the PDS. Gene expression data from various disease models and datasets were analyzed by differential analysis, combined, filtered and ranked using AUCell to collect a list of 50 common gene signatures known as the PDS. C. Heatmap of all studies used in the development of the PDS show clustering by the types of disease model.

6.1.3 PDS is podocyte-specific and is applicable to various damage models

Next, we tested the usability of the PDS and validated it for disease-type and cell-type specificity across test datasets. The PDS was first cross-validated by applying to bulk datasets after excluding disease-specific datasets, such as diabetes, slit diaphragm, or toxic damage for control and experimental conditions (Figure 6A). In addition, we tested the PDS for cell-type specificity using independent datasets sourced from Chung et al. where various disease models were characterized using scRNA-seq [206]. Here, we validated PDS using the nephrotoxic serum (NTS) nephritis model where the injection of NTS induced acute inflammatory responses followed by proteinuria that peaked 1 day after treatment, but gradually decreased within 7 days. AUCell score was calculated for all clusters (endothelium, podocytes, mesangium, juxtaglomerular apparatus, tubules and immune cells). The PDS was able to distinguish between control from nephritis conditions most significantly in the podocyte cluster. Importantly, the progression and recovery of podocyte damage was detected between control, day 1 (nephr1) and day 5 (nephr5) NTS nephritis within the podocyte cluster thus emphasizing the power of PDS to monitor disease progression (Figure 6B). We further tested the PDS on podocytes using additional scRNA-seq of other models including doxorubicin and diabetes to show that the PDS was able to differentiate between healthy and diseased podocytes across different disease models (Figure 6C).

Next, we evaluated the robustness of the PDS by randomizing the ranks and the log fold changes (LFCs) within a percentage of studies and re-calculating the PDS score to assess the separation between healthy and disease podocytes on validation datasets. A given percentage of validation studies were randomized in a stepwise fashion (0, 25%, 50%, 70%, 90% and 100%) and the 75% cutoff for inclusion of gene markers criterion was removed to recalculate the PDS. The PDS was applied to single-cell datasets including the nephritis and the doxorubicin models. After one round of randomization, more than 70% of the datasets needed to be randomized before the cell specificity of the PDS on podocytes was affected (Figure 6D). The validation datasets were further randomized for 50 rounds for each percentage of randomness. In every randomization round, the average disease score was re-calculated across control and experimental cells and tested on the nephr1 dataset to show the average disease score of control and experimental cells. More than 80% of the datasets needed to be randomized before the stability of the PDS on podocytes was affected (Figure 6E).

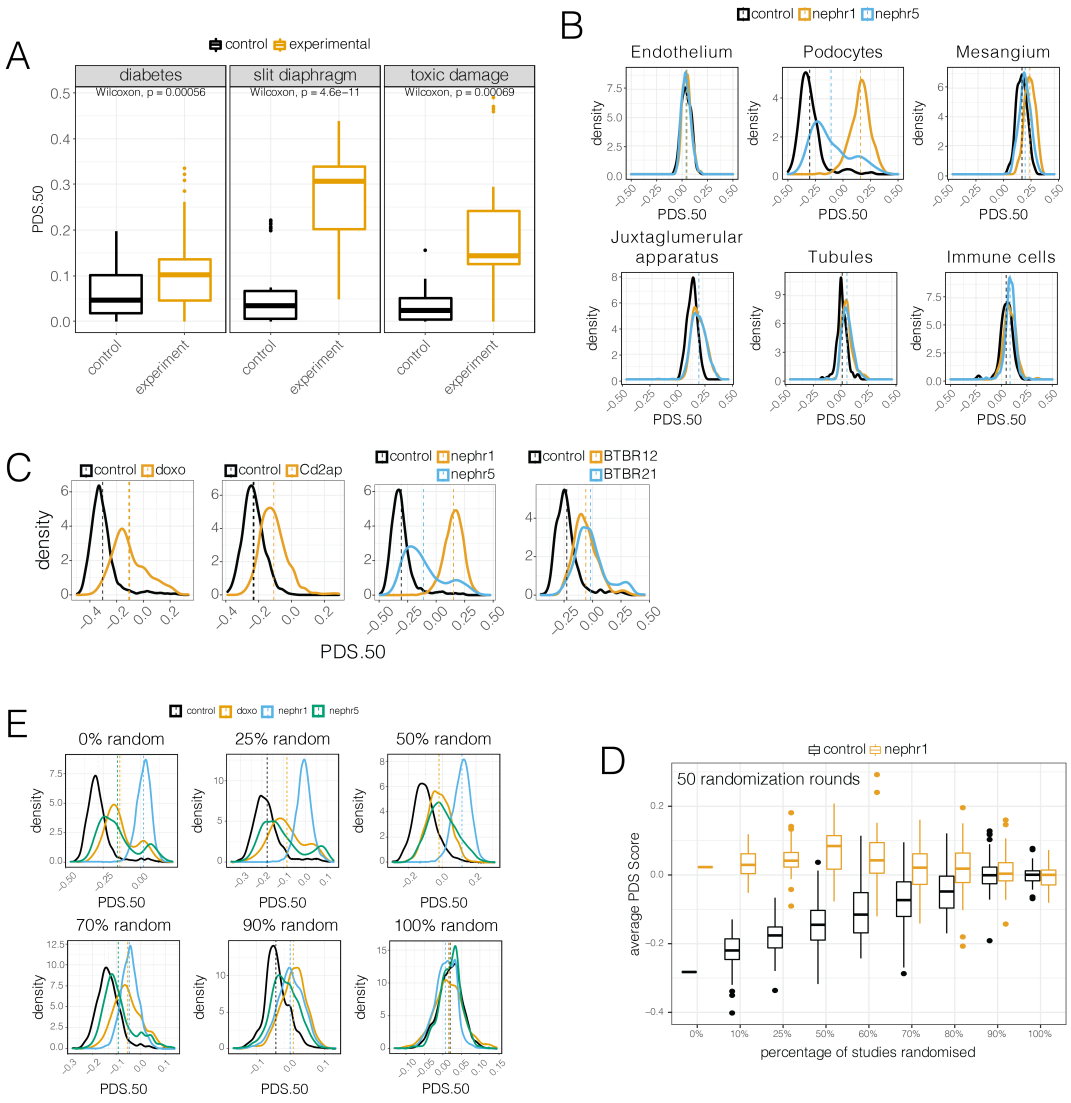

Figure 6: PDS is robust and podocyte-specific. A. Cross-validation of PDS on model-specific bulk RNA-seq datasets. Diabetes, slit diaphragm or toxic damage studies were left out and disease markers were ranked with the remaining damage models. The PDS was re-calculated for the models that were left out and the results were plotted for control and experimental studies on test datasets. B. Validation of PDS on single cell datasets from Chung et al. [206]. AUCell score was calculated for each cluster from the glomerular scRNA-seq for all conditions (control, nephr1 and nephr5). The PDS shows high sensitivity for podocytes and is able to capture disease progression (nephr1) and recovery (nephr5) in the NTS nephritis model. C. The PDS is tested on all single-cell datasets and is able to capture disease progression in all models in podocytes. D. Randomization of the PDS shows that the PDS is cell-type specific. More than 70% of all cells need to be randomized for PDS to lose specificity. E. Even after 50 rounds of randomization of studies, more than 80% of the datasets need to be randomized to affect the stability of PDS.

6.1.4 Verification of PDS marker genes

Furthermore, we verified the expression of PDS marker genes on other levels of cellular regulation to confirm the correlation between gene expression with protein expression. Expectedly, PDS marker genes were detected in most datasets on the transcript level and they clustered in two groups, up- or down-regulated upon podocyte damage (Figure 7). To correlate the changes in the transcriptome to those in the proteome, we

evaluated the expression of the PDS gene signatures using proteomics data collected from *Nphs2*$^{\text{R231Q/A286V}}$ glomeruli at 3w. Proteins that were not detected by mass spectrometry or non-protein coding genes were excluded from analysis. Of all PDS markers genes, 35 PDS proteins were detectable in either wildtype or disease mice (Figure 8A) and 19 PDS proteins were measured in both conditions. PDS marker genes that were detected in both control and disease conditions showed the same direction of change on the protein level as on the transcript level (Figure 8B).

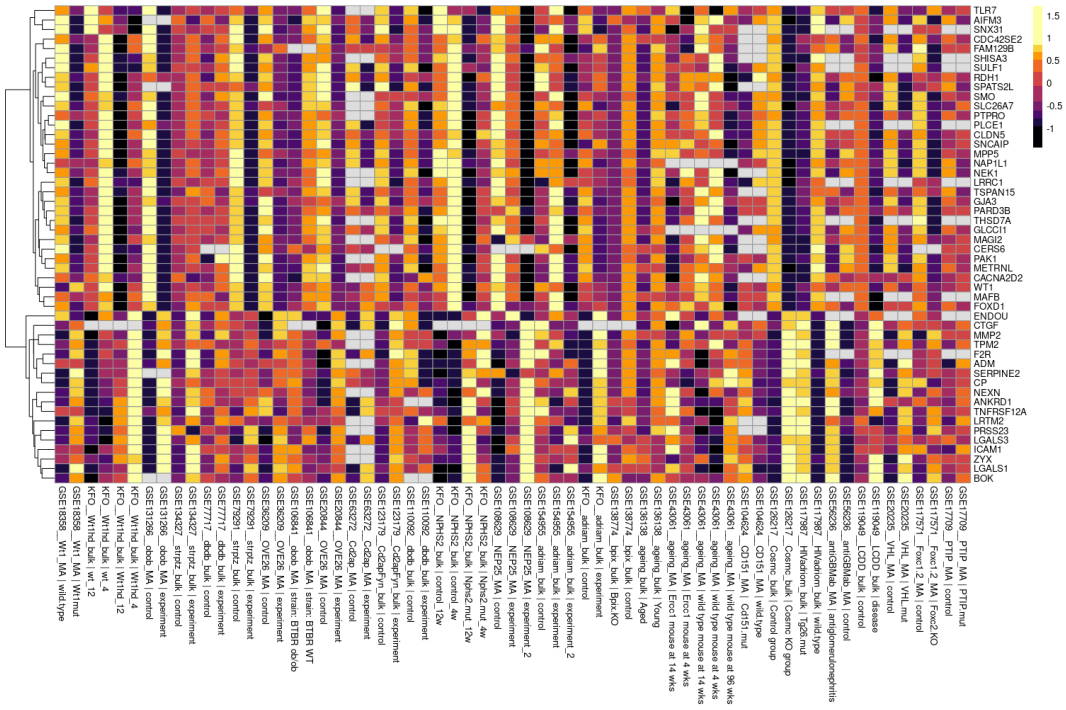

Figure 7: Transcript expression of PDS marker genes across all bulk datasets show consistent up- or down-regulation upon podocyte damage.

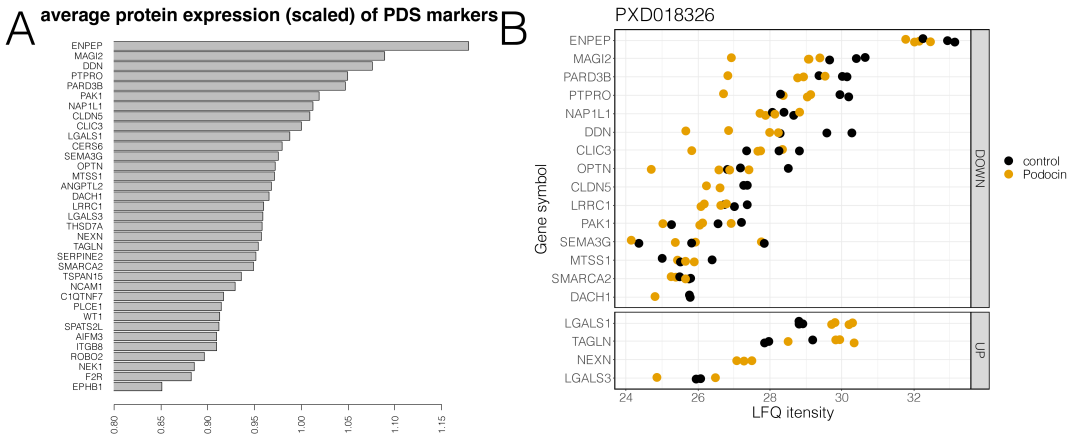

Figure 8: *Nphs2*$^{\mathrm{R231Q/A286V}}$ proteome shows the same direction of differential expression as transcriptome. A. Average protein expression of PDS markers genes where proteins were detected in the transcriptome. Data was scaled by samples and then the average Z-score across samples was calculated for all PDS proteins identified. B. Jitterplot of individual genes of PDS marker genes between control and podocin mutated mice. Proteins on the top panel are PDS markers transcripts that were commonly down-regulated those on the lower panel are PDS markers transcripts that were commonly up-regulated in podocytes upon damage.

Additionally, we verified the localization of several PDS marker genes on the cellular level using STED microscopy (Figure 9). Podocyte-specific PDS marker genes may be important in maintaining the structural integrity of podocyte architecture and may mislocalize subcellularly upon podocyte damage. THSD7A is a protein localized to the membrane and thought to play a role in actin cytoskeleton rearrangement and membranous nephropathy [223]. Claudin-5 has been shown to be expressed at plasma membranes of podocytes [224] and has been imaged by super-resolution microscopy to be localized to the slit diaphragm of podocytes [225]. SMO is a G protein-coupled receptor that might be involved in the Hedgehog signaling pathway [226]. NEK1 is a serine or threonine-protein kinase and is expressed in embryonic kidney cells most prominently in cells developing into podocytes and proximal tubules [227]. STED microscopy revealed that both THSD7A and Claudin-5 co-localize with nephrin at the podocyte slit diaphragm in wildtype mice but in 12w *Wt1*.hetdel mice, Claudin-5 showed aggregation at the slit diaphragm (Figure 9A) though THSD7A show no mislocalization at effaced slit diaphragm (Figure 9B). In wildtype kidneys, SMO did not co-localize with nephrin but with Collagen 4 (Figure 9C). Interestingly, NEK1 co-localized with both nephrin and Collagen 4 (Figure 9D). The expression and the localization of these proteins verified their specificity to podocytes.

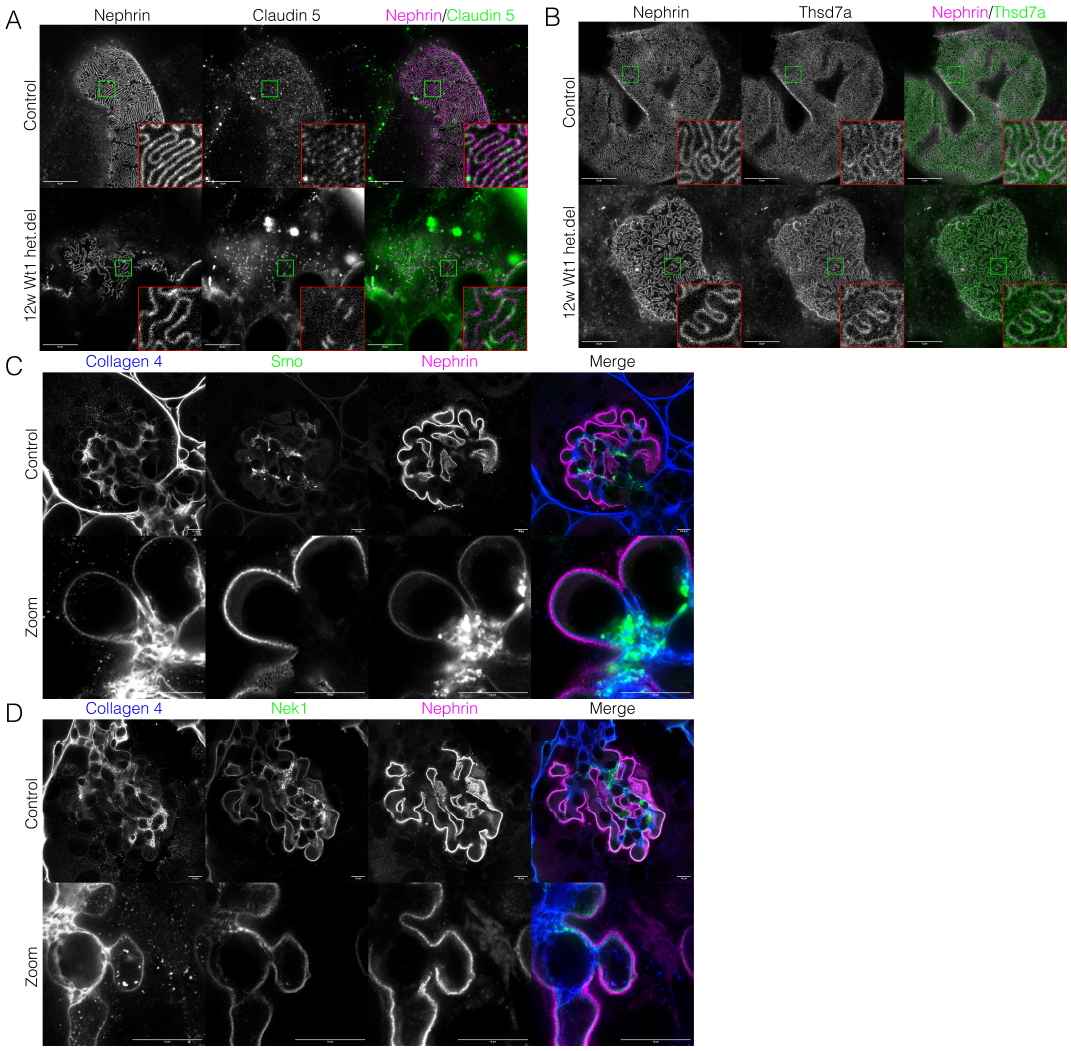

Figure 9: Cellular localization of PDS marker genes, Claudin-5, THSD7A, SMO and NEK1. The localization of some PDS marker genes (green), including Claudin-5, THSD7A, SMO and NEK1 were imaged by STED microscopy using wildtype or disease tissue from 12w *Wt1*.hetdel mice. A. Claudin-5 co-localized with nephrin (magenta) in both healthy and but showed aggregation at the slit diaphragm in disease mice (12w *Wt1*.hetdel). B. THSD7A co-localized with nephrin (magenta) in both healthy and diseased mice (12w *Wt1*.hetdel). C. SMO (green) co-localized with Collagen 4 (blue) but not with nephrin (magenta). D. NEK1 (green) co-localized with both Collagen 4 (blue) and with nephrin (magenta).

6.1.5 PDS correlates with kidney function

To relate the predictive capability of the PDS with clinical kidney function readouts, the PDS of bulk RNA-seq datasets were correlated with respective albumin/creatinine ratios (ACR) wherever described in published literature. For snRNA-seq studies, urines from mice were collected to determine the ACR of each mouse by ELISA. The PDS positively correlated with kidney function such as proteinuria for publicly available datasets (Figure 10A) as well as for in-house generated snRNA-seq (Figure 10B).

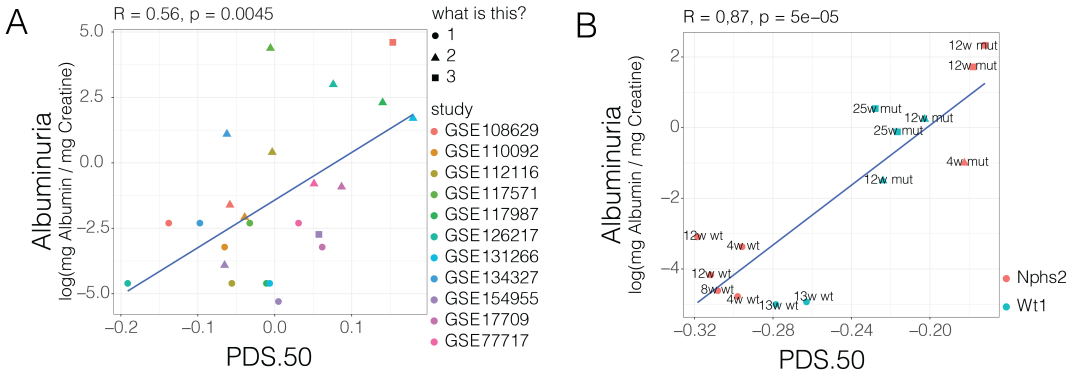

Figure 10: PDS correlates with kidney function such as proteinuria. A. For publicly available bulk datasets and B. For snRNA-seq datasets.

6.1.6 PDS is translatable to human bulk and single cell studies

To expand the application of PDS to translation medicine, we tested the PDS which was originally developed using mouse data on human data, using publicly available human bulk and single-cell RNA-seq data obtained from the Kidney Precision Medicine Project (KPMP) and (Nephrotic Syndrome Study Network) NEPTUNE consortium. KPMP also collected data on known biological phenotypes and/or clinical parameters, including albuminuria, age, and sex. We find that the PDS was applicable to human bulk and single-cell studies and was most significantly correlated with albumnuria (Figure 11A). Microarray (Figure 11B) and single cell (Figure 11C) datasets were both tested for the robustness and the cell type-specificity of the PDS on podocytes. PDS scored higher in FSGS, immunoglobulin A nephropathy (IgAN) and chronic kidney disease (CKD) patient-derived datasets suggesting that the PDS may be translated to datasets generated from patient biopsy even if the original score was derived using murine samples.

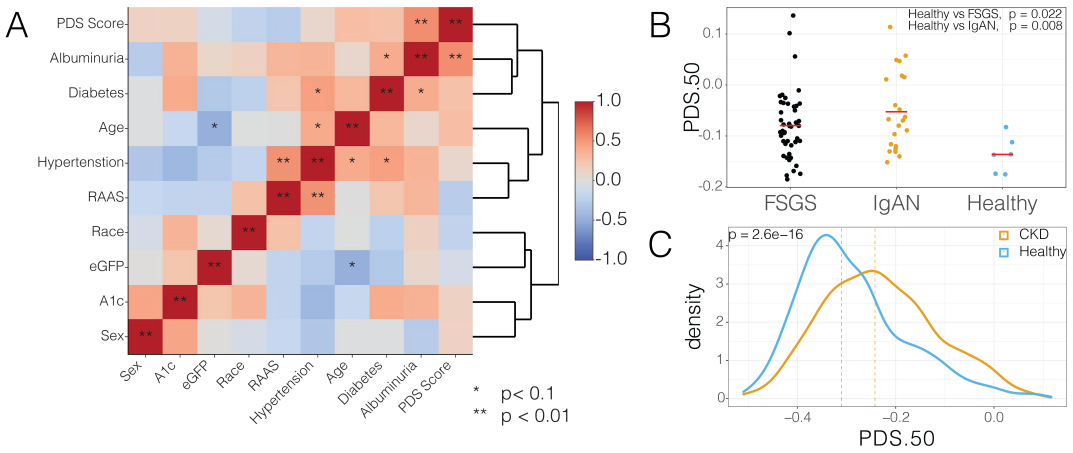

Figure 11: PDS is applicable to human bulk and single-cell datasets. A. Spearman correlation heatmap shows the highest correlation between PDS with protein-albuminuria amongst all features tested using the KPMP databank. B. PDS was applied on microarray data from GSE104066 obtained from the NEPTUNE consortium containing FSGS and immunoglobulin A nephropathy (IgAN) samples. C. snRNA-seq data was obtained from KPMP and PDS is higher in chronic kidney disease (CKD) samples in podocytes than controls.

6.1.7 PDS monitors cellular changes along disease progression and allows for direct comparison of TF and pathway activity across different models

Next, we investigated if the PDS can be used to investigate the transcriptional regulatory mechanisms in various disease models. We applied the PDS on the *Nphs2*$^{R231Q/A286V}$ snRNA-seq in the podocyte population and showed that the PDS can clearly distinguish between healthy and damaged podocytes (Figure 12A). Unexpectedly, the PDS cannot predict any trajectory within the damaged podocytes. Coincidentally, we noticed that the expression of certain genes, such as *Epha6*, show progressive changes in the sub-population of disease podocytes (Figure 12B), suggesting that there may be other aspects of transcription regulation not comprehensively captured by the gene sets that contributed to the PDS.

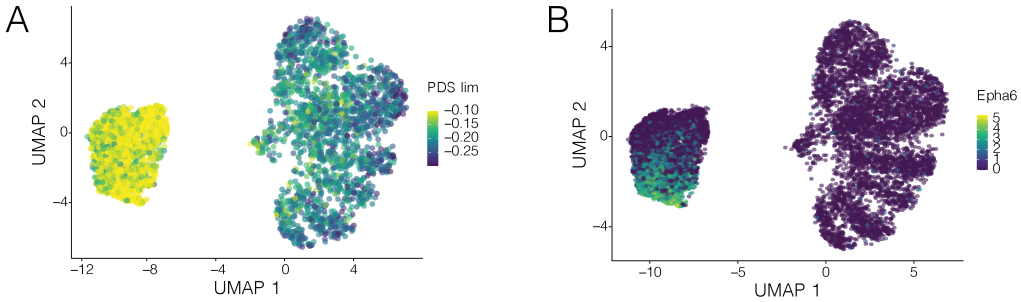

Figure 12: The PDS can clearly distinguish between healthy and damaged podocytes in *Nphs2*$^{R231Q/A286V}$ but show no trajectory within damaged podocytes. A. PDS can differentiate healthy and damaged podocytes. B. The expression of Epha6 shows progressive changes within damaged podocytes.

We anticipated that the expression of the PDS marker genes alone was insufficient to describe the status of podocyte damage because these genes were intrinsically integrated within a podocyte-specific regulatory network by TFs. Instead, we correlated the level of podocyte damage with the activity of individual TFs and biological pathways in order to generate a list of podocyte-specific TFs that may be important pathways for podocyte biology. Here, we aimed to correlate PDS with changes in TFs and TF-dependent pathway activities.

Dataset	**Type of RNA-seq**
Wt1.hetdel	sn
Nphs2 RQ/AV	sn
Pdss2 pko	sn
Coq2 ko	sn
NTS nephritis	sc
Adriamycin nephropathy	sc
Cd2ap ko	sc
Diabetic nephropathy	sc

Table 6: List of the 8 snRNA-seq or scRNA-seq used to derive podocyte-specific TFs. snRNA-seq (sn) datasets are generated in-house and scRNA-seq (sc) datasets are sourced from GSE146912. ko = knock-out, pko = podocyte-specific knock-out.

Eight scRNA-seq or snRNA-seq datasets were pooled and TFs with the median expression above zero or mean expression above 1 in podocytes were selected. 77 podocyte-specific TFs were identified as shown in

Figure 13 and their expression was correlated with the PDS. The podocytes were first ordered by their PDS from the lowest (left) to the highest (right). The activity of each TF was calculated using the difference in expression between the cell and the mean expression of control podocytes. The expression of all TFs was smoothed using the moving average for all 8 datasets. A representative heatmap for the *Nphs2*$^{\mathrm{R231Q/A286V}}$ model is shown (Figure 13A). To visualize the differential activities of TFs across all studies according to the PDS, heatmaps were generated for each of the 77 TFs. Some TFs, such as WT1, were universally downregulated in all studies. Whereas FOXD1 was only upregulated in the NTS nephritis model (Figure 13B). Similarly, the changes in pathway activities throughout the progression of podocyte damage were integrated with the Reactome and the KEGG databases. The activity of the pathway was calculated using AUCell in every cell and the top 50 pathways were selected for all 8 datasets. A representative heatmap for the *Nphs2*$^{\mathrm{R231Q/A286V}}$ model is shown for Reactome pathways (Figure 14A) and KEGG pathways (Figure 14B). Individual pathways could be plotted for all datasets. For example, the ephrin signaling negatively correlated with PDS across all models but the focal adhesion pathway showed a positive correlation with PDS in *Nphs2*$^{\mathrm{R231Q/A286V}}$ and NTS nephritis models but its activity was variable in *Cd2ap* knock-out and diabetic nephropathy models (Figure 14C).

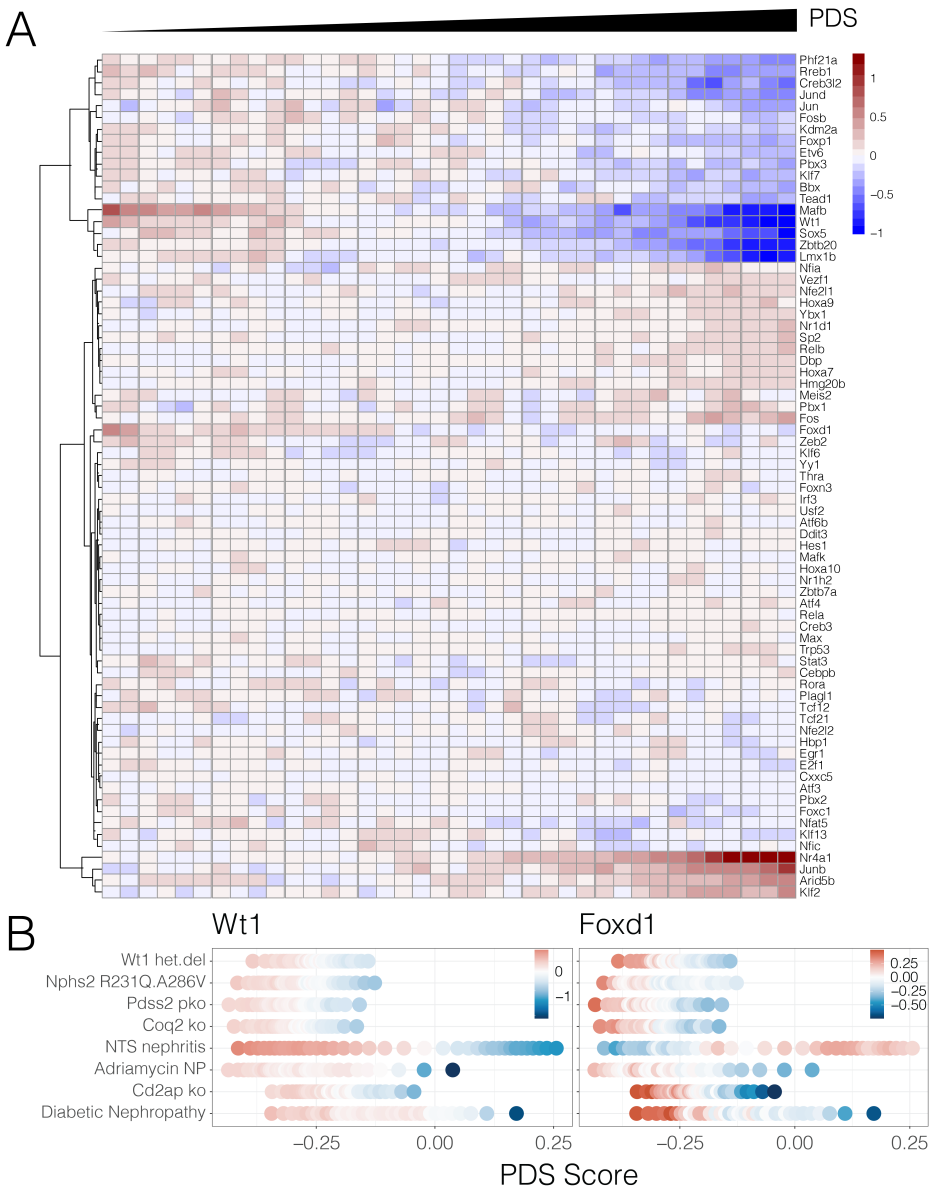

Figure 13: PDS monitors cellular changes such as TF activity in various disease models. A. Heatmap of all podocyte-specific TFs correlated with PDS at single-cell resolution in the *Nphs2*$^{\mathrm{R231Q/A286V}}$ model. B. Individual TF activity correlated with PDS in all 8 datasets.

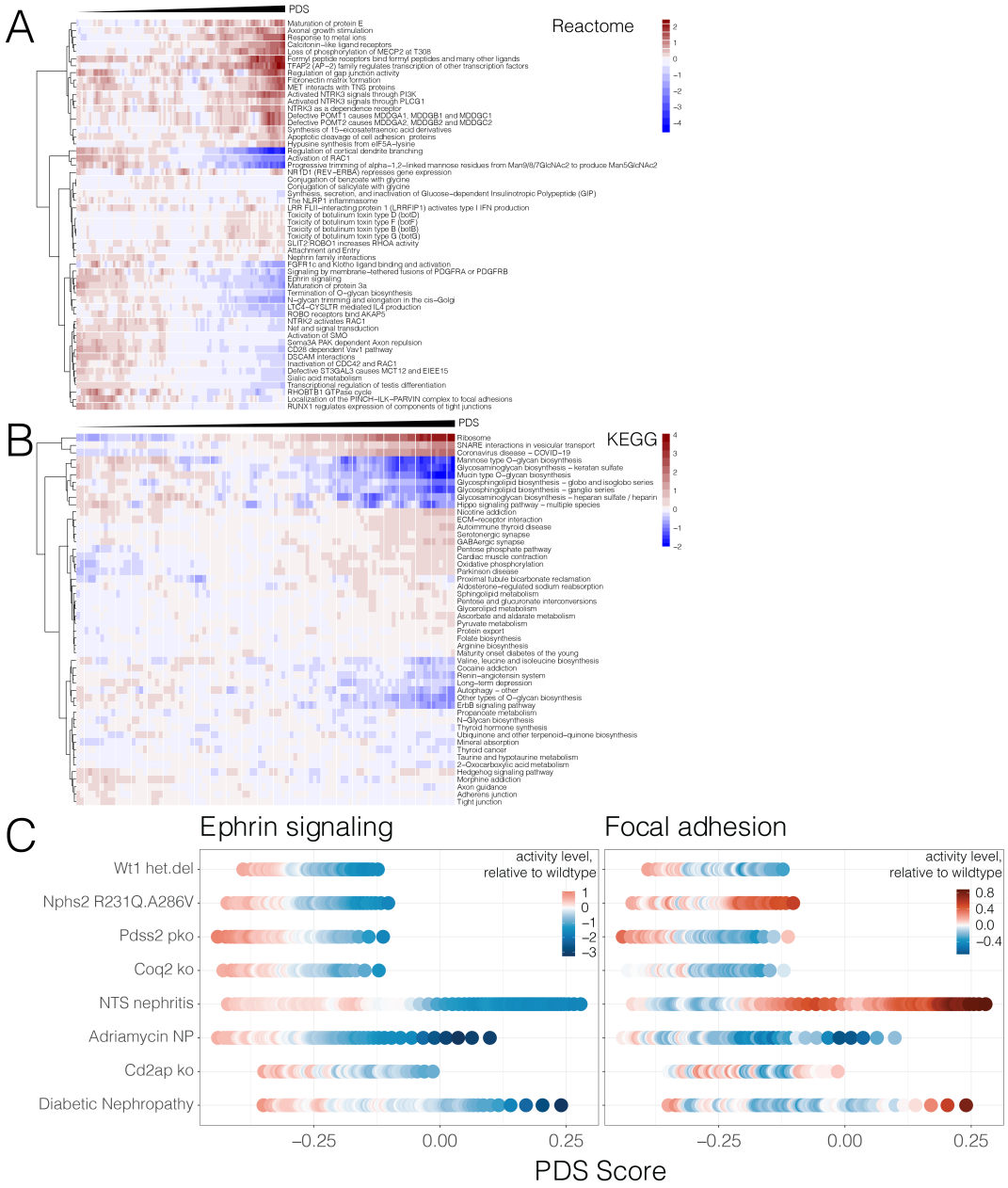

Figure 14: PDS monitors cellular changes such as pathway activity in various disease models. A. Heatmap of all Reactome pathways correlated with PDS at single-cell resolution. B. Heatmap of all KEGG pathways correlated with PDS at single-cell resolution. C. Individual pathway activity correlated with PDS in all 8 datasets.

6.1.8 Generation of the transcriptional network of the glomerulus

Next, we aimed to understand how TF and genes were interconnected with biological pathways to form a podocyte-specific transcription network and to decipher how this network dynamically responded to damage at single-cell resolution. First, we generated the transcriptional network of the glomerulus by profiling the open chromatin landscape of podocytes and endothelial cells within the glomerulus using ATAC-seq from FACS-sorted nuclei. To ensure the purity of cell population in downstream analysis, the isolation

of single nuclei from glomeruli was first established using *Rosa26*^{nTnG};Pod:cre and *Rosa26*^{nTnG};Tie2:cre mice. Glomeruli were first isolated from bead-perfused kidneys and digested to yield singlet nuclei from mice expressing cell-type specific nuclear fluorescent reporters. GFP-labeled podocyte or glomerular endothelial nuclei were sorted by FACS and collected for downstream genome-wide profiling (Figure 15).

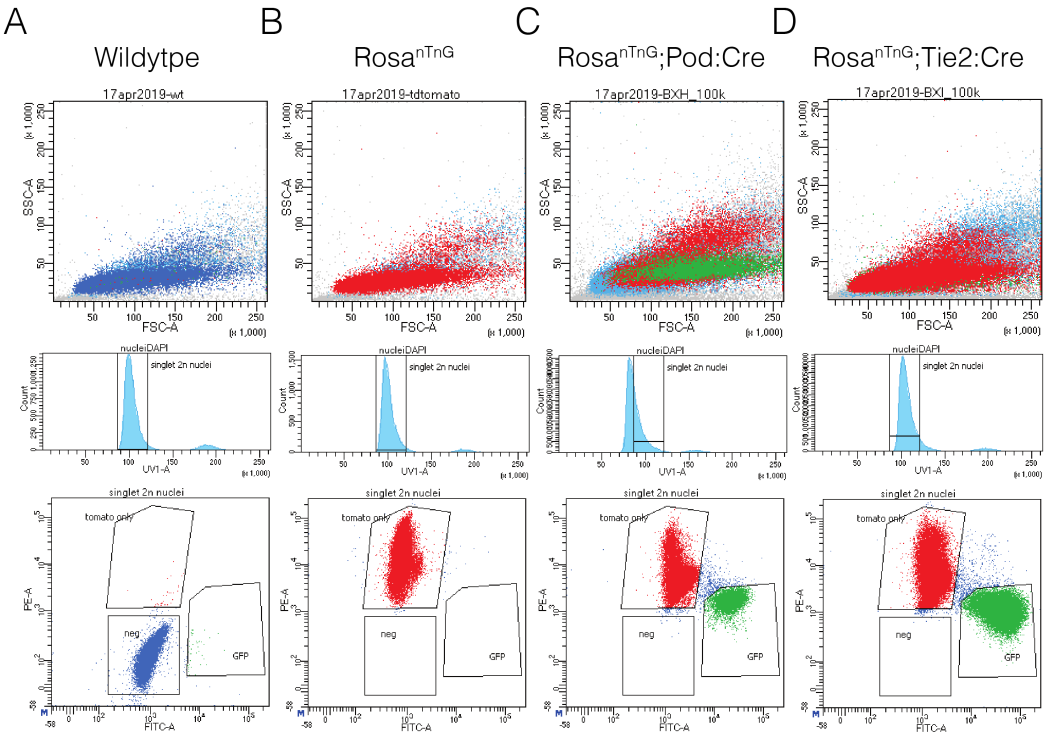

Figure 15: FACS of GFP+/tdTomato+ single nuclei from glomeruli of reporter mice. Nuclei were isolated from glomeruli wildtype mice (A), and reporter mice expressing nTnG only (B), or with Pod:cre (C) or with Tie2:cre (D). The nuclei were stained with DAPI and DAPI+ nuclei were first gated by forward- and side-scatter (top panel) and sorted for singletness (middle panel) before GFP+ or tdTomato+ nuclei were sorted (bottom panel) and collected for ATAC-seq.

50,000 sorted nuclei from healthy 8 week-old mice were subjected to ATAC-seq to profile cell-type specific chromatin accessibility in podocytes and glomerular endothelial cells (Figure 16). Peak calling was performed using Genrich. DiffBind R package was used to derive a consensus peak set and to generate principal component analysis (PCA) and heatmap using 3 podocyte and 2 non-podocyte ATAC-seq samples (Figure 16). Expectedly, loci of genes that are important for podocyte biology, such as *Lmx1b*, *Wt1* and *Nphs1*, showed significantly more open chromatin in podocytes (podo) than non-podocytes (non-podo) (Figure 16C).

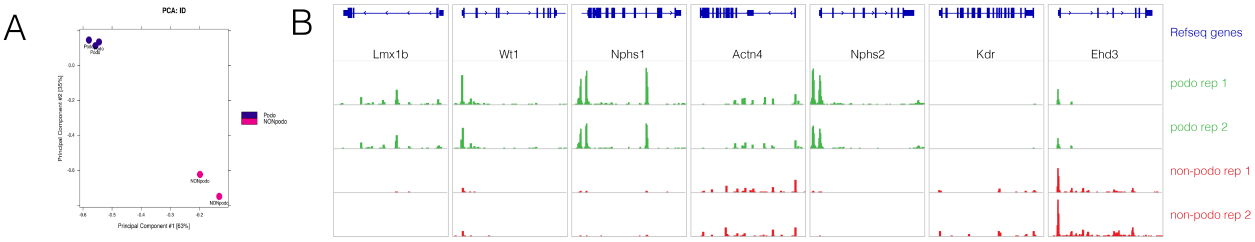

Figure 16: Quality assessment of cell type-specific glomerular ATAC-seq. A. PCA of podocyte and non-podocyte-specific ATAC-seq. B.Genome browser tracks of podo and non-podo ATAC-seq at Lmx1b, Wt1, Nphs1, Actn4, Nphs2, Kdr and Edh3 loci.

We utilized the consensus peak set derived from podocyte ATAC-seq containing 38934 peaks to build a podocyte-specific transcription regulatory network. Of the consensus peak set, 25,564 peaks were podocytes and 24,754 were non-podocyte peaks. 15,593 pekas were common for both cell types. Amongst the podocyte peaks, 7650 were found exclusively in podocytes, and amongst the non-podocyte peaks were found exclusively in non-podocytes. Differential analysis was performed using DEseq2 and discovered 13,958 differential bound peaks under qvalue < 0.01 and LFCs > 2 cut-off, composing of 36% of all consensus peaks (Figure 17A). The top 10 GO biological processes based on binned peak-to-gene distances were plotted for non-cell type-specific, podocyte-specific, and non-podocyte-specific peaks (Figure 17B). Interestingly, non-cell type-specific peaks were predominantly localized in promoter regions whereas podocyte-specific and non-podocyte-specific genes were predominantly in enhancer regions distal to the TSS. The GO terms obtained from non-podocyte-specific peaks were mostly involved in endothelial cell biology. Expectedly, podocyte-specific GO terms obtained were relevant to podocyte biology, including actin cytoskeleton reorganization, positive regulation of cell-junction assembly, and glomerulus development. The cell type-specific peaks were further analyzed using the GREAT algorithm and each peak was assigned to one or more nearest gene(s) by proximity. GREAT analysis showed that bimodal promoter-enhancer distribution of distances for all ATAC-seq peaks but an enhancer-centered distribution of distances for podocyte-specific peaks highlighting that cell type-specific peaks were mostly concentrated in enhancer regions (Figure 17C).

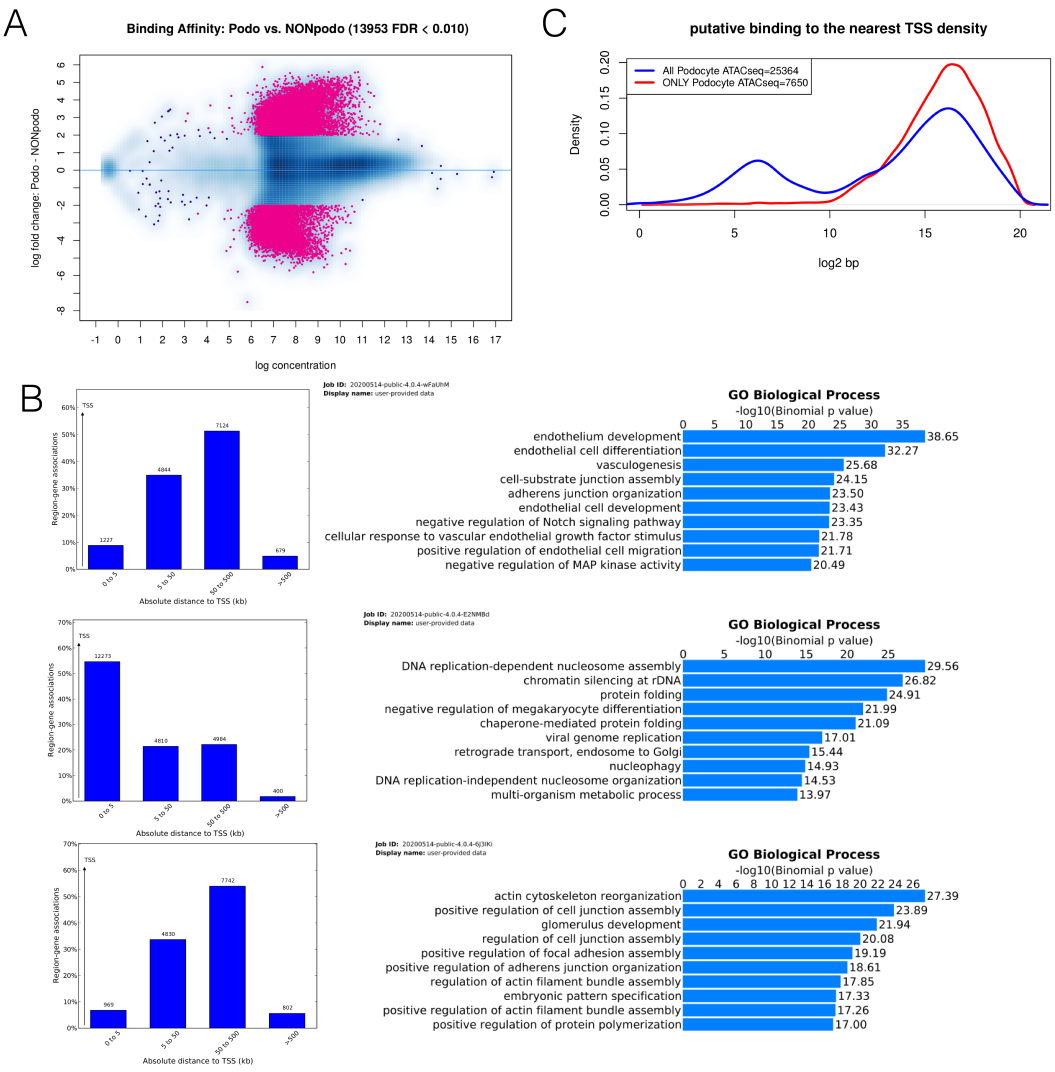

Figure 17: Differential binding analysis of podocyte-specific ATAC-seq reveals GO terms relevant to podocyte biology and GREAT analysis showed that podocyte-specific peaks are mostly located within enhancer regions. A. Differential analysis was performed using DEseq2 and discovered 13958 differential bound peaks (magenta). Binned peak-to-gene distances. B. Bar-charts of the top 10 GO biological processes of non-podocyte-specific peaks (top panels), non-cell type-specific peaks (middle panels) and podocyte-specific peaks (bottom panels). C. GREAT analysis shows a bi-modal distribution for all podocyte-specific peaks but an unimodal distribution for podocyte-exclusive peaks.

6.1.9 Podocyte-specific gene regulatory network revealed key TFs at different stages of FSGS

Next, we generated a list of priors of podocyte-specific TF-gene interaction needed to generate a regulatory network. Motif scanning was used to search for TF sequences within the podocyte-specific peaks and was combined with footprinting analysis to predict putative TF binding sites. Finally, the predicted binding events were associated with nearby genes. Motif scanning analysis identified a substantial amount of binding events, including 20,627 putative binding events of WT1 predicted on chromosome 2 (Figure 18A). After the pre-selection of footprinting using HINT, motif scanning identified 456 putative WT1 binding events on the same chromosome (Figure 18B). The analysis of footprinting before motif scanning allowed for the selection of podocyte-specific peaks that have stronger TF-binding signals. The predictions of TF binding

events performances performed better at the promoter (Figure 18C) than at enhancers (Figure 18D) because ATAC-seq signals at promoters were stronger, indicating more open chromatin.

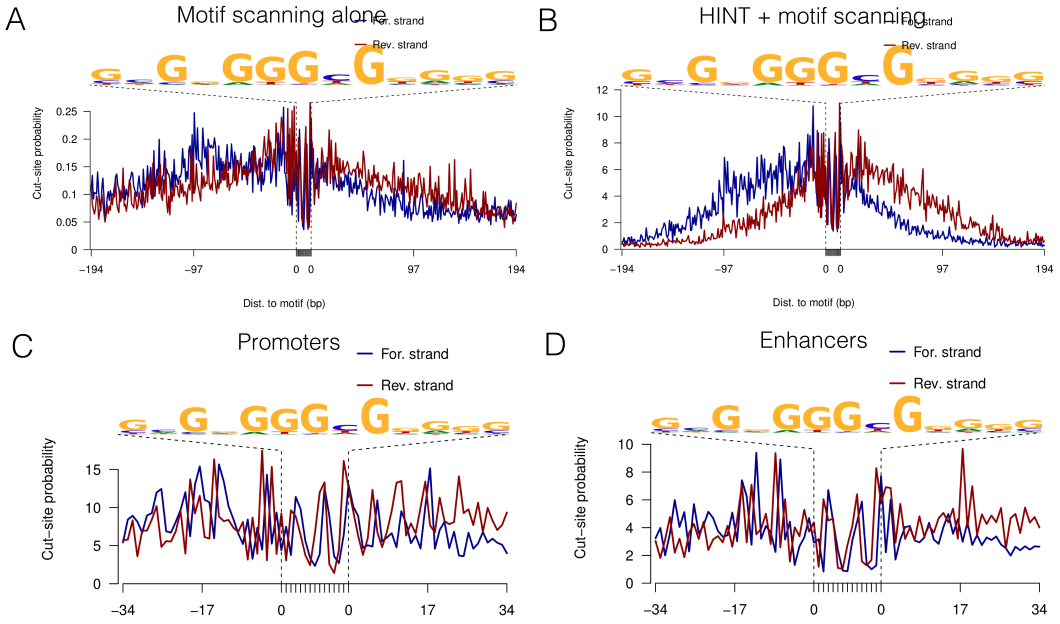

Figure 18: A combination of footprinting using HINT and motif scanning analysis was used to identify putative binding events of Wt1 on chromosome 2. A. Wt1 motif scanning of chromosome 2 produced 20,627 putative binding sites. B. Pre-selection of HINT footprinting combined with motif scanning on chromosome 2 produced 456 putative binding events. C. Wt1 footprint at base pair resolution at promoter regions. D. Wt1 footprint at base pair resolution at enhancer regions.

Next, target genes associated with each putative TF binding event were predicted using either TFtargetCaller, which was optimized for the promoter-gene association. The target genes were validated using differentially expressed genes of *Wt1*.hetdel bulk glomeruli RNA-seq data using animals sacrificed at 4 weeks (Figure 19A) and 12 weeks (Figure 19B). Other sets of TF binding events were also tested, including ATAC-seq peaks to benchmark for background and WT1 glomerular ChIP-seq peaks for benchmark for positive targets. Targets called using ATAC-seq, HINT footprinting and motif scanning for WT1 (N=38) were similar to target prediction using WT1 ChIP-seq and footprinting (N=33). There were no differences between the choices of RNA-seq datasets used. The same analysis was repeated using the ABC-score, which was optimized for enhancer-gene association (Figure 19C&D). There was little overlap in the gene target prediction between TFtargetCaller and ABC-score.

The target genes were further verified globally using the gene set enrichment analysis (GSEA) method where the predicted targets of WT1 were assessed for their enrichments against the list of genes differentiated expressed in the 4-week-old *Wt1*.hetdel bulk RNA-seq datasets. Genes called by both TFtargetCaller and ABC-score were combined in the GSEA analysis (Figure 19E) and compared to target genes predicted using glomerular WT1 ChIP-seq data [33] (Figure 19F). The prediction using TFtargetCaller and/or ABCScore applied to ATAC-seq were similar whereas the TFtargetCaller outperformed ABCscore or their union on ChIP-seq datasets.

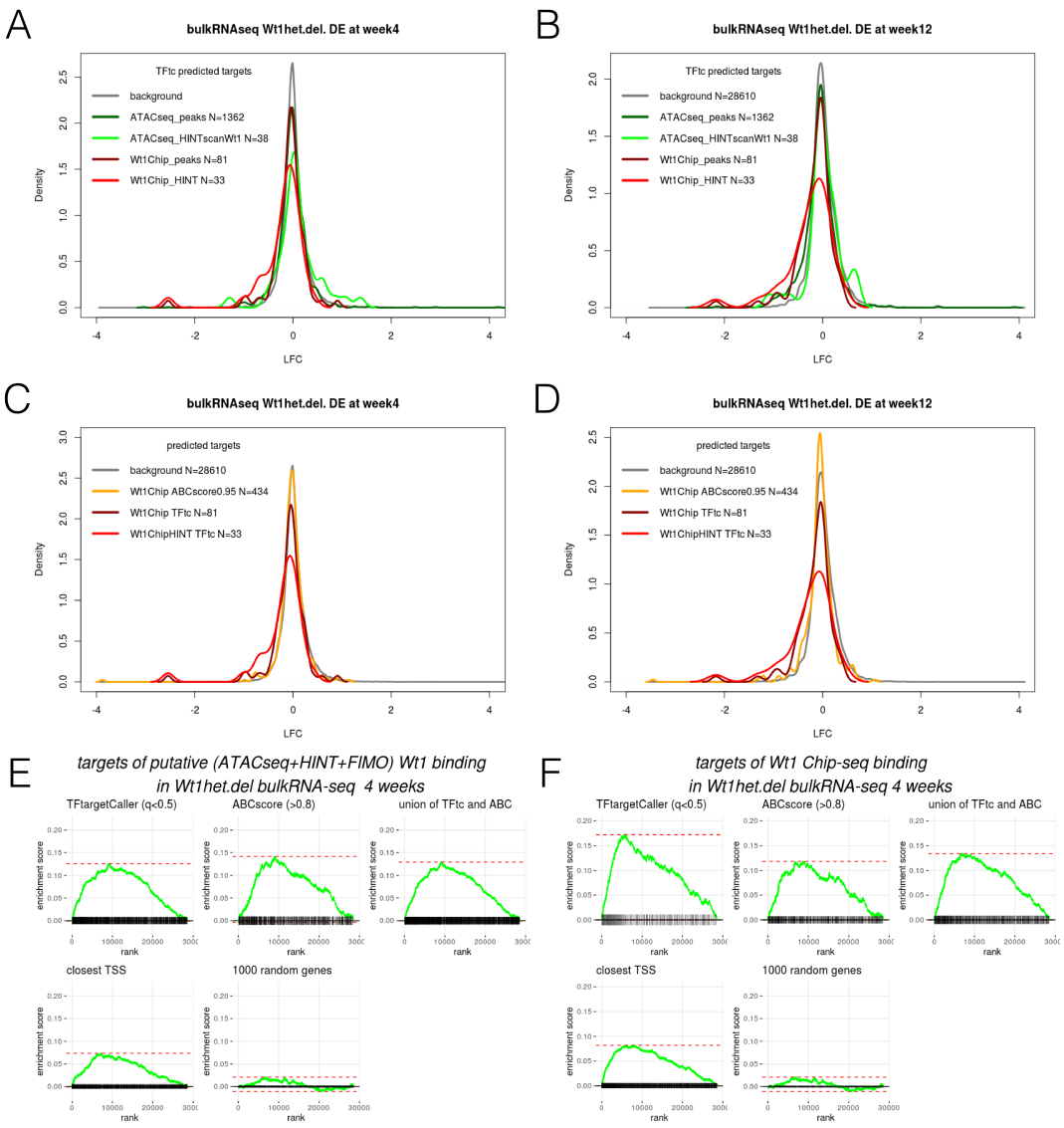

Figure 19: TFtargetCaller and ABC-score were used to associate putative TF binding events to target genes. Target calling was performed using TFtargetCaller using putative Wt1 binding events was validated by comparing to Wt1 ChIP-seq datasets and to glomerular bulk RNA-seq datasets from *Wt1*.hetdel mice at 4 weeks (A) and 12 weeks (B). Similarly, target calling was performed using ABC-score and compared to WT1 ChIP-seq datasets and to glomerular bulk RNA-seq datasets from *Wt1*.hetdel mice at 4 weeks (C) and 12 weeks (D). E. GSEA for target genes predicted with various methods from HINT+FIMO putative Wt1 binding. F. GSEA for target genes predicted from Wt1 Chip-seq data.

Finally, we called the target genes for all TFs after combining the results obtained from TFtargetCaller and ABC-score to generate the priors for the podocyte-specific gene regulatory network. We identified 906 TF regulators and 15,646 genes that have contributed to the podocyte-specific priors. The subset of TFs of the priors that were differentially regulated in *Wt1*.hetdel mice at 4 weeks (Figure 20A) and 12 weeks (Figure 20B) showed active gene regulatory network at corresponding stages of FSGS. For instance, Wt1 (blue) is a central regulatory for both the early and late stages of FSGS. Additional TFs, such as LMX1B, TCF21 and SMAD3 became differentially regulated in late-stage FSGS.

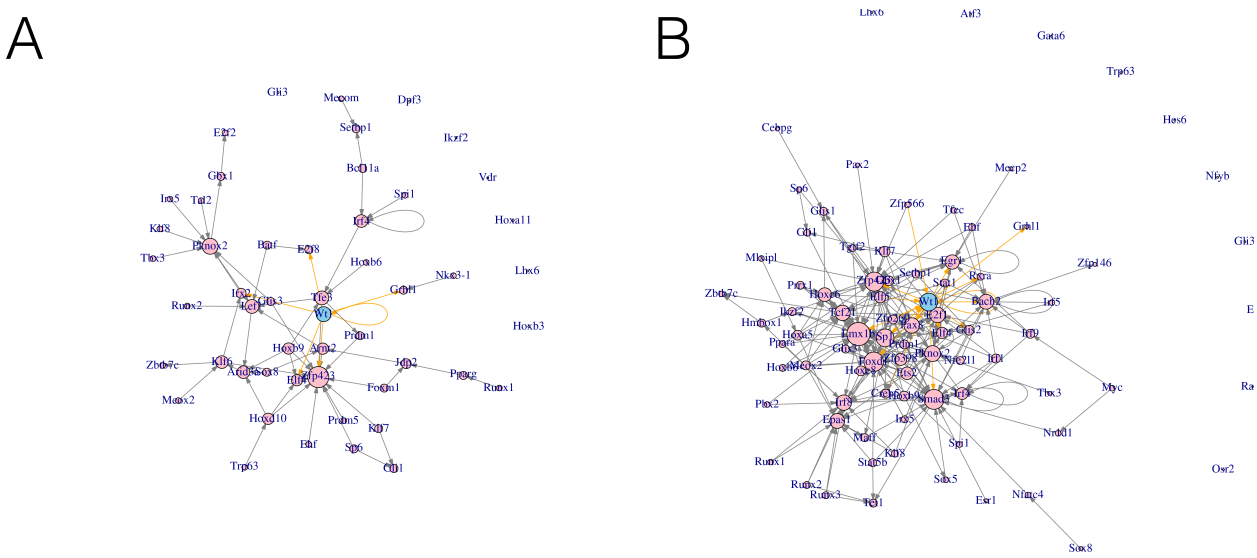

Figure 20: Podocyte-specific gene regulatory network revealed key TFs at different stages of FSGS. A. Podocyte gene regulatory network at an early stage of FSGS, in 4 week-old *Wt1*.hetdel mice. B. Podocyte gene regulatory network at late stage of FSGS, in 12 week-old *Wt1*.hetdel mice.

6.2 Mapping the epigenetic landscape in the glomerulus

6.2.1 Identification of glomerular cell type-specific enhancers and SEs

Based on the analysis of the podocyte-specific ATAC-seq, we observed that podocyte-specific peaks were highly concentrated in gene regulatory regions that were predicted to be enhancers. However, these enhancer regions were determined based on analysis *in silico* and may not reflect the true epigenetic regulatory landscape of podocyte biology. These enhancer regions may also be cell type-specific in the glomerulus and may be differentially regulated along podocyte disease progression. We aimed to map the epigenetic landscape of the glomerulus using a combination of CUT&Tag and ATAC-seq, as well as Hi-ChIP methods to annotate the gene regulatory regions and to elucidate the changes in chromatin organization and gene regulation in FSGS. First, glomeruli were isolated from bead-perfused kidneys from 8-week-old healthy transgenic mice containing nuclear fluorescent reporter allele driven under the Podocin-Cre transgene (nTnG; Pod:cre) (Figure 21A). Nuclei were sorted and collected by FACS, then GFP+ or tdTomato+ single nuclei were subjected to CUT&Tag using histone modification markers including H3K4me3, H3K27ac, H3K4me1, H3K27me3, and IgG. H3K4me3 is a marker for promoters, H3K27ac is a marker for active enhancers, H3K4me1 is for poised enhancers, H3K27me3 is for repressors, and IgG was used as an isotype control. GFP+ nuclei were podocytes (podo) and tdTomato+ nuclei were non-podocytes (non-podo) isolated from the glomeruli (Figure 21B). To map glomerular endothelial cell (GEC)-specific epigenome, CUT&Tag experiments using the same histone markers were performed using wildtype mice driven under the Tie2:cre transgene. In this mouse line, GFP+ nuclei were endothelial cells (GECs) and tdTomato+ nuclei were non-endothelial cells (non-GECs) from the glomeruli (Figure 21B).

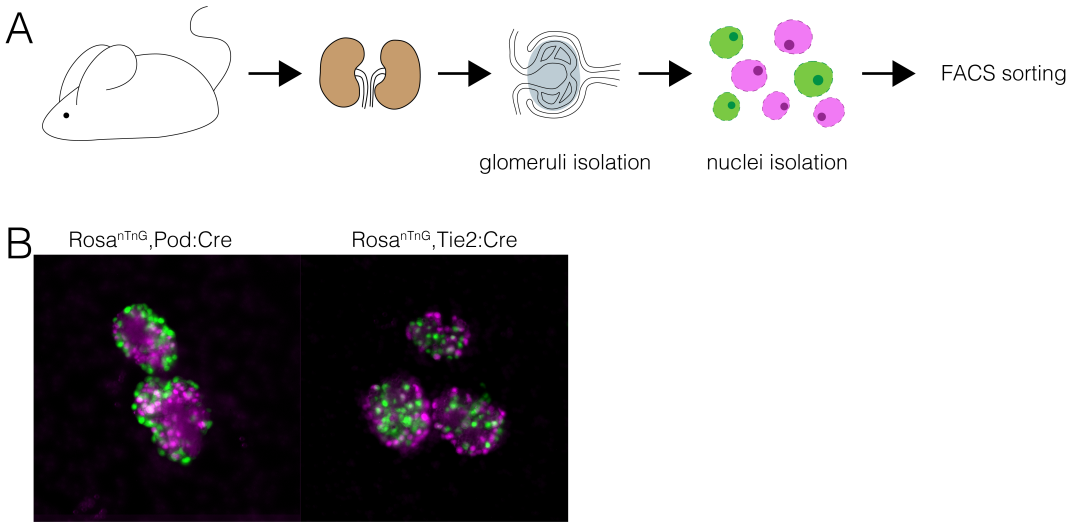

Figure 21: Schematics of mapping the epigenetic landscape of the glomerulus using wildtype animals using FACS-sorted nuclei. A. Kidneys were extracted from mice and isolated for glomeruli prior to the isolation of nuclei and the collection of single nuclei using FACS. B. Two nuclear reporter mouse lines were used to isolate podocytes (left: *Rosa*^{nTnG};Pod:cre) and GECs (right: *Rosa*^{nTnG};Tie2:cre). For *Rosa*^{nTnG};Pod:cre, GFP+ (green) nuclei were podocytes, whereas tdTomato+ (magenta) nuclei were non-podocytes. For *Rosa*^{nTnG};Tie2:cre, GFP+ (green) nuclei were GECs, whereas tdTomato+ (magenta) nuclei were non-GECs.

The specificity for podocytes was verified by visualizing the accumulation of specific histone markers at loci of known genes relevant to podocyte biology. For instance, Wt1 and *Lmx1b* are both podocyte-

specific TFs essential for the development and maintenance of podocyte function. These loci were highly enriched for active enhancer markers including H3K27ac and H3K4me1, but lacked repressor markers like H3K27me3. In contrast, Kdr is a vascular endothelial cell receptor and Pdgfrb is a receptor that critically regulates mesangial cell function. The lack of enhancer enrichment for concurrent H3K27ac and H3K4me1 was observed in podocytes at these loci, whereas the H3K27me3 marker was highly enriched. Both *Actn4* and *Smad3* loci were highly enriched for active markers in both podocyte and non-podocyte cells but lacked H3K27me3 accumulation indicating high enhancer activity in podocytes. Overall, different enhancer marker profiles for podocyte-specific specific genes were observed at single loci but genome-wide assessment of the podocyte epigenetic landscape remains to be determined (Figure 22).

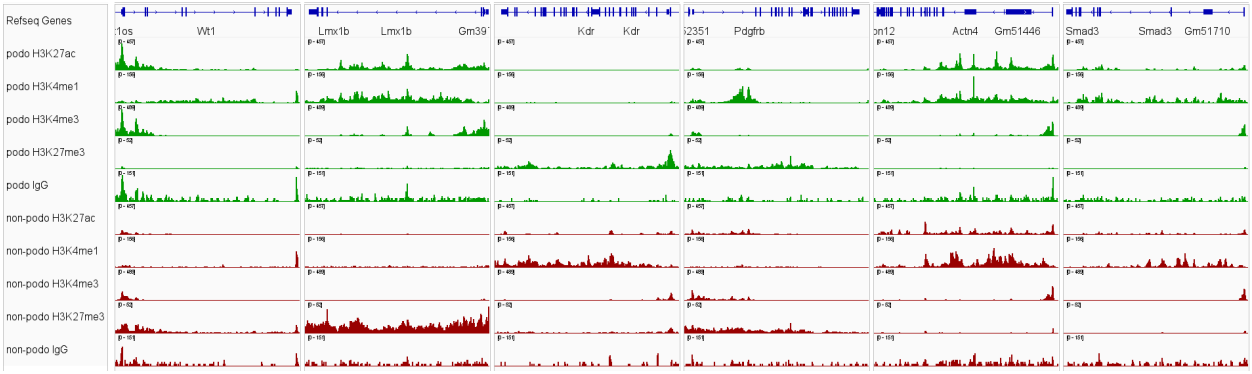

Figure 22: Genome browser tracks of H3K27ac, H3K4me1, H3K4me3, H3K27me3 and IgG of podocyte- (green) and non-podocyte- (red) specific CUT&Tag at podocyte-specific (*Lmx1b*, Wt1), glomerular endothelial-specific (Kdr), mesangial cell-specific (Pdgfrb) or general (*Actn4*, *Smad3*) loci. All tracks were grouped and normalized to the data range per each antibody marker.

In parallel, the specificity for GECs was verified using loci of genes relevant to endothelial cell biology, including Kdr and Ehd3. Compared to podocyte-specific genes, such as *Lmx1b* and Wt1, GEC-specific loci showed an accumulation of active enhancer markers whereas podocyte-specific genes were heavily enriched for H3K27me3 repressor marker (Figure 23). Similar to the podocyte-specific epigenome, GECs-specific loci were enriched for GECs-specific enhancers. In addition, both *Actn4* and *Smad3* loci were enriched for active enhancer markers, suggesting that there may be a common set of genes that have housekeeping functions across all glomerular cell types.

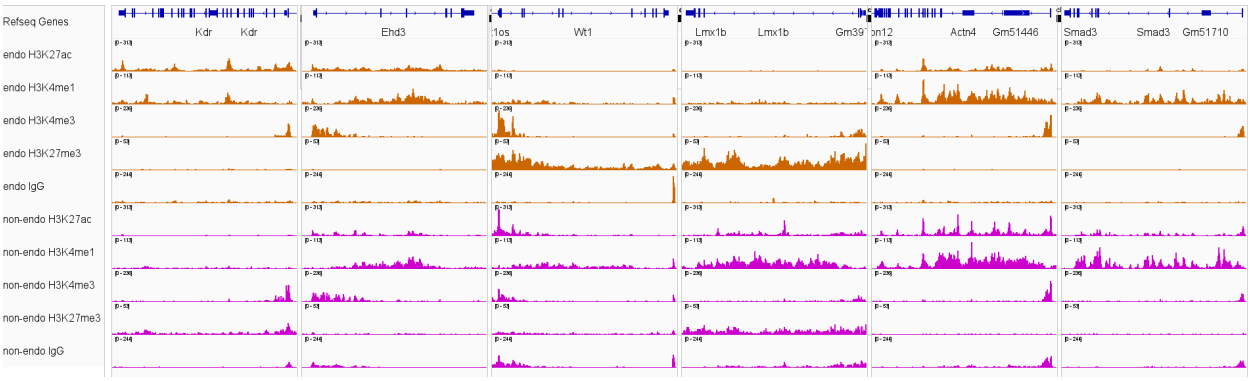

Figure 23: Genome browser tracks of H3K27ac, H3K4me1, H3K4me1, H3K27me3 and IgG of GECs- (orange) and non-GECs- (magenta) specific CUT&Tag at endothelial cell-specific (Kdr, Ehd3), glomerular endothelial-specific (*Lmx1b*, Wt1) or general (*Actn4*, *Smad3*) loci. All tracks were grouped and normalized to the data range per histone marker.

To evaluate the glomerular enhancer landscape on the genome-wide level, we defined an active cell-type specific enhancer region if signals from active enhancer markers, both H3K27ac and H3K4me1, were observed at open chromatin regions as defined by ATAC-seq but the peak was found away from promoter regions marked by H3K4me3 and was devoid of any overlap with the H3K27me3 repressor marker (Figure 24A). Cell type-specific active enhancers were called independently and exclusively using GFP+ datasets for podocytes and GECs. Active enhancers of mesangial cells were inferred using the tdTomtato+ CUT&RUN datasets generated from non-podocytes and non-GECs. We identified 11089 active podocyte-specific enhancer regions, 11735 GEC-specific enhancer regions, and 1941 inferred mesangial cell-specific enhancer regions (Figure 24B). There was minimal overlap between active enhancers specific for podocytes and GECs, though inferred active enhancers for mesangial cells showed greater overlap with the other two cell types (Figure 24C), likely resulting from poor inference, highlighting the necessity of determining the cell-type specific epigenome empirically. The sequencing-depth-normalized read coverages centered 2.5kb around active enhancers showed high specificity for cell-type specific ATAC-seq, H3K4me1+, and H3K27ac+ regions for confirming that enhancers regions were specific to their respective cell types (Figure 24D, E and F). These enhancers were assigned to the nearest genes by promixity using the GREAT algorithm and the gene sets were used for GO enrichment and Mammalian Phenotype (MP) Ontology analysis. The podocyte-specific gene sets identified GO terms highly relevant to the organization of actin and the cytoskeleton for biological processes (BP), cellular component (CC), and molecular function (MF) (Figure 24G) and similar pathways related to kidney, glomerular, and podocyte damage were expectedly revealed by human and MGI phenotypes ontology analysis (Figure 24H). Additionally, the GO and pathway analysis was performed for the genes associated with the nearest active enhancers for GECs (Figure 25A and B) and inferred mesangial cells (Figure 25C and D). Expected terms were observed for GECs including functions and phenotypes related to the vasculature and regulation of cell motility. The terms related to the mesangial cells were not identifiable to be related to mesangial cell biology likely because the active enhancers were inferred and not empirically derived using sequencing. These results demonstrate that the empirical determination of active enhancers using ATAC-seq and CUT&Tag using FACS-sorted nuclei is a valid as well as indispensable approach for reconstructing the cell type-specific glomerular epigenome.

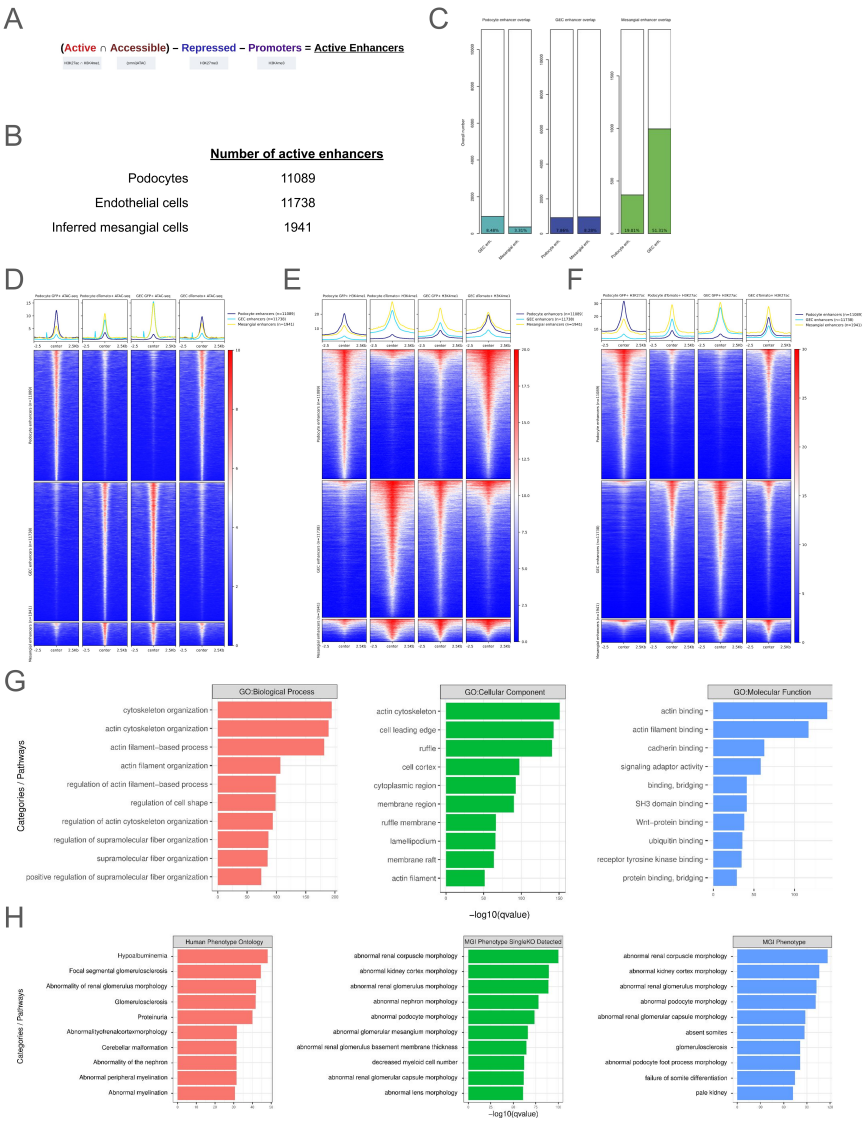

Figure 24: Active enhancers were derived from glomerular cell type-specific ATAC-seq and CUT&Tag. A. Active enhancers were defined as an overlapping peak between H3K27ac and H3K4me1 markers in the open chromatin region but devoid of H3K4me3 and H3K27me3. B. Numbers of active enhancers detected in podocytes, GECs and mesangial cells. Those of podocytes and GECs were derived from empirical data whereas that of mesangial cells were inferred based on podocytes and GECs-specific datasets. C. Percent overlap of active enhancers between glomerular cell types. D. Row-linked heatmaps of RPKM normalized number of reads across a 2.5kb genomic interval relative to the center of the active enhancer based on average density for open chromatin. Re and blue reflect high and low read densities respectively. E. Same as D but for H3K4me1 positive regions. F. Same as D but for H3K27ac positive regions. G. GO pathway analysis based on genes associated with enhancers assigned by GREAT. H. Mammalian phenotype ontology analysis based on genes associated with enhancers assigned by GREAT.

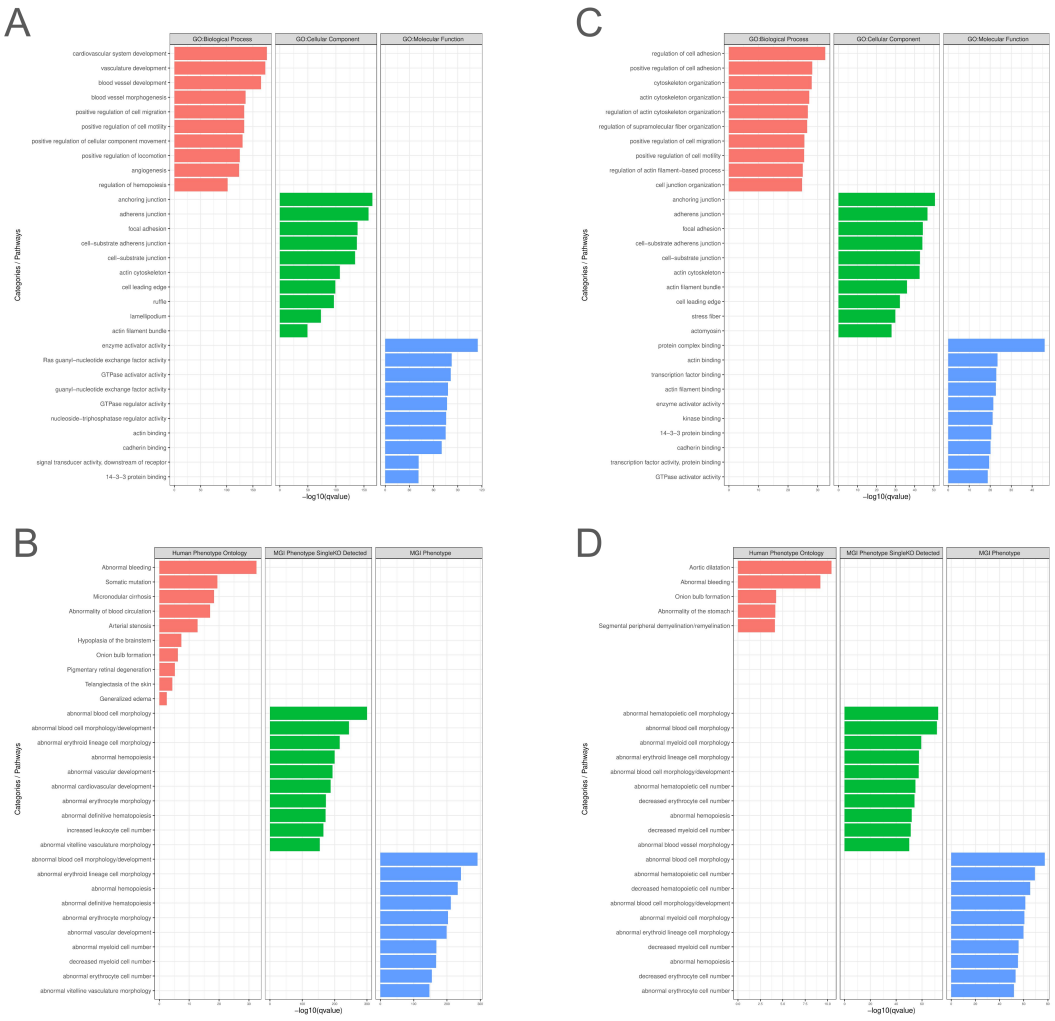

Figure 25: The GO and pathway analysis for genes associated with the nearest active enhancers of GECs and inferred mesangial cells. A. GO analysis based on genes associated with enhancers assigned by GREAT for GECs. B. Mammalian phenotype ontology analysis based on genes associated with enhancers assigned by GREAT for GECs. C. Same as A but for inferred mesangial cells. D. Same as B but for inferred mesangial cells.

6.2.2 Identification of disease-related differential podocyte-specific enhancers revealed global loss of open chromatin and acetylated enhancers in *Nphs2*$^{\mathrm{R231Q/A286V}}$ and *Phb2*$^{\mathrm{pko}}$ mice

Next, we aimed to map the podocyte epigenome in disease using two published genetic models, where the *Nphs2*$^{\mathrm{R231Q/A286V}}$ mice harbor a compound heterozygous mutation in the *Nphs2* gene and showed progressive proteinuria, structural alteration of the slit diaphragm and eventually FSGS [14], and the *Phb2*$^{\mathrm{pko}}$ mice develop early onset proteinuria at 3 weeks, glomerulosclerosis and death at 4 to 5 weeks [228]. Both proteins are required to maintain healthy podocyte foot processes. To allow for the nuclei sorting of podocytes by fluorescence, the *Nphs2*$^{\mathrm{R231Q/A286V}}$ and *Phb2*$^{\mathrm{pko}}$ mice were crossed with nTnG; Pod:cre (Figure 26A) . To collect injured podocytes, glomeruli isolation from *Nphs2*$^{\mathrm{R231Q/A286V}}$ mice was performed at 6 week-old and *Phb2*$^{\mathrm{pko}}$ mice at 4 week-old after confirming that they exhibited proteinuria at these chosen timepoints

(Figure 26B). The disorganization of the slit diaphragm was confirmed by STED super-resolution microscopy for *Nphs2*$^{\mathrm{R231Q/A286V}}$ (Figure 26D) and *Phb2*$^{\mathrm{pko}}$ (Figure 26C and D) mice by staining for nephrin and podocin and the slit length was quantified for both mouse lines (Figure 26E) to compare the relative severity of the two models. Although *Nphs2*$^{\mathrm{R231Q/A286V}}$ mice showed shorter slit length per area compared to the *Phb2*$^{\mathrm{pko}}$ mice which may suggest more severe proteinuria and podocyte injury, *Nphs2*$^{\mathrm{R231Q/A286V}}$ mice also showed longer survival than *Phb2*$^{\mathrm{pko}}$ mice, which suffered more severe renal phenotypes and earlier time of death from poor prognosis. Due to technical limitations, the mice lines were not crossed to Tie2:cre because the expression of the GFP reporter in GECs was leaky thus rendering the FACS-sorting obselete.

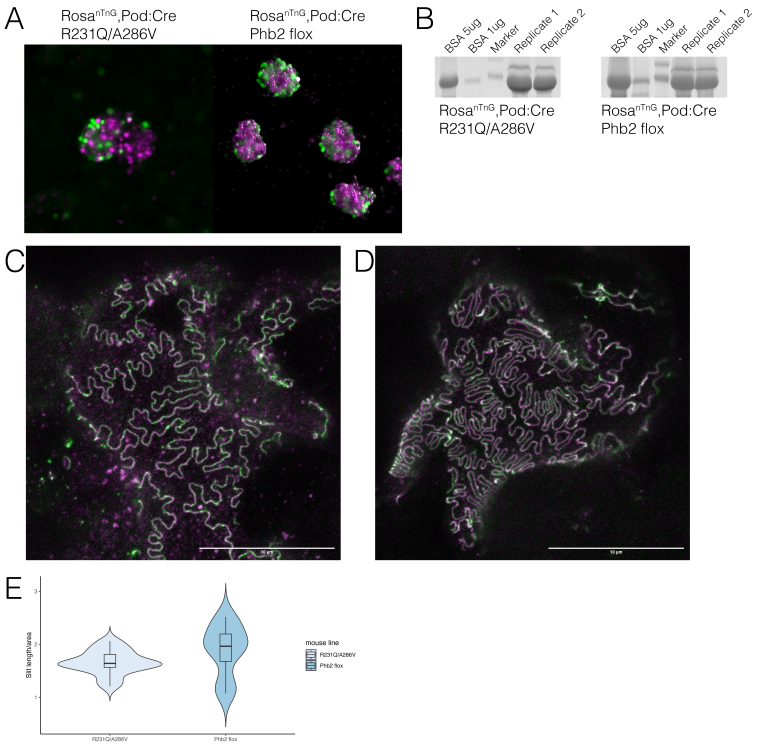

Figure 26: Basal phenotyping of the FSGS disease models used to map disease-associated enhancer epigenome. A. Podocin compound heterozygous mutant R231Q/A286V mice were crossed with *Rosa*^{nTnG},Pod:Cre reporter line to generate fluorescently labeled podocytes in FSGS model. B. Phb2 knockout mice were crossed with *Rosa*^{nTnG},Pod:Cre reporter line to generate fluorescently labelled podocytes in the FSGS model. B. Mice showed proteinuria at 6w for *Rosa*^{nTnG},Pod:Cre; R231Q/A286V mice. Mice showed proteinuria at 4w for *Rosa*^{nTnG},Pod:Cre; Phb2 fl/fl mice. C. STED staining of nephrin (magenta) and podocin (green) for *Rosa*^{nTnG},Pod:Cre; R231Q/A286V mice at 6w showed slit diaphragm effacement. D. STED staining of nephrin (magenta) and podocin (green) for *Rosa*^{nTnG},Pod:Cre; Phb2 fl/fl at 4w showed slit diaphragm effacement. E. Quantification and comparison of slit diaphragm length of *Rosa*^{nTnG},Pod:Cre; R231Q/A286V and *Rosa*^{nTnG},Pod:Cre; Phb2 fl/fl models.

Next, we isolated single nuclei and FACS sorted diseased podocyte nuclei for subsequent epigenetic profiling using H3K27ac, H3K4me1, H3K27me3 and H3K4me3 histone markers using CUT&Tag and ATAC-seq similar to wildtype mice and aimed to compare the differences in the maintenance of cell type-specific enhancers. At podocyte-specific loci, such as *Nphs1*, *Nphs2*, and *Lmx1b*, we observed decreased open chromatin in *Nphs2*$^{\mathrm{R231Q/A286V}}$ and *Phb2*$^{\mathrm{pko}}$ podocytes compared to wildtype whereat *Dock5*, *Tmod3*, and *Smad3*, there were openings of some regions in the disease models, indicating chromatin reorganization during podocyte

injury (Figure 27).

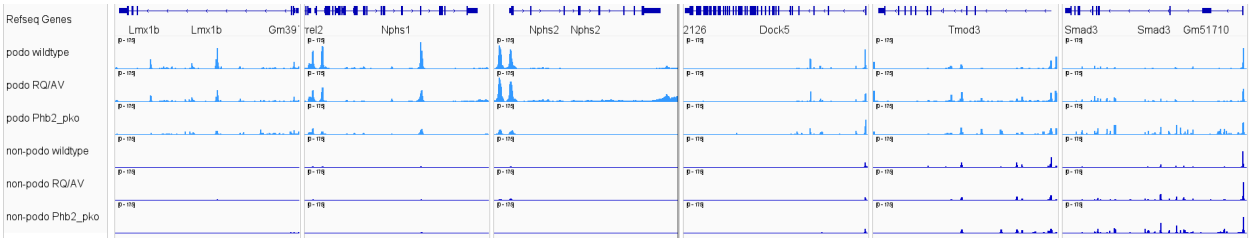

Figure 27: Genome browser tracks of open chromatin of disease models in podocyte (light blue) and non-podocytes (dark blue) of wildtype *Nphs2*$^{\mathrm{R231Q/A286V}}$ and *Phb2*$^{\mathrm{pko}}$ mice. *Lmx1b*, *Nphs1*, *Nphs2*, Dock5, Tmod3 and *Smad3* loci are shown from left to right.

To evaluate which specific type of regulatory regions were changing within the open chromatin, the changes in acetylation and methylation profiles from CUT&Tag were used to observe in regulatory regions at some loci. For example, at the Mgat5b and Hrh2 loci, there was enrichment for the H3K27me3 marker at the promoters of these genes exclusively in the *Phb2*$^{\mathrm{pko}}$ model. At the loci of *App*, *Adm*, *Vtcn1* and *Pik3r1*, acetylation markers were increased compared to wildtype for the *Nphs2*$^{\mathrm{R231Q/A286V}}$ model but not the *Phb2*$^{\mathrm{pko}}$ model suggesting there are model-specific regulations of active enhancers in diseased podocytes (Figure 28).

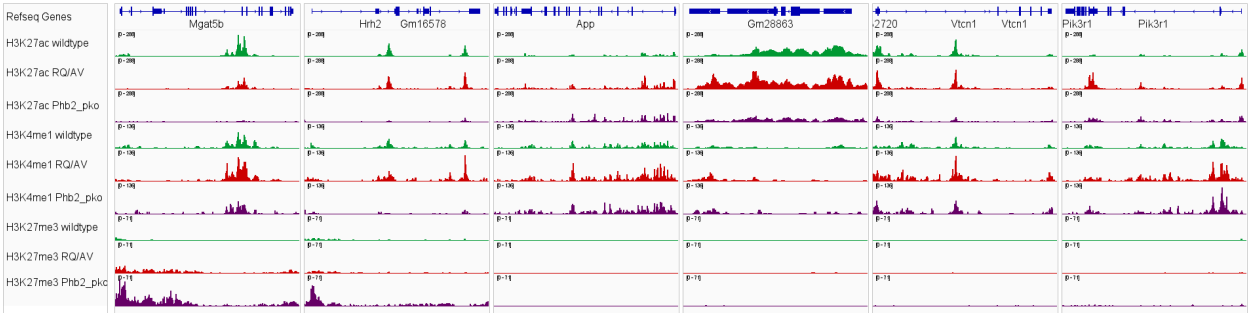

Figure 28: Genome browser tracks of H3K27ac, H3K4me1 and H3K27me3 podocyte-specific CUT&Tag of the *Nphs2*$^{\mathrm{R231Q/A286V}}$ and *Phb2*$^{\mathrm{pko}}$ models at the *Mgat5b*, *Hrh2*, *App*, *Adm*, *Vtcn1* and *Pik3r1* loci. The wildtype is green, the *Nphs2*$^{\mathrm{R231Q/A286V}}$ model is red and the *Phb2*$^{\mathrm{pko}}$ model is violet.

Next, we aimed to determine which regulatory elements in podocytes were differentially regulated on a genome-wide level in FSGS compared to wildtype and to investigate if there were differences between the *Nphs2*$^{\mathrm{R231Q/A286V}}$ and *Phb2*$^{\mathrm{pko}}$ models during disease progression. First, active enhancers were called independently from the wildtype active enhancers to determine disease-related enhancers. We performed enhancer-to-gene linkage analysis using GREAT and analyzed the gene sets using GO and Mammalian Phenotype Ontology analysis. Similar to podocyte-specific GO analysis for wildtype enhancers, terms related to the actin cytoskeleton such as "actin cytoskeleton organization", "actin filament-based process" and "cytoskeleton organization" were related to both *Nphs2*$^{\mathrm{R231Q/A286V}}$ and *Phb2*$^{\mathrm{pko}}$ models (Figure 29A and C). In the *Nphs2*$^{\mathrm{R231Q/A286V}}$ model, "hypoalbuminemia", "focal segmental glomerulosclerosis" and "nephrotic syndrome" were revealed (Figure 29B), whereas "abnormality of peripheral nerves", "abnormal myelination", and "diseased nerve conduction velocity" were revealed in the *Phb2*$^{\mathrm{pko}}$ model (Figure 29D), highlighting potential differences in etiology in the two models despite the similarity in podocyte damage and renal

phenotypes.

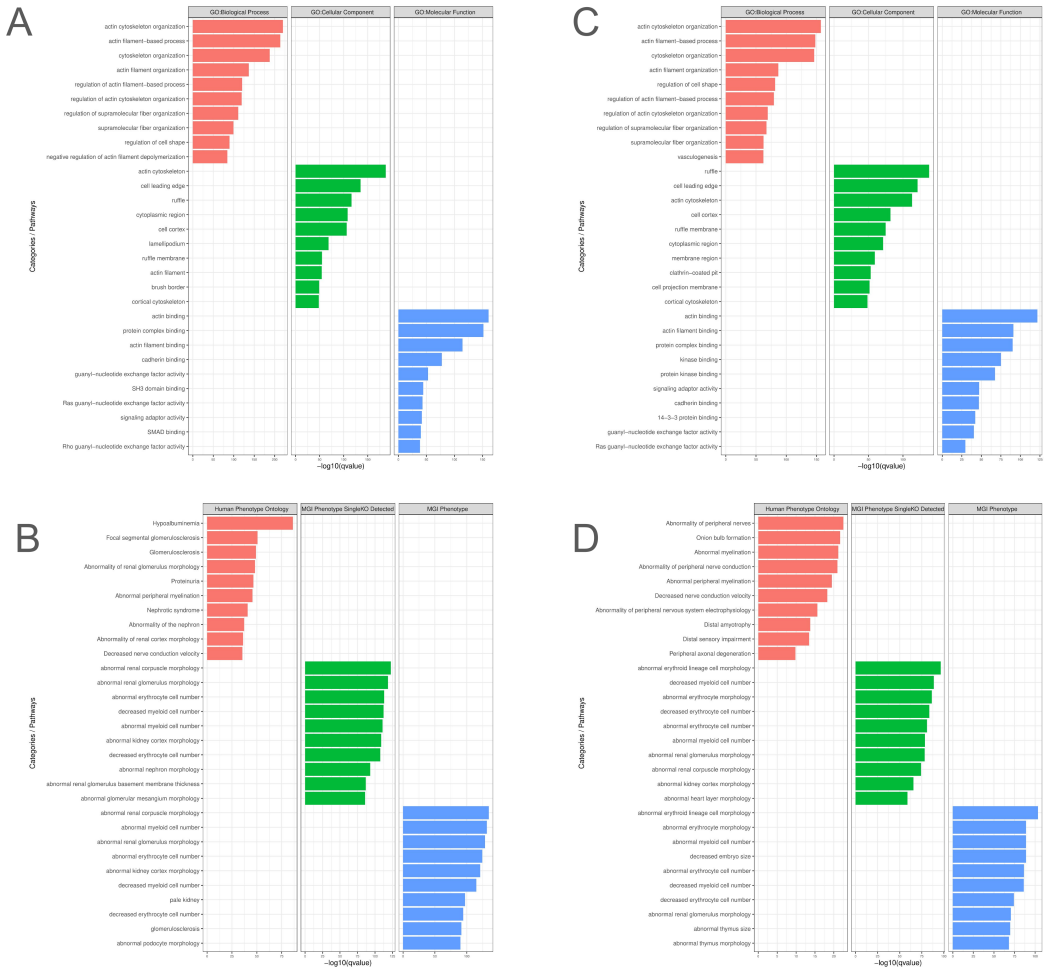

Figure 29: GO and pathway analysis for genes associated with the nearest active enhancers of podocytes from *Nphs2*$^{\mathrm{R231Q/A286V}}$ and *Phb2*$^{\mathrm{pko}}$ models. A. GO analysis based on genes associated with enhancers assigned by GREAT for podocytes from the *Nphs2*$^{\mathrm{R231Q/A286V}}$ model. B. Mammalian phenotype ontology analysis based on genes associated with enhancers assigned by GREAT podocytes from the *Nphs2*$^{\mathrm{R231Q/A286V}}$ model. C. Same as A but from the *Phb2*$^{\mathrm{pko}}$ model. D. Same as B but from the *Phb2*$^{\mathrm{pko}}$ model.

To compare and contrast with wildtype podocyte-specific enhancers, we identified 11089 for wildtype, 11789 for the *Nphs2*$^{\mathrm{R231Q/A286V}}$ model, and 6905 for the *Phb2*$^{\mathrm{pko}}$ model. The number of active enhancers in the *Nphs2*$^{\mathrm{R231Q/A286V}}$ model was comparable to wildtype but less for the *Phb2*$^{\mathrm{pko}}$ model which correlated well with the disease severity. The discrepancy in the number of active enhancers between wildtype and disease may also be explained by the presence of super-enhancers (SEs). There is growing evidence that shows SEs are drivers of gene expression that confer cell type identity and carry disease-associated variants. We defined SEs as a stretch of active enhancers using the Rank Ordering of Super-Enhancers (ROSE) tool independently for wildtype, *Nphs2*$^{\mathrm{R231Q/A286V}}$ and *Phb2*$^{\mathrm{pko}}$ models. We identified 80 SEs in wildtype podocytes, 50 SEs in the *Nphs2*$^{\mathrm{R231Q/A286V}}$ model, and 32 SEs in the *Phb2*$^{\mathrm{pko}}$ model. Unlike regular active enhancers, the majority of SEs was more unique to each model and showed less overlap between different genotypes, suggesting that most SEs may be involved in the maintenance of podocyte specificity or be

implicated in the rewiring of epigenetic regulation in podocyte injury (Figure 30A). Interestingly, the length of classic active enhancers was indistinguishable between different cell types, even between wildtype and different FSGS models, although the length of wildtype SEs was strikingly longer than the lengths of SEs from both disease models suggesting SEs erosion in podocyte disease (Figure 30B).

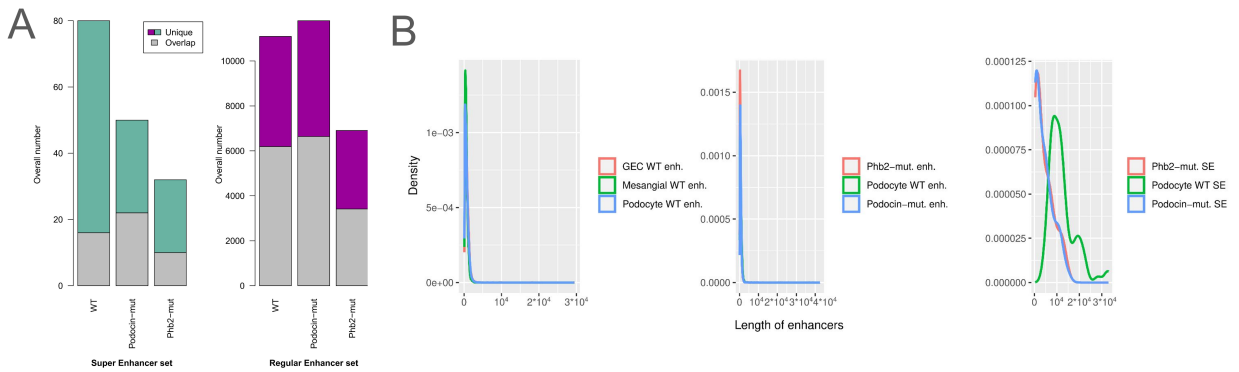

Figure 30: SEs were eroded in *Nphs2*$^{\mathrm{R231Q/A286V}}$ and *Phb2*$^{\mathrm{pko}}$ FSGS models compared to wildtype. A. Overlapping and unique super-enhancers and active enhancers in wildtype, *Nphs2*$^{\mathrm{R231Q/A286V}}$ and *Phb2*$^{\mathrm{pko}}$ models. B. The length of enhancers did not differ between cell types, nor between FSGS models and wildtype, but the length of SEs decreased in FSGS models.

Next, we investigated which histone markers were most differentially regulated upon disease, we performed differential binding analysis for both *Nphs2*$^{\mathrm{R231Q/A286V}}$ and *Phb2*$^{\mathrm{pko}}$ models to wildtype (Figure 31A and B) and the majority of the regular enhancers showed significant changes in chromatin accessibility and acetylation on H3K27, but no changes in methylation on H3K4 and H3K27 suggesting the loss of open chromatin and enhancer activity is primarily associated with podocyte damage but alteration in poised enhancers or repressor region bookmarking were trivial. The podocytes from *Phb2*$^{\mathrm{pko}}$ mice showed more changes in differential binding sites in ATAC-seq and aceytylation at enhancers than that of *Nphs2*$^{\mathrm{R231Q/A286V}}$ mice suggesting the severity of renal burden may be associated with the extent of chromatin reorganization and enhancer degradation (Figure 31A and B). Here, no differential binding was revealed when comparing SEs between wildtype and disease models since eroded enhancers would not be classified as SE by the ROSE tool in the first place.

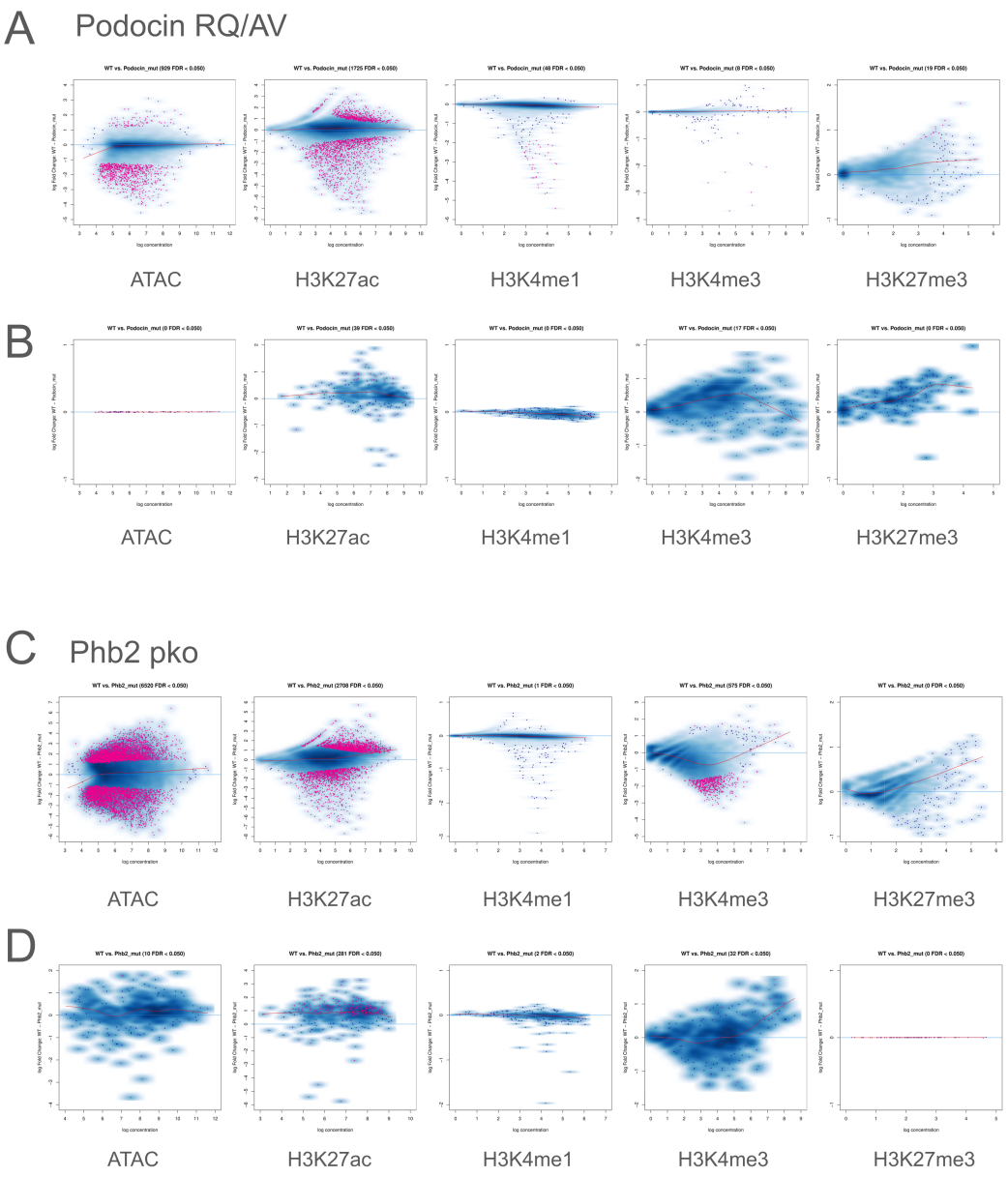

Figure 31: Differential binding analysis showed changes in open chromatin and acetylation on H3K27 between wildtype and *Nphs2*$^{\mathrm{R231Q/A286V}}$ and *Phb2*$^{\mathrm{pko}}$ FSGS models. A. MA plot displaying differential binding sites of regular enhancers in the open chromatin regions, for H3K27ac, H3K4me1, H3K4me3 and H3K27me3 between wildtype and the *Nphs2*$^{\mathrm{R231Q/A286V}}$ model. B. MA plot displaying differential binding sites of regular enhancers in the open chromatin regions, for H3K27ac, H3K4me1, H3K4me3 and H3K27me3 between wildtype and the *Phb2*$^{\mathrm{pko}}$ model. C. Same as A except for SEs. D. Same as B except for SEs.

6.2.3 Putative differential TF binding within differentially regulated enhancers implies a potential transition in TF switching during disease

Next, we analyzed the potential binding of TFs to the differential binding sites of regular enhancer regions in wildtype and disease models (Figure 32). Within the enhancer regions that were hyperacetylated in both *Nphs2*$^{\mathrm{R231Q/A286V}}$ and *Phb2*$^{\mathrm{pko}}$ models, there was putative binding of AP1 and Jun class TFs wherein

the enhancer regions that were more deacetylated and less active, there was a loss of binding for Tead and Lhx class TFs. There were subtle differences between enhancers that were hyperacetylated in the *Nphs2*$^{\mathrm{R231Q/A286V}}$ model but hypoacetylated in the *Phb2*$^{\mathrm{pko}}$ model or vice versa, where either condition showed putative binding for Tead and myogenic regulatory factors (MRFs) family TFs. The former also showed additional enrichment for NUR77, ERRA, AP4, EGR, and ZNF143 whereas the latter showed a preference for CHOP, ATF4, TBET, AP1, HAND2 and NF1 TFs indicating clear differences in the differential binding sites between these models and potential model-specific TF binding regulation of disease podocytes.

A

Rank	Motif	Name	P-value	log P-pvalue	q-value (Benjamini)	# Target Sequences with Motif	% of Targets Sequences with Motif	# Background Sequences with Motif	% of Background Sequences with Motif
1		AP-1(bZIP)/ThioMac-PU.1-ChIP-Seq(GSE21512)/Homer	1e-37	-8.599e+01	0.0000	140.0	65.42%	11796.8	23.76%
2		Fra2(bZIP)/Striatum-Fra2-ChIP-Seq(GSE43429)/Homer	1e-36	-8.497e+01	0.0000	113.0	52.80%	7492.2	15.09%
3		JunB(bZIP)/DendriticCells-Junb-ChIP-Seq(GSE36099)/Homer	1e-35	-8.251e+01	0.0000	119.0	55.61%	8595.0	17.31%
4		Fra1(bZIP)/BT549-Fra1-ChIP-Seq(GSE46166)/Homer	1e-35	-8.096e+01	0.0000	118.0	55.14%	8575.0	17.27%
5		Atf3(bZIP)/GBM-ATF3-ChIP-Seq(GSE33912)/Homer	1e-34	-8.021e+01	0.0000	128.0	59.81%	10265.3	20.67%
6		Fosl2(bZIP)/3T3L1-Fosl2-ChIP-Seq(GSE56872)/Homer	1e-34	-8.011e+01	0.0000	95.0	44.39%	5409.0	10.89%
7		BATF(bZIP)/Th17-BATF-ChIP-Seq(GSE39756)/Homer	1e-34	-7.884e+01	0.0000	127.0	59.35%	10229.3	20.60%
8		Jun-AP1(bZIP)/K562-cJun-ChIP-Seq(GSE31477)/Homer	1e-31	-7.294e+01	0.0000	78.0	36.45%	3840.8	7.73%
9		Bach2(bZIP)/OCILy7-Bach2-ChIP-Seq(GSE44420)/Homer	1e-17	-4.036e+01	0.0000	56.0	26.17%	3442.6	6.93%
10		TEAD(TEA)/Fibroblast-PU.1-ChIP-Seq(Unpublished)/Homer	1e-14	-3.333e+01	0.0000	98.0	45.79%	10729.2	21.61%

B

1		TEAD4(TEA)/Tropoblast-Tead4-ChIP-Seq(GSE37350)/Homer	1e-19	-4.496e+01	0.0000	298.0	43.57%	13376.5	27.19%
2		TEAD(TEA)/Fibroblast-PU.1-ChIP-Seq(Unpublished)/Homer	1e-15	-3.550e+01	0.0000	241.0	35.23%	10674.5	21.70%
3		TEAD2(TEA)/Py2T-Tead2-ChIP-Seq(GSE55709)/Homer	1e-15	-3.519e+01	0.0000	203.0	29.68%	8438.3	17.15%
4		Lhx1(Homeobox)/EmbryoCarcinoma-Lhx1-ChIP-Seq(GSE70957)/Homer	1e-13	-3.189e+01	0.0000	331.0	48.39%	16817.5	34.19%
5		Lhx2(Homeobox)/HFSC-Lhx2-ChIP-Seq(GSE48068)/Homer	1e-12	-2.769e+01	0.0000	316.0	46.20%	16298.4	33.13%
6		FOXM1(Forkhead)/MCF7-FOXM1-ChIP-Seq(GSE72977)/Homer	1e-11	-2.541e+01	0.0000	321.0	46.93%	16917.5	34.39%
7		Tcf21(bHLH)/ArterySmoothMuscle-Tcf21-ChIP-Seq(GSE61369)/Homer	1e-10	-2.497e+01	0.0000	307.0	44.88%	16030.7	32.59%
8		MafA(bZIP)/Islet-MafA-ChIP-Seq(GSE30298)/Homer	1e-10	-2.481e+01	0.0000	276.0	40.35%	13998.2	28.46%
9		FOXA1(Forkhead)/MCF7-FOXA1-ChIP-Seq(GSE26831)/Homer	1e-10	-2.370e+01	0.0000	305.0	44.59%	16059.7	32.65%
10		Lhx3(Homeobox)/Neuron-Lhx3-ChIP-Seq(GSE31456)/Homer	1e-10	-2.315e+01	0.0000	406.0	59.36%	23175.1	47.11%

C

Rank	Motif	Name	P-value	log P-pvalue	q-value (Benjamini)	# Target Sequences with Motif	% of Targets Sequences with Motif	# Background Sequences with Motif	% of Background Sequences with Motif
1		Nur77(NR)/K562-NR4A1-ChIP-Seq(GSE31363)/Homer	1e-10	-2.420e+01	0.0000	32.0	26.23%	3422.1	6.86%
2		TEAD4(TEA)/Tropoblast-Tead4-ChIP-Seq(GSE37350)/Homer	1e-5	-1.253e+01	0.0007	58.0	47.54%	13965.7	28.01%
3		TEAD(TEA)/Fibroblast-PU.1-ChIP-Seq(Unpublished)/Homer	1e-4	-1.048e+01	0.0034	47.0	38.52%	10983.2	22.03%
4		Erra(NR)/HepG2-Erra-ChIP-Seq(GSE31477)/Homer	1e-4	-1.015e+01	0.0035	98.0	80.33%	31622.8	63.42%
5		TEAD2(TEA)/Py2T-Tead2-ChIP-Seq(GSE55709)/Homer	1e-4	-9.941e+00	0.0035	40.0	32.79%	8878.0	17.81%
6		Ap4(bHLH)/AML-Tfap4-ChIP-Seq(GSE45738)/Homer	1e-4	-9.749e+00	0.0035	73.0	59.84%	20976.0	42.07%
7		MyoD(bHLH)/Myotube-MyoD-ChIP-Seq(GSE21614)/Homer	1e-3	-8.990e+00	0.0065	54.0	44.26%	14120.0	28.32%
8	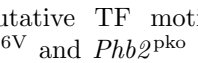	MyoG(bHLH)/C2C12-MyoG-ChIP-Seq(GSE36024)/Homer	1e-3	-8.706e+00	0.0075	66.0	54.10%	18783.2	37.67%
9	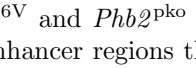	Egr1(Zf)/K562-Egr1-ChIP-Seq(GSE32465)/Homer	1e-3	-8.685e+00	0.0075	41.0	33.61%	9720.1	19.49%
10	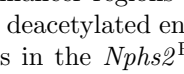	ZNF143|STAF(Zf)/CUTLL-ZNF143-ChIP-Seq(GSE29600)/Homer	1e-3	-8.211e+00	0.0099	32.0	26.23%	6985.5	14.01%

D

1		TEAD(TEA)/Fibroblast-PU.1-ChIP-Seq(Unpublished)/Homer	1e-5	-1.293e+01	0.0009	24.0	55.81%	11236.1	22.57%
2	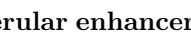	TEAD4(TEA)/Tropoblast-Tead4-ChIP-Seq(GSE37350)/Homer	1e-5	-1.213e+01	0.0010	26.0	60.47%	13599.9	27.32%
3	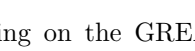	Chop(bZIP)/MEF-Chop-ChIP-Seq(GSE35681)/Homer	1e-5	-1.175e+01	0.0010	12.0	27.91%	3081.1	6.19%
4	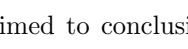	TEAD2(TEA)/Py2T-Tead2-ChIP-Seq(GSE55709)/Homer	1e-5	-1.152e+01	0.0010	20.0	46.51%	8667.8	17.41%
5		Atf4(bZIP)/MEF-Atf4-ChIP-Seq(GSE35681)/Homer	1e-4	-1.094e+01	0.0013	13.0	30.23%	3935.8	7.91%
6		Tbet(T-box)/CD8-Tbet-ChIP-Seq(GSE33802)/Homer	1e-3	-8.621e+00	0.0109	28.0	65.12%	18473.9	37.11%
7		CEBP-AP1(bZIP)/ThioMac-CEBPb-ChIP-Seq(GSE21512)/Homer	1e-3	-7.178e+00	0.0397	20.0	46.51%	11668.8	23.44%
8		MyoG(bHLH)/C2C12-MyoG-ChIP-Seq(GSE36024)/Homer	1e-2	-6.657e+00	0.0585	25.0	58.14%	17176.7	34.51%
9		Hand2(bHLH)/Mesoderm-Hand2-ChIP-Seq(GSE61475)/Homer	1e-2	-5.514e+00	0.1629	16.0	37.21%	9461.4	19.01%
10		NF1(CTF)/LNCAP-NF1-ChIP-Seq(Unpublished)/Homer	1e-2	-5.064e+00	0.2300	12.0	27.91%	6364.0	12.78%

Figure 32: Putative TF motif analysis within differentially acetylation regulatory regions of the *Nphs2*$^{\mathrm{R231Q/A286V}}$ and *Phb2*$^{\mathrm{pko}}$ FSGS models compared to wildtype. A. TF motif enrichment within hyperacetylated enhancer regions than wildtype in both *Nphs2*$^{\mathrm{R231Q/A286V}}$ and *Phb2*$^{\mathrm{pko}}$ models. B. Same as A except within deacetylated enhancer regions in both models. C. Same as A except within hyperacetylated enhancer regions in the *Nphs2*$^{\mathrm{R231Q/A286V}}$ but deacetylated in the *Phb2*$^{\mathrm{pko}}$ model. D. same as A except within deacetylated enhancer regions in the *Nphs2*$^{\mathrm{R231Q/A286V}}$ but hyperacetylated in the *Phb2*$^{\mathrm{pko}}$ model.

6.2.4 Glomerular enhancer-promoter loops pinpointed key enhancer-genes pairs in podocytes

Instead of relying on the GREAT algorithm to assign enhancer-gene pair which is predicted purely by proximity, we aimed to conclusively identify the target genes of specific enhancers by empirically pulling

down the promoter of all genes crosslinked to its interacting enhancers by performing Hi-ChIP using H3K27ac using wildtype isolated glomeruli. We identified looping events between enhancers and promoters and used the interacting anchors to tether and assign enhancers to their factual target genes. The input H3K27ac control served as a secondary method that verified the cell-type specific enhancers determined by CUT&Tag and ATAC-seq, and Hi-ChIP enabled the generation of a genome-wide 3D chromatin interaction map that showed distal looping events from the podocyte-specific enhancers or SEs to the promoters at genes of interests, for example, Wt1, Podxl and *Actn4* (Figure 33A, B and C).

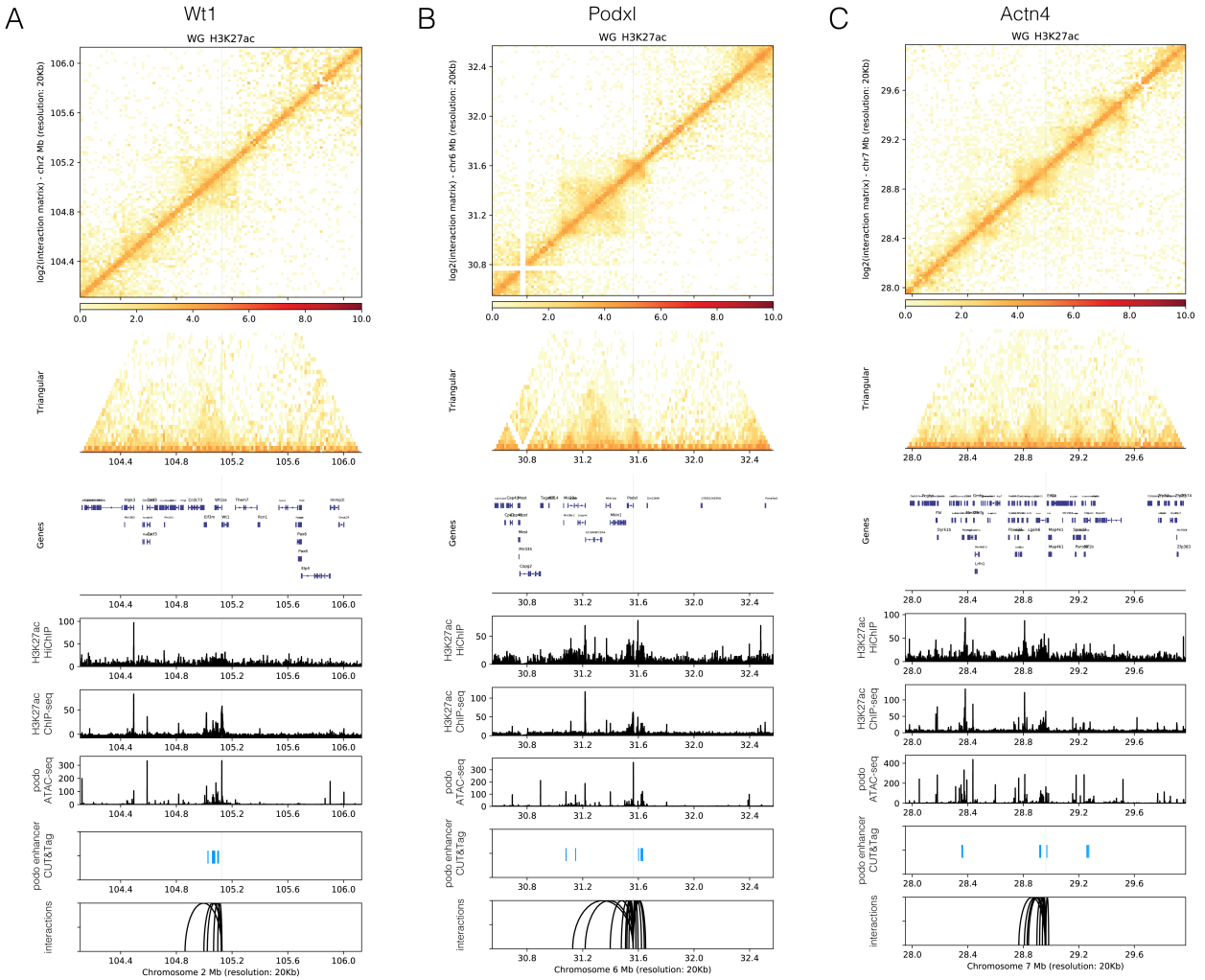

Figure 33: Glomerular HiChIP of H3K27ac identifies target genes of podocyte-specific enhancers. Interaction map of H3K27ac at Wt1 (A), Podxl (B), and *Actn4* (C) loci and corresponding peaks of H3K27ac ChIP-seq, ATAC-seq and podocyte-specific enhancer peaks and loop interactions.

6.2.5 Disease-associated target genes of enhancer or SEs revealed key pathways related to podocyte disease

To evaluate whether the changes in podocyte-specific enhancers can be functionally correlated with the changes in gene expression of their target genes, we utilized the snRNA-seq of the *Nphs2*$^{R231Q/A286V}$ model already described in Figure 4, and additionally performed snRNA-seq from isolated glomeruli us-

ing the *Phb2*$^{\text{pko}}$ model to examine the changes in target gene expression both models. Similar to the *Nphs2*$^{\text{R231Q/A286V}}$ model, we also identified the major cell types within the glomerulus including podocytes, GECs and mesangial cells in the *Phb2*$^{\text{pko}}$ model suggesting correct glomeruli isolation and nuclei isolation (Figure 34A), and cell type-specific marker genes such as *Nphs2*, *Lmx1b*, Wt1, *Nphs1*, Gata2, Gata3, Gata5 and Pecam1 were used to determine the cell type of each cluster (Figure 34B).

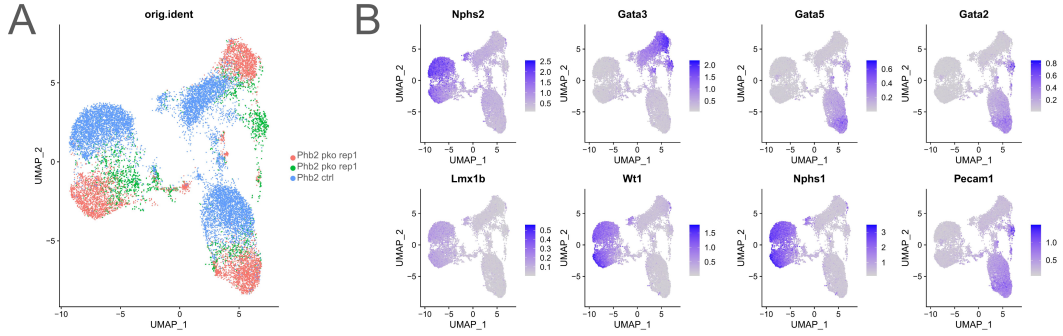

Figure 34: snRNA-seq of the *Phb2*$^{\text{pko}}$ model revealed distinct populations of glomerular cell types and shifts in global transcriptional expression in Phb2 pko mice compared to control. A. UMAP of all cells from Phb2 pko mice and control. B. Dimplot of *Nphs2*, *Lmx1b*, Gata3, Wt1, Gata5, *Nphs1*, Gata2 and Pecam1 to determine the cell type of each cluster.

To examine the functional consequences of the loss of enhancer activity in the disease models, we correlated the changes in the gene expression of the target genes to their respective differentially acetylated active enhancers or SEs in each model. The target gene sets were used for pathway analysis and the top 10 pathways were illustrated in cord plots (Figure 35 and 36). Generally, the upregulation of acetylation or enhancer activity correlated with the upregulation of target gene expression, whereas the loss of enhancer activity led to the downregulation of target genes for deacetylated enhancers. Owing to the larger number of deacetylated enhancers in the *Phb2*$^{\text{pko}}$ model compared to *Nphs2*$^{\text{R231Q/A286V}}$ model, a larger number of target genes were downregulated. Some common pathways regulated by the target genes such as EGFR1, VEGFA-VEGFR2 signaling and RHO GTPase cycle were shared between both models suggesting convergence to common downstream effectors or signaling pathways despite differential regulation of enhancers upstream of gene regulation. The discrepancy in the inverse correlation between enhancer activity and target gene expression for some genes may be explained by the regulation of the same target genes by multiple enhancers. For instance, *Nrp1* and *Nck2* both harbor hyper- and de-acetylated enhancers even though the genes themselves were downregulated in the *Phb2*$^{\text{pko}}$ model. The number of target genes and pathways inferred from SEs in each model was less than that of regular enhancers primarily due to the limited number of podocyte-specific SEs in each model. Despite this, the findings resonate with the previously mentioned conclusions, underscoring the distinctions in the regulation of target genes by model-specific SEs in diseased podocytes. This emphasizes the critical importance of preserving the integrity of enhancer activity for the maintenance of healthy podocytes.

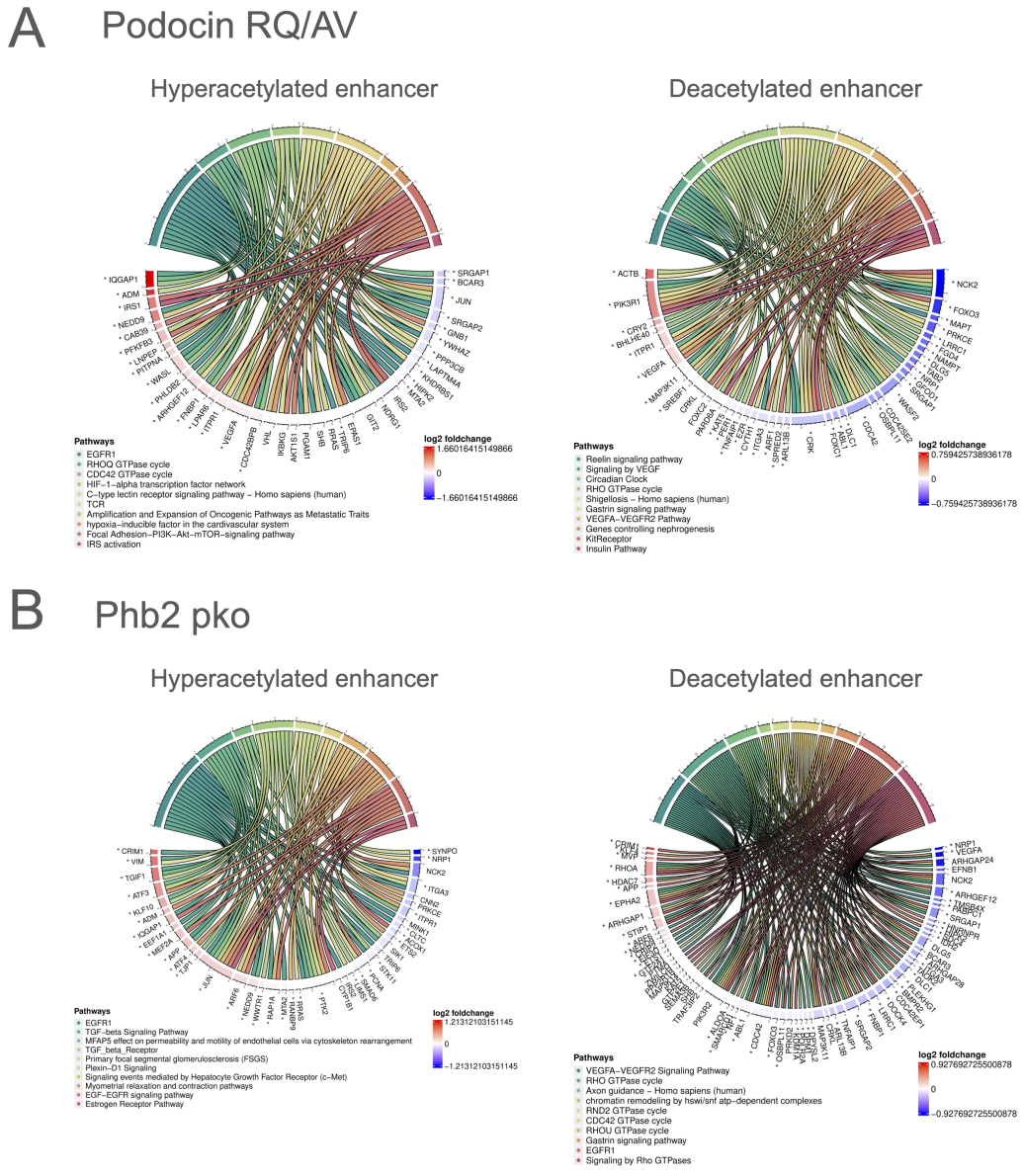

Figure 35: Cord plots of acetylated and deacetylated enhancer target genes in *Nphs2*$^{\mathrm{R231Q/A286V}}$ and *Phb2*$^{\mathrm{pko}}$ models. A. Hi-ChIP target genes of hyperacetylated enhancers region in the *Nphs2*$^{\mathrm{R231Q/A286V}}$ model. The blue-red colored heatmap represents the log2fc of gene expression. Significantly differentially expressed genes are labeled with an asterisk. B. Same as A except for deacetylated enhancers. C. Same as A except for the *Phb2*$^{\mathrm{pko}}$ model. D. Same as B except for the *Phb2*$^{\mathrm{pko}}$ model.

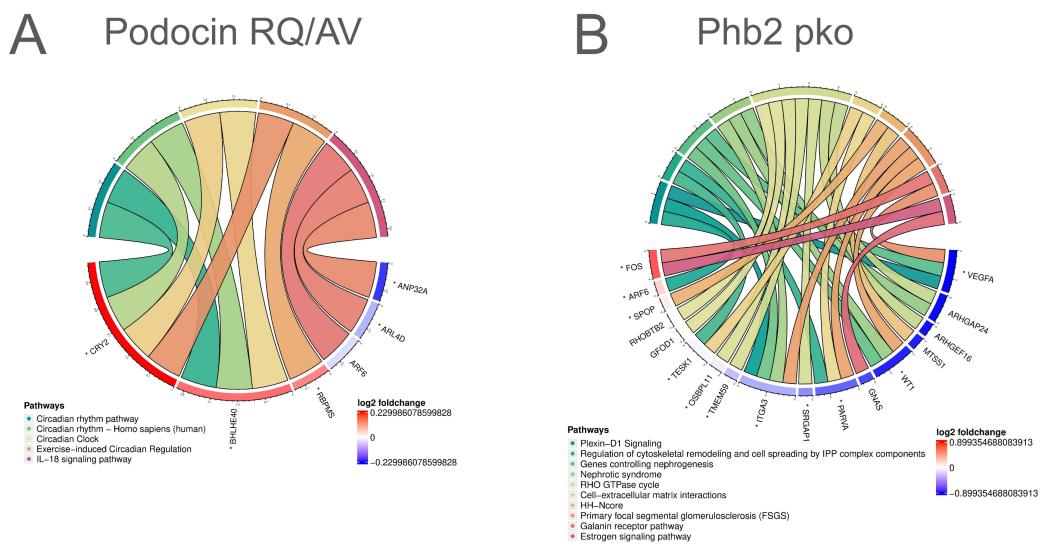

Figure 36: Cord plots of deacetylated SEs target genes in *Nphs2*$^{\mathrm{R231Q/A286V}}$ and *Phb2*$^{\mathrm{pko}}$ models.

6.3 Characterization of the function and molecular mechanism of *Lmx1b*

6.3.1 Phenotyping of the tamoxifen-inducible podocyte-specific *Lmx1b* deletion mice

We aim to more comprehensively characterize the roles of *Lmx1b* in podocytes and utilized a published tamoxifen-inducible conditional knockout of *Lmx1b* in podocytes (*Lmx1b*-ipko) mouse model that had previously been shown to cause an FSGS phenotype [110]. Similar to Burghardt et al., these mice showed similar renal and glomerular pathology upon induction. Control and experimental mice were fed *ad libitum* for short (6-day), medium (10-day) or long (14-day) durations using a tamoxifen-containing diet to induce gradual deletion of *Lmx1b* from podocytes and to simulate progressive development of FSGS. At the end of tamoxifen induction, urines and kidneys were collected from sacrificed animals before tissues were processed for histological analysis by PAS staining, STED microscopy and EM imaging to determine the extent of glomerular damage (Figure 37A). In order to assess functional levels of podocyte damage, albuminuria was quantified from urines qualitatively by Coomassie staining and quantitatively by ELISA. In both methods, weak proteinuria in mice was observed after 10-day and strong and significant levels of proteinuria after 14-day tamoxifen induction compared to the control (Figure 37B anc C). To verify the knockout, we performed immunofluorescence microscopy and *Lmx1b* showed specific co-localization with Wt1 in the podocyte nuclei but decreased protein expression in parts of the damaged glomeruli at 14-day in *Lmx1b*-ipko mice (Figure 37D). We further characterized the degrees of renal damage by PAS but there was no identifiable glomerular damage except in 14-day *Lmx1b*-ipko mice (Figure 37E). Furthermore, we used EM to verify the glomerular damage and observed clear podocyte effacement in 14-day *Lmx1b*-ipko mice (Figure 37F).

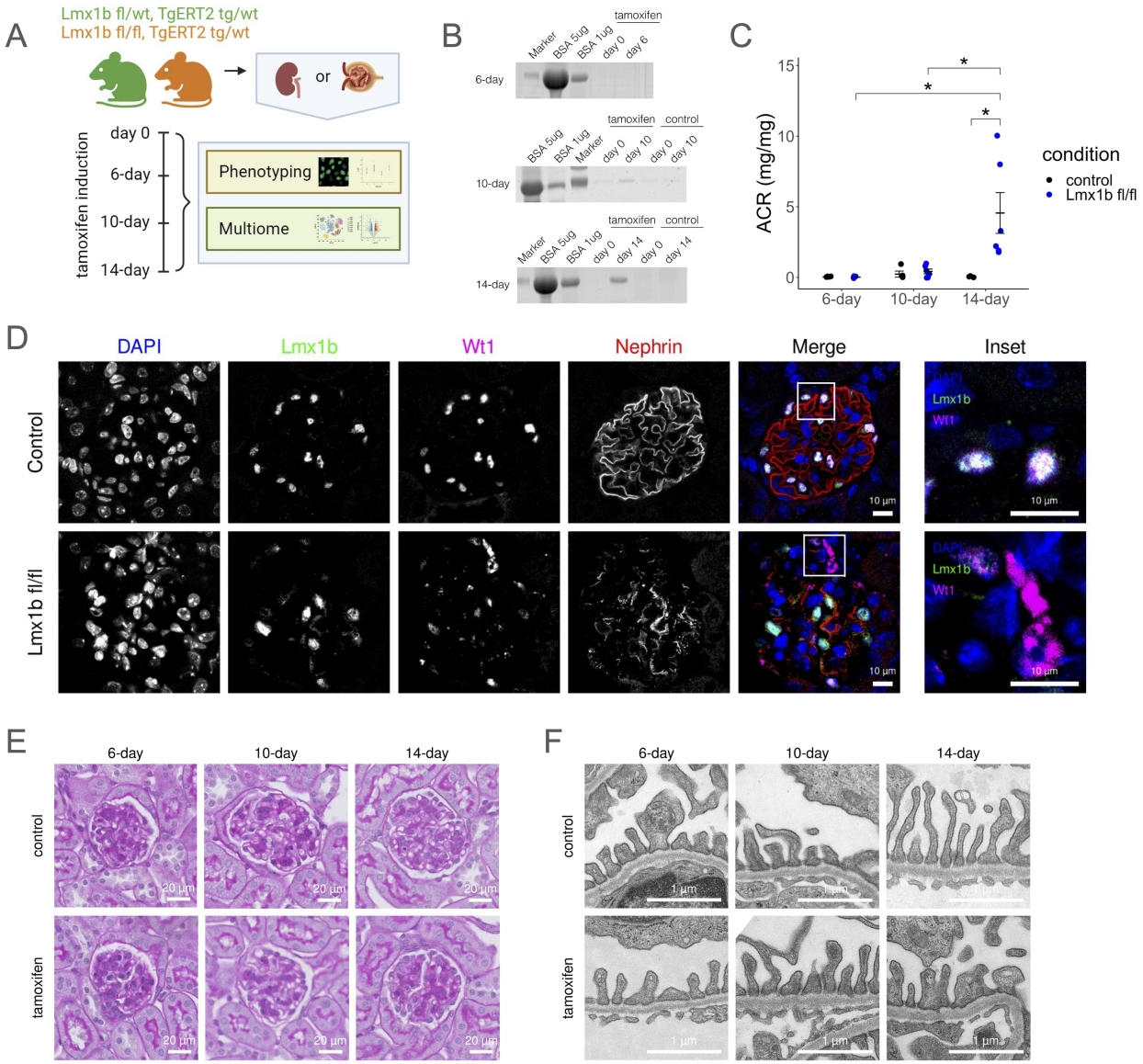

Figure 37: Phenotyping of tamoxifen-induced podocyte-specific *Lmx1b*-ipko mice showed FSGS-like phenotype and affected podocyte slit diaphragm. A. Schematic of the experimental setup. Tamoxifen-inducible podocyte-specific *Lmx1b* flox; TgERT2:cre control or experimental (*Lmx1b*-ipko) mice were treated with tamoxifen diet for 6, 10 or 14 days prior to sacrifice and tissue collection for phenotyping and 10X Multiome analysis. B. Coomassie blue staining revealed a time-dependent increase in proteinuria from 6-day, 10-day to 14-day upon tamoxifen treatment. Weak and more pronounced proteinuria were observed at 10-day and 14-day respectively. C. ACR (mg/mg) at day 6, 10, or 14 post tamoxifen induction was determined from urines collected from control or experimental animals and showed a progressive increase in *Lmx1b*-ipko mice compared to control. Error bars are mean +/- SEM. D. IF staining of *Lmx1b* on kidney tissues of *Lmx1b*-ipko mice at 14-day timepoint showed *Lmx1b* co-localization with Wt1 in podocyte nuclei and decreased protein expression in the damaged glomeruli in *Lmx1b*-ipko mice. E. PAS staining of kidney tissues at 6-day, 10-day and 14-day timepoints showed FSGS lesions in the glomerulus in *Lmx1b*-ipko mice versus control. F. Electron microscopy of kidney tissues at 6-day, 10-day and 14-day timepoints showed effacement of podocyte foot processes in *Lmx1b*-ipko mice versus control.

Owing to the lack of quantitative assessments of the slit diaphragm offered by PAS staining and EM

ultrastructural imaging, we used STED super-resolution microscopy to characterize the integrity of the podocyte slit diaphragm by staining for podocin and nephrin at all timepoints (Figure 38A). The length of the podocyte slit diaphragm can be quantified by segmenting the podocyte foot processes based on nephrin or podocin staining as slit length/area using the macros developed in [14] . The length of slits correlates with proteinuria [14]. We are the first to show by STED, that various degrees of podocyte damage were observed along FSGS progression at the level of a single glomerulus, and the differences in average slit length even differed within the same glomerulus. The gradual changes to the slit diaphragm upon *Lmx1b* loss-of-function resulted in a heterogeneous presentation characteristic of FSGS, where the changes in the average slit diaphragm length at the capillary were observed in 10-day and 14-day *Lmx1b*-ipko mice. There was no statistical difference between control and *Lmx1b*-ipko mice at 6-day but a significant decrease in slit length/area was seen at the 10-day and the 14-day timepoint. Within the tamoxifen treatment group, there was a significant decrease in slit length/area from 6-day to 14-day, and showed a progressive decline in podocyte slit diaphragm length over time (Figure 38B). Compared to conventional phenotyping using PAS or EM ultramicroscopy in Burghardt et al., STED microscopy offered a more quantitative assessment of the gradual loss of the integrity of the glomerulus and the slit diaphragm upon *Lmx1b* knockout. Interestingly, STED images used for slit diaphragm length quantification suggested a significant decrease of nephrin and podocin protein concentrations at the SD upon *Lmx1b* knockout (Figure 38A). As *Nphs2*, the gene coding for podocin, has been confirmed as a direct target of *Lmx1b* though not *Nphs1*, the gene encoding nephrin [111] Both nephrin and podocin are core components of the slit diaphragm signaling complex, and their signal intensities in STED images were quantified. The expression of podocin showed a significant decrease between *Lmx1b*-ipko and control animals at all timepoints (Figure 38C), whereas the expression of nephrin only showed a significant decrease between *Lmx1b*-ipko and control animals at 14-day (Figure 38D). This is in line with *Lmx1b* directly targeting *Nphs2* but not *Nphs1* though a presumably secondary decrease of nephrin signals at the SD becomes evident at later timepoints. In conclusion, nephrin and podocin quantification at the SD in our model corroborated an activating function of *Lmx1b* on *Nphs2* expression, rendering *Nphs2* a readout for *Lmx1b* activity on the RNA and protein level.

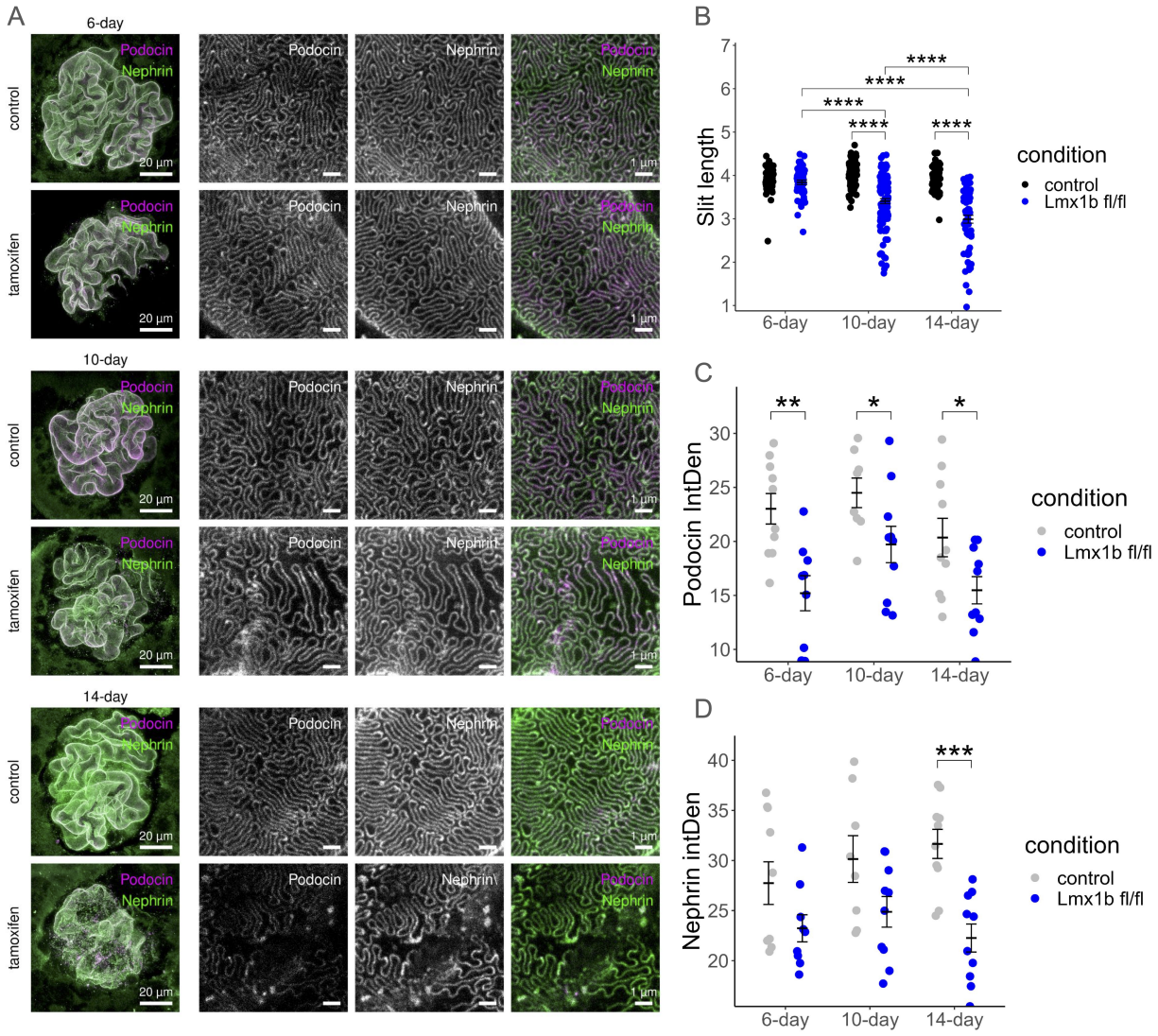

Figure 38: The slit length, and the expression of nephrin and podocin, decreased after tamoxifen induction. A. STED microscopy of nephrin and podocin showed progressive changes in slit diaphragm morphology from 6-day to 14-day versus control. Left: images of the whole glomerulus. B. Quantification of the slit diaphragm length/area from F showed a significant decrease in slit length in *Lmx1b*-ipko mice at 10-day and 14-day. C. Quantification of podocin fluorescence intensity from F showed a significant decrease in podocin intensity at all timepoints. D. Quantification of nephrin fluorescence intensity from F showed a significant decrease in nephrin tensity at 14-day timepoint.

6.3.2 10X Single Cell Multiome of *Lmx1b*-ipko glomeruli revealed dysregulation in non-canonical Wnt signaling and TF class switching in podocytes

Next, we investigated why podocytes displayed such variable degrees of damage within the same glomerulus and aimed to elucidate the role of *Lmx1b* on transcription regulation of gene expression and active regulatory sequences in the podocyte genomes using single-cell approaches. By delineating the gene regulatory programs underlying podocytes in *Lmx1b*-ipko mice, we aimed to gain a fundamental understanding of the function of *Lmx1b* in the pathophysiology of FSGS. We took advantage of the 10X Single Cell Multiome platform to examine the glomerular regulome by probing changes in gene expression and chromatin conformation

at single-cell resolution using snRNA-seq and snATAC-seq from the same nucleus. Similar to phenotyping, control or experimental *Lmx1b*-ipko mice were induced with tamoxifen for 6-day, 10-day or 14-day, and single nuclei were prepared from isolated glomeruli and processed for 10X Single Cell Multiome ATAC and Gene Expression protocol prior to analysis.

Cells from all samples were clustered and annotated based on gene expression of marker genes, both gene expression and DNA accessibility measurements were represented in the joint UMAP (Figure 39A). Major glomerular cells including podocytes (30.44 %), endothelial cells (38.08 %) and mesangial cells (17.81 %) formed the largest clusters in the datasets. Other cell types that were also profiled include distal tubule cells (7.60 %), immune cells (0.87 %), the Loop of Henle cells (1.26 %), principal cells (0.57 %), proximal tubules cells (1.68 %), renal interstitium (0.21 %), renal vesicle cells (1.21 %) and β-intercalated cells (0.25 %). Unbiased clustering revealed major cell types of the glomerulus in expected proportions demonstrating the purity of the isolated glomeruli fractions and the efficiency of our nuclei isolation method.

Since *Lmx1b* is podocyte-specific, podocytes were selected, subsetted, and reclustered for further analysis. Two subclusters of podocytes were revealed and the majority of cells from cluster 1 came exclusively from *Lmx1b*-ipko animals but not from control (Figure 39B). We suspected that cells from cluster 1 were transcriptionally and epigenetically different from cluster 0 likely due to *Lmx1b* deletion. To verify the knockout of *Lmx1b* on a multiome level, we observed the down-regulation of *Nphs2*, a target gene of *Lmx1b*, in cluster 1 (Figure 39C). Additionally, we performed motif footprinting in accessible chromatin regions and *Lmx1b* motifs itself was down-regulated in cluster 1 (Figure 39D). Taken together, the cells that originated from cluster 1 were re-annotated as sick podocytes and those from cluster 0 were re-annotated as healthy podocytes. To confirm, the podocyte cell number of these clusters was quantified over the tamoxifen induction time course, and showed a time-dependent increase in the number of the sick podocytes along FSGS progression (Figure 39E), demonstrating persisting and increasing podocyte injury linked to the loss of *Lmx1b*.

To determine the gene- and chromatin-regulatory consequences of *Lmx1b* loss-of-function, we carried out differential expression gene (DEGs) analysis using snRNA-seq between healthy and sick podocytes at each timepoint and revealed 1102, 598, and 401 DEGs at 6-day, 10-day and 14-day respectively. We also carried out differentially accessible regions (DARs) analysis using snATAC-seq between the two populations of podocytes and revealed 26786, 25551, and 21986 DARs at 6-day, 10-day and 14-day respectively (Figure 39F). Both differential analyses on the level of snRNA-seq and snATAC-seq suggest significant rewiring of the transcriptome and epigenome upon *Lmx1b* deletion.

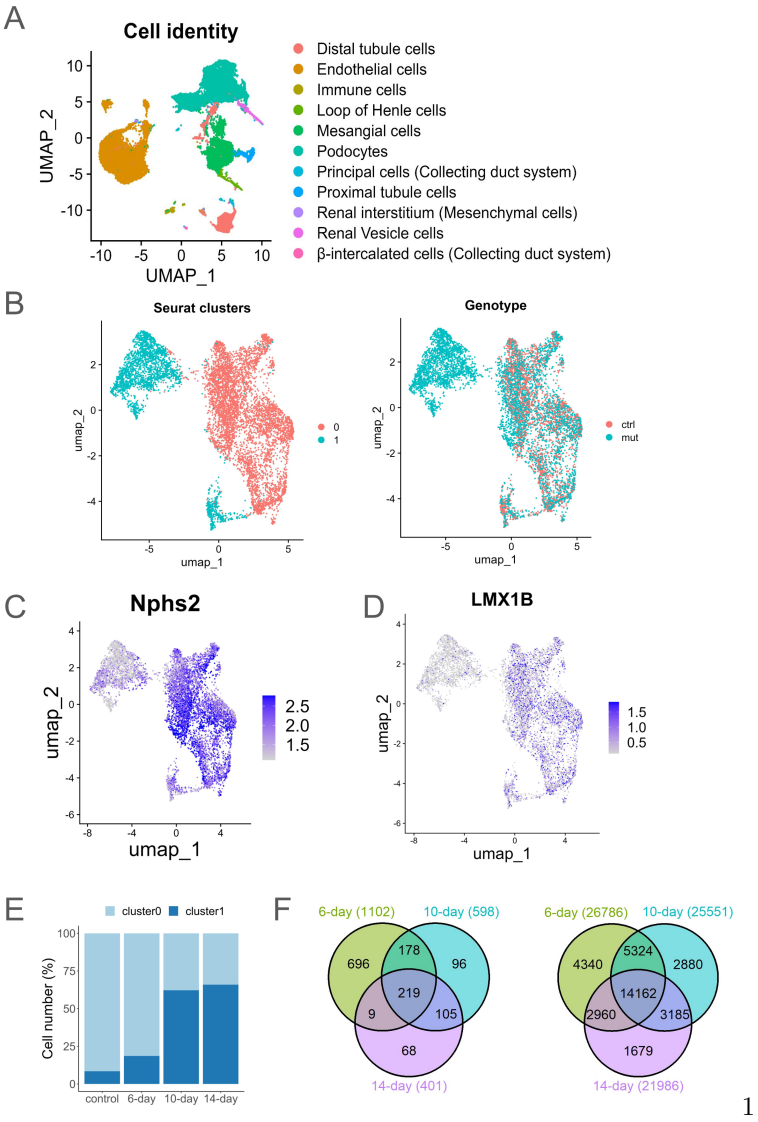

Figure 39: Single nuclei multiomic analysis of *Lmx1b*-ipko podocytes revealed time-dependent differential regulation of the non-canonical Wnt signaling pathway and transcription factor class switching in the open chromatin. A. UMAP of all cells from 6-day, 10-day and 14-day timepoints by cell type. B. (Left) UMAP of podocytes from 6-day, 10-day and 14-day timepoints by Seurat clusters. (Right) UMAP of podocytes from 6-day, 10-day and 14-day timepoints by genotype. A distinct cluster of podocytes was revealed to be contributed by cells exclusively from *Lmx1b*-ipko experimental mice. C. UMAP of the gene expression of *Nphs2* in all podocytes. D. UMAP of the motif enrichment of *Lmx1b* in all podocytes. E. Proportion of the number of podocytes contributed by cluster 0 or cluster 1. Cluster 0 was re-annotated as healthy podocytes and cluster 1 was re-annotated as sick podocytes. F. (Left) Venn diagram of differentially expressed genes (DEGs) between sick and healthy podocytes in 6-day, 10-day and 14-day timepoints. Significantly differentially regulated genes were defined as log2FC.threshold = 0.25 and FDR < 0.01. (Right) Venn diagram of differentially accessible regions (DARs) between sick and healthy podocytes in 6-day, 10-day and 14-day timepoints. Significantly differentially accessible regions were defined as log2FC.threshold = 0.4 and FDR < 0.05.

To evaluate the impact of *Lmx1b* deletion on the chromatin landscape, the genes linked to open or closed DARs were determined by correlating gene expression with accessibility at nearby peaks. Generally, genes

showed increased open chromatin at earlier timepoints but were associated with closed chromatin at later stages of FSGS (Figure 40A), suggesting that *Lmx1b* may be implicated in the maintenance of chromatin organization in podocytes. To investigate which TFs have substituted for the absence of *Lmx1b* in disease podocytes during chromatin reorganization, we further analyzed the TF motifs that were enriched within the open chromatin regions between healthy and sick podocytes and identified clear TF class switching within accessible chromatin. All mammalian transcription factors were extracted from the JASPAR database and filtered for expression in podocytes using snRNA-seq. The TFs were further categorized by TF class based on motif similarity before ranking by log2fc of motif enrichment. The motifs of TFs belonging to the Homeo domain factors, ARID, TEAD domain factors, and forkhead/winged helix factors were enriched in healthy podocytes. LMX1B is a homeodomain factor. ARID3A has been implicated in nephric tubule regeneration but its role in podocytes has not been described [229]. TEAD1 is TEAD domain transcription factor and is a major effector of the Hippo signaling pathway [43]. FOXC is a Fork head/winged helix transcription factor that has been confirmed to act with *Lmx1b* to regulate *Nphs2* combinatorial [111]. Whereas, the motifs of TFs from the basic leucine zipper factors, high-mobility group (HMG) domain factors, MADS box factors and nuclear receptors with C4 zinc fingers were more enriched in sick podocytes (Figure 40B). FOS, FOSL1 and JUNB belong to the basic leucine zipper factor class by forming the AP-1 regulator complex and are associated with the progression of immunoglobulin A nephropathy [230, 231, 232]. Sox6 belongs to the HMG domain factor class but has been described in the context of podocyte injury. The role of the myocyte enhancer factor-2 (MEF2) has not been well described in podocytes but may be involved in the Wnt signaling pathway, regulation fo α-actinin-4 by HDACs and glucose metabolism [233, 234, 235]. NR4A1 has been shown to be differentially regulated in IgA nephropathy but its transcriptional roles in podocytes are not clear [236]. Based on snATAC-seq, we demonstrated that the loss of *Lmx1b* in diseased podocytes led to changes in chromatin accessibility and induced open accessibility at differential TF binding sites.

To gain insight into the function of genes controlled by *Lmx1b*, we analyzed the DEGs on the level of gene expression, and the majority of genes expressed in podocytes showed up-regulation at 6-day compared to later stages of FSGS (Figure 40C) suggesting that *Lmx1b* may function as a transcriptional repressor in podocytes though initial damage responses mediated through non-*Lmx1b* dependent pathways may also be captured. The gene ontology (GO) analysis by biological processes of the DEGs between sick vs. healthy podocytes showed various terms that are known to be related to podocyte biology including negative regulation of adherent junction assembly, VEGF-activated platelet-derived growth factor receptor signaling pathway and filtration diaphragm assembly (Figure 40D). Curiously, some terms were related to glomerular mesangial cell development and differentiation at the early 6-day timepoint which may indicate podocyte de-differentiation.

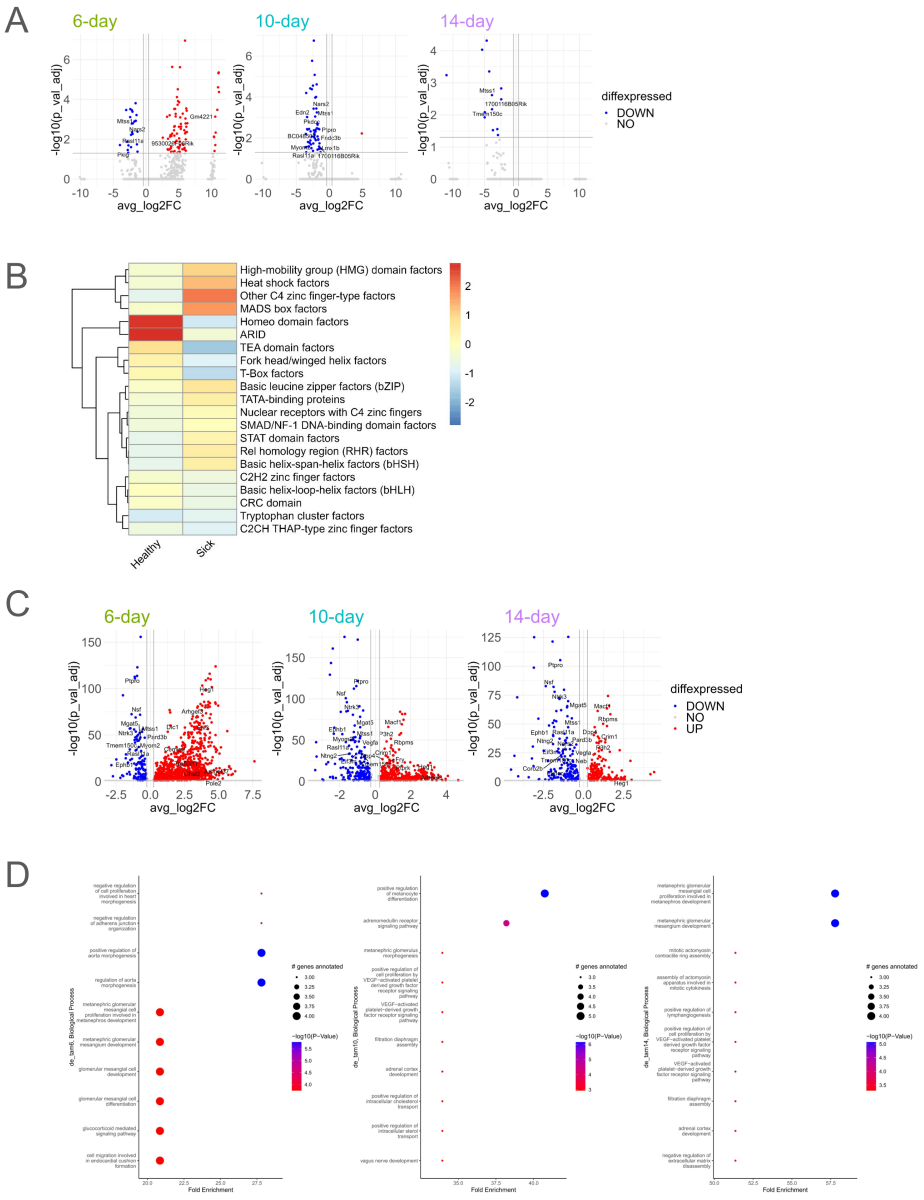

Figure 40: Single nuclei multiomic analysis of *Lmx1b*-ipko podocytes revealed time-dependent differential regulation of the non-canonical Wnt signaling pathway and transcription factor class switching in the open chromatin. A. Volcano plots of DARs (FDR < 0.01) in tamoxifen-induced mice between sick and healthy podocytes. Up-regulated genes are highlighted in red (log2FC > 0.25) and down-regulated genes are highlighted in blue (log2FC < -0.25). DARs that are putative targets of *Lmx1b* are labeled. Most regions are closed at later timepoints. B. Heatmap the fold enrichment of all significantly enriched TF motifs categorized by all classes of TFs annotated by JASPAR. C. Volcano plots of DEGs (FDR < 0.01) in tamoxifen-induced mice between sick and healthy podocytes. Up-regulated genes are highlighted in red (log2FC > 0.25) and down-regulated genes are highlighted in blue (log2FC < -0.25). DEG that are putative targets of *Lmx1b* are labeled. Most differentially regulated genes are up-regulated at earlier timepoints and down-regulated at later timepoints. D. GO BP analysis of DEGs of 6-day (left), 10-day (middle) and 14-day (right) timepoint.

Based on GO analysis, it is unclear which pathways *Lmx1b* may be implicated in, thus we also carried out pathway-centric analysis using GAGE analysis and revealed several pathways that are known to be related

to signaling pathways in podocyte biology, including the Rap1 signaling pathway, the calcium signaling pathway, and the focal adhesion pathway. Interestingly, the Wnt signaling pathway was also dysregulated in sick podocytes (Figure 41A). *Lmx1b* has been implicated in Wnt signaling during limb development [136, 137, 134, 144] and the non-canonical Wnt signaling pathway is known to then activate calcium signaling or Rho/Rac/Rap signaling to regulate actin remodeling [237]. The essential gene members that significantly contribute to each pathway were illustrated for the Wnt signaling pathway, the focal adhesion pathway, the calcium signaling pathway and the Rap1 signaling pathway (Figure 41B) and contain common genes such as *Camk2a* and *Pdgrfb* thus further demonstrating potential ability to crosstalk between these pathways. Notably, there was an up-regulation of WNT5B in sick podocytes across all timepoints compared to baseline control. WNT5B is a ligand and can activate the non-canonical Wnt signaling pathway to propagate further intracellular signaling to activate the planar cell polarity (PCP) pathway and the calcium (Ca^{2+}) signaling pathway to control actin organization, cellular polarity and migration. Overall, we identified the non-canonical Wnt signaling pathway which could regulated by *Lmx1b*, as well as WNT5B as an interesting ligand that has not been previously published to have demonstrated roles in podocytes.

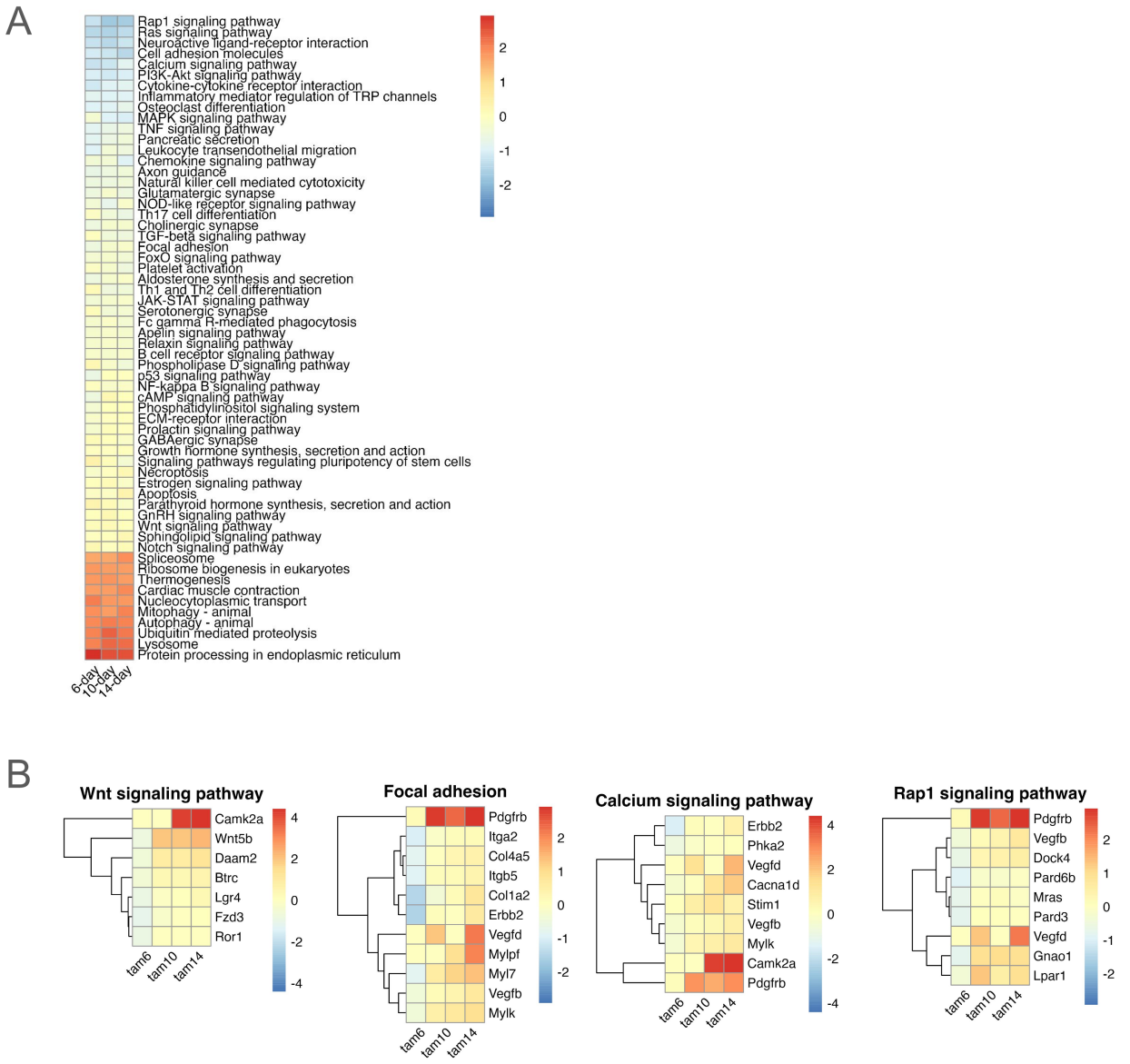

Figure 41: Single nuclei multiomic analysis of *Lmx1b*-ipko podocytes revealed time-dependent differential regulation of the non-canonical Wnt signaling pathway and transcription factor class switching in the open chromatin. A. GAGE analysis of significant up- and down-regulated pathways of DEGs across each time-points. B. Heatmaps of the expression of essential member genes that significantly contribute to gene set pathways: Wnt signaling pathway, focal adhesion, calcium signaling pathway, Rap1 signaling pathway.

Next, we tested whether WNT5B can activate the non-canonical Wnt signaling pathway in podocytes. The non-canonical arm could be further subdivided into two pathways: the Wnt/PCP or the Wnt/Ca^{2+} pathways. The former can mediate cytoskeleton rearrangement via the Rho and Rac signaling cascades and the latter can trigger intracellular calcium flux and downstream signaling cascades. WNT5B may be up-regulated and secreted by sick podocytes to act within a glomerulus in a para-/autocrine fashion on neighboring podocytes to trigger either or both pathways. Rearrangement of the cytoskeleton is associated with podocytopathy [238], and persistent high concentrations of intracellular calcium have been shown to have detrimental effects on podocytes [239].

In order to determine if WNT5B acts through the Wnt/PCP or the Wnt/Ca^{2+} pathway in podocytes, we utilized a podocyte-specific reporter mice expressing both GCaMP calcium sensor and LifeAct-mCherry which is a marker for F-actin, and extracted acute kidney slices which enabled for *ex vivo* imaging of glomeruli in living kidney tissues (Figure 42A). We observed increased calcium signal intensity in treated glomeruli compared to vehicle control at all timepoints. (Figure 42B), and the quantification of GCaMP signal intensity showed a significant increase for both low and high concentrations of WNT5B at 1 h and 2 h (Figure 42C) suggesting that WNT5B was capable of acting the Wnt/Ca^{2+} pathway and trigger intracellular calcium influx after prolonged exposure. The fluorescence intensity of F-actin in podocytes was dose-dependently and significantly increased at 1 h but this effect diminished at 2 h and 4 h (Figure 42D and E) suggesting that actin was initially reorganized but then remained static. Similar to basal GCaMP intensity, basal LifeAct intensity was also increased in vehicle after 4 h, suggesting that acute kidney slices may not allow for longer imaging without inducing damage in podocytes. In contrast to calcium signaling, which persisted with prolonged WNT5B treatment, F-actin expression was only acutely up-regulated with WNT5B treatment suggesting that WNT5B-mediated Wnt/PCP or the Wnt/Ca^{2+} signaling, albeit are pathways under the same non-canonical Wnt signaling arm, required different WNT5B concentration and elicited different temporal responses. In conclusion, WNT5B demonstrated the ability to regulate calcium signaling and actin expression, and these elicited changes may be related to podocyte injury.

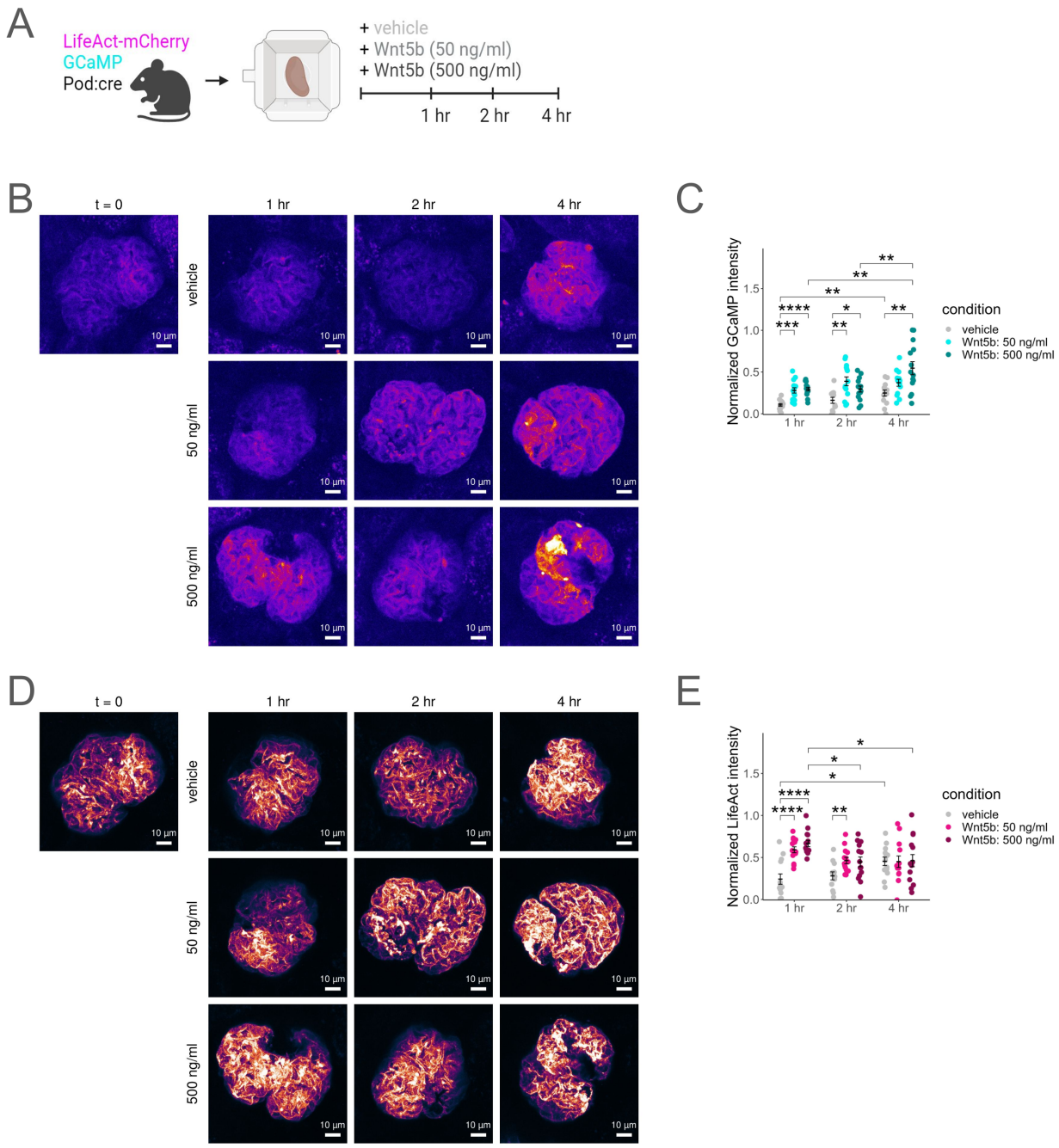

Figure 42: WNT5B regulates the non-canonical Wnt signaling pathway in podocytes. A. Schematic of WNT5B treatment on acute kidney slices from podocyte-specific LifeAct:mCherry;GCaMP mice. Acute kidney slices were incubated with PBS vehicle, low (50 ng/ml) or high (500 ng/ml) concentrations of WNT5B for 1 h, 2 h or 4 h prior to imaging by multiphoton for changes in calcium signaling or cytoskeleton rearrangement. B. Multiphoton images of GCaMP at all timepoints treated with vehicle or different concentrations of WNT5B. C. Quantification of GCaMP fluorescence intensity. A significant increase in GCaMP was observed at both low and high concentrations of WNT5B treatment across all timepoints. D. Multiphoton images of LifeAct at all timepoints treated with vehicle or different concentrations of WNT5B. E. Quantification of LifeAct fluorescence intensity. A significant increase in LifeAct was observed at early timepoints of WNT5B treatment.

6.3.3 eGFP.LMX1B undergoes LLPS under osmotic stress

Next, we aimed to understand the molecular mechanism of action of LMX1B. LMX1B is a transcription factor and is expected to localize to the nucleus. Interestingly, endogenous LMX1B was stained in kidney tissue by STED and showed a speckle-like subnuclear localization in podocytes (Figure 43 A) suggesting that LMX1B may function within nuclear condensates since such speckled staining patterns are indicative of TFs undergoing LLPS, a biophysical property of proteins to organize into complexes within a membraneless subcompartment to functionally enhance transcription in the nucleus [240]. Similarly, LMX1B speckles were also seen by immunofluorescence microscopy (Figure 37D) to validate that STED staining was not an artifact. The subcellular location of endogenous LMX1B was further confirmed in HEK293T cells, where LMX1B localized to the nucleus as expected and showed speckle-like morphology similar to that of H3K27ac (Figure 43 B). The tails of H3 have been implicated in phase separation [241]. The ability of LMX1B to undergo LLPS has not yet been demonstrated. The loss of LMX1B nuclear speckles was present in areas with abnormal ac-tubulin and nephrin staining, indicating glomerular damage likely resulting from LMX1B loss of function. Taken together, LMX1B may undergo LLPS and its competence appeared likely to be associated with a speckled staining pattern.

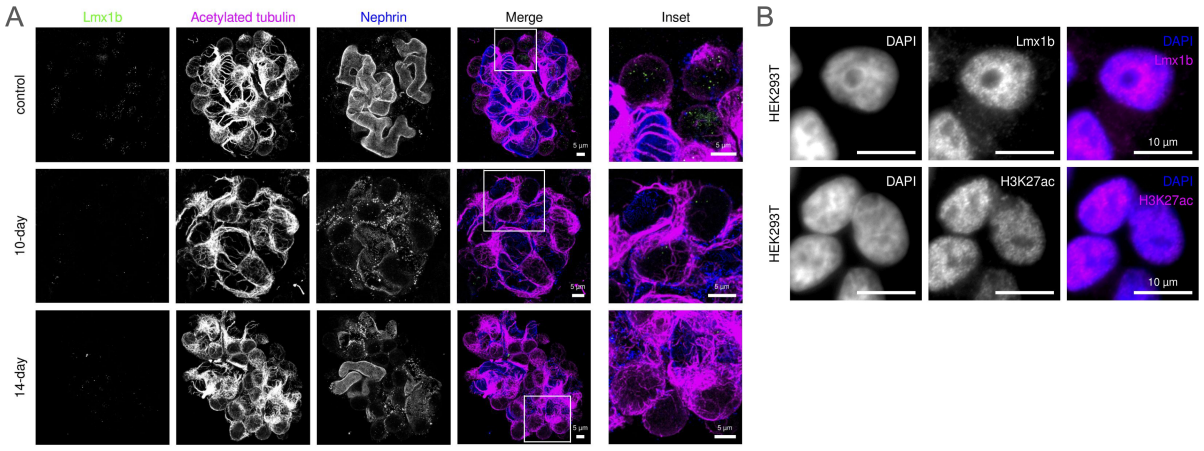

Figure 43: LMX1B showed speckle-like subnuclear localization in tissue and cells. A. STED microscopy of LMX1B , acetylated-tubulin and nephrin of tamoxifen-induced LMX1B -ipko mice at 10-day and 14-day versus control. LMX1B show speckle-like localization to the nucleus of podocytes, acetylated-tubulin localized to the primary podocyte foot processes and nephrin localized to the podocyte slit diaphragm. At 10-day and 14-day, there is a progressive loss of LMX1B expression in the podocyte nuclei. LMX1B (green), acetylated-tubulin (magenta), nephrin (blue) in merged image. B. IF staining of endogenous LMX1B localized exclusively to the nucleus in HEK293T cells and showed speckle-like subnuclear localization. LMX1B (magenta), DAPI (blue) in merged image.

Next, we wanted to determine whether LMX1B may contain the intrinsic ability to undergo LLPS. LMX1B is known to contain two protein-interacting LIM zinc-binding domains between aa. 56-106 and aa. 115-168 and one DNA-binding homeobox domain between aa. 219-278. (Figure 44 A) but the rest of the sequence may function beyond protein binding by carrying specific biophysical properties that could satisfy the requirement for LLPS. The most common way for proteins to participate in weak multivalent interactions is via disordered regions [242]. PONDR predicted the amino acid sequence of LMX1B to contain two intrinsic disordered domains (IDR) between amino acids 176-229 (IDR1) and 282-382 (IDR2), and either

or both IDRs may allow LMX1B to participate in LLPS (Figure 44 B). To corroborate the prediction, we also used AlphaFold to predict structured folding for both known protein- and DNA-interaction domains and two similarly disordered domains in the same regions (Figure 44 C). We also used prediction tools such as FuzDrop to predict droplet-promoting regions and aggregative hot spots within the LMX1B sequence (Figure 44 D). The regions of residues predicted to be droplet-promoting regions were aa. 172-238 and aa. 283-363. the regions of residues predicted to be aggregation hot spots were aa. 172-179, aa. 229-235, aa. 283-295, aa. 319-326 and aa. 344-357. In theory, the amino acid residues within LMX1B were predicted to form disordered regions that permitted LLPS.

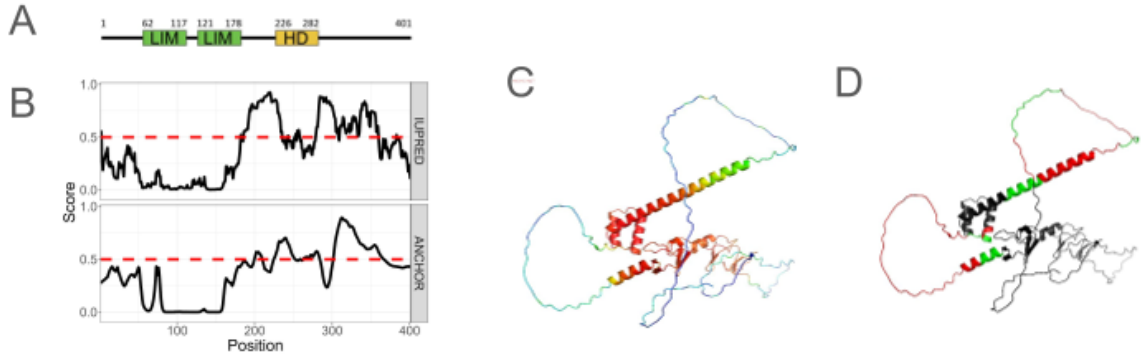

Figure 44: LMX1B contains disordered domains. A. Domain overview of full-length mouse LMX1B (LMX1B -201) with residue numbers of known domains extracted from Pfam InterPro database. Two LIM domains (green) at aa. 62-117 and aa. 121-178, and one homeobox domain (HD, yellow) at aa. 226-282. B. Disorder prediction using IUPRED2A for full-length LMX1B amino acid sequence. Values above the threshold indicated a high tendency for disorder. ANCHOR prediction for protein regions that undergo disorder-to-order transitions upon binding. A high score represents highly disordered binding regions. The threshold for IUPRED2A and ANCHOR scores are both set at 0.5 (red). C. AlphaFold predicted model of full-length LMX1B. Coloring based on the model's predicted confidence score (b-factor). D. Alphafold predicted the model of full-length LMX1B in grey. The regions of residues predicted to be droplet-promoting regions (aa. 172-238, aa. 283-363) were highlighted in green, and the regions of residues predicted to be aggregation hot spots (aa. 172-179, aa. 229-235, aa. 283-295, aa. 319-326, aa. 344-357) were highlighted in red. The prediction was based on FuzDrop.

In order to capture the liquid-like properties of LMX1B and to perform live cell imaging experiments, we cloned mouse or human LMX1B into either N-terminal or C-terminal tagged-eGFP constructs and over-expressed the constructs in HEK293T cells (Figure 45). Mouse or human LMX1B showed very similar localization. Interestingly, C-terminal eGFP-tagged LMX1B showed punctate-like subnuclear localization similar to endogenous LMX1B whereas eGFP.LMX1B showed more ubiquitous distribution in the nucleus. The differences in the localization of LMX1B were likely accounted for by the eGFP tagging. The droplet-like LMX1B puncta resembled the localization of endogenous LMX1B and was highly suggestive that C-terminal tagged LMX1B was functional whereas the N-terminal tagging interfered with LMX1B folding.

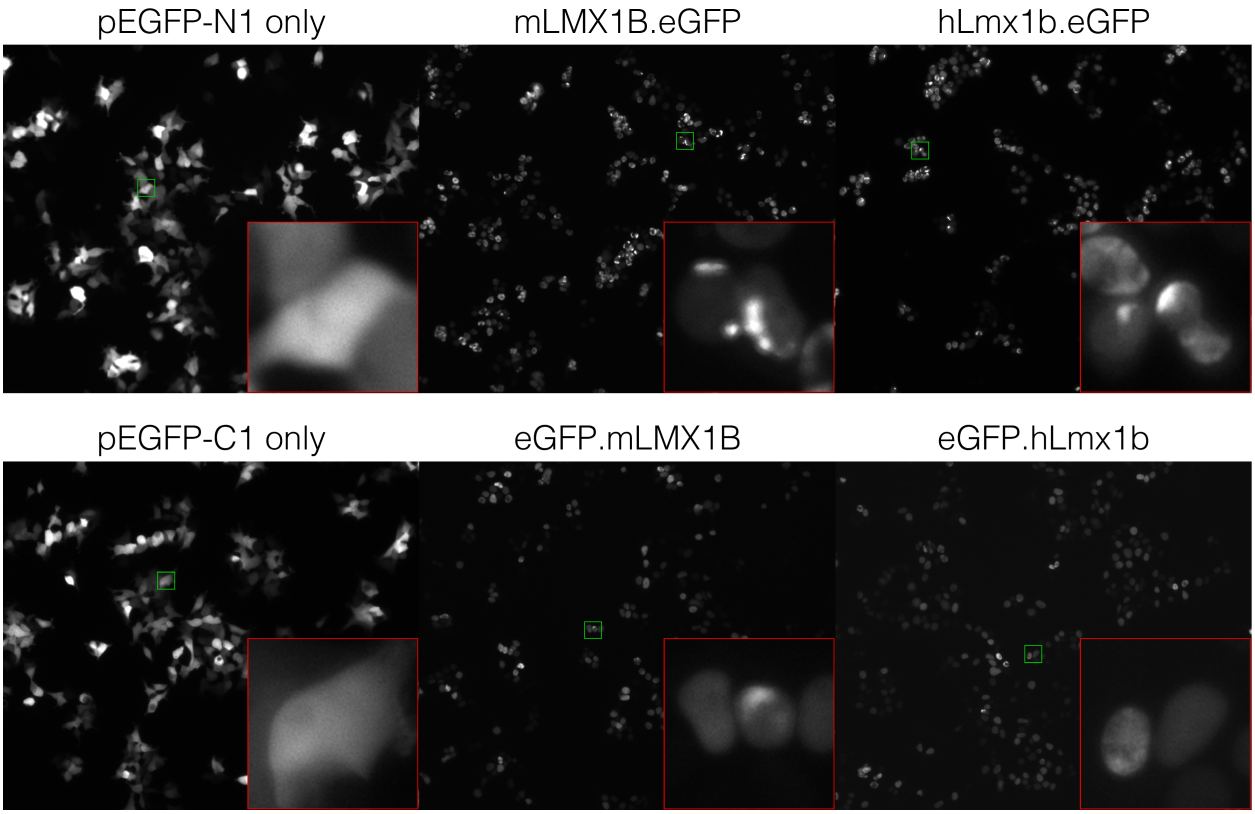

Figure 45: eGFP.LMX1B and LMX1B.eGFP show different subnuclear distributions in HEK293T cells. Mouse or human LMX1B with eGFP tagged either to the N- or C-terminus were overexpressed in HEK293T cells but showed different subnuclear localization. Empty pEGFP-N1 or pEGFP-C1 controls showed a uniform distribution of GFP in cells.

6.3.4 LMX1B.eGFP does not display LLPS-like properties

Owing to the similarity in the subnuclear localization of C-terminus eGFP-tagged LMX1B (LMX1B.eGFP) with endogenous LMX1B subnuclear localization in podocytes, LMX1B.eGFP was tested first for liquid-like properties in overexpressing cells. LMX1B was transiently expressed in HEK293T cells on glass dishes for live cell imaging and fluorescence recovery after photobleaching (FRAP) assay. Either part of the puncta or the entire puncta was photobleached and allowed to recover over time. Compared to eGFP.Taz, which is known to undergo LLPS and displayed dynamic liquid-like properties after FRAP since it is capable of replacing proteins with dead fluorophores with fluorescent TAZ (Figure 46A&B). Although LMX1B.eGFP displayed punctate-like subnuclear localization, however, the puncta did not recover after photobleaching and did not display liquid-like behaviors (Figure 46C&D). The eGFP-tagging at the C-terminus seemed to have affected the folding or the solubility of LMX1B and resulted in protein aggregation in the nucleus.

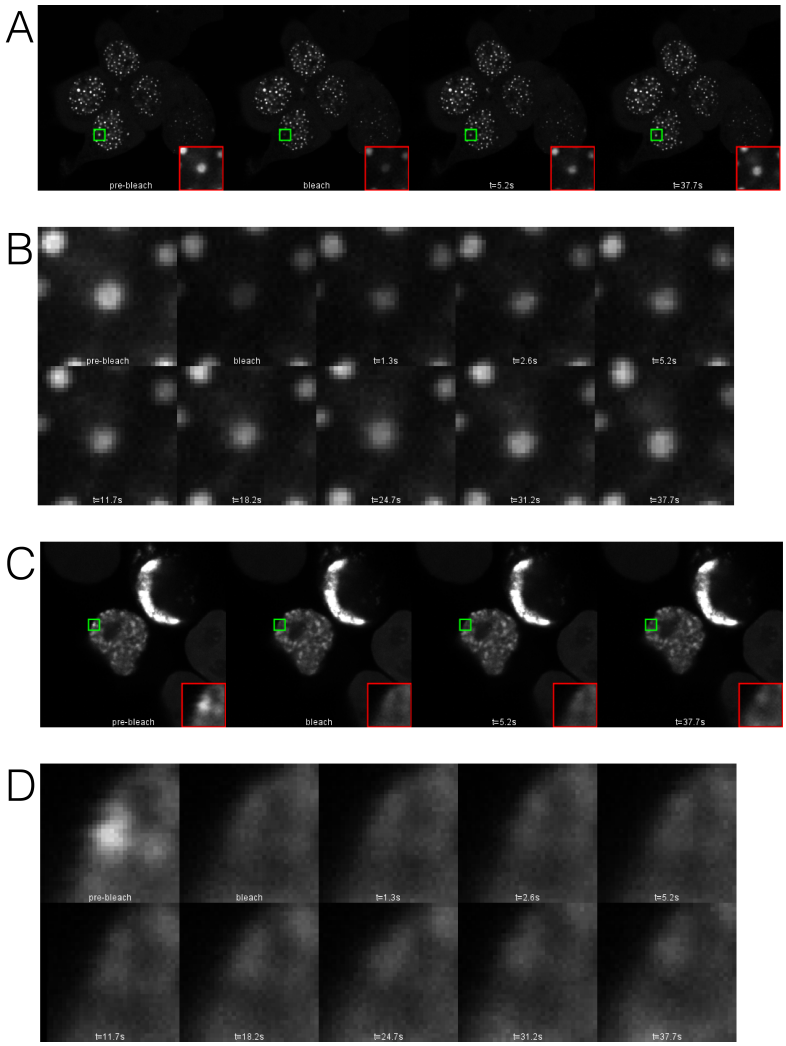

Figure 46: Live imaging and FRAP assay showed that LMX1B.eGFP puncta do not phase separate in HEK293T cells. A. eGFP.Taz was transfected into HEK293T cells and photobleached at t=0 s. The fluorescence recovered within 5 s. B. Zoom in of eGFP.TAZ puncta and its fluorescence recovery over 37.7 s. C. LMX1B.eGFP was transfected into HEK293T cells and photobleached at t=0 s. The fluorescence of the puncta did not recover over time. D. Zoom in on LMX1B.eGFP lack of fluorescence recovery over 37.7 s.

6.3.5 eGFP.LMX1B phase separates under osmotic stress

Next, we tested the N-terminus tagged LMX1B for LLPS. We transiently overexpressed eGFP.LMX1B in Moins cells but eGFP.LMX1B was ubiquitously and uniformly distributed throughout the nucleus and did not show speckle-like subnuclear localization similar to its endogenous expression. Since there were no clear speckles, we tested for the ability of eGFP.LMX1B for phase separation in cells. To induce dynamic and multivalent properties of LMX1B likely mediated through the IDRs, we simulated cellular crowding by placing the cells under hyperosmotic stress by treatment with sorbitol or high salt. Cells were incubated in Ringer's imaging buffer (283 mOsmol/kg) and treated with 2X solutions to reach a final concentration of 200mM sorbitol (502 mOsmol/kg) or 300mM NaCl (777 mOsmol/kg) prior to imaging every 15 s to follow the behavior of eGFP.LMX1B within the nucleus. When treated with 200mM sorbitol, eGFP.LMX1B dynamically fused into droplets in the nucleus (Figure 47A). Similar liquid-like fusion events between eGFP.LMX1B was

observed in cells treated with 300mM NaCl (Figure 47B). Droplet formation began within 30 s and fusion event was achieved within 3 min for sorbitol treatment but more quickly within 2 min for salt treatment. The dynamics of droplet formation and fusion were different between cells treated with 200mM sorbitol and 300mM NaCl, likely due to different osmotic pressures induced by each treatment. The number of nuclear speckles was quantified for sorbitol treatment (Figure 47D) or for high salt treatment (Figure 47F). Both treatments elicited similar effects where the relative number of nuclear speckles increased within 30 s compared to t=0, whereas eGFP.NLS control did not respond to osmotic stress (Figure 47E&G). In conclusion, eGFP.LMX1B was able to under LLPS though only under hyperosmotic stress.

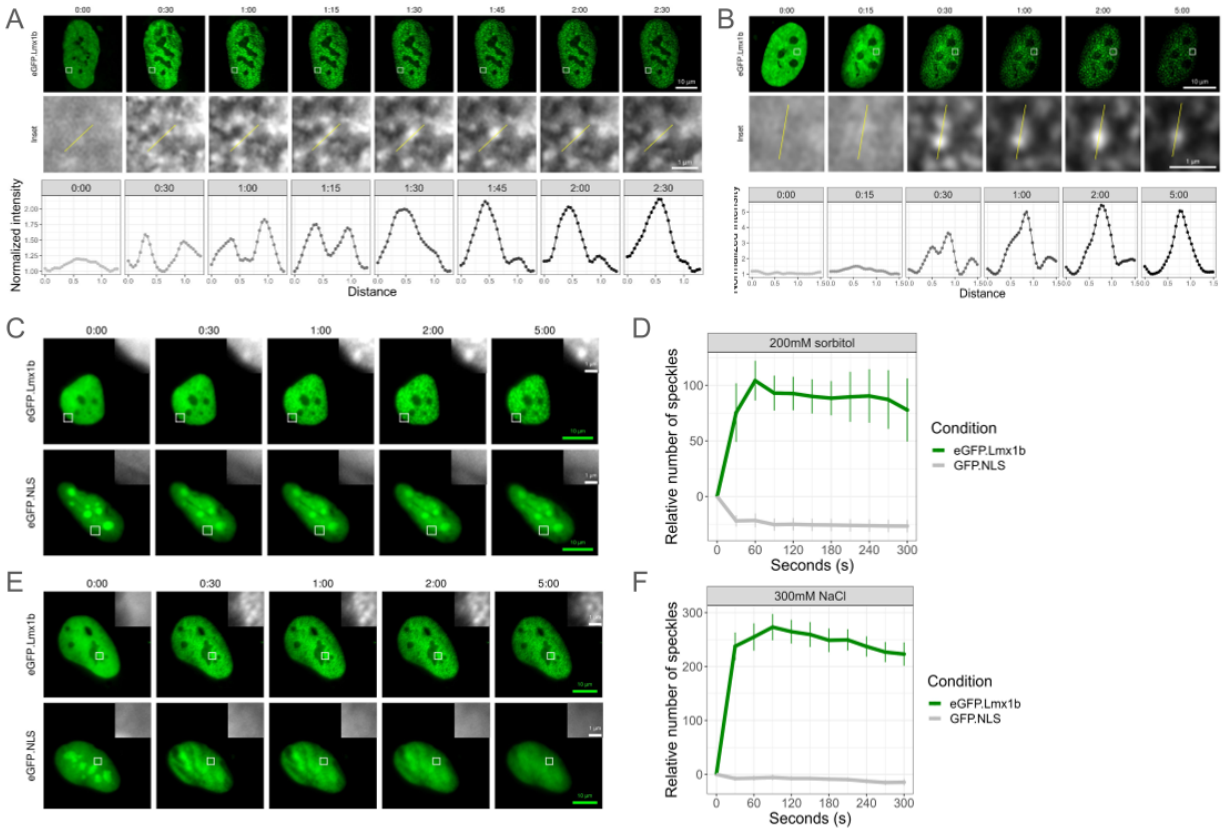

Figure 47: eGFP.LMX1B undergoes phase separation under osmotic stress. A. Full-length eGFP.LMX1B was overexpressed in Moins cells and treated with 200mM sorbitol and imaged by Airyscan confocal microscopy at 30 s intervals for 5 minutes. The nuclear speckles displayed liquid-like properties by undergoing fusion events. B. Full-length eGFP.LMX1B was overexpressed in Moins cells and treated with 300mM NaCl and imaged by Airyscan confocal microscopy at 30 s intervals for 5 minutes. The nuclear speckles displayed liquid-like properties by undergoing fusion events. C. Full-length eGFP.LMX1B or eGFP.NLS control was overexpressed in Moins cells, treated with 200mM sorbitol, and imaged by live cell imaging at 30 s intervals for 5 minutes. Upon treatment, eGFP.LMX1B underwent phase separation by collapsing into speckle-like subnuclear compartments within 30 s, whereas the localization of eGFP.NLS did not respond to sorbitol. D. Quantification of the relative number of nuclear speckles treated with 200mM sorbitol. The total number of nuclear speckles was normalized to that of t=0. E. Full-length eGFP.LMX1B or eGFP.NLS control was overexpressed in Moins cells, treated with 300mM NaCl, and imaged by live cell imaging at 30 s intervals for 5 minutes. Upon treatment, eGFP.LMX1B underwent phase separation by collapsing into speckle-like subnuclear compartments within 30 s, whereas the localization of eGFP.NLS did not respond to 300mM NaCl. F. Quantification of the relative number of nuclear speckles treated with 300mM NaCl. The total number of nuclear speckles was normalized to that of t=0.

6.3.6 IDR2 of LMX1B is responsible for phase separation

Since LMX1B was predicted to contain two IDRs and osmotic stress-induced eGFP.LMX1B to undergo LLPS, we investigated which IDR conferred the weak and multivalent interactions that drove phase separation. In order to determine the exact peptide responsible for the phase separation of LMX1B, we deleted each or both of the two IDRs of LMX1B. Deletion of IDR1 aa. 180-221 generated the eGFP.LMX1B ΔIDR1 mutant. Deletion of IDR2 aa. 288-401 generated the eGFP.LMX1B ΔIDR2 mutant. Deletion of both IDR1 and

IDR2 generated the eGFP.LMX1B ΔIDR1/2 double mutant (Figure 48A). Alphfold predicted that LIM and HD structures were not affected by the deletion of IDRs (Figure 48B).

The full-length or truncation mutants of eGFP-tagged LMX1B were transiently overexpressed in Moins cells. Interestingly, ΔIDR1 and ΔIDR1/IDR2 eGFP.LMX1B showed speckle-like distribution in the nucleus at basal levels, whereas full length and ΔIDR2 eGFP.LMX1B was more uniformly distributed in the nucleus. Upon treatment with 200mM sorbitol, both full-length and ΔIDR1 underwent phase separation, but ΔIDR2 failed to form droplets. Despite the basal increase of nuclear speckles in ΔIDR1/IDR2 double mutants, no additional nuclear speckles were formed upon osmotic stress (Figure 48C&D).

Additionally, cells were treated with 150mM NaCl (530 mOsmol/kg), which had a similar osmolarity to that of 200mM sorbitol (502 mOsmol/kg). ΔIDR1 showed weak phase separation upon treatment compared to full-length eGFP.LMX1B. ΔIDR2 and ΔIDR1/IDR2 double mutants did not form additional nuclear speckles compared to baseline upon treatment (Figure 48E&F). When cells were treated with 300mM NaCl, ΔIDR1 phase separated as well as full-length eGFP.LMX1B . ΔIDR2 and ΔIDR1/IDR2 formed nuclear speckles though at a slower rate compared to full-length eGFP.LMX1B (Figure 48G&H). This is likely due to the extremely high osmotic pressure induced by high salt or an artifact of the charge associated with salt treatment. In conclusion, we have identified IDR2 to be the disordered domain responsible for the ability of LMX1B to undergo LLPS in cells.

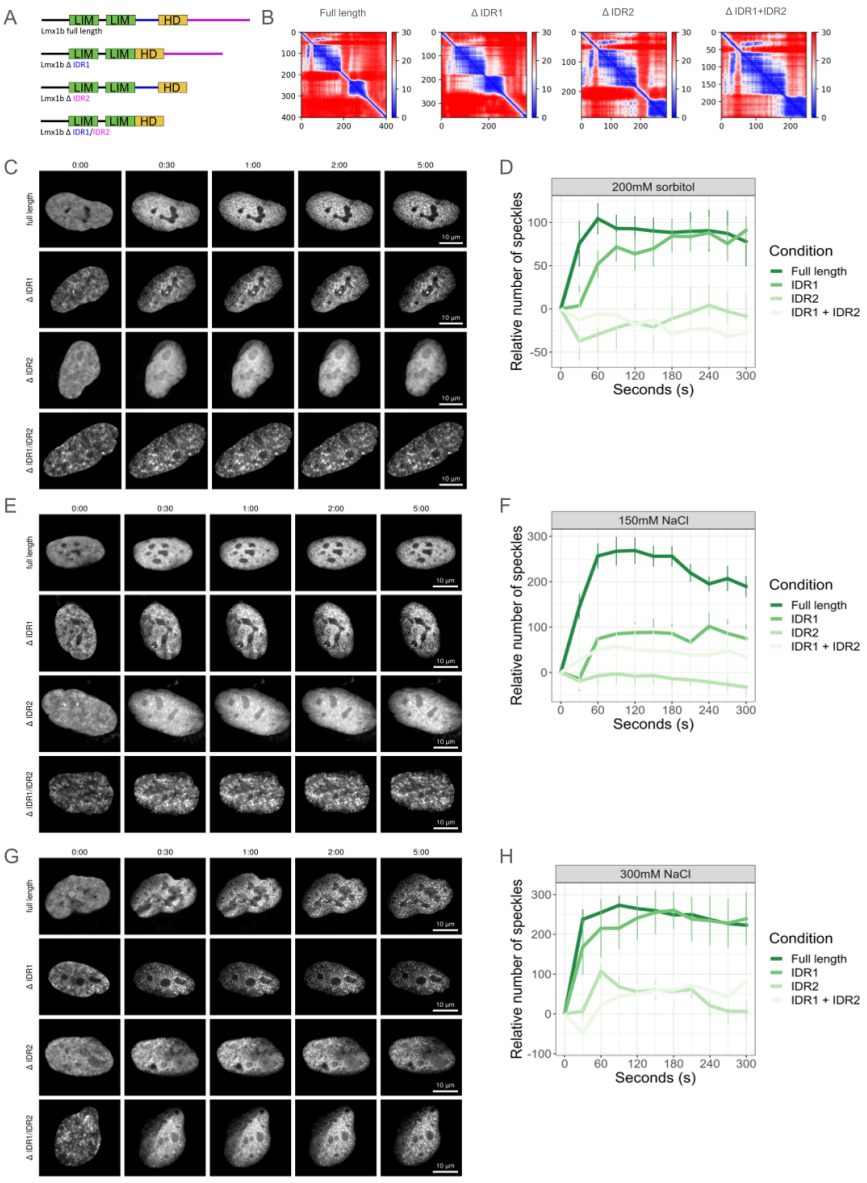

Figure 48: IDR2 is responsible for the LLPS of LMX1B. A. Schematics of full-length and LMX1B truncation mutants. IDR1 (blue) spanned from aa. 180-221 and IDR2 spanned from aa. 288-401 (magenta) as predicted by IUPRED2A. Three truncation mutants were generated from full-length LMX1B: ΔIDR1, ΔIDR2, or double mutant ΔIDR1/ΔIDR2. B. AlphaFold prediction of full-length LMX1B and truncation mutants where both LIM and Homeobox domains are predicted to retain protein folding. C. Full-length or truncation mutants of eGFP.LMX1B was overexpressed in Moins cells and treated with 200mM sorbitol. eGFP.LMX1B ΔIDR2 and ΔIDR1/ΔIDR2 did not respond to treatment and failed to undergo LLPS under osmotic stress. D. Quantification of the relative number of nuclear speckles treated with 200mM sorbitol. The total number of nuclear speckles was normalized to that of t=0. E. Full-length or truncation mutants of eGFP.LMX1B was overexpressed in Moins cells and treated with 150mM NaCl. eGFP.LMX1B ΔIDR2 and ΔIDR1/ΔIDR2 did not respond to treatment and failed to undergo LLPS under osmotic stress. F. Quantification of the relative number of nuclear speckles treated with 150mM NaCl. The total number of nuclear speckles was normalized to that of t=0. G. Full-length or truncation mutants of eGFP.LMX1B was overexpressed in Moins cells and treated with 300mM NaCl. eGFP.LMX1B ΔIDR2 and ΔIDR1/ΔIDR2 responded weakly to osmotic stress. H. Quantification of the relative number of nuclear speckles treated with 300mM NaCl. The total number of nuclear speckles was normalized to that of t=0.

7 Discussion

7.1 Gene regulatory network of podocytes and the development of the Podocyte Damage Score (PDS)

7.1.1 Generation and validation of the PDS

Current evaluation criteria for assessing podocyte damage encompass established diagnostic readouts like proteinuria and loss of renal function [243], alongside molecular assays that quantify markers related to cellular damage and stress [244], the estimation of podocyte detachment or loss [245], and the examination of podocyte morphology through histology [246, 247, 14, 248]. However, these approaches are outcompeted by the throughput and resolution offered by single-cell technology. The increasing popularity of scRNA-seq enabled the generation of high-quality data from human kidney biobanks and the deposition of datasets in publically available databases. The differences in sample preparation and data generation called for a standardized metric to assess podocyte damage. On a molecular level, the heterogeneity in disease etiology and cellular identity also demanded increasing resolution to analyze and understand the changes in molecular mechanisms and the rewiring of regulatory pathways during the progression of podocytopathy. In this study, we aim to generate a universally applicable ranking score to assess the degree of podocyte damage in the kidney at single-cell resolution.

We pooled published and in-house generated bulk and single-cell RNA-seq datasets of product damage models and systematically selected and filtered for the top 50 contributing podocyte-specific genes that were differentially expressed in disease to compile the podocyte damage score (PDS). Most genes, including *Lgals1* [249], *Thsd7a* [250, 251, 252], *Cldn5* [225, 224], *Pard3b* [253] and *Wt1* [33, 34], have been implicated in podocyte diseases but we also identified novel genes like *Lgals3*, *Lrrc1*, *Shisa3*, *Zyx*, and *Nap1l1* which have not been previously demonstrated to have significant roles in podocytes. We cross-validated that the PDS was podocyte-specific, applicable to various glomerular diseases and that the gene expression correlated with proteome expression and kidney function. We further translated the PDS onto bulk and single-cell datasets sampled from human biopsies out of the KPMP and NEPTUNE consortium and demonstrated the applicableness and robustness of the PDS on extended datasets sourced from both murine or human origins. To understand the common and differential molecular changes underlying podocytopathy from various glomerular diseases, we correlated the PDS to transcription factor (TF) and pathway activities at single-cell resolution and integrated this with the transcriptional network generated using ATAC-seq to identify key podocyte-specific TF regulatory networks that were rewired upon podocyte damage. The ranking metric that we developed facilitated the identification of podocytes undergoing damage while discerning associated modulations in the TFs and pathway activities that may have contributed to the advancement of novel therapeutic approaches.

We used super-resolution microscopy to verify the localization of PDS-derived gene products in podocytes including Thsd7a, Claudin-5, Smoothened and Nek1. Thsd7a is a transmembrane protein that localizes to the podocyte slit diaphragm [252], and circulating autoantibodies to THSD7A have been identified in patients diagnosed with idiopathic membranous nephropathy [250, 223]. Thsd7a mediates the rearrangement of the cytoskeleton, transduces signaling at the focal adhesion, and contributes to maintaining the integrity of the glomerular filtration barrier [223, 251, 252]. In parallel, several Claudin proteins, including Claudin-1 [254], Claudin-3 [255] and Claudin-5 [256, 225, 224], have been associated with the formation of the slit diaphragm and the maintenance of foot processes in podocytes. We identified Claudin-5 co-localization with nephrin

as a key slit diaphragm-associated protein that showed mislocalization under podocyte damage which is supported by similar findings from Tesch et al. [225]. Podocyte-specific deletion of *Cldn5* showed aberrant thickening of the GBM, expansion of the mesangium, proteinuria, and increased expression of Wif1, which is a secreted inhibitor that can sequester Wnt ligands in the Wnt signaling pathway [224]. We also stained for the Smoothened (*SMO*) protein which revealed localization to the podocyte membrane. SMO plays an important role in the Sonic Hedgehog (Shh) signaling pathway. Shh ligand competes with SMO for binding to the Patched-1 receptor and inhibits downstream signal transduction. The unsequestered SMO activates the translocation of Gli, a transcription factor, to the nucleus where it can activate the expression of target genes to drive cellular growth, patterning, and differentiation. The function of SMO and the Shh signaling pathway in podocytes has shown that Shh may act as an important mediator of podocyte-mesangial crosstalk [257]. Shh was upregulated in podocytes of chronic kidney diseases and the deletion of podocyte-specific Shh and the inhibition of SMO using cyclopamine inhibited mesangial cell activation but ameliorated glomerulosclerosis in the kidneys of adriamycin-treated and diabetic mice [257]. Furthermore, the inhibition of SMO using cyclopamine has also been shown to significantly attenuate renal fibrosis in murine models for ischemia-reperfusion and obstructive nephropathy [258, 259]. Lastly, we characterized by STED the localization of the NIMA-related kinases 1 (NEK1), whose function is implicated in DNA damage responses, G2-M phase progression, and renal cyst progression. Mutation in Nek1 is associated with the development of polycystic kidney disease [260], and podocytes show high expression of NEK1 and upregulation after ischemic injury which may intimate attempts by podocytes to undergo repair of DNA damage post-injury [261]. Interestingly, NEK1 may be a target gene of TAZ highlighting the potential of molecular crosstalking with the Hippo signaling pathway [262]. Through the use of super-resolution microscopy, it becomes possible to visually subtle changes in the localization of differentially regulated proteins, which cannot be known by transcriptomic and this may provide insights into the changes in the signaling pathway of injured podocytes.

7.1.2 Injury scores in other tissues

The complexity of single-cell transcriptomic datasets demands the development of metrics suitable for in-depth analysis of the rewiring in the transcription network after injury. For example, an injury score designed by Melms et al. was applied to kidney single-cell transcriptomic aimed to score individual proximal tubule cells using the 50 top differentially upregulated genes between diabetic to control mice treated with SGLT2 and/or ACE inhibitors. A significant decrease in the injury score was demonstrated after combination therapy and revealed modulation in injured proximal tubule gene regulatory networks such as dysregulation of fatty acid oxidation in diabetes [263]. Similarly, an ischemia-reperfusion injury (IRI) score was derived from gene sets from IRI and control scRNA-seq where 100 top DEGs were chosen to classify proximal cells and assess damage along temporal trajectory and to identify a maladaptive/profibrotic proximal tubular cells subcluster that express proinflammatory and profibrotic cytokines and myeloid cell chemotactic factors [264]. Li et al. have further extended the understanding of their comprehensive scRNA-seq by analyzing multiple cell types using gene sets to derive cell cycle score and ECM score to evaluate the injury and cell states during kidney fibrosis [265], but the analysis focused on proximal tubules owing to the large proportion of these cells in the kidney. Similarly, comprehensive cell state scores developed from integrated multimodal spatial kidney atlas spatial transcriptomic studies described cycling, adaptive, transitioning and degenerative states revealed key molecular signatures and biological pathways correlated with injury time-course and kidney outcomes [179]. All of the studies mostly focused on analyzing the proximal tubules owing to the large proportion of cells dominating the scRNA-seq in the kidney and did not provide in-depth insights into the

biology of podocytes.

7.1.3 Gene regulatory network in podocytes

The significance of gene regulatory networks in podocytes is underscored by comprehensive studies integrating diverse genomic approaches. Studies combining mRNA and miRNA transcriptional profiling with quantitative proteomic analyses revealed highly specific and sophisticated gene regulatory networks orchestrating the regulation of cytoskeleton dynamics, cell differentiation, endosomal transport, and peroxisome function [60]. Remarkably, these analyses not only shed light on the specificity of gene regulation but also predict the existence of podocyte-specific gene regulatory networks. Furthermore, the inclusion of alternative splicing of respective genes adds an additional layer of complexity to the understanding of podocyte biology. Exploring the intricacies of podocyte differentiation involves the scrutiny of at least six transcription factors: wt1, foxc2, hey1, tcf21, lmx1b, and mafb. The individual impact of knocking down these factors in zebrafish has implicated their roles in podocyte development. Particularly, the combined knockdown of wt1 and foxc2 resulted in a comprehensive loss of expression in all podocyte marker genes, thus underscoring the interdependence of these transcription factors [266]. This finding echoes the roles of WT1 as a key transcription factor driving podocyte cell-type specification through TF-regulatory element network interplay [34]. Furthermore, studies on the glucocorticoid effects on podocytes reveal significant regulation of genes related to cytoskeleton processes and the concurrent downregulation of genes encoding pro-inflammatory cytokines and growth factors emphasizes the impact of gene networks rewiring in response to treatment [267]. Additionally, the genome-wide expression profiling of renal biopsies across different CKD stages unveiled a multifaceted transcriptional landscape associated with CKD progression by identifying compartment- and cell-type-specific dysregulation of hypoxia-associated gene transcripts [268]. Lastly, network analysis during FSGS highlights the coordinated cellular injury response in podocytes, emphasizing the intricate interplay within the gene regulatory network, where pathways such as response to wounding and regulation of cellular processes converge. Key transcription factors, including NF-κB, STAT, SP1, and p53, play pivotal roles in orchestrating these responses. However, the investigation of the gene regulatory network is currently limited by bulk RNA-seq and lacks single-cell resolution [269]. Integrating podocyte-specific gene regulatory networks with PDS enables further exploration of molecular changes within individual cells amongst complex tissues. This integration promises a more detailed understanding of the intricate interplay within the gene regulatory network in podocytes.

7.1.4 Gene regulatory network (GRNs) in kidney

We developed the GRNS using podocyte-specific ATAC-seq which has not been generated as most studies rely on the power of single-cell technology to investigate rare cell types. The generation of GRNs not only in podocytes but in the whole kidney also plays a crucial role in understanding cell-type heterogeneity during development, as well as signal crosstalk between glomerular cells in injury. The elucidation of major gene-regulatory circuits in the kidney leveraged by scRNA-seq and scATAC-seq revealed the critical orchestration of target gene expression by cell type-specific enhancers and transcription factors during nephron progenitor differentiation highlighting early podocyte commitment and complex renal tubule cell differentiation [174]. The GRNs underlying the development of renal primordium identified key TFs that orchestrate the core regulatory circuits important for tissue morphogenesis, cellular differentiation, and the activation of glial cell line-derived neurotrophic factor (Gdnf)-Ret signaling pathway [270]. Other cell-type specific GRNs were also elucidated for other cells including the mouse nephron progenitor cells [271] and proximal tubules of kidney

organoids [272] and revealed TFs- and enhancer-regulated subcircuits that provided broader insights in the gene and epigenetic regulatory layer in the maintenance of cell-type identify and function. Boulogne et al. had developed an open-accessible KidneyNetwork which integrated various kidney RNA-seq co-expression networks aimed to predict associations between kidney-specific gene functions and disease phenotypes but lacked single-cell resolution to assess disease trajectories [273]. In summary, the multifaceted exploration of gene regulatory networks in the kidney integrated from single-cell studies provides meaningful biological insights into renal development, organoid functionality, and disease-associated gene prioritization, and contributes to a comprehensive understanding of the intricate molecular mechanisms underlying kidney biology and pathology.

7.2 Mapping the epigenetic landscape in health and disease

7.2.1 Epigenetic regulation by TF and chromatin remodelers in podocytes

Published work on epigenetic regulation in podocytes has been sparse and distributed across many research areas. In cultured podocytes infected with HIV-infected, hypomethylation at gene promoters and global upregulation of genes were detected [274]. The modification of m6A has been shown to be significantly upregulated in mice with diabetic kidney disease [275]. In diabetic nephropathy, advanced glycation end products (AGEs) reduced the expression of nuclear inhibitor of protein phosphatase 1 and enhancer of zeste homolog 2 which led to decreased H3K27me3 expression in podocytes [87]. Additionally, podocytes that were placed under hypoxic conditions showed a notable reduction in H3K27me3 [276]. Generally, a decrease in methylation has been shown in damaged podocytes. On the other hand, studies investigating the epigenetic regulation by TFs have been previously described in podocytes. Wt1, a key TF important for maintaining podocyte function, has been shown to regulate transcriptional reprogramming during podocyte injury [35]. DACH1, a TF that has been demonstrated to regulate podocyte health by recruiting and sequestering PTIP, serves as a core component capable of activating H3K4me3. This activation, in turn, leads to a reduction in global H3K4me3 marking at promoters, ultimately repressing transcription in podocytes [277]. Moreover, it was established that FOXC1/2 is intricately associated with SEs and exerts a pivotal role in orchestrating the differentiation of mature podocytes, ensuring the preservation of cell identity [82]. Massa et al. used a loss-of-function MAFB knockout mouse model and demonstrated a loss of H3K4me3 at the promoters of Mafb- and Wt1-driven target genes which suggested that MAFB may regulate chromatin accessibility at its target genes [51]. Concurrently, they have also mapped the podocyte-specific H3K4me3, H3K4me1 and H3K27me3 epigenetic landscapes using similar approaches using FACS-sorted podocytes from healthy adult mice but did not directly compare to injured podocytes as we did in our study [51]. Overall, existing research indicated the importance of epigenetic regulation in podocytes by methylation and by single TFs but lacked comprehensive genome-wide characterization of podocyte-specific changes when undergoing damage.

The function of chromatin remodelers and chromatin reorganization in damaged podocytes has undergone limited research. CTCF is an insulator protein and is associated with cohesin to maintain the boundary of topology-associated domains [278]. Full body knockout of CTCF is embryonically lethal and the inducible podocyte-specific deletion of CTCF showed loss of podocytes, proteinuria, and developed glomerular pathology thus highlighting the importance of faithfully maintaining the TADs for correct transcription regulation in podocytes [83]. We profiled the 3D chromatin organization using the Hi-ChIP method which showed transcription-centered chromatin interaction directly between enhancers and promoters but we were unfortunately unable to capture changes in enhancer-promoter contacts in disease animals due to technical

limitations. Interestingly, the single-cell RNA-seq analysis of glomerular cells in CTCF-knockout mice at earlier time points following knockout revealed dysregulation in cytoskeletal dynamics, mitochondrial function, and intraglomerular cell-cell crosstalk via VEGFA and PDGFB signaling which were also identified as differentially regulated pathways in our enhancer-centric analysis [84].

The modulation of epigenetic functions by histone deacetylases (Hdacs) in podocytes presented conflicting and inconclusive findings. Hdacs are associated with transcriptional repression through its deacetylase activity. We showed global downregulation of H3K27ac in damaged podocytes and may be associated with increased Hdac activities. The upregulation of Hdac1/2 activities has been shown in models of podocyte injury, and the administration of valproic acid, which inhibits Hdac1/2 activities, showed renal protective effects and mitigated proteinuria [279, 92, 93, 280]. Similar outcomes were also observed with the deletion of podocyte-specific Hdac1/2 in adult mice [91]. In contrast, germline deletion of Hdac1/2 in podocytes led to pronounced proteinuria, glomerulosclerosis, and evidence of DNA damage, coupled with characteristics indicative of cell senescence [94]. The precise role of Hdac1/2 in podocytes in both developmental processes and disease contexts requires further investigation.

A large amount of research has also been dedicated to unraveling the role of epigenetic regulation in kidney disease in mouse and human tissue and largely focused on the role of methylation and GWAS association studies [179, 281, 81], yet few papers characterized glomerular cells due to limitation in existing available methods to extract such cells from complex tissues or biopsies efficiently. In our study, we bridge the gap in understanding by comprehensively mapping the enhancers landscape on a genome-wide level in healthy and diseased podocytes.

7.2.2 The identification of glomerular cell type-specific enhancers and SEs in health and disease

We first mapped the epigenetic landscape of glomerular cell types in health and disease by applying the recently developed CUT&Tag technique on FACS-sorted nuclei purified from isolated glomeruli [161]. The advances in sequencing technologies combined with the availability of mouse reporter lines highly enabled novel epigenetic discoveries in rare cell types in heterogeneous tissues. FACS-sorting ensured the purity of cell lineage and conferred absolute cell type-specificity for all datasets derived from these nuclei. We were the first to exploit histone modification markers, including markers for active and poised enhancers, promoters and repressors, for the annotation of genome-wide gene regulatory regions specific to podocytes and glomerular endothelial cells, and integrated novel datasets such as ATAC-seq and HiChIP to pinpoint highly cell-type specific enhancer regions that regulate key target genes important for glomerular biology. Due to the lack of reporters driven under mesangial cell-specific cre, only a limited number of enhancers for mesangial cells were identified via indirect inference thus further highlighting the inadequacy of *in silico* prediction and the imperative to generate *de novo* datasets. A significant limitation of the Hi-ChIP method lies in its demand for substantial input materials and its inability to achieve single nucleotide resolution. We attempted to generate podocyte-specific Hi-ChIP or glomerular Hi-ChIP from disease animals but were unsuccessful. Consequently, the integration with CUT&Tag or ATAC-seq techniques proved indispensable to impart cell type specificity and enhance the resolution of datasets. Nonetheless, we identified unique podocyte- and GECs-specific enhancers and SEs that were associated with the maintenance of cell identity as revealed by the GO analysis.

To elucidate the regulation of enhancers in podocyte injury, we meticulously characterized the enhancer landscape of podocytes by using two established genetic mouse models, the *Nphs2*$^{\mathrm{R231Q/A286V}}$ and *Phb2*$^{\mathrm{pko}}$

models [14, 228]. The major findings revealed a global loss of open chromatin, an inactivation of enhancers, and an erosion of SEs that correlated with the severity of podocyte injury and may affect the putative binding of TFs within differentially regulated enhancer regions. In place of using *in silico* proximity-based linkage between enhancers and target genes, we expanded insights on the enhancer-gene connectome using Hi-ChIP and further integrated the expression of podocyte-specific targets using snRNA-seq to address which enhancer-associated gene regulatory pathways were perturbed during podocyte damage. We discovered that the activities of enhancers and SEs were not only specific to cell types but also exhibited specificity in the responses to podocyte damage. Importantly, our findings also corroborated with the conclusions from Miao et al., which also exploited single-cell technologies such as snRNA-seq correlated with ATAC-seq, to address epigenetic programming in the kidney during kidney development to demonstrate the reliance on distal enhancer elements and concordant time-dependent changes of TF to regulate the expression of predicted target genes [174].

Our data demonstrated differential and common enhancer-regulated signaling pathways that were affected in the podocytes of the *Nphs2*$^{\mathrm{R231Q/A286V}}$ and *Phb2*$^{\mathrm{pko}}$ models. Both the EGFR1 and the VEGFA-VEGFR2 signaling pathways were key pathways that are associated with podocyte diseases. EGFR has been implicated in the development of glomerulosclerosis but the exact mechanism is not known [282]. Heparin-binding EGF-like growth factor (HB-EGF) can bind to the EGF receptor (EGFR) to induce its phosphorylation on tyrosine residues leading to the transactivation of the receptor and the subsequent activation of several intracellular signaling transduction pathways including the phosphoinositide-3-kinase (PI3K)/Akt pathways, the Janus kinase/signal transducers and activators of transcription (JAK/STAT) pathways and the extracellular signal-regulated kinase (ERK) pathway. In podocytes, the upregulation of HB-EGF expression and the sustained activation of EGFR was significantly increased in mice treated with anti-GBM nephrotoxic serum (NTS) treatment, and the inhibition of EGFR also ameliorated albuminuria [283]. The upregulation of HB-EGF in the kidney was also observed in FSGS [284]. In streptozotocin-induced diabetic mice with podocyte-specific EGFR knockout, there was a significant reduction in albuminuria, decreased podocyte loss, and attenuated foot process effacement. [285, 286]. In contrast, the activation of EGFR demonstrated a renal protective role by promoting kidney recovery in cases of acute kidney injury [287, 288]. In summary, the impact of EGFR activation on kidney damage remains uncertain, necessitating further research to discern both its potential beneficial and detrimental outcomes specific to disease etiology. On the other hand, podocyte-derived VEGF has shown protective functions in the glomeruli of developing mice [289], whereas injured podocytes showed decreased production of VEGF-A and promoted glomerular endothelial injury and loss of endothelial fenestration [290]. In parallel, homozygous podocyte-specific deletion of VEGF-A is perinatal lethal whereas heterozygous loss of allele resulted in underdeveloped filtration barriers, proteinuria, and failure in the differentiation of endothelial cells [291, 292]. The identification of the EGFR and VEGF pathways may highlight the role of podocyte crosstalk with the other glomerular cell types [293]. Taken together, deeper insights into the differential regulation of podocyte enhancers may aid in the understanding of the function of cell-specific enhancers and further advance the discovery of novel therapeutics for podocyte disease.

7.3 Lmx1b is an essential transcription factor for the maintenance of podocyte function and may function via LLPS

7.3.1 Phenotyping of the *Lmx1b*-ipko mouse model

The whole body homozygous mutants of Lmx1b were perinatally lethal [105] and no renal phenotype was observed in heterozygous Lmx1b knockout animals [294], thus necessitating the use of cell-type specific deletion of Lmx1b to investigate its function in renal pathology. *Lmx1b*-ipko mice suffered renal failure, developed massive proteinuria days after birth, and did not survive longer than 14-days postnatally [187]. Lmx1b has been implicated in the regulation of Col4a3, Col4a4, CD2AP and podocin in Lmx1b knockout glomeruli in newborn mice, and therefore considered to be important for podocyte differentiation and function [295]. Compared to published inducible podocyte-specific Lmx1b knockout mice [110] which developed proteinuria only after one week of induction using doxycycline, the mice housed in our facility needed more days to reach significant ACR after induction with tamoxifen. This may be explained by the differences in the efficacy of the doxycycline or tamoxifen administration or confounding factors associated with the Tet-On/Tet-Off and Cre/loxP systems responding to each feed [296]. However, on a renal phenotypic level, published data showed foot processes disappearance after two weeks of induction which correlated with our observation at 14-day when podocyte foot processes became effaced [110]. Overall, Lmx1b knockout mice showed proteinuria, podocyte effacement, and FSGS-like phenotypes.

Furthermore, our study is the first to characterize the *Lmx1b*-ipko mouse model by using STED microscopy to quantitatively assess the changes in the morphology of the podocyte slit diaphragm, and the expression of podocin and nephrin within the glomerulus at each timepoint. At early timepoints post-tamoxifen induction, we observed significant and persistent downregulation of podocin protein expression starting at 6-day, followed by the onset of significant changes in the slit morphology at 10-day then the downregulation of nephrin protein expression at 14-day which by this point correlated with renal phenotypes including podocyte effacement and the onset of significant proteinuria. We showed changes in slit diaphragm proteins and morphology over time and these occurred prior to the onset of proteinuria. Notably, Nphs2 has been described to be transcriptionally co-regulated by Lmx1b and FoxC in podocytes [111] and may be a key mediator at the slit diaphragm that led to podocyte dysfunction in the Lmx1b knockout mice.

In contrast, published data described that the onset of proteinuria preceded the downregulation of podocin and nephrin proteins in *Lmx1b*-ipko mice by one week based on quantification using immunofluorescence images [110]. There might be differences in the quantification method of immunofluorescence and STED images. STED super-resolution microscopy can more robustly capture subtle changes in the morphology of the slit diaphragm due to its ability to resolve subcellular structures below the diffraction limit compared to conventional confocal microscopy, however, the quantification of fluorescence intensity remains variable due to the necessity for selectively deplete excited fluorophores in order to minimize the size of focal point to achieve super-resolution. A more reliable protein quantification method like mass spectrometry would be needed to conclusively determine the expression of podocin and nephrin in podocytes along disease progression in *Lmx1b*-ipko mice.

7.3.2 Lmx1b may regulate chromatin organization in podocytes

The multiome data enabled simultaneous snRNA-seq and snATAC-seq profiling from podocytes undergoing Lmx1b knockout along FSGS development. We identified a distinct cluster of diseased podocytes that were transcriptionally and epigenetically different from healthy podocytes and differential analysis revealed

dominantly global up-regulation at the initial stage of knockout and changes in open chromatin accessibility of differential TF binding sites. Our data suggests that Lmx1b functioned as a transcriptional repressor in podocytes but this is contrary to the analysis of Lmx1b knockout in adult-stage serotonin neurons, where Lmx1b largely served as a transcriptional activator to protect against transcriptomic degradation [297]. The differences may be explained by that the bulk RNA-seq of Lmx1b deleted serotonin neurons were captured at one single timepoint or that the Lmx1b loss-of-function triggered rapid but secondary injury responses. Lmx1b has been reported to regulate the chromatin accessibility in lineage-specific distal enhancer regions during neuron maturation to drive subtype identity [298]. Likely, Lmx1b may also be important in the organization of accessible chromatin for cellular specification in podocytes.

Lmx1b has been shown to interact with Ldb1 [299, 187], and mice with podocyte inactivation of Ldb1 presented proteinuria at 19-day post-brith, dilated tubules with protein casts and loss of foot processes [187] suggesting that Ldb1 is essential in the maintenance of podocyte function. Interestingly, Ldb1 has been described as an enhancer looping factor that can interact with different transcription factors and facilitate enhancer-promoter interactions to regulate cell type-specific gene expression [300, 301]. Lineage-specific transcription factors for erythropoiesis such as GATA1 and TAL1 can form the erythroid complex with LDB1 and LMO2 to activate erythroid genes mediating long-range enhancer-promoter looping for β-globin gene expression, and this loop formation is largely mediated independently of the mediator and cohesin complex [302, 129, 303]. LHX2, similarly to Lmx1b, also belongs to the LIM homeobox (LHX) transcription factor family and has been described to bind to olfactory receptor super-enhancers and to regulate the maintenance of interchromosomal contact sites via interaction with LDB1 adaptor protein [304].

Lmx1b may be in complex with Ldb1 in podocytes to organize and maintain chromatin accessibility at key podocyte-specific long-range enhancer-promoter contact sites in the genome to drive cell type-specific gene expression for podocyte differentiation and function. The lack of available Lmx1b antibodies for interactome studies, CUT&RUN, or Hi-ChIP experiments is the major bottleneck for investigating the function of Lmx1b. It would be crucial to identify the interaction partners and the genome-wide binding sites of Lmx1b in a cell type-specific manner to precisely elucidate its relationship with distal gene regulatory regions and the regulatory function of its target genes in podocytes.

In addition, we analyzed the snRNA-seq of Lmx1b knockout mice at several timepoints. Differential gene analysis between sick and healthy podocytes revealed that more genes were differentially regulated at earlier timepoints but gradually decreased over disease progression.

Surprisingly, GO analysis revealed terms related to the differentiation of mesangium and the regulation of aorta morphogenesis at earlier timepoints when most genes were upregulated, which likely suggests the failure to maintain podocyte identity and podocyte de-differentiation upon the acute loss of Lmx1b. Changes in signaling pathways such as glucocorticoid signaling pathway, VEGF-activated receptor signaling pathway, adrenomedulin signaling pathways and regulation of intracellular transport were observed at 6-day and 10-day and may support transcriptional network rewiring affected by the absence of Lmx1b targeting. At 14-day, terms related to mesangial cell proliferation, glomerular mesangial development, and negative regulation of extracellular matrix disassembly correlated well with mesangial cell expansion and increased extracellular matrix that is commonly observed in FSGS patients. At 14-day, changes in the actin cytoskeleton and slit diaphragm were intimated by GO terms involving changes in the actomyosin assembly and filtration diaphragm assembly. The major finding of Burghardt et al. was that Lmx1b may regulate the actin cytoskeleton via Abra and Arl4c, which are both actin-binding Rho-activating proteins that were up-regulated in Lmx1b knockout and may be putative Lmx1b target genes since both ABRA and ARL4C genes

harbor FLAT elements that enable Lmx1b binding within their promoter regions [110]. In our datasets, the differential analysis revealed significant upregulation of Abra at 10-day but non-significant upregulation of Arl4c at all timepoints in sick podocytes. Transgelin showed significant upregulation at 6-day in our datasets. The pathway-centric GAGE analysis did not show regulation by actin cytoskeleton as a significantly regulated KEGG pathway but essential member genes in related pathways including focal adhesion and MAPK signaling pathway were differentially regulated in Lmx1b knockout mice.

7.3.3 Wnt5b induced calcium signaling and changes in actin expression in podocytes

In order to evaluate the effect of Wnt5b on podocytes, we utilized a podocyte-specific reporter mouse expressing both calcium sensors and actin-binding proteins and generated acute kidney slices for incubation with increasing concentrations of mouse recombinant Wnt5b for an extended length of incubation time. We observed increased calcium signal compared to baseline and dose-dependent increase in actin expression though this effect showed no significance beyond 2 h of induction. We demonstrated that Wnt5b was able to induce non-canonical Wnt/calcium and Wnt/PCP signaling in podocytes and hypothesize that this effect may be mediated via the Ror1 receptor though this remains to be investigated. In chronic lymphocytic leukemia, both Wnt5a and Wnt5b can interact with the Ror1 receptor but only Wnt5a resulted in the phosphorylation of DVL3. In zebrafish, Ror1 is dispensable but the interaction between Ror2 and Wnt5b was essential for cartilage morphogenesis, chondrocyte polarization, and the organization of focal adhesion [305]. Additionally, the Wnt5b-Ror2 complex has been shown to regulate cytoneme formation, can be transported to cell protrusion, and transduced paracrine JNK signaling downstream of the Wnt–PCP signaling axis [306]. More research is needed to fully elucidate the downstream signaling of Wnt5b in podocytes and its effect on podocyte slit diaphragm morphology and function.

Overall, Lmx1b may control the balance between canonical and non-canonical Wnt signalings to maintain proper podocyte function. It is also likely that Wnt5b may function similarly to Wnt7a and act upstream of Lmx1b in podocytes but this remains an interesting facet for investigation. Fascinatingly, LDB can bind to single-stranded DNA binding protein (SSBP) proteins and can be recruited by lineage-specific LIM-domain proteins to enhancers to form a Wnt enhanceosome to regulate the Wnt signaling pathway [307, 308, 309]. Ldb2, which shares about 75% sequence similarly with Ldb1, could also bind to SSBP proteins [310]. The mechanism of action may be similar in podocytes, and it would be exciting if Lmx1b interacts with Ldb1 and SSDP proteins under steady state to form the Wnt enhanceosome at long-range enhancer-promoter contact sites to regulate the Wnt signaling pathway. In the absence of Lmx1b, changes in chromatin conformation could lead to the disassembly of enhancer-promoter contacts, and the aberrant upregulation of Ldb2 may sequester the Wnt enhanceosome to upregulate the non-canonical Wnt pathway as damage or rescue response. However, the exact molecular mechanism and target genes of Lmx1b remain to be elucidated and more insight would be gained if the genome-wide DNA binding sites of Lmx1b in podocytes can be determined by CUT&RUN or ChIP-seq.

7.3.4 Overexpressed Lmx1b undergoes phase separation under osmotic stress

Liquid-liquid phase separation is a mechanism that explains the formation of membraneless organelles or cell structures via multivalent interactions including π-π, cation-anion, dipole-dipole, and interactions via intrinsically disordered regions (IDRs) [311, 240]. Biochemical reactions are accelerated within the organelle due to increased protein concentration and lower mobility though the characteristics of these structures retain liquid-like properties. These structures have been described as bodies, puncta, granules, droplets, and

condensates. They can exist in all compartments of the cell including cytoplasm, membranes and nucleus, and they may interact with other binding partners like nucleic acids or raft [312].

Endogenous expression of Lmx1b shows a speckle-like subnuclear location by immunofluorescence and STED microscopy. The amino acid sequence of Lmx1b was used to predict its likelihood of containing intrinsic disordered regions (IDRs) and to undergo LLPS. C- or N-terminal eGFP-tagged Lmx1b were generated and tested for their ability to under LLPS. Despite the punctate-localization of Lmx1b.eGFP, FRAP assay showed a lack of liquid-like properties and suggested that Lmx1b may have precipitated within the nucleus. It also intimated that the C-terminus of Lmx1b may be important for its molecular function. In contrast, the overexpression of eGFP.Lmx1b led to a uniform nuclear distribution but responded dynamically to hyperosmotic stress induced by sorbitol and NaCl. Lmx1b was predicted to contain two IDRs and we deleted either or both and tested the truncation mutants for their ability to phase separate and determined that IDR2, located at the C-terminal tail of Lmx1b, was responsible for the LLPS property of Lmx1b. Both eGFP.Lmx1b ΔIDR2 and ΔIDR1/IDR2 truncation mutants failed to form nuclear speckles in the presence of 200mM sorbitol and 150mM NaCl, although the formation of some nuclear speckles was observed when cells were induced with 300mM NaCl. Likely, Lmx1b phase separation was also affected by charge whereas sorbitol is a non-charged polar molecule. In this study, we deleted the entire C-terminal tail of Lmx1b beyond the homeodomain but only certain peptides within the deletion likely facilitated LLPS. Generation of step-wise truncation mutants may offer more insights into which amino acids or biochemical properties are important for the multivalent interaction of Lmx1b.

Phase separation of LIM domain-containing proteins Many LIM domain-containing proteins are also able to undergo LLPS. For example, LIMD1 is a focal adhesion molecule and the LIM domains and phosphorylation status are important for phase separation [313]. LIMD1 belongs to the Ajuba family protein and can interact with kinases from the Hippo pathway and affect slit diaphragm morphology and function in Drosophila [113]. In addition, JRAB/MICAL-L2 is a LIM-domain and IDR-containing protein and induces the formation of tubular recycling endosomes via LLPS [314], and it has also been shown to interact with F-actin and colocalize with α-actinin-4 which is essential for the function of podocyte slit diaphragm [315]. Ablim1 is an actin-binding protein via its intrinsically disordered region [316] though the role of Ablim1 has not been well researched in podocytes. In Lmx1b, the phosphorylation at several serines residues within IDR1 and IDR2 were detected and further experiments with phosphorylation mutants of Lmx1b are needed to determine if LLPS of Lmx1b is regulated by phosphorylation status.

Phase separation of chromatin and podocyte transcription factors Chromatin can also phase separate in physiological salt and the C-terminal lysine-rich disordered tail of histone H1 can modulate the density and fluidity of chromatin droplets *in vitro* [317]. Chromatin remodelers such as Brd4, CTCF, HP1α, and the mediator complex have been shown to undergo LLPS [318, 319, 320, 321]. Nuclear condensates have been proposed as transcriptional hubs that facilitate 3D chromatin rearrangement and coordinate with transcription factors to activate gene expression [322, 321, 323]. Recently, it has been proposed that transcription factors can bind to RNA and may mediate negative feedback transcriptional control by tightly balancing the stability of nuclear condensate by titrating the stoichiometry of TF to RNA at the stage of transcription initiation or elongation [324, 75]. Phase separation may be a novel macroscopic regulatory mechanism that explains transcriptional control by incorporating all interacting partners including DNA, RNA, and proteins on a spatial level.

WW domain-containing transcription regulator protein 1 (TAZ) and Yes-associated Protein (YAP), share about 45% amino acid identity and are both transcription coactivators that can act downstream of the Hippo signaling pathway and regulate mechanosignaling in podocytes [325]. Podocyte-specific deletion of Yap or Taz leads to proteinuria and causes FSGS [326, 327]. Taz readily forms nuclear condensates via its coiled-coil domain and compartmentalizes with a DNA-binding co-activator to enable transcriptional activation of the Hippo pathway [328]. Unlike Taz but similar to Lmx1b, Yap immediately formed condensates under hyperosmotic stress induced by sorbitol and upregulated its target genes [329]. Unlike both Yap and Taz, Lmx1b has so far not been implicated in mechanosensing mechanisms. In STED, endogenous Lmx1b seems to form distinct subnuclear droplets in podocytes but this does not correlate with the localization of eGFP.Lmx1b in Moins cells. It is possible that in overexpression systems, eGFP.Lmx1b saturated the nucleoplasm and thus only formed condensates at the correct concentration which induced cell shrinkage. This is supported by the fact that LLPS is a biological phenomenon that is highly dependent on protein concentration and proper multivalent interactions with co-factors ([240]). The concentration-dependent effect of LLPS of Lmx1b could be tested *in vivo* using purified recombinant Lmx1b proteins. Moreover, it is currently unclear if other stressors like pH, temperature, amino acid starvation, and even Wnt ligands would also induce the nuclear condensation of Lmx1b, and identifying additional triggers of Lmx1b condensates could uncover additional insights into the dynamics of the DNA-binding activity of Lmx1b.

7.4 Conclusion and future perspective

We aim to better understand underlying molecular pathways that contributed to podocytopathy in FSGS by investigating the transcriptional and epigenetic regulation of podocytes. We developed the podocyte damage score (PDS) to assess the healthy state of podocytes based on transcriptomics datasets, and validated that the PDS is robust, cell-type specific and highly applicable to various podocyte injury models. We derived a podocyte-specific transcription network using murine ATAC-seq datasets but more insights would be gained by translating such network onto human datasets to obtain a deeper understanding of the underlying rewiring in biological pathways and cellular mechanisms to pave the way for targeted therapy. Additionally, we mapped the epigenome of the cell type-specific enhancers in the glomerulus and studies the transcriptional function and molecular mechanisms of *Lmx1b* in podocytes. Our work highly benefited from the power of a booming field supported by single-cell technologies and robust bioinformatics pipelines that streamlined the in-depth analysis of cell type-specific gene regulation. In future studies, we aim to identify actively transcribed enhancer subsets, examine the dynamics of enhancer activity in health and disease, and unravel the mechanism of action between podocyte-specific eRNA, TF, and gene expression along FSGS progression.

Fortunately, single-cell technologies have greatly aided in investigating scarce cell types. However, the major bottleneck of the low sequencing depth offered by the high-throughput yet expensive 10X sequencing platform limited most research to the abundant tubular cells rather than the glomerular cell types [175]. Our snRNA-seq benefited from prior glomeruli isolation to ensure that a large number of podocytes were assayed. Instead of using snATAC-seq, which suffered from sparser peaks and epigenetic profiling restricted to chromatin accessibility, we resorted to the purification of podocytes by FACS which although more laborious in terms of animal crossings and husbandry, was more adaptable to versatile downstream sequencing techniques. In the future, we aim to establish the single nucleus CUT&Tag (snCUT&Tag) technique which provides a multi-modality approach to assay rare cells from complex tissues for histone or TF markers of interest along with snRNA-seq from the same nucleus. Our preliminary attempts at generating an H3K27ac Hi-ChIP from the glomeruli of disease animals were unsuccessful due to low input but insights into the

chromatin enhancer-promoter re-arrangement would be essential in understanding the epigenetic regulome of podocytes in FSGS and will remain one of our most prioritized goals.

As a future perspective, we aim to advance our understanding of the mechanism of how enhancers regulate target genes in podocytes by investigating the role of enhancer RNAs in gene regulation. The regulation of enhancers by eRNA is an exciting field of research that may explain the function and mechanism of enhancers in gene regulation. eRNAs are a subcategory of long non-coding RNAs (lncRNAs) that are bi-directionally transcribed short-lived RNA from enhancers whose exact functions are unclear but may be implicated in the recruitment of cell type-specific TFs and gene expression have not been described in podocytes [73]. We aim to carry out nascent RNA-seq from glomerular nuclei and integrate it with our existing reservoir of podocyte-specific enhancers and SEs to understand the regulation of eRNA in disease. The expression of eRNA is likely necessary for the maintenance of podocyte function and identity and eRNA dysregulation may compromise kidney function and lead to FSGS. Versions of nascent RNA-seq including 5'-GRO-Seq, PRO-cap or NET-CAGE are useful in the identification of enhancer RNA. The major challenge would be the amount of input material required for these sensitive and laborious assays. Once surmounting these challenges, the identification and understanding of eRNA regulation will significantly enhance our understanding of the intricate interplay between transcription factors (TFs) and eRNAs in the regulation of 3D chromatin structure and gene expression.

In this thesis, we also aimed to understand the role of *Lmx1b* and its molecular mechanism of action. We phenotyped the *Lmx1b*-ipko mice and implicated the role of *Lmx1b* in the non-canonical Wnt pathway and showed that Wnt5b is capable of inducing the calcium signaling and modulating the actin cytoskeleton in podocytes. We demonstrated that the overexpression of LMX1B can phase separate under osmotic pressure and the IDR domain near the C-terminal end facilitated LMX1B to undergo LLPS. The generation of ChIP-seq or CUT&RUN datasets to profile the exact binding sites of LMX1B is crucial in the understanding of the regulatory network of *Lmx1b*. So far, we have been limited by the lack of high-quality commercially available antibodies against LMX1B suitable for ChIP-seq or CUT&RUN. It will also be interesting to elucidate and compare the genome-wide binding profile of LDB1 in podocytes relative to LMX1B as well as investigate the localization of LDB1 in association with LMX1B nuclear condensation. The identification of eRNAs driven by LMX1B may shed light on another layer of epigenetic regulation of gene expression by interactions between TFs and eRNAs. The current limitation in technology does not yet offer the resolution possible to capture and quantify transient short-lived eRNAs in a cell-type specific manner but optimization of RNAscope may be an alternative solution.

Faithful epigenetic regulation of cell type identity and maintenance may be crucial to avert disease pathogenesis, and robust sequencing and bioinformatics techniques are indispensable for the annotation of genomic regions of interest and for understanding the intricate molecular and biological processes driving podocytopathy. Future effort in the investigation of additional layers of epi-regulome and the mechanisms of TFs may present novel insights into the therapeutic strategies that benefit the prevention and intervention of podocytopathy.

A Appendix

A.1 Genotyping

Genotyping	Reaction mix per sample		Cycling Parameter			Product size
$Lmx1b^{flox}$	ddH_2O	13.6 µL	1:	94 °C	5 min	wt: 330 bp tg: 220 bp
	5X GoTaq buffer	5 µL	2:	94 °C	45 s	
	25 mM $MgCl_2$	1.5 µL	3:	58 °C	60 s	
	25 mM dNTP	0.2 µL	4:	72 °C	45 s	
	10 µM Lmx1b lox2 fw	1.25 µL	5:	cycle step 2-4	35 times	
	10 µM Lmx1b lox2 rv	1.25 µL	6:	72 °C	5 min	
	Taq polymerase	0.2 µL	7:	10 °C	forever	
	DNA	2 µL				
Pod:cre or Tie2:cre	ddH_2O	14.7 µL	1:	94 °C	3 min	wt: 494 bp tg: 269 bp
	5X GoTaq buffer	5 µL	2:	94 °C	30 s	
	25 mM $MgCl_2$	2 µL	3:	55 °C	30 s	
	25 mM dNTP	0.2 µL	4:	72 °C	30 s	
	10 µM Beta-globin fw	0.4 µL	5:	cycle step 2-4	35 times	
	10 µM Beta-globin rv	0.4 µL	6:	72 °C	5 min	
	10 µM Cre fw	0.4 µL	7:	15 °C	forever	
	10 µM Cre rv	0.4 µL				
	Taq polymerase	0.2 µL				
	DNA	2 µL				
$Rosa26^{nTnG}$ or $Rosa26^{mTmG}$	ddH_2O	12.0 µL	1:	94 °C	3 min	wt: 330 bp tg: 250 bp
	5X GoTaq buffer	5 µL	2:	94 °C	30 s	
	25 mM $MgCl_2$	2 µL	3:	61 °C	60 s	
	25 mM dNTP	0.2 µL	4:	72 °C	60 s	
	10 µM Rosa26 wt fw	1.2 µL	5:	cycle step 2-4	35 times	
	10 µM Rosa26 wt rv	0.8 µL	6:	72 °C	2 min	
	10 µM Rosa26 tg rv	1.6 µL	7:	10 °C	forever	
	Taq polymerase	0.2 µL				
	DNA	2 µL				

Genotyping	Reaction mix per sample		Cycling Parameter			Product size
Wt1.hetdel	dH_2O	12.0 µL	1:	95 °C	2 min	wt: 320 bp tg: 260 bp
	5X GoTaq buffer	5 µL	2:	95 °C	30 s	
	25 mM $MgCl_2$	1.5 µL	3:	54 °C	30 s	
	Q-solution	5 µL	4:	72 °C	120 s	
	25 mM dNTP	0.2 µL	5:	cycle step 2-4	34 times	
	10 µM Wt1 wt fw	1.4 µL	6:	72 °C	10 min	
	10 µM Wt1 wt rv	1.8 µL	7:	15 °C	forever	
	10 µM Wt1 tg rv	2.0 µL				
	Taq polymerase	0.5 µL				
	DNA	2 µL				
Cre:ERT2	ddH_2O	11.6 µL	1:	94 °C	3 min	wt: 351 bp tg: 500 bp
	5X GoTaq buffer	5 µL	2:	94 °C	30 s	
	25 mM $MgCl_2$	1.5 µL	3:	57 °C	30 s	
	25 mM dNTP	0.2 µL	4:	72 °C	45 s	
	10 µM Cre:ERT2 fw 1	1.0 µL	5:	cycle step 2-4	35 times	
	10 µM Cre:ERT2 rv 1	1.0 µL	6:	72 °C	10 min	
	10 µM Cre:ERT2 fw 2	1.0 µL	7:	10 °C	forever	
	10 µM Cre:ERT2 rv 2	1.0 µL				
	Taq polymerase	0.5 µL				
	DNA	2 µL				
Podocin^{flox}	ddH_2O	13.1 µL	1:	94 °C	5 min	wt: 236 bp tg: 285 bp
	5X GoTaq buffer	5 µL	2:	94 °C	30 s	
	25 mM $MgCl_2$	1.5 µL	3:	62 °C	45 s	
	25 mM dNTP	0.2 µL	4:	72 °C	30 s	
	10 µM Nphs2 lox2 fw	1.25 µL	5:	cycle step 2-4	35 times	
	10 µM Nphs2 lox2 rv	1.25 µL	6:	72 °C	7 min	
	Taq polymerase	0.2 µL	7:	10 °C	forever	
	DNA	2 µL				
Podocin^{R231Q}	ddH_2O	11.1 µL	1:	94 °C	3 min	wt: 176 bp tg: 285 bp
	5X GoTaq buffer	5 µL	2:	94 °C	45 s	
	25 mM $MgCl_2$	1.5 µL	3:	55 °C	60 s	
	25 mM dNTP	0.2 µL	4:	72 °C	30 s	
	10 µM R231Q fw 1	1.25 µL	5:	cycle step 2-4	29 times	
	10 µM R231Q rv 1	1.25 µL	6:	72 °C	3 min	
	10 µM R231Q fw 2	1.25 µL	7:	15 °C	forever	
	10 µM R231Q rv 2	1.25 µL				
	Taq polymerase	0.2 µL				
	DNA	2 µL				

Genotyping	Reaction mix per sample		Cycling Parameter			Product size
Podocin^{A286V}	ddH_2O	13.6 µL				sequencing
	5X GoTaq buffer	5 µL				
	25 mM $MgCl_2$	1.5 µL				
	25 mM dNTP	0.2 µL	1:	94 ℃	3 min	
	10 µM A286V fw	1.25 µL	2:	94 ℃	45 s	
	10 µM A286V rv	1.25 µL	3:	55 ℃	60 s	
	Taq polymerase	0.2 µL	4:	72 ℃	30 s	
	DNA	2 µL	5:	cycle step 2-4	29 times	
			6:	72 ℃	3 min	
	ddH_2O	1.625 µL	7:	15 ℃	forever	
	SAP	0.3 µL				
	EXO1	0.075 µL				
	PCR product	8 µL				
Phb2^{flox}			1:	95 ℃	2 min	wt: 378 bp tg: 506 bp
	ddH_2O	5.5 µL	2:	95 ℃	30 s	
	2X REDTaq buffer	12.5 µL	3:	62 ℃	30 s	
	10 µM Phb2 P1	1 µL	4:	72 ℃	45 s	
	10 µM Phb2 P2	0.5 µL	5:	cycle step 2-4	40 times	
	DNA	5 µL	6:	72 ℃	90 s	
			7:	15 ℃	forever	

Table 7: PCR and cycling parameters for Genotyping.

A.2 Plasmid maps

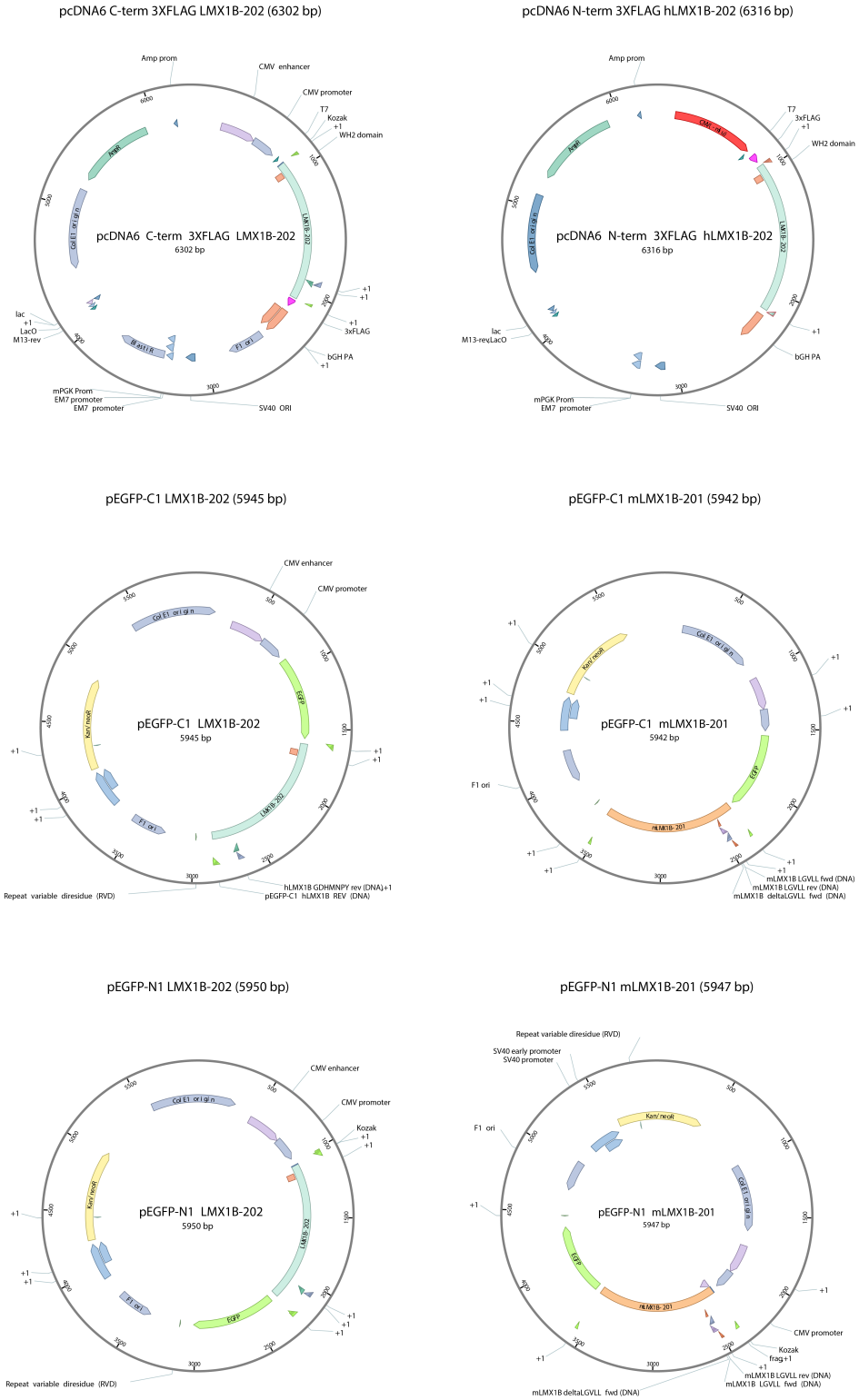

Figure 49: Plasmid maps of all plasmids generated in-house.

A.3 Contribution from others

A.3.1 Gene regulatory network of podocytes and the development of the Podocyte Damage Score (PDS)

The bioinformatics analysis for the Podocyte damage score project was carried out by Tim Padvitski, who generated all figures within the chapter except Figure 9 and Figure 15

A.3.2 Mapping the epigenetic landscape in the glomerulus

The bioinformatics analysis for the CUT&Tag, Hi-ChIP and snRNA-seq, and the Hi-ChIP on isolated glomeruli were performed by Dr. Giuliano Crispatzu, and generated Figure 24, Figure 25, Figure 29, Figure 30, Figure 31, Figure 32, Figure 33, Figure 34, Figure 35 and Figure 36.

A.3.3 Characterization of the function and molecular mechanism of *Lmx1b*

The bioinformatics analysis for the Lmx1b multiome project was carried out by Dr. Antonios Papadakis, who generated Figure 39A, 39B, 39C and 39D. He also performed the differential gene and peak analysis corresponding to Figure 39F, Figure 40A and 40C. The macro used to analyze the GO terms in Figure 40D was provided by Dr. Katrin Bohl. The GCaMP/Lifeact;Pod:cre mouse model in Figure 42A was created by Dr. Julia Binz-Lotter. The multiphoton microscopy for the Wnt5b treated acute kidney slices experiment was performed and imaged by Eva Wiesner, corresponding to images in Figure 42B and 42D. The macro used to quantify nuclear speckles in Figure 47D and 47F, and Figure 48D, 48F and 48H, was written by Dr. Martin Höhne.

References

[1] Martin R. Pollak, Susan E. Quaggin, Melanie P. Hoenig, and Lance D. Dworkin. The glomerulus: the sphere of influence. *Clinical journal of the American Society of Nephrology : CJASN*, 9:1461–1469, 2014.

[2] Hermann Pavenstädt, Wilhelm Kriz, and Matthias Kretzler. Cell biology of the glomerular podocyte. *Physiological reviews*, 83:253–307, 2003.

[3] Jeffrey B. Kopp, Hans Joachim Anders, Katalin Susztak, Manuel A. Podestà, Giuseppe Remuzzi, Friedhelm Hildebrandt, and Paola Romagnani. Podocytopathies. *Nature reviews. Disease primers*, 6, 12 2020.

[4] Rajasree Menon, Edgar A. Otto, Celine C. Berthier, Viji Nair, Evan A. Farkash, Jeffrey B. Hodgin, Yingbao Yang, Jinghui Luo, Kenneth J. Woodside, Haniyeh Zamani, Silas P. Norman, Roger C. Wiggins, Matthias Kretzler, and Abhijit S. Naik. Glomerular endothelial cell-podocyte stresses and crosstalk in structurally normal kidney transplants. *Kidney international*, 101:779–792, 4 2022.

[5] Tillmann Bork, Wei Liang, Oliver Kretz, Simon Lagies, Kosuke Yamahara, Camila Hernando-erhard, Martin Helmstädter, Christoph Schell, Bernd Kammerer, and Tobias B. Huber. Beclin1 is essential for podocyte secretory pathways mediating vegf secretion and podocyte-endothelial crosstalk. *International journal of molecular sciences*, 23, 4 2022.

[6] Anna Greka and Peter Mundel. Cell biology and pathology of podocytes. *Annual review of physiology*, 74:299–323, 2012.

[7] Koichiro Ichimura, Soichiro Kakuta, Yuto Kawasaki, Takayuki Miyaki, Takahiro Nonami, Naoyuki Miyazaki, Tomoyo Nakao, Sakiko Enomoto, Shigeo Arai, Masato Koike, Kazuyoshi Murata, and Tatsuo Sakai. Morphological process of podocyte development revealed by block-face scanning electron microscopy. *Journal of cell science*, 130:132–142, 2017.

[8] Puneet Garg. A review of podocyte biology. *American journal of nephrology*, 47 Suppl 1:3–13, 6 2018.

[9] V. D. D'Agati. Podocyte injury in focal segmental glomerulosclerosis: Lessons from animal models (a play in five acts). *Kidney international*, 73:399–406, 2008.

[10] Elena Torban, Fabian Braun, Nicola Wanner, Tomoko Takano, Paul R. Goodyer, Rachel Lennon, Pierre Ronco, Andrey V. Cybulsky, and Tobias B. Huber. From podocyte biology to novel cures for glomerular disease. *Kidney International*, 96:850–861, 10 2019.

[11] Stuart J. Shankland, Yuliang Wang, Andrey S. Shaw, Joshua C. Vaughan, Jeffrey W. Pippin, and Oliver Wessely. Podocyte aging: Why and how getting old matters. *Journal of the American Society of Nephrology : JASN*, 32:2697–2713, 11 2021.

[12] Taiji Matsusaka, Eric Sandgren, Ayumi Shintani, Valentina Kon, Ira Pastan, Agnes B. Fogo, and Iekuni Ichikawa. Podocyte injury damages other podocytes. *Journal of the American Society of Nephrology : JASN*, 22:1275, 7 2011.

[13] Thomas Benzing and David Salant. Insights into glomerular filtration and albuminuria. *The New England journal of medicine*, 384:1437–1446, 4 2021.

[14] Linus Butt, David Unnersjö-Jess, Martin Höhne, Aurelie Edwards, Julia Binz-Lotter, Dervla Reilly, Robert Hahnfeldt, Vera Ziegler, Katharina Fremter, Markus M. Rinschen, Martin Helmstädter, Lena K. Ebert, Hayo Castrop, Matthias J. Hackl, Gerd Walz, Paul T. Brinkkoetter, Max C. Liebau, Kálmán Tory, Peter F. Hoyer, Bodo B. Beck, Hjalmar Brismar, Hans Blom, Bernhard Schermer, and Thomas Benzing. A molecular mechanism explaining albuminuria in kidney disease. *Nature Metabolism 2020 2:5*, 2:461–474, 5 2020.

[15] Peter Mundel. Podocytes and the quest for precision medicines for kidney diseases. *Pflugers Archiv : European journal of physiology*, 469:1029–1037, 8 2017.

[16] Marina de Cos, Kristin Meliambro, and Kirk N. Campbell. Novel treatment paradigms: Focal segmental glomerulosclerosis. *Kidney International Reports*, 8:30, 1 2023.

[17] An S. De Vriese, Jack F. Wetzels, Richard J. Glassock, Sanjeev Sethi, and Fernando C. Fervenza. Therapeutic trials in adult fsgs: lessons learned and the road forward. *Nature reviews. Nephrology*, 17:619–630, 9 2021.

[18] Agnes B. Fogo. Causes and pathogenesis of focal segmental glomerulosclerosis. *Nature Reviews Nephrology 2014 11:2*, 11:76–87, 12 2014.

[19] Amir Shabaka, Ana Tato Ribera, and Gema Fernández-Juárez. Focal segmental glomerulosclerosis: State-of-the-art and clinical perspective. *Nephron*, 144:413–427, 9 2020.

[20] Ania Koziell, Victor Grech, Sagair Hussain, Gary Lee, Ulla Lenkkeri, Karl Tryggvason, and Peter Scambler. Genotype/phenotype correlations of nphs1 and nphs2 mutations in nephrotic syndrome advocate a functional inter-relationship in glomerular filtration. *Human molecular genetics*, 11:379–88, 2 2002.

[21] J M Kaplan, S H Kim, K N North, H Rennke, L A Correia, H Q Tong, B J Mathis, J C Rodríguez-Pérez, P G Allen, A H Beggs, and M R Pollak. Mutations in actn4, encoding alpha-actinin-4, cause familial focal segmental glomerulosclerosis. *Nature genetics*, 24:251–6, 3 2000.

[22] Sanna Lehtonen, Fang Zhao, and Eero Lehtonen. Cd2-associated protein directly interacts with the actin cytoskeleton. *American journal of physiology. Renal physiology*, 283:F734–43, 10 2002.

[23] Yu-Xing Liu, Ai-Qian Zhang, Fang-Mei Luo, Yue Sheng, Chen-Yu Wang, Yi Dong, Liangliang Fan, and Lv Liu. Case report: A novel heterozygous mutation of cd2ap in a chinese family with proteinuria leads to focal segmental glomerulosclerosis. *Frontiers in pediatrics*, 9:687455, 2021.

[24] M M Löwik, P J T A Groenen, I Pronk, M R Lilien, R Goldschmeding, H B Dijkman, E N Levtchenko, L A Monnens, and L P van den Heuvel. Focal segmental glomerulosclerosis in a patient homozygous for a cd2ap mutation. *Kidney international*, 72:1198–203, 11 2007.

[25] Maddalena Gigante, Paola Pontrelli, Eustacchio Montemurno, Leonarda Roca, Filippo Aucella, Rosa Penza, Gianluca Caridi, Elena Ranieri, Gian Marco Ghiggeri, and Loreto Gesualdo. Cd2ap mutations are associated with sporadic nephrotic syndrome and focal segmental glomerulosclerosis (fsgs). *Nephrology, dialysis, transplantation : official publication of the European Dialysis and Transplant Association - European Renal Association*, 24:1858–64, 6 2009.

[26] Dmitry Tsvetkov, Michael Hohmann, Yoland Marie Anistan, Marwan Mannaa, Christian Harteneck, Birgit Rudolph, and Maik Gollasch. A cd2ap mutation associated with focal segmental glomerulosclerosis in young adulthood. *Clinical medicine insights. Case reports*, 9:15–9, 2016.

[27] D N Feng, Y H Yang, D J Wang, D C Meng, R Fu, J J Wang, and Z H Yu. Mutational analysis of podocyte genes in children with sporadic steroid-resistant nephrotic syndrome. *Genetics and molecular research : GMR*, 13:9514–22, 11 2014.

[28] M Little, G Holmes, W Bickmore, V van Heyningen, N Hastie, and B Wainwright. Dna binding capacity of the wt1 protein is abolished by denys-drash syndrome wt1 point mutations. *Human molecular genetics*, 4:351–8, 3 1995.

[29] D A Haber, R L Sohn, A J Buckler, J Pelletier, K M Call, and D E Housman. Alternative splicing and genomic structure of the wilms tumor gene wt1. *Proceedings of the National Academy of Sciences of the United States of America*, 88:9618–22, 11 1991.

[30] Olivia Boyer, Stéphanie Woerner, Fan Yang, Edward J Oakeley, Bolan Linghu, Olivier Gribouval, Marie-Josèphe Tête, José S Duca, Lloyd Klickstein, Amy J Damask, Joseph D Szustakowski, Françoise Heibel, Marie Matignon, Véronique Baudouin, François Chantrel, Jacqueline Champigneulle, Laurent Martin, Patrick Nitschké, Marie-Claire Gubler, Keith J Johnson, Salah-Dine Chibout, and Corinne Antignac. Lmx1b mutations cause hereditary fsgs without extrarenal involvement. *Journal of the American Society of Nephrology : JASN*, 24:1216–22, 7 2013.

[31] Noel Edwards, Sarah J Rice, Shreya Raman, Ann Marie Hynes, Shalabh Srivastava, Iain Moore, Mohamed Al-Hamed, Yaobo Xu, Mauro Santibanez-Koref, David T Thwaites, Daniel P Gale, and John A Sayer. A novel lmx1b mutation in a family with end-stage renal disease of 'unknown cause'. *Clinical kidney journal*, 8:113–9, 2 2015.

[32] Nicole K Andeen, Jennifer Schleit, Christopher D Blosser, Michael O Dorschner, Fuki Marie Hisama, and Kelly D Smith. Lmx1b-associated nephropathy with type iii collagen deposition in the glomerular and tubular basement membranes. *American journal of kidney diseases : the official journal of the National Kidney Foundation*, 72:296–301, 8 2018.

[33] Martin Kann, Eunnyung Bae, Maximilian O. Lenz, Liangji Li, Bao Tran Trannguyen, Valerie A. Schumacher, Mary E. Taglienti, Liliana Bordeianou, Sunny Hartwig, Markus M. Rinschen, Bernhard Schermer, Thomas Benzing, Chen Ming Fan, and Jordan A. Kreidberg. Wt1 targets gas1 to maintain nephron progenitor cells by modulating fgf signals. *Development (Cambridge, England)*, 142:1254–1266, 4 2015.

[34] Martin Kann, Sandrine Ettou, Youngsook L. Jung, Maximilian O. Lenz, Mary E. Taglienti, Peter J. Park, Bernhard Schermer, Thomas Benzing, and Jordan A. Kreidberg. Genome-wide analysis of wilms' tumor 1-controlled gene expression in podocytes reveals key regulatory mechanisms. *Journal of the American Society of Nephrology*, 26:2097–2104, 9 2015.

[35] Sandrine Ettou, Youngsook L. Jung, Tomoya Miyoshi, Dhawal Jain, Ken Hiratsuka, Valerie Schumacher, Mary E. Taglienti, Ryuji Morizane, Peter J. Park, and Jordan A. Kreidberg. Epigenetic transcriptional reprogramming by wt1 mediates a repair response during podocyte injury. *Science advances*, 6, 7 2020.

[36] Amelia Casamassimi and Alfredo Ciccodicola. Transcriptional regulation: Molecules, involved mechanisms, and misregulation. *International Journal of Molecular Sciences*, 20, 3 2019.

[37] Sumant S. Chugh. Transcriptional regulation of podocyte disease. *Translational research : the journal of laboratory and clinical medicine*, 149:237, 2007.

[38] Akihito Hishikawa, Kaori Hayashi, Takaya Abe, Mari Kaneko, Hideki Yokoi, Tatsuhiko Azegami, Mari Nakamura, Norifumi Yoshimoto, Takeshi Kanda, Yusuke Sakamaki, and Hiroshi Itoh. Decreased kat5 expression impairs dna repair and induces altered dna methylation in kidney podocytes. *Cell reports*, 26:1318–1332.e4, 1 2019.

[39] Anne Rascle, Hani Suleiman, Tanja Neumann, and Ralph Witzgall. Role of transcription factors in podocytes. *Nephron. Experimental nephrology*, 106, 6 2007.

[40] Lihua Dong, Stefan Pietsch, Zenglai Tan, Birgit Perner, Ralph Sierig, Dagmar Kruspe, Marco Groth, Ralph Witzgall, Hermann Josef Gröne, Matthias Platzer, and Christoph Englert. Integration of cistromic and transcriptomic analyses identifies nphs2, mafb, and magi2 as wilms' tumor 1 target genes in podocyte differentiation and maintenance. *Journal of the American Society of Nephrology : JASN*, 26:2118–2128, 9 2015.

[41] Annette Hammes, Jian Kan Guo, Gudrun Lutsch, Joerg Robert Leheste, Danilo Landrock, Ulrike Ziegler, Marie Claire Gubler, and Andreas Schedl. Two splice variants of the wilms' tumor 1 gene have distinct functions during sex determination and nephron formation. *Cell*, 106:319–329, 8 2001.

[42] Julie Wells, Miguel N. Rivera, Woo Jae Kim, Kristen Starbuck, and Daniel A. Haber. The predominant wt1 isoform (+kts) encodes a dna binding protein targeting the planar cell polarity gene scribble in renal podocytes. *Molecular cancer research : MCR*, 8:975, 7 2010.

[43] Morgan A. Burt, Titilola D. Kalejaiye, Rohan Bhattacharya, Nikolaos Dimitrakakis, and Samira Musah. Adriamycin-induced podocyte injury disrupts the yap-tead1 axis and downregulates cyr61 and ctgf expression. *ACS chemical biology*, 17:3341–3351, 12 2022.

[44] Manuel Rogg, Jasmin I. Maier, Martin Helmstädter, Alena Sammarco, Felix Kliewe, Oliver Kretz, Lisa Weißer, Clara Van Wymersch, Karla Findeisen, Anna L. Koessinger, Olga Tsoy, Jan Baumbach, Markus Grabbert, Martin Werner, Tobias B. Huber, Nicole Endlich, Oliver Schilling, and Christoph Schell. A yap/taz-arhgap29-rhoa signaling axis regulates podocyte protrusions and integrin adhesions. *Cells*, 12, 7 2023.

[45] Yoshiro Maezawa, Tuncer Onay, Rizaldy P. Scott, Lindsay S. Keir, Henrik Dimke, Chengjin Li, Vera Eremina, Yuko Maezawa, Marie Jeansson, Jingdong Shan, Matthew Binnie, Moshe Lewin, Asish Ghosh, Jeffrey H. Miner, Seppo J. Vainio, and Susan E. Quaggin. Loss of the podocyte-expressed transcription factor tcf21/pod1 results in podocyte differentiation defects and fsgs. *Journal of the American Society of Nephrology : JASN*, 25:2459–2470, 11 2014.

[46] Felix Kliewe, Andreas W. Kuss, Florian Siegerist, Sindy Schröder, Sandra Schordan, Nadine Artelt, Frances Kindt, Kerstin Amann, Maja T. Lindenmeyer, Karlhans Endlich, and Nicole Endlich. Studies on the role of the transcription factor tcf21 in the transdifferentiation of parietal epithelial cells into podocyte-like cells. *Cellular physiology and biochemistry : international journal of experimental cellular physiology, biochemistry, and pharmacology*, 55:48–67, 2021.

[47] Joichi Usui, Misa Yaguchi, Satoshi Yamazaki, Mayumi Takahashi-Kobayashi, Tetsuya Kawamura, Shuzo Kaneko, Surya V. Seshan, Pierre Ronco, and Kunihiro Yamagata. Transcription factor 21 expression in injured podocytes of glomerular diseases. *Scientific reports*, 10, 12 2020.

[48] Naoki Morito, Toshiaki Usui, Shun Ishibashi, and Kunihiro Yamagata. Podocyte-specific transcription factors: Could mafb become a therapeutic target for kidney disease? *Internal medicine (Tokyo, Japan)*, 62:11–19, 2023.

[49] Toshiaki Usui, Naoki Morito, Hossam H. Shawki, Yoshinori Sato, Hiroyasu Tsukaguchi, Michito Hamada, Hyojung Jeon, Manoj Kumar Yadav, Akihiro Kuno, Yuki Tsunakawa, Risa Okada, Takaaki Ojima, Maho Kanai, Keigo Asano, Yuki Imamura, Ryusuke Koshida, Keigyou Yoh, Joichi Usui, Hideki Yokoi, Masato Kasahara, Ashio Yoshimura, Masafumi Muratani, Takashi Kudo, Hisashi Oishi, Kunihiro Yamagata, and Satoru Takahashi. Transcription factor mafb in podocytes protects against the development of focal segmental glomerulosclerosis. *Kidney international*, 98:391–403, 8 2020.

[50] Yoshinori Sato, Hiroyasu Tsukaguchi, Hiroyuki Morita, Koichiro Higasa, Mai Thi Nhu Tran, Michito Hamada, Toshiaki Usui, Naoki Morito, Shoichiro Horita, Takao Hayashi, Junko Takagi, Izumi Yamaguchi, Huan Thanh Nguyen, Masayo Harada, Kiyoko Inui, Yuichi Maruta, Yoshihiko Inoue, Fumihiko Koiwa, Hiroshi Sato, Fumihiko Matsuda, Shinya Ayabe, Seiya Mizuno, Fumihiro Sugiyama, Satoru Takahashi, and Ashio Yoshimura. A mutation in transcription factor mafb causes focal segmental glomerulosclerosis with duane retraction syndrome. *Kidney international*, 94:396–407, 8 2018.

[51] Filippo M Massa, Fariba Jian-Motamedi, Marijus Šerys, Amelie Tison, Agnès Loubat, Sandra Lacas-Gervais, Luc Martin, Hassiba Belahbib, Sandrine Sarrazin, Michael H Sieweke, and Andreas Schedl. Mafb drives differentiation by permitting wt1 binding to podocyte specific promoters. *eLife*, 9 2023.

[52] Lori L. O'Brien, Michael Grimaldi, Zachary Kostun, Rebecca A. Wingert, Rori Selleck, and Alan J. Davidson. Wt1a, foxc1a, and the notch mediator rbpj physically interact and regulate the formation of podocytes in zebrafish. *Developmental biology*, 358:318–330, 2011.

[53] Sato Magassa, Liviu Aron, Clement Hoguin, Pierre Isnard, Fabiola Terzi, Christophe Legendre, Bruce A. Yankner, and Guillaume Canaud. Rest and stress resistance in the aging kidney. *Journal of the American Society of Nephrology : JASN*, 32:1974–1986, 8 2021.

[54] Ikhlak Ahmed, Mubarak Ziab, Sahar Da'as, Waseem Hasan, Sujitha P. Jeya, Elbay Aliyev, Sabah Nisar, Ajaz A. Bhat, Khalid Adnan Fakhro, and Ammira S. Alshabeeb Akil. Network-based identification and prioritization of key transcriptional factors of diabetic kidney disease. *Computational and structural biotechnology journal*, 21:716–730, 1 2023.

[55] Xiao Zhu, Liping Tang, Jingxin Mao, Yasir Hameed, Jingyu Zhang, Ning Li, Danny Wu, Yongmei Huang, and Chen Li. Decoding the mechanism behind the pathogenesis of the focal segmental glomerulosclerosis. *Computational and mathematical methods in medicine*, 2022, 2022.

[56] Yingxue Ding, Zongli Diao, Hong Cui, Aijun Yang, Wenhu Liu, and Lina Jiang. Bioinformatics analysis reveals the roles of cytoskeleton protein transgelin in occurrence and development of proteinuria. *Translational pediatrics*, 10:2250–2268, 9 2021.

[57] Thaddäus Struk, Viji Nair, Felix Eichinger, Matthias Kretzler, Roland Wedlich-Söldner, Samet Bayraktar, and Hermann Pavenstädt. Transcriptome analysis of primary podocytes reveals novel calcium regulated regulatory networks. *FASEB journal : official publication of the Federation of American Societies for Experimental Biology*, 34:14490–14506, 11 2020.

[58] Eva Nora Bukosza, Klaus Kratochwill, Christoph Kornauth, Helga Schachner, Christoph Aufricht, and Christoph A. Gebeshuber. Podocyte rna sequencing reveals wnt- and ecm-associated genes as central in fsgs. *PloS one*, 15, 4 2020.

[59] Jia Fu, Zhengzi Yi, Minchao Cai, Weijie Yuan, Weijia Zhang, Kyung Lee, and John Cijiang He. Global transcriptomic changes in glomerular endothelial cells in mice with podocyte depletion and glomerulosclerosis. *Cell death & disease*, 12, 7 2021.

[60] Melanie Boerries, Florian Grahammer, Sven Eiselein, Moritz Buck, Charlotte Meyer, Markus Goedel, Wibke Bechtel, Stefan Zschiedrich, Dietmar Pfeifer, Denis Laloë, Christelle Arrondel, Sara Gonçalves, Marcus Krüger, Scott J Harvey, Hauke Busch, Joern Dengjel, and Tobias B Huber. Molecular fingerprinting of the podocyte reveals novel gene and protein regulatory networks. *Kidney international*, 83:1052–64, 6 2013.

[61] Waddington C. H. The epigenotype. *Endeavour*, 1:18–20, 1942.

[62] Susan W. Herring. Formation of the vertebrate face epigenetic and functional influences. *Integrative and Comparative Biology*, 33:472–483, 8 1993.

[63] Nikolas Zagris. Aristotle (384-322 bc): the beginnings of embryology. *The International journal of developmental biology*, 66:5–8, 2022.

[64] D. Haig. The (dual) origin of epigenetics. *Cold Spring Harbor symposia on quantitative biology*, 69:67–70, 2004.

[65] E. R. Gibney and C. M. Nolan. Epigenetics and gene expression. *Heredity 2010 105:1*, 105:4–13, 5 2010.

[66] Aimée M. Deaton and Adrian Bird. Cpg islands and the regulation of transcription. *Genes & Development*, 25:1010, 5 2011.

[67] Lisa D. Moore, Thuc Le, and Guoping Fan. Dna methylation and its basic function. *Neuropsychopharmacology 2013 38:1*, 38:23–38, 7 2012.

[68] Steven Henikoff and Mitchell M. Smith. Histone variants and epigenetics. *Cold Spring Harbor Perspectives in Biology*, 7, 1 2015.

[69] Andrew J. Bannister and Tony Kouzarides. Regulation of chromatin by histone modifications. *Cell Research 2011 21:3*, 21:381–395, 2 2011.

[70] Nathaniel D. Heintzman, Rhona K. Stuart, Gary Hon, Yutao Fu, Christina W. Ching, R. David Hawkins, Leah O. Barrera, Sara Van Calcar, Chunxu Qu, Keith A. Ching, Wei Wang, Zhiping Weng, Roland D. Green, Gregory E. Crawford, and Bing Ren. Distinct and predictive chromatin signatures of transcriptional promoters and enhancers in the human genome. *Nature Genetics 2007 39:3*, 39:311–318, 2 2007.

[71] Karin J. Ferrari, Andrea Scelfo, Sri Ganesh Jammula, Alessandro Cuomo, Iros Barozzi, Alexandra Stützer, Wolfgang Fischle, Tiziana Bonaldi, and Diego Pasini. Polycomb-dependent h3k27me1 and h3k27me2 regulate active transcription and enhancer fidelity. *Molecular cell*, 53:49–62, 1 2014.

[72] Lili Liao, Joseph R. Testa, and Haifeng Yang. The roles of chromatin-remodelers and epigenetic modifiers in kidney cancer. *Cancer genetics*, 208:206, 5 2015.

[73] Michael Ignarski, Rashidul Islam, and Roman Ulrich Müller. Long non-coding rnas in kidney disease. *International journal of molecular sciences*, 20, 7 2019.

[74] Alla A. Sigova, Brian J. Abraham, Xiong Ji, Benoit Molinie, Nancy M. Hannett, Yang Eric Guo, Mohini Jangi, Cosmas C. Giallourakis, Phillip A. Sharp, and Richard A. Young. Transcription factor trapping by rna in gene regulatory elements. *Science*, 350:978–991, 11 2015.

[75] Jonathan E Henninger, Ozgur Oksuz, Krishna Shrinivas, Ido Sagi, Gary LeRoy, Ming M Zheng, J Owen Andrews, Alicia V Zamudio, Charalampos Lazaris, Nancy M Hannett, Tong Ihn Lee, Phillip A Sharp, Ibrahim I Cissé, Arup K Chakraborty, and Richard A Young. Rna-mediated feedback control of transcriptional condensates. *Cell*, 184:207–225.e24, 1 2021.

[76] Benjamin R. Sabari, Alessandra Dall'Agnese, Ann Boija, Isaac A. Klein, Eliot L. Coffey, Krishna Shrinivas, Brian J. Abraham, Nancy M. Hannett, Alicia V. Zamudio, John C. Manteiga, Charles H. Li, Yang E. Guo, Daniel S. Day, Jurian Schuijers, Eliza Vasile, Sohail Malik, Denes Hnisz, Tong Ihn Lee, Ibrahim I. Cisse, Robert G. Roeder, Phillip A. Sharp, Arup K. Chakraborty, and Richard A. Young. Coactivator condensation at super-enhancers links phase separation and gene control. *Science (New York, N.Y.)*, 361, 7 2018.

[77] MARCUS J. MOELLER, IULIA A. KOVARI, and LAWRENCE B. HOLZMAN. Evaluation of a new tool for exploring podocyte biology: mouse nphs1 5' flanking region drives lacz expression in podocytes. *Journal of the American Society of Nephrology : JASN*, 11:2306–2314, 12 2000.

[78] Marcus J. Moeller, Silja K. Sanden, Abdulsalam Soofi, Roger C. Wiggins, and Lawrence B. Holzman. Two gene fragments that direct podocyte-specific expression in transgenic mice. *Journal of the American Society of Nephrology : JASN*, 13:1561–1567, 2002.

[79] Marcus J. Moeller, Abdulsalam Soofi, Silja Sanden, Jürgen Floege, Wilhelm Kriz, and Lawrence B. Holzman. An efficient system for tissue-specific overexpression of transgenes in podocytes in vivo. *American journal of physiology. Renal physiology*, 289, 2005.

[80] Sebastian Pott and Jason D. Lieb. What are super-enhancers? *Nature Genetics 2015 47:1*, 47:8–12, 12 2014.

[81] Karsten B Sieber, Anna Batorsky, Kyle Siebenthall, Kelly L Hudkins, Jeff D Vierstra, Shawn Sullivan, Aakash Sur, Michelle McNulty, Richard Sandstrom, Alex Reynolds, Daniel Bates, Morgan Diegel, Douglass Dunn, Jemma Nelson, Michael Buckley, Rajinder Kaul, Matthew G Sampson, Jonathan Himmelfarb, Charles E Alpers, Dawn Waterworth, and Shreeram Akilesh. Integrated functional genomic analysis enables annotation of kidney genome-wide association study loci. *Journal of the American Society of Nephrology : JASN*, 30:421–441, 3 2019.

[82] Jingping Yang, Difei Zhang, Masaru Motojima, Tsutomu Kume, Qing Hou, Yu Pan, Aiping Duan, Mingchao Zhang, Song Jiang, Jinhua Hou, Jingsong Shi, Zhaohui Qin, and Zhihong Liu. Super-enhancer-associated transcription factors maintain transcriptional regulation in mature podocytes. *Journal of the American Society of Nephrology*, 32:1323–1337, 6 2021.

[83] Marta Christov, Abbe R Clark, Braden Corbin, Samy Hakroush, Eugene P Rhee, Hiroaki Saito, Dan Brooks, Eric Hesse, Mary Bouxsein, Niels Galjart, Ji Yong Jung, Peter Mundel, Harald Jüppner, Astrid Weins, and Anna Greka. Inducible podocyte-specific deletion of ctcf drives progressive kidney disease and bone abnormalities. *JCI insight*, 3, 2 2018.

[84] Abbe R Clark, Jamie Marshall, Yiming Zhou, Monica S Montesinos, Haiqi Chen, Lan Nguyen, Fei Chen, and Anna Greka. Single-cell transcriptomics reveal disrupted kidney filter cell-cell interactions after early and selective podocyte injury. *The American journal of pathology*, 192:281–294, 2 2022.

[85] Hong Wang, Aiping Duan, Jing Zhang, Qi Wang, Yuexian Xing, Zhaohui Qin, Zhihong Liu, and Jingping Yang. Glucocorticoid receptor wields chromatin interactions to tune transcription for cytoskeleton stabilization in podocytes. *Communications biology*, 4, 12 2021.

[86] Syamantak Majumder, Karina Thieme, Sri N. Batchu, Tamadher A. Alghamdi, Bridgit B. Bowskill, M. Golam Kabir, Youan Liu, Suzanne L. Advani, Kathryn E. White, Laurette Geldenhuys, Karthik K. Tennankore, Penelope Poyah, Ferhan S. Siddiqi, and Andrew Advani. Shifts in podocyte histone h3k27me3 regulate mouse and human glomerular disease. *The Journal of Clinical Investigation*, 128:483, 1 2018.

[87] Marita Liebisch and Gunter Wolf. Age-induced suppression of ezh2 mediates injury of podocytes by reducing h3k27me3. *American journal of nephrology*, 51:676–692, 2020.

[88] Kent Doi, Asada Leelahavanichkul, Peter S.T. Yuen, and Robert A. Star. Animal models of sepsis and sepsis-induced kidney injury. *The Journal of Clinical Investigation*, 119:2868, 10 2009.

[89] Takayuki Fujino and Naoyuki Hasebe. Alteration of histone h3k4 methylation in glomerular podocytes associated with proteinuria in patients with membranous nephropathy. *BMC nephrology*, 17:1–15, 11 2016.

[90] Gaelle M. Lefevre, Sanjeevkumar R. Patel, Doyeob Kim, Lino Tessarollo, and Gregory R. Dressler. Altering a histone h3k4 methylation pathway in glomerular podocytes promotes a chronic disease phenotype. *PLoS genetics*, 6:1–15, 2010.

[91] Kazunori Inoue, Geliang Gan, Maria Ciarleglio, Yan Zhang, Xuefei Tian, Christopher E. Pedigo, Corey Cavanaugh, Janet Tate, Ying Wang, Elizabeth Cross, Marwin Groener, Nathan Chai, Zhen Wang, Amy Justice, Zhenhai Zhang, Chirag R. Parikh, Francis P. Wilson, and Shuta Ishibe. Podocyte histone deacetylase activity regulates murine and human glomerular diseases. *The Journal of clinical investigation*, 129:1295–1313, 3 2019.

[92] Sabbir Khan, Gopabandhu Jena, Kulbhushan Tikoo, and Vinod Kumar. Valproate attenuates the proteinuria, podocyte and renal injury by facilitating autophagy and inactivation of nf-κb/inos signaling in diabetic rat. *Biochimie*, 110:1–16, 3 2015.

[93] Shokichi Naito, Kenichi Nakayama, and Nagako Kawashima. Enhanced levels of glycosphingolipid gm3 delay the progression of diabetic nephropathy. *International journal of molecular sciences*, 24:11355, 7 2023.

[94] Paulina X Medina Rangel, Elizabeth Cross, Chang Liu, Christopher E Pedigo, Xuefei Tian, Elena Gutiérrez-Calabrés, Soichiro Nagata, Anupama Priyadarshini, Gabriel Lerner, Patricia Bunda, Sudhir Perincheri, Jianlei Gu, Hongyu Zhao, Ying Wang, Kazunori Inoue, and Shuta Ishibe. Cell cycle and senescence regulation by podocyte histone deacetylase 1 and 2. *Journal of the American Society of Nephrology : JASN*, 34:433–450, 3 2023.

[95] Susan E. Quaggin. Transcriptional regulation of podocyte specification and differentiation. *Microscopy research and technique*, 57:208–211, 5 2002.

[96] Jun Li, Jinshu Xu, Huihui Jiang, Ting Zhang, Aarthi Ramakrishnan, Li Shen, and Pin Xian Xu. Chromatin remodelers interact with eya1 and six2 to target enhancers to control nephron progenitor cell maintenance. *Journal of the American Society of Nephrology*, 32:2815–2833, 11 2021.

[97] Miklos Gaszner and Gary Felsenfeld. Insulators: exploiting transcriptional and epigenetic mechanisms. *Nature reviews. Genetics*, 7:703–713, 9 2006.

[98] Timur M. Yusufzai, Hideaki Tagami, Yoshihiro Nakatani, and Gary Felsenfeld. Ctcf tethers an insulator to subnuclear sites, suggesting shared insulator mechanisms across species. *Molecular cell*, 13:291–298, 1 2004.

[99] Kerstin S. Wendt, Keisuke Yoshida, Takehiko Itoh, Masashige Bando, Birgit Koch, Erika Schirghuber, Shuichi Tsutsumi, Genta Nagae, Ko Ishihara, Tsuyoshi Mishiro, Kazuhide Yahata, Fumio Imamoto, Hiroyuki Aburatani, Mitsuyoshi Nakao, Naoko Imamoto, Kazuhiro Maeshima, Katsuhiko Shirahige, and Jan Michael Peters. Cohesin mediates transcriptional insulation by ccctc-binding factor. *Nature*, 451:796–801, 2 2008.

[100] Abraham S. Weintraub, Charles H. Li, Alicia V. Zamudio, Alla A. Sigova, Nancy M. Hannett, Daniel S. Day, Brian J. Abraham, Malkiel A. Cohen, Behnam Nabet, Dennis L. Buckley, Yang Eric Guo, Denes Hnisz, Rudolf Jaenisch, James E. Bradner, Nathanael S. Gray, and Richard A. Young. Yy1 is a structural regulator of enhancer-promoter loops. *Cell*, 171:1573, 12 2017.

[101] Giacomo Cavalli and Tom Misteli. Functional implications of genome topology. *Nature structural & molecular biology*, 20:290–299, 3 2013.

[102] Geet Duggal, Hao Wang, and Carl Kingsford. Higher-order chromatin domains link eqtls with the expression of far-away genes. *Nucleic acids research*, 42:87–96, 1 2014.

[103] Kabsun Kim, Jung Ha Kim, Inyoung Kim, Semun Seong, Jeong Eun Han, Keun Bae Lee, Jeong Tae Koh, and Nacksung Kim. Transcription factor lmx1b negatively regulates osteoblast differentiation and bone formation. *International Journal of Molecular Sciences*, 23, 5 2022.

[104] Jeffry M. Cesario, André Landin Malt, Jong Uk Chung, Michael P. Khairallah, Krishnakali Dasgupta, Kesava Asam, Lindsay J. Deacon, Veronica Choi, Asma A. Almaidhan, Nadine A. Darwiche, Jimin Kim, Randy L. Johnson, and Juhee Jeong. Anti-osteogenic function of a lim-homeodomain transcription factor lmx1b is essential to early patterning of the calvaria. *Developmental biology*, 443:103–116, 11 2018.

[105] Haixu Chen, Yi Lun, Dmitry Ovchinnikov, Hiroki Kokubo, Kerby C. Oberg, Carmen V. Pepicelli, Lin Gan, Brendan Lee, and Randy L. Johnson. Limb and kidney defects in lmx1b mutant mice suggest an involvement of lmx1b in human nail patella syndrome. *Nature Genetics 1998 19:1*, 19:51–55, 1998.

[106] Nobuhisa Morimoto, Kiyotaka Nagahama, Takayasu Mori, Takuya Fujimaru, Yukio Tsuura, Ayumi Terai, Madoka Tanabe, Megumi Otani, Shingo Shioji, Suguru Hirasawa, Shota Aki, Makoto Aoyagi, Eisei Sohara, Shinichi Uchida, and Hiroyuki Tanaka. A novel lmx1b variant identified in a patient presenting with severe renal involvement and thin glomerular basement membrane. *Nephron*, 145:776–782, 11 2021.

[107] Homare Shimohata, Yusuke Miyake, Yu Yoshida, Joichi Usui, Takayasu Mori, Eisei Sohara, Shinichi Uchida, Kouichi Hirayama, and Masaki Kobayashi. Lmx1b-associated nephropathy that showed myelin figures on electron microscopy. *CEN case reports*, 10:588–591, 11 2021.

[108] Tian Biao Zhou and Yuan Han Qin. The signaling pathways of lmx1b and its role in glomerulosclerosis. *Journal of receptor and signal transduction research*, 32:285–289, 12 2012.

[109] Gentzon Hall, Brandon Lane, Megan Chryst-Ladd, Guanghong Wu, Jen Jar Lin, Xue Jun Qin, Elizabeth R. Hauser, and Rasheed Gbadegesin. Dysregulation of wti (-kts) is associated with the kidney-specific effects of the lmx1b r246q mutation. *Scientific reports*, 7, 1 2017.

[110] Tillmann Burghardt, Jürgen Kastner, Hani Suleiman, Eric Rivera-Milla, Natalya Stepanova, Claudio Lottaz, Marion Kubitza, Carsten A. Böger, Sarah Schmidt, Mathias Gorski, Uwe De Vries, Helga Schmidt, Irmgard Hertting, Jeffrey Kopp, Anne Rascle, Markus Moser, Iris M. Heid, Richard Warth, Rainer Spang, Joachim Wegener, Claudia T. Mierke, Christoph Englert, and Ralph Witzgall. Lmx1b is essential for the maintenance of differentiated podocytes in adult kidneys. *Journal of the American Society of Nephrology : JASN*, 24:1830–1848, 11 2013.

[111] Bing He, Lwaki Ebarasi, Zhe Zhao, Jing Guo, Juha R.M. Ojala, Kjell Hultenby, Sarah De Val, Christer Betsholtz, and Karl Tryggvason. Lmx1b and foxc combinatorially regulate podocin expression in podocytes. *Journal of the American Society of Nephrology : JASN*, 25:2764–2777, 12 2014.

[112] Endika Haro, Florence Petit, Charmaine U Pira, Conor D Spady, Sara Lucas-Toca, Lauren I Yorozuya, Austin L Gray, Fabienne Escande, Anne-Sophie Jourdain, Andy Nguyen, Florence Fellmann, Jean-Marc Good, Christine Francannet, Sylvie Manouvrier-Hanu, Marian A Ros, and Kerby C Oberg. Identification of limb-specific lmx1b auto-regulatory modules with nail-patella syndrome pathogenicity. *Nature communications*, 12:5533, 9 2021.

[113] Haixu Chen and Randy L Johnson. Interactions between dorsal-ventral patterning genes lmx1b, engrailed-1 and wnt-7a in the vertebrate limb. *The International journal of developmental biology*, 46:937–41, 2002.

[114] Stefan J Schunk, Jürgen Floege, Danilo Fliser, and Thimoteus Speer. Wnt-β-catenin signalling - a versatile player in kidney injury and repair. *Nature reviews. Nephrology*, 17:172–184, 3 2021.

[115] Haiying Wang, Ran Zhang, Xinjie Wu, Yafen Chen, Wei Ji, Jingsuo Wang, Yawen Zhang, Yong Xia, Yiqun Tang, and Jinxiang Yuan. The wnt signaling pathway in diabetic nephropathy. *Frontiers in cell and developmental biology*, 9:701547, 2021.

[116] Hongxia Zhang, Weili Luo, Yonghong Sun, Yanchun Qiao, Liying Zhang, Zhilian Zhao, and Shijun Lv. Wnt/β-catenin signaling mediated-uch-l1 expression in podocytes of diabetic nephropathy. *International journal of molecular sciences*, 17, 8 2016.

[117] Xiaowen Chen, Huishi Tan, Jie Xu, Yuan Tian, Qian Yuan, Yangyang Zuo, Qiyan Chen, Xue Hong, Haiyan Fu, Fan Fan Hou, Lili Zhou, and Youhua Liu. Klotho-derived peptide 6 ameliorates diabetic kidney disease by targeting wnt/β-catenin signaling. *Kidney international*, 102:506–520, 9 2022.

[118] Hideki Kato, Antje Gruenwald, Jung Hee Suh, Jeffrey H Miner, Laura Barisoni-Thomas, Makoto M Taketo, Christian Faul, Sarah E Millar, Lawrence B Holzman, and Katalin Susztak. Wnt/β-catenin pathway in podocytes integrates cell adhesion, differentiation, and survival. *The Journal of biological chemistry*, 286:26003–15, 7 2011.

[119] Chunsun Dai, Donna B Stolz, Lawrence P Kiss, Satdarshan P Monga, Lawrence B Holzman, and Youhua Liu. Wnt/beta-catenin signaling promotes podocyte dysfunction and albuminuria. *Journal of the American Society of Nephrology : JASN*, 20:1997–2008, 9 2009.

[120] Lei Jiang, Lingling Xu, Yuxian Song, Jianzhong Li, Junhua Mao, Allan Zijian Zhao, Weichun He, Junwei Yang, and Chunsun Dai. Calmodulin-dependent protein kinase ii/camp response element-binding protein/wnt/β-catenin signaling cascade regulates angiotensin ii-induced podocyte injury and albuminuria. *The Journal of biological chemistry*, 288:23368–79, 8 2013.

[121] Dan Wang, Chunsun Dai, Yingjian Li, and Youhua Liu. Canonical wnt/β-catenin signaling mediates transforming growth factor-β1-driven podocyte injury and proteinuria. *Kidney international*, 80:1159–1169, 12 2011.

[122] Lili Zhou, Xiaowen Chen, Meizhi Lu, Qinyu Wu, Qian Yuan, Chengxiao Hu, Jinhua Miao, Yunfang Zhang, Hongyan Li, Fan Fan Hou, Jing Nie, and Youhua Liu. Wnt/β-catenin links oxidative stress to podocyte injury and proteinuria. *Kidney international*, 95:830–845, 4 2019.

[123] Lili Zhou, Yingjian Li, Weichun He, Dong Zhou, Roderick J Tan, Jing Nie, Fan Fan Hou, and Youhua Liu. Mutual antagonism of wilms' tumor 1 and β-catenin dictates podocyte health and disease. *Journal of the American Society of Nephrology : JASN*, 26:677–91, 3 2015.

[124] Ying Yu, Hongyan Mo, Hui Zhuo, Chen Yu, and Youhua Liu. High fat diet induces kidney injury via stimulating wnt/β-catenin signaling. *Frontiers in medicine*, 9:851618, 2022.

[125] Weichun He, Young Sun Kang, Chunsun Dai, and Youhua Liu. Blockade of wnt/β-catenin signaling by paricalcitol ameliorates proteinuria and kidney injury. *Journal of the American Society of Nephrology : JASN*, 22:90–103, 1 2011.

[126] Jiao Wan, Xiaoyan Hou, Zhanmei Zhou, Jian Geng, Jianwei Tian, Xiaoyan Bai, and Jing Nie. Wt1 ameliorates podocyte injury via repression of ezh2/β-catenin pathway in diabetic nephropathy. *Free radical biology & medicine*, 108:280–299, 7 2017.

[127] Dong Zhou, Yuanyuan Wang, Yuan Gui, Haiyan Fu, Shanshan Zhou, Yanlin Wang, Sheldon I Bastacky, Donna B Stolz, and Youhua Liu. Non-canonical wnt/calcium signaling is protective against podocyte injury and glomerulosclerosis. *Kidney international*, 102:96–107, 7 2022.

[128] Yinqiu Wang, George Jarad, Piyush Tripathi, Minggui Pan, Jeanette Cunningham, Daniel R Martin, Helen Liapis, Jeffrey H Miner, and Feng Chen. Activation of nfat signaling in podocytes causes glomerulosclerosis. *Journal of the American Society of Nephrology : JASN*, 21:1657–66, 10 2010.

[129] LiQi Li, Johannes Freudenberg, Kairong Cui, Ryan Dale, Sang-Hyun Song, Ann Dean, Keji Zhao, Raja Jothi, and Paul E Love. Ldb1-nucleated transcription complexes function as primary mediators of global erythroid gene activation. *Blood*, 121:4575–85, 5 2013.

[130] Sima Babayeva, Yulia Zilber, and Elena Torban. Planar cell polarity pathway regulates actin rearrangement, cell shape, motility, and nephrin distribution in podocytes. *American journal of physiology. Renal physiology*, 300:F549–60, 2 2011.

[131] Sima Babayeva, Brittany Rocque, Lamine Aoudjit, Yulia Zilber, Jane Li, Cindy Baldwin, Hiroshi Kawachi, Tomoko Takano, and Elena Torban. Planar cell polarity pathway regulates nephrin endocytosis in developing podocytes. *The Journal of biological chemistry*, 288:24035–48, 8 2013.

[132] Andrea Babelova, Felix Jansen, Kerstin Sander, Matthias Löhn, Liliana Schäfer, Christian Fork, Hartmut Ruetten, Oliver Plettenburg, Holger Stark, Christoph Daniel, Kerstin Amann, Hermann Pavenstädt, Oliver Jung, and Ralf P Brandes. Activation of rac-1 and rhoa contributes to podocyte injury in chronic kidney disease. *PloS one*, 8:e80328, 2013.

[133] Keiichiro Matoba, Yusuke Takeda, Yosuke Nagai, Kensuke Sekiguchi, Rikako Ukichi, Hiroshi Takahashi, Daisuke Aizawa, Masahiro Ikegami, Toshiaki Tachibana, Daiji Kawanami, Yasushi Kanazawa, Tamotsu Yokota, Kazunori Utsunomiya, and Rimei Nishimura. Rock2-induced metabolic rewiring in diabetic podocytopathy. *Communications biology*, 5:341, 4 2022.

[134] Jennifer M Feenstra, Kohei Kanaya, Charmaine U Pira, Sarah E Hoffman, Richard J Eppey, and Kerby C Oberg. Detection of genes regulated by lmx1b during limb dorsalization. *Development, growth & differentiation*, 54:451–62, 5 2012.

[135] Gemma L Johnson, Morgan B Glasser, Julia F Charles, Jeffrey Duryea, and Jessica A Lehoczky. En1 and lmx1b do not recapitulate embryonic dorsal-ventral limb patterning functions during mouse digit tip regeneration. *Cell reports*, 41:111701, 11 2022.

[136] R D Riddle, M Ensini, C Nelson, T Tsuchida, T M Jessell, and C Tabin. Induction of the lim homeobox gene lmx1 by wnt7a establishes dorsoventral pattern in the vertebrate limb. *Cell*, 83:631–40, 11 1995.

[137] M Kengaku, J Capdevila, C Rodriguez-Esteban, J De La Peña, R L Johnson, J C Izpisúa Belmonte, and C J Tabin. Distinct wnt pathways regulating aer formation and dorsoventral polarity in the chick limb bud. *Science (New York, N.Y.)*, 280:1274–7, 5 1998.

[138] Julia von Maltzahn, C Florian Bentzinger, and Michael A Rudnicki. Wnt7a-fzd7 signalling directly activates the akt/mtor anabolic growth pathway in skeletal muscle. *Nature cell biology*, 14:186–91, 12 2011.

[139] Maja Adamska, Allison C Billi, Susannah Cheek, and Miriam H Meisler. Genetic interaction between wnt7a and lrp6 during patterning of dorsal and posterior structures of the mouse limb. *Developmental dynamics : an official publication of the American Association of Anatomists*, 233:368–72, 6 2005.

[140] Jan M Stenman, Jay Rajagopal, Thomas J Carroll, Makoto Ishibashi, Jill McMahon, and Andrew P McMahon. Canonical wnt signaling regulates organ-specific assembly and differentiation of cns vasculature. *Science (New York, N.Y.)*, 322:1247–50, 11 2008.

[141] Julia von Maltzahn, Radoslav Zinoviev, Natasha C Chang, C Florian Bentzinger, and Michael A Rudnicki. A truncated wnt7a retains full biological activity in skeletal muscle. *Nature communications*, 4:2869, 2013.

[142] K A Adams, J M Maida, J A Golden, and R D Riddle. The transcription factor lmx1b maintains wnt1 expression within the isthmic organizer. *Development (Cambridge, England)*, 127:1857–67, 5 2000.

[143] Chao Guo, Hai-Yan Qiu, Ying Huang, Haixu Chen, Rong-Qiang Yang, Sheng-Di Chen, Randy L Johnson, Zhou-Feng Chen, and Yu-Qiang Ding. Lmx1b is essential for fgf8 and wnt1 expression in the isthmic organizer during tectum and cerebellum development in mice. *Development (Cambridge, England)*, 134:317–25, 1 2007.

[144] Sangmi Chung, Amanda Leung, Baek-Soo Han, Mi-Yoon Chang, Jung-Il Moon, Chun-Hyung Kim, Sunghoi Hong, Jan Pruszak, Ole Isacson, and Kwang-Soo Kim. Wnt1-lmx1a forms a novel autoregulatory loop and controls midbrain dopaminergic differentiation synergistically with the shh-foxa2 pathway. *Cell stem cell*, 5:646–58, 12 2009.

[145] Gangqi Wang, Bram Heijs, Sarantos Kostidis, Rosalie G.J. Rietjens, Marije Koning, Lushun Yuan, Gesa L. Tiemeier, Ahmed Mahfouz, Sébastien J. Dumas, Martin Giera, Jesper Kers, Susana M. Chuva de Sousa Lopes, Cathelijne W. van den Berg, Bernard M. van den Berg, and Ton J. Rabelink. Spatial dynamic metabolomics identifies metabolic cell fate trajectories in human kidney differentiation. *Cell stem cell*, 29:1580–1593.e7, 11 2022.

[146] Florian Witte, Janine Dokas, Franziska Neuendorf, Stefan Mundlos, and Sigmar Stricker. Comprehensive expression analysis of all wnt genes and their major secreted antagonists during mouse limb development and cartilage differentiation. *Gene expression patterns : GEP*, 9:215–23, 4 2009.

[147] Elizabeth W Bradley and M Hicham Drissi. Wnt5b regulates mesenchymal cell aggregation and chondrocyte differentiation through the planar cell polarity pathway. *Journal of cellular physiology*, 226:1683–93, 6 2011.

[148] Barbara E Sisson, Rodney M Dale, Stephanie R Mui, Jolanta M Topczewska, and Jacek Topczewski. A role of glypican4 and wnt5b in chondrocyte stacking underlying craniofacial cartilage morphogenesis. *Mechanisms of development*, 138 Pt 3:279–90, 11 2015.

[149] F H J van Tienen, H Laeremans, C J H van der Kallen, and H J M Smeets. Wnt5b stimulates adipogenesis by activating ppargamma, and inhibiting the beta-catenin dependent wnt signaling pathway together with wnt5a. *Biochemical and biophysical research communications*, 387:207–11, 9 2009.

[150] R Scott Heller, Darwin S Dichmann, Jan Jensen, Chris Miller, Gordon Wong, Ole D Madsen, and Palle Serup. Expression patterns of wnts, frizzleds, sfrps, and misexpression in transgenic mice suggesting a role for wnts in pancreas and foregut pattern formation. *Developmental dynamics : an official publication of the American Association of Anatomists*, 225:260–70, 11 2002.

[151] Silvia Mazzotta, Carlos Neves, Rory J Bonner, Andreia S Bernardo, Kevin Docherty, and Stefan Hoppler. Distinctive roles of canonical and noncanonical wnt signaling in human embryonic cardiomyocyte development. *Stem cell reports*, 7:764–776, 10 2016.

[152] Xiaobin Han and Zhongjie Sun. Adult mouse kidney stem cells orchestrate the de novo assembly of a nephron via sirt2-modulated canonical wnt/β-catenin signaling. *Advanced science (Weinheim, Baden-Wurttemberg, Germany)*, 9:e2104034, 5 2022.

[153] Jenny Schneider, Alaa A Arraf, Mor Grinstein, Ronit Yelin, and Thomas M Schultheiss. Wnt signaling orients the proximal-distal axis of chick kidney nephrons. *Development (Cambridge, England)*, 142:2686–95, 8 2015.

[154] Jason D. Buenrostro, Paul G. Giresi, Lisa C. Zaba, Howard Y. Chang, and William J. Greenleaf. Transposition of native chromatin for fast and sensitive epigenomic profiling of open chromatin, dna-binding proteins and nucleosome position. *Nature Methods 2013 10:12*, 10:1213–1218, 10 2013.

[155] Pei Fen Kuan, Dana Huebert, Audrey Gasch, and Sunduz Keles. A non-homogeneous hidden-state model on first order differences for automatic detection of nucleosome positions. *Statistical Applications in Genetics and Molecular Biology*, 8, 1 2009.

[156] Alan P. Boyle, Sean Davis, Hennady P. Shulha, Paul Meltzer, Elliott H. Margulies, Zhiping Weng, Terrence S. Furey, and Gregory E. Crawford. High-resolution mapping and characterization of open chromatin across the genome. *Cell*, 132:311–322, 1 2008.

[157] Paul G. Giresi and Jason D. Lieb. Isolation of active regulatory elements from eukaryotic chromatin using faire (formaldehyde assisted isolation of regulatory elements). *Methods (San Diego, Calif.)*, 48:233, 7 2009.

[158] M. Ryan Corces, Alexandro E. Trevino, Emily G. Hamilton, Peyton G. Greenside, Nicholas A. Sinnott-Armstrong, Sam Vesuna, Ansuman T. Satpathy, Adam J. Rubin, Kathleen S. Montine, Beijing Wu, Arwa Kathiria, Seung Woo Cho, Maxwell R. Mumbach, Ava C. Carter, Maya Kasowski, Lisa A. Orloff, Viviana I. Risca, Anshul Kundaje, Paul A. Khavari, Thomas J. Montine, William J. Greenleaf, and Howard Y. Chang. An improved atac-seq protocol reduces background and enables interrogation of frozen tissues. *Nature methods*, 14:959–962, 10 2017.

[159] Jason D. Buenrostro, Beijing Wu, Ulrike M. Litzenburger, Dave Ruff, Michael L. Gonzales, Michael P. Snyder, Howard Y. Chang, and William J. Greenleaf. Single-cell chromatin accessibility reveals principles of regulatory variation. *Nature 2015 523:7561*, 523:486–490, 6 2015.

[160] Peter J. Skene and Steven Henikoff. An efficient targeted nuclease strategy for high-resolution mapping of dna binding sites. *eLife*, 6, 1 2017.

[161] Hatice S. Kaya-Okur, Steven J. Wu, Christine A. Codomo, Erica S. Pledger, Terri D. Bryson, Jorja G. Henikoff, Kami Ahmad, and Steven Henikoff. Cut&tag for efficient epigenomic profiling of small samples and single cells. *Nature Communications 2019 10:1*, 10:1–10, 4 2019.

[162] Haojia Wu, Yuhei Kirita, Erinn L. Donnelly, and Benjamin D. Humphreys. Advantages of single-nucleus over single-cell rna sequencing of adult kidney: Rare cell types and novel cell states revealed in fibrosis. *Journal of the American Society of Nephrology : JASN*, 30:23–32, 1 2019.

[163] Michal Slyper, Caroline B.M. Porter, Orr Ashenberg, Julia Waldman, Eugene Drokhlyansky, Isaac Wakiro, Christopher Smillie, Gabriela Smith-Rosario, Jingyi Wu, Danielle Dionne, Sébastien Vigneau, Judit Jané-Valbuena, Timothy L. Tickle, Sara Napolitano, Mei Ju Su, Anand G. Patel, Asa Karlstrom, Simon Gritsch, Masashi Nomura, Avinash Waghray, Satyen H. Gohil, Alexander M. Tsankov, Livnat Jerby-Arnon, Ofir Cohen, Johanna Klughammer, Yanay Rosen, Joshua Gould, Lan Nguyen, Matan Hofree, Peter J. Tramontozzi, Bo Li, Catherine J. Wu, Benjamin Izar, Rizwan Haq, F. Stephen Hodi, Charles H. Yoon, Aaron N. Hata, Suzanne J. Baker, Mario L. Suvà, Raphael Bueno, Elizabeth H. Stover, Michael R. Clay, Michael A. Dyer, Natalie B. Collins, Ursula A. Matulonis, Nikhil Wagle, Bruce E. Johnson, Asaf Rotem, Orit Rozenblatt-Rosen, and Aviv Regev. A single-cell and single-nucleus rna-seq toolbox for fresh and frozen human tumors. *Nature Medicine*, 26:792, 5 2020.

[164] Dries Deleersnijder, Jasper Callemeyn, Ingrid Arijs, Maarten Naesens, Amaryllis H. Van Craenenbroeck, Diether Lambrechts, and Ben Sprangers. Current methodological challenges of single-cell and single-nucleus rna-sequencing in glomerular diseases. *Journal of the American Society of Nephrology : JASN*, 32:1838–1852, 8 2021.

[165] Jiarui Ding, Xian Adiconis, Sean K. Simmons, Monika S. Kowalczyk, Cynthia C. Hession, Nemanja D. Marjanovic, Travis K. Hughes, Marc H. Wadsworth, Tyler Burks, Lan T. Nguyen, John Y.H. Kwon, Boaz Barak, William Ge, Amanda J. Kedaigle, Shaina Carroll, Shuqiang Li, Nir Hacohen, Orit Rozenblatt-Rosen, Alex K. Shalek, Alexandra Chloé Villani, Aviv Regev, and Joshua Z. Levin. Systematic comparison of single-cell and single-nucleus rna-sequencing methods. *Nature biotechnology*, 38:737–746, 6 2020.

[166] Belinda Phipson, Pei X. Er, Alexander N. Combes, Thomas A. Forbes, Sara E. Howden, Luke Zappia, Hsan Jan Yen, Kynan T. Lawlor, Lorna J. Hale, Jane Sun, Ernst Wolvetang, Minoru Takasato, Alicia Oshlack, and Melissa H. Little. Evaluation of variability in human kidney organoids. *Nature methods*, 16:79–87, 1 2019.

[167] Haojia Wu, Kohei Uchimura, Erinn L. Donnelly, Yuhei Kirita, Samantha A. Morris, and Benjamin D. Humphreys. Comparative analysis and refinement of human psc-derived kidney organoid differentiation with single-cell transcriptomics. *Cell stem cell*, 23:869–881.e8, 12 2018.

[168] Hongbo Liu, Tomohito Doke, Dong Guo, Xin Sheng, Ziyuan Ma, Joseph Park, Ha My T. Vy, Girish N. Nadkarni, Amin Abedini, Zhen Miao, Matthew Palmer, Benjamin F. Voight, Hongzhe Li, Christopher D. Brown, Marylyn D. Ritchie, Yan Shu, and Katalin Susztak. Epigenomic and transcriptomic analyses define core cell types, genes and targetable mechanisms for kidney disease. *Nature Genetics 2022 54:7*, 54:950–962, 6 2022.

[169] Alexander N. Combes, Luke Zappia, Pei Xuan Er, Alicia Oshlack, and Melissa H. Little. Single-cell analysis reveals congruence between kidney organoids and human fetal kidney. *Genome medicine*, 11, 1 2019.

[170] Nick R. Glass, Minoru Takasako, Pei Xuan Er, Drew M. Titmarsh, Alejandro Hidalgo, Ernst J. Wolvetang, Melissa H. Little, and Justin J. Cooper-White. Multivariate patterning of human pluripotent cells under perfusion reveals critical roles of induced paracrine factors in kidney organoid development. *Science advances*, 6, 1 2020.

[171] Yuhei Kirita, Haojia Wu, Kohei Uchimura, Parker C. Wilson, and Benjamin D. Humphreys. Cell profiling of mouse acute kidney injury reveals conserved cellular responses to injury. *Proceedings of the National Academy of Sciences of the United States of America*, 117:15874–15883, 7 2020.

[172] Parker C. Wilson, Haojia Wu, Yuhei Kirita, Kohei Uchimura, Nicolas Ledru, Helmut G. Rennke, Paul A. Welling, Sushrut S. Waikar, and Benjamin D. Humphreys. The single-cell transcriptomic landscape of early human diabetic nephropathy. *Proceedings of the National Academy of Sciences of the United States of America*, 116:19619–19625, 9 2019.

[173] Darren A. Cusanovich, Riza Daza, Andrew Adey, Hannah A. Pliner, Lena Christiansen, Kevin L. Gunderson, Frank J. Steemers, Cole Trapnell, and Jay Shendure. Multiplex single-cell profiling of chromatin accessibility by combinatorial cellular indexing. *Science*, 348:910–914, 5 2015.

[174] Zhen Miao, Michael S. Balzer, Ziyuan Ma, Hongbo Liu, Junnan Wu, Rojesh Shrestha, Tamas Aranyi, Amy Kwan, Ayano Kondo, Marco Pontoglio, Junhyong Kim, Mingyao Li, Klaus H. Kaestner, and Katalin Susztak. Single cell regulatory landscape of the mouse kidney highlights cellular differentiation programs and disease targets. *Nature Communications 2021 12:1*, 12:1–17, 4 2021.

[175] Yoshiharu Muto, Parker C. Wilson, Nicolas Ledru, Haojia Wu, Henrik Dimke, Sushrut S. Waikar, and Benjamin D. Humphreys. Single cell transcriptional and chromatin accessibility profiling redefine cellular heterogeneity in the adult human kidney. *Nature Communications 2021 12:1*, 12:1–17, 4 2021.

[176] Parker C. Wilson, Yoshiharu Muto, Haojia Wu, Anil Karihaloo, Sushrut S. Waikar, and Benjamin D. Humphreys. Multimodal single cell sequencing implicates chromatin accessibility and genetic background in diabetic kidney disease progression. *Nature Communications 2022 13:1*, 13:1–20, 9 2022.

[177] Xin Sheng, Yuting Guan, Ziyuan Ma, Junnan Wu, Hongbo Liu, Chengxiang Qiu, Steven Vitale, Zhen Miao, Matthew J. Seasock, Matthew Palmer, Myung K. Shin, Kevin L. Duffin, Steven S. Pullen, Todd L. Edwards, Jacklyn N. Hellwege, Adriana M. Hung, Mingyao Li, Benjamin F. Voight, Thomas M. Coffman, Christopher D. Brown, and Katalin Susztak. Mapping the genetic architecture of human traits to cell types in the kidney identifies mechanisms of disease and potential treatments. *Nature Genetics 2021 53:9*, 53:1322–1333, 8 2021.

[178] Tara K. Sigdel, Paul D. Piehowski, Sudeshna Roy, Juliane Liberto, Joshua R. Hansen, Adam C. Swensen, Rui Zhao, Ying Zhu, Priyanka Rashmi, Andrew Schroeder, Izabella Damm, Swastika Sur, Jinghui Luo, Yingbao Yang, Wei Jun Qian, and Minnie M. Sarwal. Near-single-cell proteomics profiling of the proximal tubular and glomerulus of the normal human kidney. *Frontiers in medicine*, 7, 9 2020.

[179] Blue B Lake, Rajasree Menon, Seth Winfree, Qiwen Hu, Ricardo Melo Ferreira, Kian Kalhor, Daria Barwinska, Edgar A Otto, Michael Ferkowicz, Dinh Diep, Nongluk Plongthongkum, Amanda Knoten, Sarah Urata, Laura H Mariani, Abhijit S Naik, Sean Eddy, Bo Zhang, Yan Wu, Diane Salamon, James C Williams, Xin Wang, Karol S Balderrama, Paul J Hoover, Evan Murray, Jamie L Marshall, Teia Noel, Anitha Vijayan, Austin Hartman, Fei Chen, Sushrut S Waikar, Sylvia E Rosas, Francis P Wilson, Paul M Palevsky, Krzysztof Kiryluk, John R Sedor, Robert D Toto, Chirag R Parikh, Eric H Kim, Rahul Satija, Anna Greka, Evan Z Macosko, Peter V Kharchenko, Joseph P Gaut, Jeffrey B Hodgin, KPMP Consortium, Michael T Eadon, Pierre C Dagher, Tarek M El-Achkar, Kun Zhang, Matthias Kretzler, and Sanjay Jain. An atlas of healthy and injured cell states and niches in the human kidney. *Nature*, 619:585–594, 7 2023.

[180] Jitske Jansen, Bartholomeus T. van den Berge, Martijn van den Broek, Rutger J. Maas, Deniz Daviran, Brigith Willemsen, Rona Roverts, Marit van der Kruit, Christoph Kuppe, Katharina C. Reimer, Gianluca Di Giovanni, Fieke Mooren, Quincy Nlandu, Helmer Mudde, Roy Wetzels, Dirk den Braanker, Naomi Parr, James S. Nagai, Vedran Drenic, Ivan G. Costa, Eric Steenbergen, Tom Nijenhuis, Henry Dijkman, Nicole Endlich, Nicole C.A.J. van de Kar, Rebekka K. Schneider, Jack F.M. Wetzels, Anat Akiva, Johan van der Vlag, Rafael Kramann, Michiel F. Schreuder, and Bart Smeets. Human pluripotent stem cell-derived kidney organoids for personalized congenital and idiopathic nephrotic syndrome modeling. *Development (Cambridge)*, 149, 5 2022.

[181] Tim Stuart, Stephanie Hao, Bingjie Zhang, Levan Mekerishvili, Dan A. Landau, Silas Maniatis, Rahul Satija, and Ivan Raimondi. Nanobody-tethered transposition enables multifactorial chromatin profiling at single-cell resolution. *Nature Biotechnology 2022 41:6*, 41:806–812, 12 2022.

[182] Marek Bartosovic and Gonçalo Castelo-Branco. Multimodal chromatin profiling using nanobody-based single-cell cut&tag. *Nature Biotechnology 2022 41:6*, 41:794–805, 12 2022.

[183] Sneha Gopalan and Thomas G. Fazzio. Multi-cut&tag to simultaneously profile multiple chromatin factors. *STAR Protocols*, 3, 3 2022.

[184] Justin R. Prigge, James A. Wiley, Emily A. Talago, Elise M. Young, Laura L. Johns, Jean A. Kundert, Katherine M. Sonsteng, William P. Halford, Mario R. Capecchi, and Edward E. Schmidt. Nuclear double-fluorescent reporter for in vivo and ex vivo analyses of biological transitions in mouse nuclei. *Mammalian genome : official journal of the International Mammalian Genome Society*, 24:389–399, 10 2013.

[185] Mandar Deepak Muzumdar, Bosiljka Tasic, Kazunari Miyamichi, Ng Li, and Liqun Luo. A global double-fluorescent cre reporter mouse. *genesis*, 45:593–605, 9 2007.

[186] Carsten Merkwirth, Sascha Dargazanli, Takashi Tatsuta, Stefan Geimer, Beatrix Löwer, F. Thomas Wunderlich, Jürgen Christoph Von Kleist-Retzow, Ari Waisman, Benedikt Westermann, and Thomas Langer. Prohibitins control cell proliferation and apoptosis by regulating opa1-dependent cristae morphogenesis in mitochondria. *Genes & Development*, 22:476, 2 2008.

[187] Hani Suleiman, Daniel Heudobler, Anne Sarah Raschta, Yangu Zhao, Qi Zhao, Irmgard Hertting, Helga Vitzthum, Marcus J. Moeller, Lawrence B. Holzman, Reinhard Rachel, Randy Johnson, Heiner Westphal, Anne Rascle, and Ralph Witzgall. The podocyte-specific inactivation of lmx1b, ldb1 and e2a yields new insight into a transcriptional network in podocytes. *Developmental Biology*, 304:701–712, 4 2007.

[188] Jordan A. Kreidberg, Hannu Sariola, Janet M. Loring, Masahiro Maeda, Jerry Pelletier, David Housman, and Rudolf Jaenisch. Wt-1 is required for early kidney development. *Cell*, 74:679–691, 8 1993.

[189] Marcus J. Moeller, Silja K. Sanden, Abdulsalam Soofi, Roger C. Wiggins, and Lawrence B. Holzman. Podocyte-specific expression of cre recombinase in transgenic mice. *Genesis (New York, N.Y. : 2000)*, 35:39–42, 1 2003.

[190] Yaz Y. Kisanuki, Robert E. Hammer, Jun ichi Miyazaki, S. Clay Williams, James A. Richardson, and Masashi Yanagisawa. Tie2-cre transgenic mice: A new model for endothelial cell-lineage analysis in vivo. *Developmental Biology*, 230:230–242, 2 2001.

[191] Jinrong Wang, Yin Wang, Jianyin Long, Benny H.J. Chang, Mathew H. Wilson, Paul Overbeek, and Farhad R. Danesh. Tamoxifen-inducible podocyte-specific icre recombinase transgenic mouse provides a simple approach for modulation of podocytes in vivo. *Genesis (New York, N.Y. : 2000)*, 48:446–451, 2010.

[192] Gary E. Truett, P. Heeger, R. L. Mynatt, A. A. Truett, J. A. Walker, and M. L. Warman. Preparation of pcr-quality mouse genomic dna with hot sodium hydroxide and tris (hotshot). *https://doi.org/10.2144/00291bm09*, 29:52–54, 8 2018.

[193] Xiaodan Liu, Qiuling Fan, Gang Yang, Nan Liu, Dong Chen, Yi Jiang, and Lining Wang. Isolating glomeruli from mice: A practical approach for beginners. *Experimental and Therapeutic Medicine*, 5:1322, 5 2013.

[194] Weijun Luo, Michael S Friedman, Kerby Shedden, Kurt D Hankenson, and Peter J Woolf. Gage: generally applicable gene set enrichment for pathway analysis. *BMC bioinformatics*, 10:161, 5 2009.

[195] Julien Ratelade, Christelle Arrondel, Ghislaine Hamard, Serge Garbay, Scott Harvey, Nathalie Biebuyck, Herbert Schulz, Nick Hastie, Marco Pontoglio, Marie Claire Gubler, Corinne Antignac, and Laurence Heidet. A murine model of denys-drash syndrome reveals novel transcriptional targets of wt1 in podocytes. *Human molecular genetics*, 19:1–15, 9 2010.

[196] Masaru Motojima, Tsutomu Kume, and Taiji Matsusaka. Foxc1 and foxc2 are necessary to maintain glomerular podocytes. *Experimental cell research*, 352:265–272, 3 2017.

[197] Eric W. Brunskill and S. Steven Potter. Pathogenic pathways are activated in each major cell type of the glomerulus in the cd2ap mutant mouse model of focal segmental glomerulosclerosis. *BMC nephrology*, 16, 5 2015.

[198] Brooke M. Steenhard, Kathryn Isom, Larysa Stroganova, Patricia L. St. John, Adrian Zelenchuk, Paul B. Freeburg, Lawrence B. Holzman, and Dale R. Abrahamson. Deletion of von hippel-lindau in glomerular podocytes results in glomerular basement membrane thickening, ectopic subepithelial deposition of collagen {alpha}1{alpha}2{alpha}1(iv), expression of neuroglobin, and proteinuria. *The American journal of pathology*, 177:84–96, 2010.

[199] Simone Reichelt-Wurm, Tobias Wirtz, Dominik Chittka, Maja Lindenmeyer, Robert M. Reichelt, Sebastian Beck, Panagiotis Politis, Aristidis Charonis, Markus Kretz, Tobias B. Huber, Shuya Liu, Bernhard Banas, and Miriam C. Banas. Glomerular expression pattern of long non-coding rnas in the type 2 diabetes mellitus btbr mouse model. *Scientific reports*, 9, 12 2019.

[200] Masahiro Okabe, Masaru Motojima, Yoichi Miyazaki, Ira Pastan, Takashi Yokoo, and Taiji Matsusaka. Global polysome analysis of normal and injured podocytes. *American journal of physiology. Renal physiology*, 316:F241–F252, 2019.

[201] Nina Reiniger, Kai Lau, Daren McCalla, Bonnie Eby, Bin Cheng, Yan Lu, Wu Qu, Nosirudeen Quadri, Radha Ananthakrishnan, Maryana Furmansky, Rosa Rosario, Fei Song, Vivek Rai, Alan Weinberg, Richard Friedman, Ravichandran Ramasamy, Vivette D'Agati, and Ann Marie Schmidt. Deletion of the receptor for advanced glycation end products reduces glomerulosclerosis and preserves renal function in the diabetic ove26 mouse. *Diabetes*, 59:2043–2054, 8 2010.

[202] Yiqing Guo, Jesse Pace, Zhengzhe Li, Avi Ma'ayan, Zichen Wang, Monica P. Revelo, Edward Chen, Xiangchen Gu, Ahmed Attalah, Yaqi Yang, Chelsea Estrada, Vincent W. Yang, John C. He, and Sandeep K. Mallipattu. Podocyte-specific induction of krüppel-like factor 15 restores differentiation markers and attenuates kidney injury in proteinuric kidney disease. *Journal of the American Society of Nephrology : JASN*, 29:2529–2545, 10 2018.

[203] Andrew S. Potter, Keri Drake, Eric W. Brunskill, and S. Steven Potter. A bigenic mouse model of fsgs reveals perturbed pathways in podocytes, mesangial cells and endothelial cells. *PloS one*, 14, 8 2019.

[204] Brian R. Stotter, Brianna E. Talbot, Diane E. Capen, Nadine Artelt, Junwei Zeng, Yasuyuki Matsumoto, Nicole Endlich, Richard D. Cummings, and Johannes S. Schlondorff. Cosmc-dependent mucin-type o-linked glycosylation is essential for podocyte function. *American journal of physiology. Renal physiology*, 318:F518–F530, 2 2020.

[205] Jia Fu, Kemal M. Akat, Zeguo Sun, Weijia Zhang, Detlef Schlondorff, Zhihong Liu, Thomas Tuschl, Kyung Lee, and John Cijiang He. Single-cell rna profiling of glomerular cells shows dynamic changes in experimental diabetic kidney disease. *Journal of the American Society of Nephrology : JASN*, 30:533–545, 4 2019.

[206] Jun Jae Chung, Leonard Goldstein, Ying Jiun J. Chen, Jiyeon Lee, Joshua D. Webster, Merone Roose-Girma, Sharad C. Paudyal, Zora Modrusan, Anwesha Dey, and Andrey S. Shaw. Single-cell transcriptome profiling of the kidney glomerulus identifies key cell types and reactions to injury. *Journal of the American Society of Nephrology*, 31:2341–2354, 10 2020.

[207] Sébastien Bender, Maria Victoria Ayala, Amélie Bonaud, Vincent Javaugue, Claire Carrion, Christelle Oblet, Alexia Rinsant, Sihem Kaaki, Zeliha Oruc, François Boyer, Agnès Paquet, Nicolas Pons, Bastien Hervé, Mohamad Omar Ashi, Arnaud Jaccard, Laurent Delpy, Guy Touchard, Michel Cogné, Frank Bridoux, and Christophe Sirac. Immunoglobulin light-chain toxicity in a mouse model of monoclonal immunoglobulin light-chain deposition disease. *Blood*, 136:1645–1656, 10 2020.

[208] Mai Sugahara, Shinji Tanaka, Tetsuhiro Tanaka, Hisako Saito, Yu Ishimoto, Takeshi Wakashima, Masatoshi Ueda, Kenji Fukui, Akira Shimizu, Reiko Inagi, Toshimasa Yamauchi, Takashi Kadowaki, and Masaomi Nangaku. Prolyl hydroxylase domain inhibitor protects against metabolic disorders and associated kidney disease in obese type 2 diabetic mice. *Journal of the American Society of Nephrology : JASN*, 31:560–577, 2020.

[209] Jun Matsuda, Mirela Maier, Lamine Aoudjit, Cindy Baldwin, and Tomoko Takano. Arhgef7 (β-pix) is required for the maintenance of podocyte architecture and glomerular function. *Journal of the American Society of Nephrology : JASN*, 31:996–1008, 5 2020.

[210] Yifei Zhong, Kyung Lee, Yueyi Deng, Yueming Ma, Yiping Chen, Xueling Li, Chengguo Wei, Shumin Yang, Tianming Wang, Nicholas J. Wong, Alecia N. Muwonge, Evren U. Azeloglu, Weijia Zhang, Bhaskar Das, John Cijiang He, and Ruijie Liu. Arctigenin attenuates diabetic kidney disease through the activation of pp2a in podocytes. *Nature communications*, 10, 12 2019.

[211] Chengguo Wei, Khadija Banu, Felipe Garzon, John M. Basgen, Nimrod Philippe, Zhengzi Yi, Ruijie Liu, Jui Choudhuri, Miguel Fribourg, Tong Liu, Arun Cumpelik, Jenny Wong, Mubeen Khan, Bhaskar Das, Karen Keung, Fadi Salem, Kirk N. Campbell, Lewis Kaufman, Paolo Cravedi, Weijia

Zhang, Philip J. O'Connell, John Cijiang He, Barbara Murphy, and Madhav C. Menon. Shroom3-fyn interaction regulates nephrin phosphorylation and affects albuminuria in allografts. *Journal of the American Society of Nephrology*, 29:2641–2657, 11 2018.

[212] Lucy M. Hinder, Meeyoung Park, Amy E. Rumora, Junguk Hur, Felix Eichinger, Subramaniam Pennathur, Matthias Kretzler, Frank C. Brosius, and Eva L. Feldman. Comparative rna-seq transcriptome analyses reveal distinct metabolic pathways in diabetic nerve and kidney disease. *Journal of cellular and molecular medicine*, 21:2140–2152, 9 2017.

[213] Crystal Naudin, Brian Smith, Danielle R. Bond, Matthew D. Dun, Rodney J. Scott, Leonie K. Ashman, Judith Weidenhofer, and Séverine Roselli. Characterization of the early molecular changes in the glomeruli of cd151 -/- mice highlights induction of mindin and mmp-10. *Scientific reports*, 7, 12 2017.

[214] Long Jianyin, Shawn S. Badal, Ye Zengchun, Wang Yin, Bernard A. Ayanga, Daniel L. Galvan, Nathanael H. Green, Benny H. Chang, Paul A. Overbeek, and Farhad R. Danesh. Long noncoding rna tug1 regulates mitochondrial bioenergetics in diabetic nephropathy. *The Journal of clinical investigation*, 126:4205–4218, 11 2016.

[215] Xiaoyi Zheng, Fariborz Soroush, Jin Long, Evan T. Hall, Puneeth K. Adishesha, Sanchita Bhattacharya, Mohammad F. Kiani, and Vivek Bhalla. Murine glomerular transcriptome links endothelial cell-specific molecule-1 deficiency with susceptibility to diabetic nephropathy. *PloS one*, 12, 9 2017.

[216] Jia Fu, Chengguo Wei, Kyung Lee, Weijia Zhang, Wu He, Peter Chuang, Zhihong Liu, and John Cijiang He. Comparison of glomerular and podocyte mrna profiles in streptozotocin-induced diabetes. *Journal of the American Society of Nephrology : JASN*, 27:1006–1014, 2016.

[217] Susan B. Gurley, Sujoy Ghosh, Stacy A. Johnson, Kengo Azushima, Rashidah Binte Sakban, Simi E. George, Momoe Maeda, Timothy W. Meyer, and Thomas M. Coffman. Inflammation and immunity pathways regulate genetic susceptibility to diabetic nephropathy. *Diabetes*, 67:2096–2106, 10 2018.

[218] Laurent Mesnard, Dominique Cathelin, Sophie Vandermeersch, Cédric Rafat, Yosu Luque, Julie Sohier, Dominique Nochy, Loïc Garcon, Patrice Callard, Chantal Jouanneau, Marie Christine Verpont, Pierre Louis Tharaux, Alexandre Hertig, and Eric Rondeau. Genetic background-dependent thrombotic microangiopathy is related to vascular endothelial growth factor receptor 2 signaling during anti-glomerular basement membrane glomerulonephritis in mice. *The American journal of pathology*, 184:2438–2449, 2014.

[219] Bernhard Schermer, Valerie Bartels, Peter Frommolt, Bianca Habermann, Fabian Braun, Joachim L. Schultze, Marianne Roodbergen, Jan H.J. Hoeijmakers, Björn Schumacher, Peter Nürnberg, Martijn E.T. Dollé, Thomas Benzing, Roman Ulrich Müller, and Christine E. Kurschat. Transcriptional profiling reveals progeroid ercc1(-/δ) mice as a model system for glomerular aging. *BMC genomics*, 14, 8 2013.

[220] Jeffrey B. Hodgin, Viji Nair, Hongyu Zhang, Ann Randolph, Raymond C. Harris, Robert G. Nelson, E. Jennifer Weil, James D. Cavalcoli, Jignesh M. Patel, Frank C. Brosius, and Matthias Kretzler. Identification of cross-species shared transcriptional networks of diabetic nephropathy in human and mouse glomeruli. *Diabetes*, 62:299–308, 1 2013.

[221] Wanning Wang, Saizhi Jiang, Xiaoqiang Tang, Lu Cai, Paul N. Epstein, Yanli Cheng, Weixia Sun, Zhonggao Xu, and Yi Tan. Sex differences in progression of diabetic nephropathy in ove26 type 1 diabetic mice. *Biochimica et biophysica acta. Molecular basis of disease*, 1866, 1 2020.

[222] Yuliang Wang, Diana G. Eng, Natalya V. Kaverina, Carol J. Loretz, Abbal Koirala, Shreeram Akilesh, Jeffrey W. Pippin, and Stuart J. Shankland. Global transcriptomic changes occur in aged mouse podocytes. *Kidney international*, 98:1160–1173, 11 2020.

[223] Nicola M. Tomas, Elion Hoxha, Anna T. Reinicke, Lars Fester, Udo Helmchen, Jens Gerth, Friederike Bachmann, Klemens Budde, Friedrich Koch-Nolte, Gunther Zahner, Gabriele Rune, Gerard Lambeau, Catherine Meyer-Schwesinger, and Rolf A.K. Stahl. Autoantibodies against thrombospondin type 1 domain-containing 7a induce membranous nephropathy. *The Journal of clinical investigation*, 126:2519–2532, 7 2016.

[224] Hui Sun, Hui Li, Jie Yan, Xiangdong Wang, Mengyuan Xu, Mingxia Wang, Baozhen Fan, Jieying Liu, Ninghua Lin, Xin Wang, Li Li, Shengtian Zhao, and Yongfeng Gong. Loss of cldn5 in podocytes deregulates wif1 to activate wnt signaling and contributes to kidney disease. *Nature Communications 2022 13:1*, 13:1–18, 3 2022.

[225] Florian Tesch, Florian Siegerist, Eleonora Hay, Nadine Artelt, Christoph Daniel, Kerstin Amann, Uwe Zimmermann, Panagiotis Kavvadas, Olaf Grisk, Christos Chadjichristos, Karlhans Endlich, Christos Chatziantoniou, and Nicole Endlich. Super-resolved local recruitment of cldn5 to filtration slits implicates a direct relationship with podocyte foot process effacement. *Journal of cellular and molecular medicine*, 25:7631–7641, 8 2021.

[226] Setsu Endoh-Yamagami, Marie Evangelista, Deanna Wilson, Xiaohui Wen, Jan Willem Theunissen, Khanhky Phamluong, Matti Davis, Suzie J. Scales, Mark J. Solloway, Frederic J. de Sauvage, and Andrew S. Peterson. The mammalian cos2 homolog kif7 plays an essential role in modulating hh signal transduction during development. *Current biology : CB*, 19:1320–1326, 8 2009.

[227] Yumay Chen, Huai Chin Chiang, Patricia Litchfield, Michelle Pena, Charity Juang, and Daniel J. Riley. Expression of nek1 during kidney development and cyst formation in multiple nephron segments in the nek1-deficient kat2j mouse model of polycystic kidney disease. *Journal of biomedical science*, 21, 7 2014.

[228] Christina Ising, Sybille Koehler, Sebastian Brähler, Carsten Merkwirth, Martin Höhne, Olivier R Baris, Henning Hagmann, Martin Kann, Francesca Fabretti, Claudia Dafinger, Wilhelm Bloch, Bernhard Schermer, Andreas Linkermann, Jens C Brüning, Christine E Kurschat, Roman-Ulrich Müller, Rudolf J Wiesner, Thomas Langer, Thomas Benzing, and Paul Thomas Brinkkoetter. Inhibition of insulin/igf-1 receptor signaling protects from mitochondria-mediated kidney failure. *EMBO molecular medicine*, 7:275–287, 3 2015.

[229] Nanoka Suzuki, Kodai Hirano, Hajime Ogino, and Haruki Ochi. Arid3a regulates nephric tubule regeneration via evolutionarily conserved regeneration signal-response enhancers. *eLife*, 8, 1 2019.

[230] Hae Jeong Park, Jong Woo Kim, Byoung-Soo Cho, and Joo-Ho Chung. Association of fos-like antigen 1 promoter polymorphism with podocyte foot process effacement in immunoglobulin a nephropathy patients. *Journal of clinical laboratory analysis*, 28:391–7, 9 2014.

[231] Sha Jia, Xiaofeng Peng, Ludan Liang, Ying Zhang, Meng Li, Qin Zhou, Xiujin Shen, Yucheng Wang, Cuili Wang, Shi Feng, Jianghua Chen, Pingping Ren, and Hong Jiang. The study of angptl4-modulated podocyte injury in iga nephropathy. *Frontiers in physiology*, 11:575722, 2020.

[232] Zhejun Chen, Ting Zhang, Kaiqiong Mao, Xinghua Shao, Yao Xu, Minyan Zhu, Hang Zhou, Qin Wang, Zhenyuan Li, YuanYuan Xie, Xiaodong Yuan, Liang Ying, Ming Zhang, Jiajia Hu, and Shan Mou. A single-cell survey of the human glomerulonephritis. *Journal of cellular and molecular medicine*, 25:4684–4695, 5 2021.

[233] Zhimei Lv, Mengsi Hu, Minghua Fan, Xiaobing Li, Jiangong Lin, Junhui Zhen, Ziyang Wang, Haijun Jin, and Rong Wang. Podocyte-specific rac1 deficiency ameliorates podocyte damage and proteinuria in stz-induced diabetic nephropathy in mice. *Cell death & disease*, 9:342, 3 2018.

[234] Andrey V Cybulsky and Chris R J Kennedy. Podocyte injury associated with mutant α-actinin-4. *Journal of signal transduction*, 2011:563128, 2011.

[235] Toshiyuki Imasawa, Emilie Obre, Nadège Bellance, Julie Lavie, Tomoko Imasawa, Claire Rigothier, Yahsou Delmas, Christian Combe, Didier Lacombe, Giovanni Benard, Stéphane Claverol, Marc Bonneu, and Rodrigue Rossignol. High glucose repatterns human podocyte energy metabolism during differentiation and diabetic nephropathy. *FASEB journal : official publication of the Federation of American Societies for Experimental Biology*, 31:294–307, 1 2017.

[236] Sehoon Park, Minji Kang, Yong Chul Kim, Dong Ki Kim, Kook-Hwan Oh, Kwon Wook Joo, Yon Su Kim, Hyun Je Kim, Kyung Chul Moon, and Hajeong Lee. Glomerular spatial transcriptomics of iga nephropathy according to the presence of mesangial proliferation. *Scientific reports*, 14:2211, 1 2024.

[237] Raymond Habas and Xi He. Cell signaling: moving to a wnt-rap. *Current biology : CB*, 17:R474–7, 6 2007.

[238] Sijia Ma, Yang Qiu, and Chun Zhang. Cytoskeleton rearrangement in podocytopathies: An update. *International journal of molecular sciences*, 25, 1 2024.

[239] Julia Binz-Lotter, Christian Jüngst, Markus M Rinschen, Sybille Koehler, Peter Zentis, Astrid Schauss, Bernhard Schermer, Thomas Benzing, and Matthias J Hackl. Injured podocytes are sensitized to angiotensin ii-induced calcium signaling. *Journal of the American Society of Nephrology : JASN*, 31:532–542, 3 2020.

[240] Pilong Li, Sudeep Banjade, Hui-Chun Cheng, Soyeon Kim, Baoyu Chen, Liang Guo, Marc Llaguno, Javoris V Hollingsworth, David S King, Salman F Banani, Paul S Russo, Qiu-Xing Jiang, B Tracy Nixon, and Michael K Rosen. Phase transitions in the assembly of multivalent signalling proteins. *Nature*, 483:336–40, 3 2012.

[241] Erin F Hammonds, Megan Cleland Harwig, Emeleeta A Paintsil, Emma A Tillison, R Blake Hill, and Emma A Morrison. Histone h3 and h4 tails play an important role in nucleosome phase separation. *Biophysical chemistry*, 283:106767, 4 2022.

[242] Priyesh Mohanty, Utkarsh Kapoor, Dinesh Sundaravadivelu Devarajan, Tien Minh Phan, Azamat Rizuan, and Jeetain Mittal. Principles governing the phase separation of multidomain proteins. *Biochemistry*, 61:2443–2455, 11 2022.

[243] Michio Nagata. Podocyte injury and its consequences. *Kidney international*, 89:1221–30, 6 2016.

[244] Abhijit S Naik, Dustin Le, Jawad Aqeel, Su Q Wang, Mahboob Chowdhury, Lisa M Walters, Diane M Cibrik, Milagros Samaniego, and Roger C Wiggins. Podocyte stress and detachment measured in urine are related to mean arterial pressure in healthy humans. *Kidney international*, 98:699–707, 9 2020.

[245] Lan Xu, Hai-Chun Yang, Chuan-Ming Hao, Shan-Tan Lin, Yong Gu, and Ji Ma. Podocyte number predicts progression of proteinuria in iga nephropathy. *Modern pathology : an official journal of the United States and Canadian Academy of Pathology, Inc*, 23:1241–50, 9 2010.

[246] Christoph Kuppe, Hermann-Josef Gröne, Tammo Ostendorf, Toin H van Kuppevelt, Peter Boor, Jürgen Floege, Bart Smeets, and Marcus J Moeller. Common histological patterns in glomerular epithelial cells in secondary focal segmental glomerulosclerosis. *Kidney international*, 88:990–8, 11 2015.

[247] David Unnersjö-Jess, Linus Butt, Martin Höhne, German Sergei, Arash Fatehi, Anna Witasp, Annika Wernerson, Jaakko Patrakka, Peter F Hoyer, Hans Blom, Bernhard Schermer, Katarzyna Bozek, and Thomas Benzing. Deep learning-based segmentation and quantification of podocyte foot process morphology suggests differential patterns of foot process effacement across kidney pathologies. *Kidney international*, 103:1120–1130, 6 2023.

[248] Linus Butt, David Unnersjö-Jess, Martin Höhne, Robert Hahnfeldt, Dervla Reilly, Markus M Rinschen, Ingo Plagmann, Paul Diefenhardt, Sebastian Brähler, Paul T Brinkkötter, Hjalmar Brismar, Hans Blom, Bernhard Schermer, and Thomas Benzing. Super-resolution imaging of the filtration barrier suggests a role for podocin r229q in genetic predisposition to glomerular disease. *Journal of the American Society of Nephrology : JASN*, 33:138–154, 1 2022.

[249] Mariko Shimizu, Jamshid Khoshnoodi, Yoshihiro Akimoto, Hayato Kawakami, Hiroshi Hirano, Eiji Higashihara, Makoto Hosoyamada, Yuji Sekine, Ryota Kurayama, Hideaki Kurayama, Kensuke Joh, Jun Hirabayashi, Kenichi Kasai, Karl Tryggvason, Noriko Ito, and Kunimasa Yan. Expression of galectin-1, a new component of slit diaphragm, is altered in minimal change nephrotic syndrome. *Laboratory investigation; a journal of technical methods and pathology*, 89:178–95, 2 2009.

[250] Nicola M Tomas, Laurence H Beck, Catherine Meyer-Schwesinger, Barbara Seitz-Polski, Hong Ma, Gunther Zahner, Guillaume Dolla, Elion Hoxha, Udo Helmchen, Anne-Sophie Dabert-Gay, Delphine Debayle, Michael Merchant, Jon Klein, David J Salant, Rolf A K Stahl, and Gérard Lambeau. Thrombospondin type-1 domain-containing 7a in idiopathic membranous nephropathy. *The New England journal of medicine*, 371:2277–2287, 12 2014.

[251] Nicola M Tomas, Catherine Meyer-Schwesinger, Hanning von Spiegel, Ahmed M Kotb, Gunther Zahner, Elion Hoxha, Udo Helmchen, Nicole Endlich, Friedrich Koch-Nolte, and Rolf A K Stahl. A heterologous model of thrombospondin type 1 domain-containing 7a-associated membranous nephropathy. *Journal of the American Society of Nephrology : JASN*, 28:3262–3277, 11 2017.

[252] Johanna Herwig, Sinah Skuza, Wiebke Sachs, Marlies Sachs, Antonio Virgilio Failla, Gabriele Rune, Tobias N Meyer, Lars Fester, and Catherine Meyer-Schwesinger. Thrombospondin type 1 domain-containing 7a localizes to the slit diaphragm and stabilizes membrane dynamics of fully differentiated podocytes. *Journal of the American Society of Nephrology : JASN*, 30:824–839, 5 2019.

[253] Sybille Koehler, Frederik Tellkamp, Carien M Niessen, Wilhelm Bloch, Dontscho Kerjaschki, Bernhard Schermer, Thomas Benzing, and Paul T Brinkkoetter. Par3a is dispensable for the function of the glomerular filtration barrier of the kidney. *American journal of physiology. Renal physiology*, 311:F112–9, 7 2016.

[254] Yongfeng Gong, Abby Sunq, Robyn A Roth, and Jianghui Hou. Inducible expression of claudin-1 in glomerular podocytes generates aberrant tight junctions and proteinuria through slit diaphragm destabilization. *Journal of the American Society of Nephrology : JASN*, 28:106–117, 1 2017.

[255] S C Doné, M Takemoto, L He, Y Sun, K Hultenby, C Betsholtz, and K Tryggvason. Nephrin is involved in podocyte maturation but not survival during glomerular development. *Kidney international*, 73:697–704, 3 2008.

[256] Ryo Koda, Linning Zhao, Eishin Yaoita, Yutaka Yoshida, Sachiko Tsukita, Atsushi Tamura, Masaaki Nameta, Ying Zhang, Hidehiko Fujinaka, Sameh Magdeldin, Bo Xu, Ichiei Narita, and Tadashi Yamamoto. Novel expression of claudin-5 in glomerular podocytes. *Cell and tissue research*, 343:637–48, 3 2011.

[257] Dong Zhou, Haiyan Fu, Yang Han, Lu Zhang, Shijia Liu, Lin Lin, Donna B Stolz, and Youhua Liu. Sonic hedgehog connects podocyte injury to mesangial activation and glomerulosclerosis. *JCI insight*, 4, 11 2019.

[258] Dong Zhou, Yingjian Li, Lili Zhou, Roderick J Tan, Liangxiang Xiao, Min Liang, Fan Fan Hou, and Youhua Liu. Sonic hedgehog is a novel tubule-derived growth factor for interstitial fibroblasts after kidney injury. *Journal of the American Society of Nephrology : JASN*, 25:2187–200, 10 2014.

[259] Hong Ding, Dong Zhou, Sha Hao, Lili Zhou, Weichun He, Jing Nie, Fan Fan Hou, and Youhua Liu. Sonic hedgehog signaling mediates epithelial-mesenchymal communication and promotes renal fibrosis. *Journal of the American Society of Nephrology : JASN*, 23:801–13, 5 2012.

[260] P Upadhya, E H Birkenmeier, C S Birkenmeier, and J E Barker. Mutations in a nima-related kinase gene, nek1, cause pleiotropic effects including a progressive polycystic kidney disease in mice. *Proceedings of the National Academy of Sciences of the United States of America*, 97:217–21, 1 2000.

[261] Yumay Chen, Huai-Chin Chiang, Patricia Litchfield, Michelle Pena, Charity Juang, and Daniel J Riley. Expression of nek1 during kidney development and cyst formation in multiple nephron segments in the nek1-deficient kat2j mouse model of polycystic kidney disease. *Journal of biomedical science*, 21:63, 7 2014.

[262] Hyungshin Yim, Chang K Sung, John You, Yu Tian, and Thomas Benjamin. Nek1 and taz interact to maintain normal levels of polycystin 2. *Journal of the American Society of Nephrology : JASN*, 22:832–7, 5 2011.

[263] Haojia Wu, Romer Gonzalez Villalobos, Xiang Yao, Dermot Reilly, Tao Chen, Matthew Rankin, Eugene Myshkin, Matthew D Breyer, and Benjamin D Humphreys. Mapping the single-cell transcriptomic response of murine diabetic kidney disease to therapies. *Cell metabolism*, 34:1064–1078.e6, 7 2022.

[264] Michael S Balzer, Tomohito Doke, Ya-Wen Yang, Daniel L Aldridge, Hailong Hu, Hung Mai, Dhanunjay Mukhi, Ziyuan Ma, Rojesh Shrestha, Matthew B Palmer, Christopher A Hunter, and Katalin Susztak.

Single-cell analysis highlights differences in druggable pathways underlying adaptive or fibrotic kidney regeneration. *Nature communications*, 13:4018, 7 2022.

[265] Haikuo Li, Eryn E Dixon, Haojia Wu, and Benjamin D Humphreys. Comprehensive single-cell transcriptional profiling defines shared and unique epithelial injury responses during kidney fibrosis. *Cell metabolism*, 34:1977–1998.e9, 12 2022.

[266] Jeffrey T White, Bo Zhang, Débora M Cerqueira, Uyen Tran, and Oliver Wessely. Notch signaling, wt1 and foxc2 are key regulators of the podocyte gene regulatory network in xenopus. *Development (Cambridge, England)*, 137:1863–73, 6 2010.

[267] Lulu Jiang, Charles C T Hindmarch, Mark Rogers, Colin Campbell, Christy Waterfall, Jane Coghill, Peter W Mathieson, and Gavin I Welsh. Rna sequencing analysis of human podocytes reveals glucocorticoid regulated gene networks targeting non-immune pathways. *Scientific reports*, 6:35671, 10 2016.

[268] Natallia Shved, Gregor Warsow, Felix Eichinger, David Hoogewijs, Simone Brandt, Peter Wild, Matthias Kretzler, Clemens D Cohen, and Maja T Lindenmeyer. Transcriptome-based network analysis reveals renal cell type-specific dysregulation of hypoxia-associated transcripts. *Scientific reports*, 7:8576, 8 2017.

[269] Ivica Grgic, Andreas F Hofmeister, Giulio Genovese, Andrea J Bernhardy, Hua Sun, Omar H Maarouf, Vanesa Bijol, Martin R Pollak, and Benjamin D Humphreys. Discovery of new glomerular disease-relevant genes by translational profiling of podocytes in vivo. *Kidney international*, 86:1116–29, 12 2014.

[270] Michael Marcotte, Richa Sharma, and Maxime Bouchard. Gene regulatory network of renal primordium development. *Pediatric nephrology (Berlin, Germany)*, 29:637–44, 4 2014.

[271] Sylvia Hilliard, Giovane Tortelote, Hongbing Liu, Chao-Hui Chen, and Samir S El-Dahr. Single-cell chromatin and gene-regulatory dynamics of mouse nephron progenitors. *Journal of the American Society of Nephrology : JASN*, 33:1308–1322, 7 2022.

[272] Yasuhiro Yoshimura, Yoshiharu Muto, Kohei Omachi, Jeffrey H Miner, and Benjamin D Humphreys. Elucidating the proximal tubule hnf4a gene regulatory network in human kidney organoids. *Journal of the American Society of Nephrology : JASN*, 34:1672–1686, 10 2023.

[273] Floranne Boulogne, Laura R Claus, Henry Wiersma, Roy Oelen, Floor Schukking, Niek de Klein, Shuang Li, Harm-Jan Westra, Bert van der Zwaag, Franka van Reekum, Genomics England Research Consortium, Dana Sierks, Ria Schönauer, Zhigui Li, Emilia K Bijlsma, Willem Jan W Bos, Jan Halbritter, Nine V A M Knoers, Whitney Besse, Patrick Deelen, Lude Franke, and Albertien M van Eerde. Kidneynetwork: using kidney-derived gene expression data to predict and prioritize novel genes involved in kidney disease. *European journal of human genetics : EJHG*, 31:1300–1308, 11 2023.

[274] Huilin Li, Weijia Zhang, Fang Zhong, Gokul C Das, Yifan Xie, Zhengzhe Li, Weijing Cai, Gengru Jiang, Jae Choi, Mohamad Sidani, Deborah P Hyink, Kyung Lee, Paul E Klotman, and John Cijiang He. Epigenetic regulation of rcan1 expression in kidney disease and its role in podocyte injury. *Kidney international*, 94:1160–1176, 12 2018.

[275] Ling Jiang, Xueqi Liu, Xueru Hu, Li Gao, Hanxu Zeng, Xian Wang, Yuebo Huang, Wei Zhu, Jianan Wang, Jiagen Wen, Xiaoming Meng, and Yonggui Wu. Mettl3-mediated m6a modification of timp2 mrna promotes podocyte injury in diabetic nephropathy. *Molecular therapy : the journal of the American Society of Gene Therapy*, 30:1721–1740, 4 2022.

[276] Johanna Barth, Ivonne Loeffler, Tzvetanka Bondeva, Marita Liebisch, and Gunter Wolf. The role of hypoxia on the trimethylation of h3k27 in podocytes. *Biomedicines*, 11, 9 2023.

[277] Aili Cao, Jianhua Li, Morad Asadi, John M Basgen, Bingbing Zhu, Zhengzi Yi, Song Jiang, Tomohito Doke, Osama El Shamy, Niralee Patel, Paolo Cravedi, Evren U Azeloglu, Kirk N Campbell, Madhav Menon, Steve Coca, Weijia Zhang, Hao Wang, Ke Zen, Zhihong Liu, Barbara Murphy, John C He, Vivette D D'Agati, Katalin Susztak, and Lewis Kaufman. Dach1 protects podocytes from experimental diabetic injury and modulates ptip-h3k4me3 activity. *The Journal of clinical investigation*, 131, 5 2021.

[278] Iain F Davidson, Roman Barth, Maciej Zaczek, Jaco van der Torre, Wen Tang, Kota Nagasaka, Richard Janissen, Jacob Kerssemakers, Gordana Wutz, Cees Dekker, and Jan-Michael Peters. Ctcf is a dna-tension-dependent barrier to cohesin-mediated loop extrusion. *Nature*, 616:822–827, 4 2023.

[279] Katrien Van Beneden, Caroline Geers, Marina Pauwels, Inge Mannaerts, Dierik Verbeelen, Leo A van Grunsven, and Christiane Van den Branden. Valproic acid attenuates proteinuria and kidney injury. *Journal of the American Society of Nephrology : JASN*, 22:1863–75, 10 2011.

[280] Nagako Kawashima, Shokichi Naito, Masaki Nagane, Tadashi Yamashita, and Ken-Ichi Nakayama. Progression of albuminuria and podocyte injury in focal segmental glomerulosclerosis inhibited by enhanced glycosphingolipid gm3 via valproic acid. *Scientific reports*, 13:22487, 12 2023.

[281] Seong Kyu Han, Michelle T McNulty, Christopher J Benway, Pei Wen, Anya Greenberg, Ana C Onuchic-Whitford, Nephrotic Syndrome Study Network (NEPTUNE), Dongkeun Jang, Jason Flannick, Noël P Burtt, Parker C Wilson, Benjamin D Humphreys, Xiaoquan Wen, Zhe Han, Dongwon Lee, and Matthew G Sampson. Mapping genomic regulation of kidney disease and traits through high-resolution and interpretable eqtls. *Nature communications*, 14:2229, 4 2023.

[282] Alexandre Lautrette, Shunqiang Li, Rohia Alili, Susan W Sunnarborg, Martine Burtin, David C Lee, Gérard Friedlander, and Fabiola Terzi. Angiotensin ii and egf receptor cross-talk in chronic kidney diseases: a new therapeutic approach. *Nature medicine*, 11:867–74, 8 2005.

[283] Guillaume Bollée, Martin Flamant, Sandra Schordan, Cécile Fligny, Elisabeth Rumpel, Marine Milon, Eric Schordan, Nathalie Sabaa, Sophie Vandermeersch, Ariane Galaup, Anita Rodenas, Ibrahim Casal, Susan W Sunnarborg, David J Salant, Jeffrey B Kopp, David W Threadgill, Susan E Quaggin, Jean-Claude Dussaule, Stéphane Germain, Laurent Mesnard, Karlhans Endlich, Claude Boucheix, Xavier Belenfant, Patrice Callard, Nicole Endlich, and Pierre-Louis Tharaux. Epidermal growth factor receptor promotes glomerular injury and renal failure in rapidly progressive crescentic glomerulonephritis. *Nature medicine*, 17:1242–50, 9 2011.

[284] K Paizis, G Kirkland, T Khong, M Katerelos, S Fraser, J Kanellis, and D A Power. Heparin-binding epidermal growth factor-like growth factor is expressed in the adhesive lesions of experimental focal glomerular sclerosis. *Kidney international*, 55:2310–21, 6 1999.

[285] Jianchun Chen, Jian-Kang Chen, and Raymond C Harris. Egf receptor deletion in podocytes attenuates diabetic nephropathy. *Journal of the American Society of Nephrology : JASN*, 26:1115–25, 5 2015.

[286] Yan Li, Yu Pan, Shirong Cao, Kensuke Sasaki, Yinqiu Wang, Aolei Niu, Xiaofeng Fan, Suwan Wang, Ming-Zhi Zhang, and Raymond C Harris. Podocyte egfr inhibits autophagy through upregulation of rubicon in type 2 diabetic nephropathy. *Diabetes*, 70:562–576, 2 2021.

[287] H D Humes, D A Cieslinski, T M Coimbra, J M Messana, and C Galvao. Epidermal growth factor enhances renal tubule cell regeneration and repair and accelerates the recovery of renal function in postischemic acute renal failure. *The Journal of clinical investigation*, 84:1757–61, 12 1989.

[288] J Norman, Y K Tsau, A Bacay, and L G Fine. Epidermal growth factor accelerates functional recovery from ischaemic acute tubular necrosis in the rat: role of the epidermal growth factor receptor. *Clinical science (London, England : 1979)*, 78:445–50, 5 1990.

[289] Ji Ma, Taiji Matsusaka, Hai-Chun Yang, Jianyong Zhong, Nobuaki Takagi, Agnes B Fogo, Valentina Kon, and Iekuni Ichikawa. Induction of podocyte-derived vegf ameliorates podocyte injury and subsequent abnormal glomerular development caused by puromycin aminonucleoside. *Pediatric research*, 70:83–9, 7 2011.

[290] Md Abdul Masum, Osamu Ichii, Yaser Hosny Ali Elewa, Teppei Nakamura, Yuki Otani, Marina Hosotani, and Yasuhiro Kon. Modified scanning electron microscopy reveals pathological crosstalk between endothelial cells and podocytes in a murine model of membranoproliferative glomerulonephritis. *Scientific reports*, 8:10276, 7 2018.

[291] Vera Eremina, Manish Sood, Jody Haigh, András Nagy, Ginette Lajoie, Napoleone Ferrara, Hans-Peter Gerber, Yamato Kikkawa, Jeffrey H Miner, and Susan E Quaggin. Glomerular-specific alterations of vegf-a expression lead to distinct congenital and acquired renal diseases. *The Journal of clinical investigation*, 111:707–16, 3 2003.

[292] Delma Veron, Pardeep K Aggarwal, Qi Li, Gilbert Moeckel, Michael Kashgarian, and Alda Tufro. Podocyte vegf-a knockdown induces diffuse glomerulosclerosis in diabetic and in enos knockout mice. *Frontiers in pharmacology*, 12:788886, 2021.

[293] Ilse Daehn, Gabriella Casalena, Taoran Zhang, Shaolin Shi, Franz Fenninger, Nicholas Barasch, Liping Yu, Vivette D'Agati, Detlef Schlondorff, Wilhelm Kriz, Borje Haraldsson, and Erwin P Bottinger. Endothelial mitochondrial oxidative stress determines podocyte depletion in segmental glomerulosclerosis. *The Journal of clinical investigation*, 124:1608–21, 4 2014.

[294] Sabine Endele, Sabine Klein, Sabine Richter, Tina Molter, Kerstin Amann, Bernd Klanke, Ralph Witzgall, Randy L. Johnson, Karl F. Hilgers, and Andreas Winterpacht. Renal phenotype in heterozygous lmx1b knockout mice (lmx1b+/-) after unilateral nephrectomy. *Transgenic research*, 16:723–729, 12 2007.

[295] Jeffrey H. Miner, Roy Morello, Kaya L. Andrews, Cong Li, Corinne Antignac, Andrey S. Shaw, and Brendan Lee. Transcriptional induction of slit diaphragm genes by lmx1b is required in podocyte differentiation. *The Journal of clinical investigation*, 109:1065–1072, 4 2002.

[296] Rob C.I. Wüst, Riekelt H. Houtkooper, and Johan Auwerx. Reproducibility: Confounding factors from inducible systems for spatiotemporal gene expression regulation. *The Journal of Cell Biology*, 219, 7 2020.

[297] Meagan M Kitt, Nobuko Tabuchi, W Clay Spencer, Heath L Robinson, Xinrui L Zhang, Brent A Eastman, Katherine J Lobur, Jerry Silver, Lin Mei, and Evan S Deneris. An adult-stage transcriptional program for survival of serotonergic connectivity. *Cell reports*, 39:110711, 4 2022.

[298] Xinrui L. Zhang, W. Clay Spencer, Nobuko Tabuchi, Meagan M. Kitt, and Evan S. Deneris. Reorganization of postmitotic neuronal chromatin accessibility for maturation of serotonergic identity. *eLife*, 11, 4 2022.

[299] Monica Marini, Ernie M H F Bongers, Roberto Cusano, Marco Di Duca, Marco Seri, Nine V A M Knoers, and Roberto Ravazzolo. Confirmation of clim2/lmx1b interaction by yeast two-hybrid screening and analysis of its involvement in nail-patella syndrome. *International journal of molecular medicine*, 12:79–82, 7 2003.

[300] Guoyou Liu and Ann Dean. Enhancer long-range contacts: The multi-adaptor protein ldb1 is the tie that binds. *Biochimica et biophysica acta. Gene regulatory mechanisms*, 1862:625–633, 6 2019.

[301] Guoyou Liu, Lei Wang, Jürgen Wess, and Ann Dean. Enhancer looping protein ldb1 regulates hepatocyte gene expression by cooperating with liver transcription factors. *Nucleic acids research*, 50:9195–9211, 9 2022.

[302] Sang-Hyun Song, Chunhui Hou, and Ann Dean. A positive role for nli/ldb1 in long-range beta-globin locus control region function. *Molecular cell*, 28:810–22, 12 2007.

[303] Ivan Krivega and Ann Dean. Ldb1-mediated enhancer looping can be established independent of mediator and cohesin. *Nucleic acids research*, 45:8255–8268, 8 2017.

[304] Kevin Monahan, Adan Horta, and Stavros Lomvardas. Lhx2- and ldb1-mediated trans interactions regulate olfactory receptor choice. *Nature*, 565:448–453, 1 2019.

[305] Daniel B Dranow, Pierre Le Pabic, and Thomas F Schilling. The non-canonical wnt receptor ror2 is required for cartilage cell polarity and morphogenesis of the craniofacial skeleton in zebrafish. *Development (Cambridge, England)*, 150, 4 2023.

[306] Chengting Zhang, Lucy Brunt, Yosuke Ono, Sally Rogers, and Steffen Scholpp. Cytoneme-mediated transport of active wnt5b-ror2 complexes in zebrafish. *Nature*, 625:126–133, 1 2024.

[307] Marc Fiedler, Michael Graeb, Juliusz Mieszczanek, Trevor J Rutherford, Christopher M Johnson, and Mariann Bienz. An ancient pygo-dependent wnt enhanceosome integrated by chip/ldb-ssdp. *eLife*, 4, 8 2015.

[308] Miha Renko, Marc Fiedler, Trevor J Rutherford, Jonas V Schaefer, Andreas Plückthun, and Mariann Bienz. Rotational symmetry of the structured chip/ldb-ssdp core module of the wnt enhanceosome. *Proceedings of the National Academy of Sciences of the United States of America*, 116:20977–20983, 10 2019.

[309] Hongyang Wang, Juhyun Kim, Zhizhi Wang, Xiao-Xue Yan, Ann Dean, and Wenqing Xu. Crystal structure of human ldb1 in complex with ssbp2. *Proceedings of the National Academy of Sciences of the United States of America*, 117:1042–1048, 1 2020.

[310] Tetsuo Ohnishi, Yuji Kiyama, Fumiko Arima-Yoshida, Mitsutaka Kadota, Tomoe Ichikawa, Kazuyuki Yamada, Akiko Watanabe, Hisako Ohba, Kaori Tanaka, Akihiro Nakaya, Yasue Horiuchi, Yoshimi Iwayama, Manabu Toyoshima, Itone Ogawa, Chie Shimamoto-Mitsuyama, Motoko Maekawa, Shabeesh Balan, Makoto Arai, Mitsuhiro Miyashita, Kazuya Toriumi, Yayoi Nozaki, Rumi Kurokawa, Kazuhiro Suzuki, Akane Yoshikawa, Tomoko Toyota, Toshihiko Hosoya, Hiroyuki Okuno, Haruhiko Bito, Masanari Itokawa, Shigehiro Kuraku, Toshiya Manabe, and Takeo Yoshikawa. Cooperation of lim domain-binding 2 (ldb2) with egr in the pathogenesis of schizophrenia. *EMBO molecular medicine*, 13:e12574, 4 2021.

[311] Jie Wang, Jeong-Mo Choi, Alex S Holehouse, Hyun O Lee, Xiaojie Zhang, Marcus Jahnel, Shovamayee Maharana, Régis Lemaitre, Andrei Pozniakovsky, David Drechsel, Ina Poser, Rohit V Pappu, Simon Alberti, and Anthony A Hyman. A molecular grammar governing the driving forces for phase separation of prion-like rna binding proteins. *Cell*, 174:688–699.e16, 7 2018.

[312] Bin Wang, Lei Zhang, Tong Dai, Ziran Qin, Huasong Lu, Long Zhang, and Fangfang Zhou. Liquid-liquid phase separation in human health and diseases. *Signal transduction and targeted therapy*, 6:290, 8 2021.

[313] Yuan Wang, Chunlei Zhang, Wenzhong Yang, ShiPeng Shao, Xinmin Xu, Yujie Sun, Pilong Li, Ling Liang, and Congying Wu. Limd1 phase separation contributes to cellular mechanics and durotaxis by regulating focal adhesion dynamics in response to force. *Developmental cell*, 56:1313–1325.e7, 5 2021.

[314] Ayuko Sakane, Taka-Aki Yano, Takayuki Uchihashi, Kazuki Horikawa, Yusuke Hara, Issei Imoto, Shusaku Kurisu, Hiroshi Yamada, Kohji Takei, and Takuya Sasaki. Jrab/mical-l2 undergoes liquid-liquid phase separation to form tubular recycling endosomes. *Communications biology*, 4:551, 5 2021.

[315] Hiroyoshi Nakatsuji, Noriyuki Nishimura, Rie Yamamura, Hiro-Omi Kanayama, and Takuya Sasaki. Involvement of actinin-4 in the recruitment of jrab/mical-l2 to cell-cell junctions and the formation of functional tight junctions. *Molecular and cellular biology*, 28:3324–35, 5 2008.

[316] Sen Yang, Chunxia Liu, Yuting Guo, Guoqing Li, Dong Li, Xiumin Yan, and Xueliang Zhu. Self-construction of actin networks through phase separation-induced ablim1 condensates. *Proceedings of the National Academy of Sciences of the United States of America*, 119:e2122420119, 7 2022.

[317] Bryan A Gibson, Lynda K Doolittle, Maximillian W G Schneider, Liv E Jensen, Nathan Gamarra, Lisa Henry, Daniel W Gerlich, Sy Redding, and Michael K Rosen. Organization of chromatin by intrinsic and regulated phase separation. *Cell*, 179:470–484.e21, 10 2019.

[318] Chao Wei, Lumeng Jia, Xiaona Huang, Jin Tan, Mulan Wang, Jing Niu, Yingping Hou, Jun Sun, Pengguihang Zeng, Jia Wang, Li Qing, Lin Ma, Xinyi Liu, Xiuxiao Tang, Fenjie Li, Shaoshuai Jiang, Jingxin Liu, Tingting Li, Lili Fan, Yujie Sun, Juntao Gao, Cheng Li, and Junjun Ding. Ctcf organizes inter-a compartment interactions through rybp-dependent phase separation. *Cell research*, 32:744–760, 8 2022.

[319] Adam G Larson, Daniel Elnatan, Madeline M Keenen, Michael J Trnka, Jonathan B Johnston, Alma L Burlingame, David A Agard, Sy Redding, and Geeta J Narlikar. Liquid droplet formation by hp1α suggests a role for phase separation in heterochromatin. *Nature*, 547:236–240, 7 2017.

[320] Xinye Han, Di Yu, Ruirui Gu, Yanjie Jia, Qi Wang, Anbalagan Jaganathan, Xuelan Yang, Miaomiao Yu, Nicolas Babault, Chengcheng Zhao, Huanfa Yi, Qiang Zhang, Ming-Ming Zhou, and Lei Zeng. Roles of the brd4 short isoform in phase separation and active gene transcription. *Nature structural & molecular biology*, 27:333–341, 4 2020.

[321] Alicia V Zamudio, Alessandra Dall'Agnese, Jonathan E Henninger, John C Manteiga, Lena K Afeyan, Nancy M Hannett, Eliot L Coffey, Charles H Li, Ozgur Oksuz, Benjamin R Sabari, Ann Boija, Isaac A Klein, Susana W Hawken, Jan-Hendrik Spille, Tim-Michael Decker, Ibrahim I Cisse, Brian J Abraham, Tong I Lee, Dylan J Taatjes, Jurian Schuijers, and Richard A Young. Mediator condensates localize signaling factors to key cell identity genes. *Molecular cell*, 76:753–766.e6, 12 2019.

[322] Ann Boija, Isaac A Klein, Benjamin R Sabari, Alessandra Dall'Agnese, Eliot L Coffey, Alicia V Zamudio, Charles H Li, Krishna Shrinivas, John C Manteiga, Nancy M Hannett, Brian J Abraham, Lena K Afeyan, Yang E Guo, Jenna K Rimel, Charli B Fant, Jurian Schuijers, Tong Ihn Lee, Dylan J Taatjes, and Richard A Young. Transcription factors activate genes through the phase-separation capacity of their activation domains. *Cell*, 175:1842–1855.e16, 12 2018.

[323] Justin Demmerle, Siyuan Hao, and Danfeng Cai. Transcriptional condensates and phase separation: condensing information across scales and mechanisms. *Nucleus (Austin, Tex.)*, 14:2213551, 12 2023.

[324] Ozgur Oksuz, Jonathan E Henninger, Robert Warneford-Thomson, Ming M Zheng, Hailey Erb, Adrienne Vancura, Kalon J Overholt, Susana Wilson Hawken, Salman F Banani, Richard Lauman, Lauren N Reich, Anne L Robertson, Nancy M Hannett, Tong I Lee, Leonard I Zon, Roberto Bonasio, and Richard A Young. Transcription factors interact with rna to regulate genes. *Molecular cell*, 83:2449–2463.e13, 7 2023.

[325] Markus M Rinschen, Florian Grahammer, Ann-Kathrin Hoppe, Priyanka Kohli, Henning Hagmann, Oliver Kretz, Sabine Bertsch, Martin Höhne, Heike Göbel, Malte P Bartram, Rajesh Kumar Gandhirajan, Marcus Krüger, Paul-Thomas Brinkkoetter, Tobias B Huber, Martin Kann, Sara A Wickström, Thomas Benzing, and Bernhard Schermer. Yap-mediated mechanotransduction determines the podocyte's response to damage. *Science signaling*, 10, 4 2017.

[326] Monica Schwartzman, Antoine Reginensi, Jenny S Wong, John M Basgen, Kristin Meliambro, Susanne B Nicholas, Vivette D'Agati, Helen McNeill, and Kirk N Campbell. Podocyte-specific deletion of yes-associated protein causes fsgs and progressive renal failure. *Journal of the American Society of Nephrology : JASN*, 27:216–26, 1 2016.

[327] Jianchun Chen, Xiaoyong Wang, Qian He, and Raymond C Harris. Taz is important for maintenance of the integrity of podocytes. *American journal of physiology. Renal physiology*, 322:F419–F428, 4 2022.

[328] Yi Lu, Tiantian Wu, Orit Gutman, Huasong Lu, Qiang Zhou, Yoav I Henis, and Kunxin Luo. Phase separation of taz compartmentalizes the transcription machinery to promote gene expression. *Nature cell biology*, 22:453–464, 4 2020.

[329] Danfeng Cai, Daniel Feliciano, Peng Dong, Eduardo Flores, Martin Gruebele, Natalie Porat-Shliom, Shahar Sukenik, Zhe Liu, and Jennifer Lippincott-Schwartz. Phase separation of yap reorganizes genome topology for long-term yap target gene expression. *Nature cell biology*, 21:1578–1589, 12 2019.

Acknowledgement

I am grateful for Prof. Thomas Benzing and Prof. Bernhard Schermer for the encouragement and kind guidance throughout my PhD and remarkable support during a difficult and dangerous pandemic. I am thankful for the bioinformatic support from Dr. Giuliano Crispatzu, Dr. Antonios Papadakis and Tim Padvitski, which if without their help, would not realize the projects in their current state. I would like to thank my family and everyone in the Nephrolab for their wonderful inspiration, motivation and help whenever I needed in and out of the lab. I am particularly indebted to my direct supervisor Dr. Martin Kann for his incredible open-mindedness and unending patience for some of my research ideas.